NOISE GENERATION BY HIGH-SPEED AXISYMMETRIC JET FLOWS INTERACTED WITH RADIALLY IMPINGING ANNULAR JET FLOWS

by

Francis J. Montegani

Darshan S. Dosanjh

Syracuse University, Syracuse, New York 13210

Submitted to

National Aeronautics and Space Administration

Final Report Prepared Under Grant No: NsG-431
December 1967

Syracuse University Research Institute
Department of Mechanical and Aerospace Engineering
SURI Report Number 1620.1085 67 12 F

SYRACUSE UNIVERSITY RESEARCH INSTITUTE

NOISE GENERATION BY HIGH-SPEED AXISYMMETRIC JET FLOWS INTERACTED WITH RADIALLY IMPINGING ANNULAR JET FLOWS

by

Francis J. Montegani
Darshan S. Dosanjh

Syracuse University, Syracuse, New York 13210

Submitted to

National Aeronautics and Space Administration

Final Report Prepared Under Grant No: NsG-431
December 1967

Syracuse University Research Institute
Department of Mechanical and Aerospace Engineering
SURI Report Number 1620.1085 67 12 F

ACKNOWLEDGEMENT

The sponsorship of these investigations by the National Aeronautics and Space Administration under Grant No. NsG-431 is gratefully acknowledged. In addition, computer expenses were supported in part by the National Science Foundation under Grant GP-1137 administered by the Syracuse University Computing Center. The authors thank James Yu and Amr Abdelhamid for their assistance in the gathering and reduction of the experimental data. Appreciation is also extended to Mrs. Virginia Nortman for typing the report.

SUMMARY

Supersonic jet noise investigations were conducted using the impingement of a radial annular jet flow on the first shock-cell region of a moderately underexpanded axisymmetric converging main jet flow. Acoustical data and spark shadowgraphs of the interacting jet flows were recorded in an anechoic chamber. The principal experimental variables were the main jet total pressure, the impinging jet total pressure, and the impingement location. Various nozzle arrangements were employed which differed principally in regard to the provision made for entrainment of air by the jets upstream of the impingement location.

Due to such interaction of the two jet flows, the strong shock pattern in the main underexpanded jet flow is modified. Under all main jet operating conditions, a characteristic variation of the total acoustic power level with the amount of impinging flow was observed. Moreover under certain operating conditions the total acoustic power emitted by the interacted jet flows was lower than that emitted by the main jet flow alone. A maximum sound pressure level reduction of 3 1/2 dB was achieved. The observed variations in noise level were accompanied by characteristic variations of the shock pattern of the interacted jet flows. The emergence of new repetitive shock structure interposed between the original repetitive shock pattern of the main jet flow was observed. The shadowgraphs of the interacting jet flows also revealed an apparently spherical acoustic emission originating at each oblique shock tip. On the basis of these observations, an acoustic model of the flow is proposed as a distribution of wideband acoustic monopole sources on a line, which correspond to the apparent sources at each oblique shock-end. The results of this analysis are in qualitative agreement with those obtained experimentally.

CONTENTS

LIST OF SYMBOLS

A	jet exit area
A_i	elemental area on measurement sphere; acoustic source strength factor
a_o	speed of sound in undisturbed atmosphere
D	jet exit diameter
DI	directivity index
F	narrow band acoustic source strength factor
f	frequency
G	acoustic source strength factor
I	acoustic intensity
i	measuring station
$\underline{j}$	$\sqrt{-1}$
M_c	convection Mach number based on a_o
p	pressure; sound pressure
PWL	acoustic power level
Q	acoustic source strength
R	radius; acoustic power ratio
s	shock-cell or acoustic source spacing
SPL	sound pressure level
T_{ij}	stress tensor
t	time
U	jet exit velocity
W	acoustic power

GREEK

δ_{ij}	Kroneker delta
η	acoustic efficiency
θ	azimuth angle
λ	wavelength
ν	wave number
ρ	density
ω	angular frequency

INTRODUCTION

The development of the modern turbojet engine has led to serious engineering interest in jet noise generation. The continued development of more powerful jet propulsion systems for high speed aircraft and the growth of jet air traffic have focused public and scientific attention on the ever growing jet noise problems such as human annoyance and injury, and structural fatigue.[1,2*] Jet noise has become a challenging part of a wider contemporary problem of "noise pollution" which is suspected of having adverse long-term physiological and psychological effects on man.[3] Effective jet noise abatement is not yet at hand. Recently, the scope of the jet noise problem has been widened as a result of the development of giant space-age booster rockets.[4] The associated noise is extremely intense and may threaten the integrity of vehicle operations and adversely affect entire communities.

The inability of engineers and scientists to combat effectively this growth serves to assert the inherent difficulties of the problem. These follow firstly from the complexities of the phenomena of jet noise generation, and secondly from the practical obstacles to implementing abatement measures without incurring crippling performance and weight penalties.

The noise generation from both subsonic and supersonic jet flows is of current interest. To date, subsonic jet noise generation has been studied more extensively. This in part has led to a government supported program[5] directed towards the development of a quiet jet engine. The program is a consolidated effort to optimally reduce all noise sources in a jet engine

while not affecting its performance. Unfortunately, for supersonic jet flows which are more responsible for contemporary jet noise problems, no comparable motivating body of knowledge exists. In such flows, compressibility effects on turbulence and the presence of shock waves become complicating factors. The subsonic jet noise generating mechanisms change their character and become more complex as the flow becomes supersonic, and new mechanisms emerge. The relative contribution to the total noise from each of the mechanisms in supersonic jet flows is not yet established. The practical approaches to noise abatement evolving from subsonic considerations are not directly applicable either to rocket exhausts where the high speed flow invariably has shock structure or to the jet engine exhaust if it is operated above the critical pressure ratio.

Basically, jet noise generating mechanisms arise from convected turbulence and the interaction of convected turbulence with shock waves. In an investigation of interacting two dimensional high-speed jet flows, Dosanjh and Sheeran[6] observed that the shock structure of a supersonic jet flow was markedly altered by the impingement of a low-energy side jet flow. Concurrently, a subjective "softening" of the emitted noise was observed. Since the formation and the presence of shock fronts plays an important role in jet noise generation, any modification and weakening of the shock pattern may be expected to lead to a modified and possibly a reduced radiation of noise. It is to explore this idea that the present research was undertaken. Previously, Ingard and Maling[7] investigated the noise generation by two axially interacting high subsonic jet flows and found the noise so generated to be greater than the combined noise of the individual jets. This however was an asymmetric

interaction of two equal jet flows with no apparent physical basis for possible noise reduction. In the present case, the approach is new and stems from the primary attempt to systematically modify the shock structure of a high-speed axisymmetric converging main jet flow using radially impinging annular jet flow.

To present the scope and results of this research in a logical sequence, the report is organized into three sections. The first section contains a brief review of the nature and mechanisms of jet noise generation with emphasis on supersonic jet flows. This is necessary to provide a context in which the specific motivations, the procedures, and the results of this research can be suitably discussed and interpreted. The second section comprises a description of the overall experimental facilities and apparatus which were designed and built specifically for these investigations. These facilities were provided with ample operational flexibility so that they can be subsequently used to conduct other acoustical and flow investigations. Included in this section is a discussion of the general methods used to obtain the acoustical and optical data. In the third section, the results of the experimental and analytical investigations of the noise generation by high-speed interacting jet flows are presented. It is shown that this new attempt at jet noise reduction did achieve positive results which hopefully may be of some practical value, and new and interesting phenomena concerning noise and flow characteristics of high-speed jet flows have been discovered which are fertile areas for further investigations.

I - MECHANISMS OF JET NOISE GENERATION

SUBSONIC AND SHOCK-FREE SUPERSONIC JET FLOWS

Aerodynamic noise, by definition, encompasses only the noise generated as a by-product of an airflow and jet noise is a special case of such noise. Up until 1952, little was understood of the fundamental mechanisms of aerodynamic noise generation by turbulent flows although turbulence per se was receiving considerable scientific attention. In 1952 and 1954, M. J. Lighthill[8,9] advanced a theory for aerodynamic noise generation by turbulent flows and established some needed fundamental direction for the emerging scientific and engineering interest in jet noise generation. This has come to be the classic work in the field.

A fundamental result describing the far field noise caused by a region of turbulence absent of sinks, sources, or solid boundaries in Lighthill's[8,10] notation, is

$$\rho - \rho_o = \sum_{i=1}^{3} \sum_{j=1}^{3} \frac{1}{4\pi a_o^2} \frac{x_i x_j}{x^3} \int \frac{1}{a_o^2} \frac{\partial^2}{\partial t^2} T_{ij}\left(\underline{y}, t - \frac{|\underline{x}-\underline{y}|}{a_o}\right) d\underline{y} \tag{1}$$

where

ρ = instantaneous density

ρ_o = density of undisturbed atmosphere

a_o = speed of sound in undisturbed atmosphere

$\underline{x}$ = far field position vector

x = magnitude of $\underline{x}$

x_i = component of $\underline{x}$

$\underline{y}$ = position vector in turbulent region

t = time.

The tensor T_{ij} is Lighthill's turbulence stress tensor, defined by

$$T_{ij} = \rho v_i v_j + p_{ij} - a_o^2 \rho_{ij} \tag{2}$$

where

v_i, v_j = instantaneous velocity

p_{ij} = surface stress tensor

δ_{ij} = Kroneker delta.

Equation 1 is readily explained with reference to figure 1. The origin of the coordinate system is located within the turbulence field, and $\underline{y}$ is the position vector of an element of volume $d\underline{y}$ within the turbulence field. The vector $\underline{x}$ denotes the position of a point $P(\underline{x})$ away from the turbulence field such that $|\underline{x}-\underline{y}| \sim x$. The quantity

$$t - \frac{|\underline{x}-\underline{y}|}{a_o}$$

is the "retarded time", where $|\underline{x}-\underline{y}|/a_o$ is the time it takes a signal to reach $\underline{x}$ from $\underline{y}$. Equation 1 thus gives the instantaneous density perturbation $\rho - \rho_o$ at a far field point in terms of a volume integration throughout the turbulence region of the second time derivative of the stress tensor T_{ij} evaluated at retarded time. Using summation convention, equation 1 may be simply written as

$$p - p_o \simeq \frac{x_i x_j}{4\pi a_o^2 x^3} \int_\tau [\ddot{T}_{ij}] d\tau, \tag{3}$$

where $p - p_o$ replaces its acoustic equivalent $a_o^2(\rho-\rho_o)$ in the far field. The second time derivative is denoted with double dots, and the square brackets denote evaluation at retarded time.

Thus, the determination of the sound field (fluctuating acoustic pressure $p - p_o$) generated by a turbulent flow has been put on a quantitative analytical basis and brought to within a direct integration of actual evaluation. However, although the Lighthill theory proceeds on an assumed a priori knowledge of the stress tensor T_{ij}, it is apparent from the outset that because of the statistical nature of turbulence, analytical descriptions of T_{ij} are unattainable for arbitrary flows. This is so in spite of making a good first approximation of the stress tensor (equation 2) for subsonic flows as

$$T_{ij} \approx \rho_o v_i v_j .$$

Experimental evaluations of the integrand of equation 3 or equivalent forms, using the approximate form of the stress tensor, are quite untenable as the necessary measurements count in the thousands.[11] Recently Chu[12] has accomplished some limited measurements in this regard with low subsonic flows. Direct experimental hot wire measurements in high speed flows encounter added difficulties in separating the simultaneous presence of temperature and velocity fluctuations.[13]

From dimensional considerations and using experimental evidence on the structure of jet flows, Lighthill deduced the so-called "eighth power law" for the acoustic power radiated by a jet, i.e.,

$$\text{Acoustic power} \propto \frac{\rho_o A U^8}{a_o^5} \tag{4}$$

where U is the jet exit velocity, and A is the jet exit area. This result is valid over the entire subsonic flow regime. From this result it follows that the acoustic efficiency η of a subsonic jet, that is, the ratio of the emitted acoustic power to the jet power, varies as U^5. Experimentally, the variation has been established[14] approximately as

$$\eta = 10^{-4}(U/a_o)^5 \tag{5}$$

The important regions of a subsonic jet flow are illustrated in Figure 2a. These comprise an initial mixing region extending about four diameters downstream of the exit, followed by an adjustment region to about eight diameters and then by a region of turbulent decay. Among the considerations leading to the U^8 law, is the empirical fact that the greatest fraction of the total noise is generated in the mixing region within a few diameters of the jet exit. The mixing region is characterized as a region of high shear giving rise to high turbulence levels which account for the significant noise emission. In this region, the acoustic power emitted per unit length is constant, while in the adjustment region it begins to fall off, and in the region of turbulent decay starting at 8D, the acoustic power per unit length varies inversely as the seventh power of the downstream distance.[15]

Therefore two fundamental ways of reducing the noise of subsonic jets suggest themselves. The first is to reduce the jet exit velocity which will reduce the acoustic efficiency (equation 5) of the jet. This is the basis for the current trend to development of high bypass ratio engines. These use turbine shaft work to impel additional inlet air through the engine, bypassing the combustion chamber and achieving the same thrust (with lower exit velocities) as a non-bypass unit. There is a practical limit to the effectiveness of this approach however, since a penalty is paid in terms of increased inlet fan noise. Any other means of reducing shear in addition to reducing jet velocity will also reduce the acoustic emission. This is one of the principles of operation of jet engine silencers. These achieve reduced shear by enhancing induced secondary entrainment flow from the surrounding air into the jet flow. The second fundamental way to reduce the total noise emission at its source is to diminish the extent of the mixing region in which the noise generated per unit length is high and constant. This might be accomplished by suitably modifying the flow so that the region of turbulent decay, where the noise per unit length falls off sharply, is moved closer to the nozzle exit.

The Lighthill theory is particularly notable in that it relates the sound produced by turbulence to classical acoustic theory. From classical acoustics, a monopole is the simplest sound source, being nondirectional, and creates sound by fluctuating mass injection. This may be physically represented by a uniformly pulsating sphere and is illustrated schematically in figure 3. Higher order sound sources which have a directional character may be constructed by bringing together a number of phase related monopoles. For example, as illustrated in figure 3, a dipole is constituted of two opposed-phase monopoles.

A dipole may be physically represented by a laterally oscillating sphere, and further, it is equivalent to a fluctuating force acting in the medium. A quadrupole in turn may be constructed from two opposed dipoles, which, being equivalent to balanced forces in opposition, are equated with fluctuating stresses in the medium. This is physically represented by a symmetrically deforming sphere in figure 3.

If such sources are presumed to be convected at a Mach number M_c referred to ambient sound velocity, the acoustic fields they generate are given, using summation convention, by

$$p - p_o = \underset{(a)}{\frac{m(t-x/a_o)}{4\pi x(1-M_c\cos\theta)}} \quad , \quad \underset{(b)}{\frac{x_i \dot{P}_i(t-x/a_o)}{4\pi x^2(1-M_c\cos\theta)^2}} \quad , \quad \underset{(c)}{\frac{x_i x_j \ddot{T}_{ij}(t-x/a_o)}{4\pi x^3(1-M_c\cos\theta)^3}} \tag{6}$$

for a monopole, a dipole, and a quadrupole respectively where $m(t)$, $P_i(t)$, and $T_{ij}(t)$ are the respective source strengths at time t. Here θ is the angle between the direction of emission and the direction of convection, and x is the distance from the point of emission.

If the turbulence in a jet flow is convected with velocities which are not negligible, equation 3 can be reformulated as

$$p - p_o = \frac{x_i x_j}{4\pi a_o^2 x^3} \int_\tau \frac{[\ddot{T}_{ij}]}{(1-M_c\cos\theta)^3} \, d\tau \tag{7}$$

where M_c is the turbulence convection Mach number and θ becomes the angle between the jet axis and the direction of emission from an elemental volume. The convection velocity is responsible only for the $(1-M_c\cos\theta)^3$ term which becomes simply a directional factor. A comparison of the pressure field of an

acoustic quadrupole (equation 6c) with the integrand of equation 7 identifies the integrand as being due to a spatial distribution of convected acoustic quadrupoles. Further, these quadrupoles, because of the directional factor, are greatly influenced by the convection velocity. An understanding of the effects of convection velocity is important to explain the changes that the noise generation undergoes with increasing Mach number.

A quadrupole, being comprised of four elementary monopoles, radiates energy to distant points with reduced efficiency compared to a single monopole with the same strength. This is because of cancellation effects among the signals of the composite simple sources. Indeed, these cancellation effects are responsible for the nature of the quadrupole. As the convection speed of the quadrupole increases, the efficiency of the radiation increases. This follows from the directionality factor which increases the sound emitted forward more than it decreases the sound emitted backward so that the integrated intensity in all directions (acoustic power) increases with M_c.

To an observer being approached by a convected quadrupole at Mach 1, the basic nature of the acoustic emission changes. This comes about since, to the observer, no cancellation effects occur as the composite monopole sources move along with the wave fronts they create. Mathematically, under such conditions singularities arise in the Lighthill theory because of the directional factor. Recognizing the nature of the singularities, and on the basis of earlier work by Phillips[16] with supersonic boundary layers, Ffowcs-Williams[17] extended the Lighthill theory to sonic and shock-free supersonic jet flows. The new nature of the acoustic emission under these circumstances has been described in terms of "eddy Mach waves". Physically these may be envisioned as rudimentary

bow shocks attached to convected coherent regions of turbulence. Such radiation propagates in a direction perpendicular to the Mach line of the convected supersonic source.

The Mach wave radiation has been observed experimentally, among others, by Lowson and Ollerhead.[18] Also see Figure 15 for such directional acoustic emission originating near the nozzle exit. However the relative importance of this type of acoustic emission is not yet well established and the theory yields no quantitative information. Moreover, on the basis of experimental observations of the acoustic emission from a number of actual rocket engine exhausts, it has been concluded[19] that the major part of the noise is generated from the downstream portion of the subsonic region of the jet flow.

Ffowcs-Williams established a U^3 variation of acoustic emission for supersonic flows and showed that for Mach number flows above two or three, the acoustic efficiency should remain constant. This has been borne out by some limited evidence.[20]

THE ROLE OF SHOCK STRUCTURE IN JET NOISE GENERATION

For supersonic flows, the character of the acoustic emission changes because of the presence of shock waves in the flow. Most practical supersonic jet flows possess a complex shock pattern. Shock-free supersonic jet flow exists only for properly contoured converging-diverging nozzles, and only at a single specified operating condition for which the flow issues with the same static pressure as the ambient medium. Operation at any other condition above the critical pressure ratio results in an over- or underexpanded flow condition and the establishment of a shock pattern. Not all practical supersonic nozzles are of the contoured type, and of those that are, most certainly none operate

solely at their shock free condition. Therefore the role of shock waves in jet flow noise generation must be considered.

Kovasznay[21] showed that a general compressible flow disturbance may be described in terms of three modes: a) a vorticity (or velocity) mode, b) an entropy (or temperature) mode, and c) a sound (or pressure) mode. The interaction of any of these disturbance modes with a shock wave gives rise to all three fluctuation modes downstream of the shock front. Consequently, the interaction of turbulence (velocity mode) with the shock structure of a high-speed jet flow is a source of sound. For weak disturbances, these modes behave independently, whereas for strong disturbances there is a non-linear coupling between them.

The qualitative importance of the role of shock waves in jet noise generation is well established. Franklin[22] investigated acoustic emission from a number of converging-diverging nozzles operating over a continuous range of pressure ratios spanning the shock-free condition. He observed a reduced acoustic emission in all cases at the shock free condition suggesting a significant contribution to the total radiated noise from shock-turbulence interaction. This is supported by Howes[23] who likewise observed marked acoustical effects because of shock structure variations in supersonic flows. Howes further concluded that there is no adequate relation for predicting total acoustic power based on the geometric and fluid properties of supersonic jets over a wide range of conditions. This is in contrast with the U^3 prediction by Ffowcs-Williams for shock-free supersonic jet flows.

Taking a more fundamental approach to the problem, various investigators have considered the interaction of a simple velocity mode disturbance with a shock

wave. Ribner[24] considered the problem of a sinusoidal shear wave (which is taken to represent a single component of the turbulence spectrum) interacting with a shock wave. His results showed a refracted, amplified shear wave and an intense sound wave to be produced and convected downstream. His results were qualitatively verified experimentally with the interaction of a single vortex with a shock wave by Hollingsworth and Richards.[25] These experiments revealed the creation of a single growing cylindrical acoustical wave by the passage of a shock wave over an isolated vortex. Using interferometric techniques, Weeks and Dosanjh[26] obtained quantitative results on the intensity of the cylindrica sound wave. Ribner[27] extended his earlier shock-shear wave interaction analysis to shock-turbulence interaction by constructing a Fourier integral of superposed shear waves to represent turbulent velocity field. With this approach he was able to compute the sound levels downstream of an infinite plane shock wave in terms of the intensity of upstream isotropic turbulence. These results provide only a qualitative guide to the generation of noise by the shock structure in jet flows because of the field variation of the turbulence and the complicated shock pattern. Recently, in an extension of this work, Ribner[28] has determined the ratio of acoustic energy flux (i.e., the acoustic energy emitted per unit area of shock wave) to the turbulent energy flux as a function of upstream Mach number.

The application of all these basic results, deduced under simplifying assumptions, to actual supersonic jet flows is somewhat limited in scope because of the physical complexity of actual jet flows in which field variations of velocity, turbulence, and shock structure occur concomittantly. The lack of systematic methods of quantitative noise prediction for general supersonic jet

flows illustrates this. Nevertheless, two important observations can be made concerning noise reduction of supersonic jet flows in addition to those which carry over from subsonic jet flows. First, if shock waves are a significant noise source, the total noise emitted by supersonic jet flows may be modified and/or reduced by modifying and/or diminishing the total extent of shock waves. This would be particularly true for portions of the shock structure in high turbulence regions of the flow. Second, noise reduction might be accomplished by any severe weakening of the strong shock pattern. These points will be referred to later.

Shock-turbulence interaction phenomena in jets can become amplified by resonance effects. Under some operating conditions, these may be the cause of an intense discrete acoustic emission variously termed "screech" or "whistle" which dominates the noise emitted by a jet. The mechanism responsible for this effect has been explained by Powell.[29] For a cold model, converging jet operating slightly above choked conditions, a repetitive shock pattern is established as illustrated schematically in figure 2b. A flow disturbance originating at the nozzle exit is amplified in the shear layer as it is convected downstream where it interacts with the shock wave and emits a strong acoustic signal. This signal, in propagating in the upstream direction perturbs the local ambient pressure at the nozzle exit. In turn, the jet expansion angle is perturbed (being dependent on the jet exit operating pressure ratio) and gives rise to a new eddy which, in propagating downstream, perpetuates the process. The succession of shock cells all contribute to the phenomenon and once established it manifests large undular oscillations of the flow, and intense discrete directional acoustic emission results. The fundamental frequency of the emitted

tone is given by

$$f = \frac{a_o M_c}{s(1+M_c)} ,$$

where s is the successive shock spacing, and M_c is the disturbance convection Mach number. If three or more phase related acoustic sources identifiable with the consecutive shock cells are presumed to contribute to the sound emission, the resultant far field emission is computed to comprise a strong fundamental tone emitted in the upstream direction, and a first harmonic of comparable intensity emitted normal to the jet axis. This agrees with the experimentally observed sound field. The correctness of the feedback nature of this mechanism has been verified by Hammitt[30] who, by interfering with the upstream propagating acoustic emission, was able to suppress the flow oscillations and discrete emission. The hot jets, however, do not favor the existence of this feedback mechanism. Also, such feedback effects can be suppressed by proper attention to nozzle design with the introduction of teeth or notches.[31]

On the basis of the preceding review it is evident that as yet no concise systematic analytical treatment of the problem of jet noise generation exists covering all the wide range of operating conditions of interest. Practical understanding follows from a piecemeal application of combinations of theory and experiment. Scientific knowledge is being acquired gradually through carefully executed investigations of elementary flows designed to shed light on specific phenomena. For example such work is typified by references 12 and 13. The systematic experimental model studies such as those by Barnett[32], Morgan et al[33], and Pernet[34] are typical of the applied research on the problem.

Such investigations are important for shedding more light on the nature of the mechanisms involved, and for pointing the way for further analytical and semi-empirical methods of analysis. Also, from such investigations, hopefully, will come needed new approaches to jet noise abatement. The present research with interacting jets was undertaken in this spirit.

It was indicated in relation to the mixing region that reduced noise emission may be accomplished by: 1) modifying the flow such as to reduce shear and 2) reducing the extent of the mixing region. In addition, for supersonic flow, it followed that noise reduction could be accomplished by: 3) reducing the total extent of shock structure in the flow, and 4) eliminating or weakening the existing shock structure. Dosanjh and Sheeran[6] established that the impingement of a low-energy side jet flow on an underexpanded main jet flow would radically alter the main jet flow and its shock structure. With the addition of the impinging flow, a subjective "softening" of the emitted sound was observed. The apparent connection between these observations and approaches 3 and 4, above is clear. In addition, the impingement of a side jet flow on a main jet flow would alter the turbulence structure of the main jet flow and items 1 and 2 would be relevant in this regard. Therefore, by impinging a low-energy side jet flow on an underexpanded main jet flow, the four modifying effects as noted above could contribute to noise modification and possible reduction. To verify this hypothesis and expectation, the noise studies of interacting high speed axisymmetric jet flows were undertaken.

II - EXPERIMENTAL FACILITIES AND METHODS

The noise emission is variable with direction around the jet flow. The total acoustic power (which is an integrated effect) is therefore more easily related to jet operating conditions. But total acoustic power is not a sufficient criterion for evaluating effective noise abatement as it may not directly reveal other changes occurring in the directional sound field which may be contributory to effective noise abatement.

In general terms, effective abatement of the noise emitted by a source may be accomplished by:

a) reduction of the total acoustic power radiated, by uniform reduction of the acoustic intensity in all directions,

b) selective reduction of the sound intensity in certain directions where it is particularly objectionable, and

c) modification of the spectrum of the sound so it is less offensive either to hearing or to a responsive structure.

The "effective abatement" may be accomplished even with an increase in total power radiated if changes described in b) and c) above are effective. Therefore to properly examine the noise abatement merits of flow impingement technique, all aspects of the sound field must be investigated. These are the total acoustic power, the directivity, and the spectrum. The facilities developed and described in this section were designed to meet these three specific needs.

ANECHOIC CHAMBER

In a laboratory situation, the total acoustic power radiated and the power spectrum can be determined with relative ease using a reverberant-room where a diffuse sound field is established. This type of facility however is

the antithesis of that necessary for the determination of directivity data. For the latter, an anechoic chamber is required in which a free field is established. It must be noted that in a diffuse field no quantitative directivity information may be obtained either directly or indirectly, whereas a free field permits the ultimate determination of all noise radiating properties of the object under test since the total power and the power spectrum may be established by computation from the directivity information. For these investigations therefore, the more general facility, a fully anechoic chamber was constructed with particular attention to the requirements of operating continuously running model jets within it.

The site made available for the construction of the anechoic chamber was a below ground open concrete walled loading pit having dimensions of 14' -6" x 17' -0" x 11' -1" deep, opening through an 8' x 10' doorway into the basement level of a building where a control room could be located. The below ground site exterior to the building was desirable on the basis of lessened background structural noise. Having finalized the site size which was the basic constraint in the design of the anechoic chamber, there remained the problems of optimizing the other construction features, particularly the cutoff frequency employed. For the most generally useful anechoic chamber, the lowest possible cutoff frequency is desired. However, for a given cutoff frequency, the anechoic wall treatment thickness required is approximately 1/4 wavelength. Therefore a low cutoff frequency implies a deep wall treatment. This results in a small working space in the anechoic chamber, whereas for many reasons as large a working area as possible is desired. Other considerations had to be made for the ultimate size of the model jets employed (whose characteristic sound wavelength varies with

jet diameter which was determined by the choice of cutoff frequency). An upper size limit on the jet diameter was imposed by the finite air supply, and a lower limit was imposed by the high frequency response of the instrumentation available. Without elaborating on merits of various decisions and compromises made in these matters, the resulting facilities are described below.

To prepare the open pit for the installation of the anechoic chamber, the walls were extended upward 3' -3" from ground level with face brick (to match the building exterior) backed with 8 inch solid concrete block. The structure was capped with an 8 inch reinforced concrete slab and a built-up gravel surface roof. The water in the no longer functioning trap in a floor drain was replaced with oil to prevent ultimate evaporation and gas release. The 8' x 10' doorway was temporarily left open to allow maximum access for construction of the anechoic chamber. The resulting hard walled enclosure had final interior dimensions of 14' -6" x 17' -0" x 14' -2" high. A spring-isolated anechoic chamber was constructed and the basic configuration of the facility is that of an isolated anechoic room within a room. A four inch air gap was allowed between walls of the isolated room and adjacent interior surfaces of the enclosure consistent with standard practice for maximum airborne noise attenuation.[35] At the completion of the isolated anechoic chamber installation, the 8' x 10' opening was walled up with 8 inch solid concrete block and a soundproof access door installed to match a corresponding interior door in the isolated chamber.

The anechoic chamber was designed for a cutoff frequency of 200 Hz. A blanket-type fiberglass covered wedge was used in lieu of the usual wire-cloth covered wedge in order to eliminate the possibility of difficulties with ultrasonic reflections. The finished interior dimensions of the chamber were

10' -6" x 13' -0" x 9' -2" high, wedge tip to wedge tip. A 3/32 inch diameter wire cable floor with 2 inch spacing was installed 10 inches above the floor wedge tips, and a removable steel grating floor was provided though not used in these investigations to avoid high frequency reflections. Two lights and nine instrumentation hangers were installed in the ceiling. A sound-attenuating air-piping and instrumentation penetration was provided through the double walls between the anechoic chamber and the control room.

Of particular importance for the utilization of the chamber for jet noise investigations was the installation of two sound-attenuating air vents to allow exit for the jet efflux. For each vent, two silencers were employed in series. One was fastened to the isolated structure and one to the rigid structure in the ceiling. These were connected by flexible ducting. The vent openings in the chamber were overhead on either side at the downstream end of the anechoic chamber and the air was conducted to the outside of the building. Together the vents provided a flow capacity of 2600 standard cubic feet per minute at 0.25 inch H_2O. This volume rate approximates the mass flow for a one inch diameter jet operating at 200 psig total pressure.

It was subsequently determined that the impingement of the flows from one inch diameter jet on the downstream wall caused buffeting of the wedges which threatened their integrity owing to the fragile fiberglass structure. To eliminate the likelihood of damage, a fiberglass-lined impingement funnel and a duct which vented the efflux directly to the ceiling exhaust, were installed in the wall treatment. This was accomplished with minimal disturbance to the wall wedge treatment, and the installation may be seen in figure 4. The impingement funnel acted as a diffuser through which all the jet efflux exited

while at the same time entraining additional air. The additional air entered the chamber through the other (now inlet) duct. The net result was an actual reduction in the ambient pressure of about 0.01 inch H_2O in the closed anechoic chamber while the jets were in operation.

The determination of the actual field conditions achieved in the finished anechoic chamber was done in a direct manner relevant to the way in which the chamber was to be used for the interacting-jet noise measurements. A speaker was fastened in place at the location normally occupied by the interacting jet nozzles and the decay in sound pressure level with radial distance in a horizontal plane was determined. This was done for a number of radial horizontal lines. The radial decay was determined for each frequency an octave apart from 100 Hz to 80 kHz. (A 12 inch speaker was used for frequencies of 1600 Hz and below, and a high-frequency speaker having an effective diameter of approximately one inch was used for frequencies of 3150 Hz and above.) The direction of the axis of the speaker, in general, was different from that of the line of sound pressure level decay measurements. For a theoretical free field, the sound pressure level will decay by 6.02 dB for each doubling of distance from the source (avoiding measurements in the immediate vicinity of the speaker). In an anechoic chamber, the theoretical decay is usually not achieved at low frequencies close to the wedge tips. By calibration of the anechoic chamber it was established that for the 6 foot circular arc about the jets on which sound pressure level measurements were made, free field conditions prevailed within one dB for all frequencies between 400 Hz and 80 kHz, with the greatest deviations occurring at the lowest frequencies when the measuring arc was in the vicinity of the wedge tips. Considering that the spectra from the inter-

acting jets possessed negligible components below 1000 Hz, it followed that free field conditions prevailed in the anechoic chamber for all conditions of noise emission from the interacting jets, within the reliability of the measured data. The background noise level in the closed anechoic chamber was below the sensitivity of the acoustical instrumentation employed in the interacting-jet noise investigations.

AIR SUPPLY AND FLOW CONTROL SYSTEM

The compressed air was supplied by a reciprocating two-stage compressor which had a pumping capacity of 270 cubic feet per minute with a maximum obtainable pressure of 350 psig. The compressed air was passed through an after-cooler and separator which removed some of the water vapor and oil in the air. Oil and water vapor were also removed by an oil filter and an electrically reactivated dual tower type dryer which employs silica gel and molecular sieves as drying agents. The dry compressed air was stored in four storage tanks with a total capacity of 450 cubic feet. From the storage tanks the compressed air flowed through approximately 150 feet of 2" diameter piping, a dust filter and the pressure control system. The tank supply pressure fell continuously as the jets discharged. The function of the air flow control system was to automatically maintain the total pressure in the jet reservoirs at constant operating values as the pressure in the storage tanks fell. A schematic diagram of the system used to accomplish this is given in figure 5. Air from the main supply line after passing through a dust filter in the control room, was branched into two lines, one each for the main and impinging jets. The air for each jet was throttled to proper operating pressure by a separate diaphragm-actuated control valve. Each of the control valves was actuated by

low pressure air from a corresponding valve pilot which detected the total pressure in the appropriate jet reservoir in the anechoic chamber. The detected air pressure was mechanically compared with the desired preset value at the pilot which automatically adjusted the control valve accordingly. After an initial period of stabilization (approx. 5 min.), the system held the jet operating pressures within 0.25 psi of the preset value as the main supply pressure continuously fell. The period of the 0.25 psi fluctuation cycle was on the order of one or two minutes. The total pressures in the reservoirs were determined with precision Bourdon tube gages accurate to 0.1%. A view in the control room showing the valves, the valve pilots, and the precision gages is shown in figure 6.

For the simultaneous operation of both the main and impinging jets, in spite of the availability of two independent automatic control systems, the two air flows were not separately controlled. The impinging jet air was drawn from the automatically controlled main jet air using a hand operated valve (figure 5) bypassing the impinging jet automatic control valve entirely. This simplified the problem of flow system stabilization by eliminating the use of one controller. Further, it maintained the ratio of the impinging jet pressure to the main jet pressure (which ratio was a basic experimental variable) at a constant value compared to the ratio which would have been attained if the two pressures varied independently, each with a 0.25 psi maximum deviation. This followed since, for any setting of the impinging jet flow control handvalve, the impinging jet pressure was proportional to the main jet pressure for small excursions of the main jet pressure, and the handvalve setting, corresponding to the proportionality constant, could be interpreted as percent

impingement. The 0.25 psi deviation of the main jet pressure had no detectable effect on the acoustical measurements.

The controlled air from the flow system in the control room was piped to reservoirs in the anechoic chamber through flexible high-pressure rubber hoses passing through the penetration provided in the double walls. The reservoirs (one each for the main and impinging jets) were supported by a pipe stand constructed for the purpose, and mounted in four of the supports originally provided for the removable steel grating floor for the anechoic chamber. Each reservoir had internal dimensions of 5 inches diameter by 30 inches long with tapering end sections. The jet nozzles investigated (which are described in detail in section III) were mounted on the end of the main jet reservoir and supported approximately midway between the ceiling and floor wedge tips. The impinging jet reservoir was suspended immediately beneath the main jet reservoir. The arrangement is shown in figure 7, with the covering fiberglass removed. The plan location of the nozzles in the chamber is shown in figure 8. The pipe stands and reservoirs can be removed from the anechoic chamber very simply.

TECHNIQUE OF ACOUSTIC MEASUREMENTS

The free field environment in the anechoic chamber made it possible to determine the directivity of a sound source. This could be done for the wideband (entire frequency range of a spectrum of interest) sound or for its narrow band components (frequency bandwidths of 1/3 octave or less). From this basic information, which was important in itself, the overall total acoustic power radiated (which is more readily related to the gross jet operating characteristics), and the power spectrum, were computed. The computational

method in conjunction with the method of acoustical measurement is next described.

The acoustic radiation from an arbitrary sound source varies with direction, and the intensity of the noise is thus generally a function of three space coordinates. In these investigations the jet flows are axisymmetric, having axisymmetric sound fields for which the intensity is a function of r the radial distance and θ the azimuth angle measured from the downstream jet axis. From symmetry, the sound intensity is constant on a circle of radius $r \sin \theta$ normal to the jet axis. Denote the wideband intensity from the jets as $I(r,\theta)$. (Alternately, the discussion could be restricted to narrow band radiation which will be denoted $I_f(r,\theta)$.) The wideband acoustic power radiated by the jets is given as

$$W = \int_{\sigma} I(r,\theta)\, d\sigma(r,\theta) \tag{8}$$

where σ is any imaginary enclosing surface. Referring to figure 9, let the enclosing surface be spherical of radius R and equation 8 may be expressed as

$$W = \int_{o}^{\pi} I(\theta)\, dA(\theta) \tag{9}$$

where $I(\theta)$ denotes $I(r,\theta)$ evaluated at $r = R$, and the elemental area dA is given by

$$dA = 2\pi R^2 \sin\theta\, d\theta \quad .$$

For far field noise radiation, the intensity is given by

$$I(\theta) = \frac{p^2(\theta)}{\rho_o a_o} \tag{10}$$

where $p(\theta)$ is the wideband rms acoustic pressure. This is defined as

$$p(\theta) = \left[\lim_{T\to\infty} \frac{1}{T} \int_o^T p^2(\theta,t)dt \right]^{1/2} \tag{11}$$

where $p(\theta,t)$ is the instantaneous acoustic pressure at the azimuth angle θ. Thus, if R is sufficiently large to insure far field measurements, substitution of equation 10 into equation 9 yields

$$P = \int_o^\pi \frac{p^2(\theta)}{\rho_o a_o} \, dA(\theta) \quad . \tag{12}$$

With reference to figure 9, for experimental purposes assume $p(\theta)$ to be constant on a thin annular strip of width $R\Delta\theta$. Let $\pi/\Delta\theta$ be an integral value q, such that there are $q + 1$ stations, numbered consecutively from 0 to q, at which $p(\theta)$ is to be measured. The angle of the i^{th} station at which $p(\theta)$ is measured is given by $i\Delta\theta$. This angle locates an elemental annular area A_i of arc width $R\Delta\theta$ bounded by the angles $i\Delta\theta \pm \Delta\theta/2$. The annular areas at each station are given exactly by

$$A_i = 4\pi R^2 \sin(i\Delta\theta) \sin \Delta\theta/2 \qquad i = 1,2,\ldots, q-1 \tag{13}$$

where $\Delta\theta$ may be large. The polar areas at $\theta = 0,\pi$ are respectively

$$A_o = A_q = 2\pi R^2[1-\cos \Delta\theta/2] \; . \tag{14}$$

It follows that the integral of equation 12, approximated by a finite sum, yields for the total acoustic power radiated:

$$P = \sum_{i=o}^{q} \frac{p_i^2}{\rho_o a_o} A_i \qquad (15)$$

where the subscript i denotes θ-dependent variables evaluated at the i^{th} measuring station, and the A_i are given by equations 13 and 14.

MICROPHONE POSITIONING MECHANISM

Experimental determination of p_i was accomplished by successively positioning a microphone at a number of measuring stations in a horizontal plane at fixed radius from the jet exit. Various means of conveniently positioning a microphone may be contrived with different degrees of complexity and cost. The system developed here accomplished the task accurately, reliably, and at low cost using relatively simple hardware. The design details of the system, including a positioning mechanism and a position readout device, are given in Appendix A. The positioning mechanism was suspended near the ceiling in the anechoic chamber, and supported a counterweighted boom which moved in a horizontal plane and pivoted about a vertical axis through the jet flows. The microphone was suspended by its own cable from the boom and was directed horizontally towards the axis of rotation using a simple wire bracket. See figure 7. The arc of microphone travel is shown in figure 8. The signal from the microphone was conducted via double shielded cable run along the boom to the center of rotation where it was embedded in the wedge treatment and let through the instrumentation penetration to the control room.

ACOUSTICAL INSTRUMENTATION

The acoustical instrumentation can be seen in figure 6. The principal equipment employed for the acoustical measurements included:

1. Quarter inch free field response condenser microphones with appropriate cathode followers. Frequency response from 20 Hz to 200 kHz $\pm$ 2 dB, with frequency calibration curves supplied by the manufacturer. Dynamic range from 64 dB to 174 dB re 2×10^{-4} μ bar.
2. Pistonphone. (Accuracy $\pm$ 0.2 dB.) Used as a laboratory sound pressure standard.
3. Microphone Amplifier. General purpose instrument used in conjunction with condenser microphones as a precision sound level meter. Frequency response from 10 Hz to 200 kHz. Provision made for bandpass filter insertion for spectrum analysis.
4. Bandpass filter set. A 1/1 or 1/3 octave band filter set with center frequency (the geometric mean of the upper and lower limiting frequencies of a frequency band) range from 25 Hz to 40 kHz. Specific unit employed was custom modified by the manufacturer by the addition of four upper 1/3 octave band filters raising the upper center frequency limit to 100 kHz. Used in conjunction with microphone amplifier and level recorder for automatic spectrum analysis.
5. Level recorder. Graphic strip recorder used in conjunction with microphone amplifier and 1/3 octave band filters for automatic spectrum analysis. Frequency response from 10 Hz to 200 kHz. 50 dB dynamic range.

6. Beat frequency oscillator. Frequency range from 200 Hz to 200 kHz. Used for frequency response evaluations of 1/3 octave band filters and tape recording system.
7. Record/reproduce tape system with three active direct-record channels. Frequency response from 100 Hz to 100 kHz $\pm$ 3 dB. Frequency calibration curves determined with beat frequency oscillator. Loop adapter provided for continuous analysis of short term recordings.

The tape system was employed primarily to permit 1/3 octave band spectrum analysis under conditions when the available jet run time (limited by air supply capacity) was insufficient to accomplish the noise survey directly. In use, the wideband noise signal at each of the measuring stations was recorded on tape. Each recorded signal was of 15 seconds duration. At a later time, the tape was cut and formed into loops, one for each station, and the data on each of these loops was analyzed by continuously running it through the tape system using the loop adapter. No significant differences were noted between the results obtained with the tape system and those obtained from direct measurements with the level recorder technique except that the dynamic response of the tape system was limited to approximately 30 dB.

In the actual investigations, the tape system was employed only on a limited basis as it was determined that the jet run times could be extended considerably by running the air supply compressor continuously. Prior to instituting the investigations, the ability to do this was not assured because of possible induced noise by the compressor through the piping. However the piping is about 150 feet in length and there was no detectable variation

between the data obtained with the compressor stopped and that obtained with it continuously running.

OPTICAL INSTRUMENTATION AND TECHNIQUE

In support of the acoustical measurements, spark shadowgraphs of the jet flows were obtained to determine shock structure changes brought about by the impinging flow, and to observe acoustic emission and sources. To accomplish this, portable shadowgraphic apparatus was constructed which could be conveniently assembled in the anechoic chamber. Removable pipestands were fabricated to fit into the grating floor supports and the components of the shadowgraph system were mounted on these stands. The actual setup in the anechoic chamber is shown in figure 10a, and a schematic of the arrangement is given in figure 10b.

The spark source incorporated six 0.24 μfd, 10 kV maximum rated capacitors, connected in parallel, which discharged across magnesium electrodes yielding an intense transient spark light source of approximately 1-2 μ sec. duration. The capacitor discharge was triggered across the magnesium electrodes by a low energy ionizing spark from a standard automotive ignition coil. A capacitor charge voltage of 2 1/2 kV provided optimum film exposure.

Obtaining shadowgraphs in the anechoic chamber posed an unusual problem since the flow controls and pressure gages were situated in the control room. Moreover, the level of acoustic intensity was so high that presence of the experimenter in the anechoic chamber during the recording of the optical data was hazardous. Therefore a special motorized filmholder/shutter was constructed (figure 11) to circumvent the problem. Essentially the unit is a filmholder, but significantly, it is light-tight and incorporates a motor driven slow speed guillotine-type focal plane shutter which

is opened and closed remotely from the control room. In operation, under ordinary lighting conditions, a conventional filmholder was set in place in the unit, and the slide withdrawn in preparation for the exposure. The investigator could then leave the anechoic chamber, darken it from the outside, and from the control panel, maintain the jet operating conditions while remotely uncovering the film and obtaining the shadowgraph exposure. The unit was constructed to accept three standard size filmholders using different metal inserts (see figure 11). The shutter was opened and closed with the simple throw of a switch at the control panel, and the fully open or closed position was indicated by panel lights.

For all shadowgraphs, Kodak Contrast Process Ortho film was used exclusively, developed in D-8 for four minutes at 70°F. The processing time and temperature were greater than recommended by the manufacturer, but were used for improved contrast, and no degradation of quality was apparent except for a very occasional emulsion reticulation. For yet better image contrast, the films were printed on a grade 4 high contrast enlarging paper.

In recording shadowgraphs, a small film-to-flow distance results in sharply defined shock waves. Alternately, large film-to-flow distances result in greatly accented acoustic emission at the expense of clear delineation of the shock waves. Since the motivation for these investigations lay fundamentally in modification of the jet flow shock structure, a small film-to-flow distance was used to permit the most clear observation of the shock wave variations. The film-to-flow distance used for all shadowgraphs presented here was 4 1/2 inches. Under such conditions, the sound fields do not receive maximum visual emphasis although they are still well defined as a result of

the high contrast photographic processing technique employed. These shadowgraphic records do serve to identify positive noise generating regions of the flow, and thus have played an important role in this investigation.

III - INTERACTING JET NOISE INVESTIGATIONS

EXPERIMENTAL PROGRAM

1. The interaction of a two-dimensional main jet flow impinged upon by a single two-dimensional side jet flow was investigated earlier by Dosanjh and Sheeran.[6] Because of its interaction, the main jet flow deflected. In the present case, ultimately practical results of use in jet or rocket propulsion are sought. Therefore a non-deflected axisymmetric flow is preferred. Such a flow may be achieved by a symmetric distribution of an even number of impinging jets about the main axisymmetric jet. However, such a flow as an acoustic source is three-dimensional so that the amount of acoustical data necessary to document the sound field is prohibitive, particularly as the investigations of a wide range of operating conditions and arrangements of flows were planned. Therefore uniformly axisymmetric non-deflected interacting jet flows were desired. To achieve this a continuous annular impinging jet was employed. This had one disadvantage in that the noise generating characteristics of the annular jet alone could not be separately obtained as the flow would impinge upon itself. This was not a serious restriction as will become apparent in the discussion of the results.

2. The converging axisymmetric main jet was operated at moderately high pressure ratios such as to yield an underexpanded jet flow with normal shock (Mach) disc. (Fig.2c) Such operating conditions were employed principally because the original observations with two-dimensional jet flows by Dosanjh and Sheeran[6] were made with underexpanded flows. The subjective softening of the noise noticed by them was thought to be due to the weakening or the observed

elimination of the normal shock (Riemann wave). For the present investigations the operating pressure ratios for the underexpanded jet flows were higher than the range in which the Powell mechanism is effective. Therefore the possible masking or distortion of other acoustic effects by the associated dominant "screech type" noise emission was avoided.

3. The impinging and main jet exit areas were equal. The annular jet exit was D/8 wide by 2D in diameter, where D is the main jet exit diameter.

These decisions followed from a reasonable optimizing of the parameters involved. The annular jet diameter had to be sufficiently large to avoid interference with the expanded flow from the main jet. For a fixed value of impinging jet annular exit area, the annulus width varies inversely as the diameter, and for very small annulus widths, machining tolerances become significant. The main jet diameter D was chosen 3/8 inch as a suitable compromise between the available run time (which favored small jets) and the frequency response of the instrumentation (which favored large jets).

4. The Basic Variables chosen were:

a) Main jet total pressure

b) Amount of Impinging Flow

c) Downstream Impingement Location

d) Impingement Angle.

For the greatest portion of the experimental data a main jet total pressure of 100 psig was employed. The amount of impinging flow is denoted by "percent impingement" which is defined as the percent ratio of the impinging jet total gage pressure to the main jet total gage pressure. Since the main jet was operated at 100 psig, the percent impingement is numerically equal to

the impinging jet total gage pressure. Main jet total pressures of 75, 150, and 200 psig were also used for the interacting-jet noise investigations.

The impingement location is specified by the ratio x/D, where x is the downstream distance from the plane of the main jet exit to the plane of the centroid of the (line) generatrix of the annular jet exit, and D is the main jet exit diameter.

Nozzle Geometry

During the course of the investigations, three nozzle arrangements were used. Each of these varied in relation to provision made for entrainment by the interacting jet flows upstream of the impingement location. These nozzle arrangements are illustrated in figures 12, 13, and 14, and are referred to as nozzle arrangement I, II, and III respectively. Each arrangement comprised a main jet converging nozzle with a 3/8 inch diameter exit, and a concentric annular converging nozzle of equal exit area, 3/4 inch diameter by 3/64 inch wide. Flow from the impinging jet nozzle was directed radially inward at right angles to the main jet flow. In addition, impinging flow inclined 45^{o} downstream to the main jet flow was employed with nozzle arrangement I.

The main jet nozzles were screwed into the end of the main jet reservoir and the interior mating surfaces were smooth. The main jet nozzle interior was machined with a No. 1 standard Morse taper smoothly blending to a straight exit section 3/8 inch diameter by 3/8 inch long. All interior nozzle surfaces were polished.

The main jet nozzle served to support a small annular buffer reservoir (except for nozzle arrangement III) to which was fastened a set of nozzle rings

which when assembled in place formed the annular jet nozzle. The entire impinging jet nozzle assembly could be positioned as desired in an axial direction on the main jet nozzle allowing the impingement location to be varied. The impingement location is specified by the ratio x/D.

Air for the impinging jet flow was drawn from a manifold in the end of the impinging jet reservoir through four equal-length plastic lines connected in parallel to the impinging jet buffer reservoir. These may be seen in figure 7. The buffer reservoirs and the impinging nozzles in all cases were designed to tangentially distribute the incoming four airstreams so that, at the annular nozzle exits, uniform flows were established with no tangential velocity components or tangential variations of radial velocity. The impinging jet flow total pressure was measured using four parallel connected pitot probes directed upstream in the four incoming airstreams in the buffer reservoirs. An exception to this was nozzle arrangement III which had no buffer reservoir as such, but incorporated carefully installed screens for uniform flow distribution which resulted in a significant pressure drop depending on the flow rate. This arrangement was calibrated beforehand by measuring the exit total pressure as a function of the reservoir pressure.

Procedure

For the investigation of each of the interacting jet arrangements the experimental procedure was to select an x/D value, and then, after having stabilized the main jet flow operating total pressure, adjust the impinging flow total pressure as desired. At each condition of impinging jet pressure, the required acoustical or optical data were obtained. The procedures for obtaining the acoustical data are discussed on the following page. The method of

gathering the optical data is evident from the discussion of the optical instrumentation (see pp. 30-32).

For obtaining acoustical data, the anechoic chamber was cleared of all equipment which was not essential either to support the jet nozzles and reservoirs or the microphone boom. All remaining hard surfaces except the actual nozzles were liberally covered with blanket fiberglass to eliminate acoustical reflections. Once the x/D value for the nozzles was set, the anechoic chamber was vacated and the door closed. The operating conditions for the jets were selected and stabilized with the flow control system. By remote control the microphone was positioned successively at the desired measuring stations and the acoustical data at each station was recorded. Usually eight measuring stations from 15° to 120° were used with a 15° increment angle. Every two complete surveys, the anechoic chamber was entered and the reading of the ambient temperature was obtained from a mercury thermometer suspended on the microphone cable. This also provided a regular visual check of the in-chamber conditions. The barometric pressure outside the anechoic chamber was recorded as this was well in agreement with that in the closed anechoic chamber under all circumstances.

The pistonphone (with $\pm$ 0.2 dB accuracy) was employed frequently to calibrate the sound pressure level meter and the graphic level recorder. However, during runs, random amplitude modulation of the jet noise caused oscillations of the meter needle which lowered the precision of the readings to 0.5 dB. At each measuring station either a wideband sound pressure level or a 1/3 octave band spectrum, or both were determined. Under limited circumstances the signal was recorded on magnetic tape for subsequent analysis.

Computations

Total Acoustic Power.- The wideband sound pressure levels were used to compute the total acoustic power radiated in the following way. From the definition of sound pressure level, SPL, re $0.0002\ \mathrm{dyne/cm^2}$:

$$\mathrm{SPL}_i = 20 \log_{10} \frac{p_i}{(0.0002\ \frac{\mathrm{dyne}}{\mathrm{cm}^2})} \quad [\mathrm{dB}]$$

(where p_i is the wideband rms acoustic pressure defined by equation 11), the mean square acoustic pressure for the i^{th} measuring station becomes

$$p_i^2 = 4 \times 10^{-8} \ \mathrm{antilog} \ (\frac{\mathrm{SPL}_i}{10}) \quad [\frac{\mathrm{dyne}}{\mathrm{cm}^2}] \tag{16}$$

Noting that

$$1 \ \mathrm{watt} = 10^7 \ \frac{\mathrm{dyne\text{-}cm}}{\mathrm{sec}} \ ,$$

and substituting this and equation 16 into equation 15, there results for the total acoustic power

$$W_t = \frac{4 \times 10^{-15}}{\rho_o a_o} \sum_{i=o}^{q} \mathrm{antilog} \ (\frac{\mathrm{SPL}_i}{10}) \ A_i \quad [\mathrm{watt}] \ , \tag{17}$$

where the product $\rho_o a_o$ is the characteristic impedance of air in cgs units and A_i is in cm^2. Finally, expressing this as power level, PWL, re 10^{-12} watt defined by

$$\mathrm{PWL} = 10 \log_{10} \frac{W_t}{[10^{-12} \ \mathrm{watt}]} \quad [\mathrm{dB}] \ ,$$

obtain

$$PWL = 10 \log \left[\frac{4\times10^{-3}}{\rho_o a_o} \sum_{i=o}^{q} \text{antilog} \left(\frac{SPL_i}{10}\right) A_i\right] \quad [dB] \ . \tag{18}$$

The minimum value of θ at which the microphone could be placed to determine SPL_i without also detecting a significant flow convection signal* was experimentally established at 15^o. The maximum value of θ was arrived at as the best compromise which allowed the most reliable data to be obtained, considering the sound level drop-off with upstream azimuth angle, and the need to keep the microphone in the far field requiring a long boom which was not designed to rotate a full 180^o in the anechoic chamber. This angle was established at 120^o. See figure 8.

Confining the measuring stations to the circular arc between 15^o and 120^o, constrains the upper and lower limits respectively on the previous summation to

$$m \geq \frac{15^o}{\Delta\theta}$$

and

$$n \leq \frac{120^o}{\Delta\theta}$$

where m and n are integers. This eliminates the polar areas from consideration, and a final working expression is obtained from equation 18, after substituting the expression for A_i (equation 13), as

$$PWL = 10 \log \left[\frac{16\times10^{-3}}{\rho_o a_o} \pi R^2 \sin\frac{\Delta\theta}{2} \sum_{i=m}^{n} \sin(i\Delta\theta) \text{ antilog} \left(\frac{SPL_i}{10}\right)\right] \quad [dB]. \tag{19}$$

---

*Such a signal is termed "pseudosound" since it is manifested to a microphone as sound, but the convected density fluctuations which are its source are not propagated as sound.

The center of rotation of the microphone about the jets (corresponding to the center of the imaginary enclosing sphere) was selected to be on the jet axis, 3 diameters or 1 1/8 inches downstream of the jet exit. The radius from this point to the microphone was 6 feet or 192 D, which insured far field measurements since the dominant wavelengths of the emitted sound were on the order of 5 D. Because of the voluminous data to be reduced using equation 19, a digital computer was used for the task. In most cases, eight measuring stations at 15^{o} increments from 15^{o} to 120^{o} were employed. Under these circumstances, 20% of the spherical area (primarily beyond 120^{o}) was neglected. The error introduced in the total power level by neglecting the sound field beyond 120^{o} was computed to be less than 1 dB if the sound pressure level measured at 120^{o} is assumed to remain constant between 120^{o} to 180^{o}. Since the sound pressure level generally falls off with high θ values, the actual error in the total power level is even less. The magnitude of the actual error is of the order of the reliability of the measured sound pressure level data. Therefore all total power level values reported here were computed from the actual measured data from 15^{o} to 120^{o}.

Directivity Index.- The directivity index $DI(\theta)$ is the difference between the sound pressure level of a directional source and the sound pressure level at the same location of a non-directional source emitting the same acoustic power. Symbolically this is written for the axisymmetric jet as

$$DI(\theta) = SPL(r,\theta) - SPL(r) \tag{20}$$

where $SPL(r,\theta)$ denotes the wideband measured sound pressure level, at a point, of the directional source, and $SPL(r)$ is the level at the same point of a non-directional source emitting the same acoustic power. (As with the acoustic power computation these considerations may also be restricted to a narrow frequency band.) The expression for power level (eq. 18) for the directional jet source is

$$PWL = 10 \log_{10} \left[\frac{4\times10^{-3}}{\rho_o a_o} \sum_{i=o}^{q} antilog \left(\frac{SPL(r)_i}{10}\right) \cdot A_i\right] \quad [dB] .$$

For a non-directional source the $SPL(r)_i$ are all equal and may be taken out of the summation as $SPL(r)$, yielding

$$SPL(r) = PWL - 10 \log_{10} \left[\frac{4\times10^{-3}}{\rho_o a_o} \sum_{i=o}^{q} A_i\right] \quad [dB], \tag{21}$$

where it is noted that

$$\sum_{i=o}^{q} A_i$$

is the area of the imaginary enclosing sphere on which measurements were taken. Rather than consider the acoustic radiation to be evenly distributed over a completely enclosing sphere, consider it uniformly distributed over the actual area between stations m through n on which measurements were taken. Equation 21 then becomes

$$SPL(r) = PWL - 10 \log_{10}\left[\frac{16\times10^{-3}}{\rho_o a_o} \pi R^2 \sin\frac{\Delta\theta}{2} \sum_{i=m}^{n} \sin(i\Delta\theta)\right] \quad [dB] \tag{22}$$

which, in conjunction with the definition

$$DI(\theta) = SPL(r,\theta) - SPL(r) ,$$

yields the directivity index.

The quantity SPL(r) is termed the mean level of the directional radiation and is noted wherever the directivity index is presented. By adding the directivity index to the mean level, the measured sound pressure level at any value of θ may be obtained. The directivity index permits comparison of the directional radiation character of the different jet flows without regard to their relative levels. A completely non-directional source, regardless of the total acoustic power radiated, would have a zero directivity index at all azimuth angles.

1/3 Octave Band Power Spectra.- The directivity of the emitted sound of jets is dependent on frequency. Consequently the sound spectrum varies with azimuth angle. Experimentally, the spectrum variation with azimuth angle is the most convenient to measure, and by cross-plotting the data, the directivity dependence on frequency may be determined, which is the more meaningful form of the data. However, such a presentation as a large set of parametric curves (one for each frequency band), prevents making simple comparisons among the results of the various test conditions. To allow a simpler, systematic comparison of the spectrum characteristics at the various test conditions, 1/3 octave band power spectra were obtained.

The 1/3 octave band power spectra were computed from 1/3 octave band intensity spectra at each measuring station in the same manner as the wideband power level, but utilizing a separate computation for each spectrum band.

The results are plotted as power level versus frequency band, and each plotted point represents the integrated power emitted by the jet in all directions in a particular frequency band.

RESULTS

Main Jet Alone

To establish a basis for comparison of the experimental results for the interacting jets, the noise emission of the main jet alone* was investigated. A typical shadowgraph of the converging underexpanded main jet flow at a total pressure of 100 psig is reproduced as figure 15 where the characteristic shock structure, comprising intercepting shocks, a normal shock (Mach) disc and reflected oblique shocks is evident. The variations of the geometry of the shock structure with jet operating pressure ratios recorded during the present investigation were in good agreement with those reported by Love et al.[36]

The apparently spherical sound waves emanating from just downstream of the reflected shock cell end can be seen in all shadowgraphs of the underexpanded jet flows. This demonstrates, in part, the role of shock structure in inducing a noise source. This shock end emission has also been noted previously by others,[37] and will be considered later as a phenomenon of considerable interest to noise investigations from high speed jet flows. In the shadowgraph a directional acoustic emission originating at the nozzle exit edge is also evident.[18] For total acoustic power considerations, this source may not be significant as the acoustic emission is confined to a small angle representing a small portion of the integrated sound in all directions. The acoustic power radiated by the main jet alone as a function of jet total pressure is given in figure 16a, and is approximately linear over the greater portion

---

*Main jet with no impinging jet nozzle in place.

of the pressure range investigated. The nearly linear power level increase starts at approximately 60 psig which corresponds to the condition reported by Lassiter and Hubbard[38] where the screech attributable to the Powell mechanism described previously, ceases. The directivity index is given in figure 16b showing the maximum sound pressure level occurring at 30^{o}. The 1/3 octave band power spectrum for the main jet alone at 100 psig with the impinging jet nozzle removed is given in figure 16c. The spectrum displays no discrete components.

For the main jet alone, a typical computer printout of the 1/3 octave band sound pressure levels, re 2×10^{-4} μ bar, is reproduced in Figure 17 from which the directivity variation with frequency may be obtained. For each measuring station the wideband sound pressure level is computed from the 1/3 octave band data (see Appendix B) and appears below the spectrum analysis. From the computed wideband sound pressure levels, the total acoustic power radiated is computed (equation 20) and appears last, both in dB re 10^{-12} watt, and in watts. A tabulation of spectrum determinations obtained for each of the nozzle arrangements at various operating conditions is given in Appendix D.

Nozzle Arrangement I: 90^{o} Impingement

Acoustical Investigations.- For nozzle arrangment I, shown in figure 12, which has no provision for entrainment by the jet flows upstream of the impingement location, the wideband acoustic power variations with percent impingement for 90^{o} impinging flow are given in figure 18. For the x/D values shown, the power level value at zero percent impingement (with the impinging jet nozzle in place) agrees closely with that of the main jet alone operated at

the same total pressure. Locating the impinging jet nozzle more than 0.8D downstream caused the zero percent impingement power level to fall off sharply, indicating that under those conditions the impinging jet nozzle housing in some manner effected the results. For this reason, the data curves for $x/D > 0.8$ are not shown in figure 18. For $x/D = 0.2$, the dip in the power level curve was not as pronounced, although the zero percent value was in agreement, and this data curve also is not shown in figure 18. However, these data which are not plotted are tabulated in Appendix C.

The variation in power level with percent impingement for $0.4 \leq x/D \leq 0.8$ is well-defined and typical of the noise behavior for the interacting high speed jet flows. For discussion purposes, consider the power level variation at $x/D = 0.6$. From 0 to 8% impingement, the power level increases. At 8% it peaks 5 dB ® above the starting level. Significantly then, the total power emitted DECREASES with INCREASING percent impingement. It subsequently drops to a relative minimum value, at 18% impingement, approximately 1 1/2 dB above the starting level. (A 1 1/2 dB increase in power level represents an acoustic power (watts) increase of 41%. This may be compared with the mass flow increase of 18% to obtain an idea of the magnitudes involved.) At higher values of percent impingement, the power level increases once again.

The decrease in power level with increasing percent impingement, and the relative minimum power level achieved is of considerable interest. In each case shown in figure 18, the relative minimum power level is greater than the one at zero percent impingement. The value of percent impingement at which the relative minimum power level occurs increases with decreasing x/D. The relative minimum power level value is the lowest at $x/D = 0.6$ and increases

with higher or lower x/D values. There is no obvious way to ascertain the significance of the relative minimum power level value in terms of the amount of impinging flow. That is, the power radiated by the interacting jet flows at 18% impingement, for example, cannot be compared with the sum of the power radiated by the main jet flow alone at 100 psig and the annular flow alone at 18 psig. This follows since the power emission of the annular flow cannot be determined as it will impinge upon itself making the results questionable. However, one can be certain that if the relative minimum power level at any non-zero value of percent impingement can be brought as low as the level at zero percent impingement, a noise reduction for the main jet alone will have occurred. As will be shown, such a result does occur with the other nozzle arrangements used.

Plots of directivity index for nozzle arrangement I at zero percent impingement and at percent impingement values corresponding to the conditions of relative maximum and minimum power levels respectively are given in figure 19. These demonstrate a peak emission at 30^{o} which is characteristic of the bulk of the data for all the nozzles investigated. Also typifying the data for nozzle arrangement I for all x/D is a lesser peak at 90^{o} at conditions of maximum power level. A complete tabulation of the directivity index for all conditions is given in Appendix C.

Spectrum analysis of the sound radiated by the interacting jet flows was carried out at $x/D = 0.6$ from which the 1/3 octave band power spectra were computed. Four such typical spectra are presented in figure 20. With the exception of the spectrum at minimum power emission, the spectra display a relatively sharp jump in the 6300 or 8000 Hz center frequency

band indicating the presence of a discrete signal. Such a peak did not appear in the data for the main jet alone with the impinging jet nozzle removed, although it did appear for conditions of no impinging flow but with the impinging jet nozzle in place. Consequently, the peak in the spectrum is attributed to the geometry of the nozzle arrangement and not to the flow interaction. Carefully sealing the impinging jet nozzle exit with lead, but otherwise not altering the exit cavity formed by the annular and the main jet nozzles diminished the peak in the spectrum but did not eliminate it. Thus the discrete signal appears not to be due solely to the cavity formed by the exterior surfaces of the impinging jet nozzle but is probably also due to a Helmholtz-type resonance in the cavity upstream in the impinging jet nozzle. Tabulations of the 1/3 octave band spectrum data may be found in Appendix D.

To establish the influence of the geometry-attributable discrete signal on the previously discussed power level variation with percent impingement, total power levels were computed from 1/3 octave band spectra data in the manner discussed in Appendix B, and discounting the power contribution made by the peak wherever it occurred. The results are presented in figure 21. The upper curve is the power level computed from 1/3 octave band spectrum data without modification and reproduces reasonably the results presented in figure 18 for $x/D = 0.6$. The lower curve was computed from the same data from which the peak was discounted; that is, a smooth spectrum spanning the frequency where the peak occurred was assumed. Though slightly attenuated, the lower curve still demonstrates the previously described power level variation with percent impingement, and therefore the characteristic power level variation is

attributed primarily to changes in the flow and associated acoustic sources of the combined interacted jet flows.

Shadowgraphic Investigations.- Using nozzle arrangement I with 90° impingement, shadowgraphs of the main jet flow alone and also its interaction with the impinging jet flow were recorded at operating conditions identical to those at which the acoustical data were gathered. A sequence of typical shadowgraphs is reproduced in figure 22 showing the development of the flow and shock structure with percent impingement at $x/D = 0.6$.

At zero percent impingement and with the impinging jet nozzles in place, the distance from the main jet nozzle exit to the normal shock disc and the normal shock diameter are identical with those of a free convergent axisymmetric jet operating at 100 psig. Compare figure 22 at zero percent impingement with figure 15. Therefore the effect of the impinging jet nozzle housing on the stand-off distance and size of the Mach disc is not discernible.

With the addition and increase of impinging flow, the intercepting shocks move inward, the diameter of the normal shock decreases, and the reflected shocks grow in length. As this development of shock structure progresses with percent impingement, the total acoustic power radiated increases markedly (figure 18). The normal shock disc does not disappear completely but reaches a minimum diameter of approximately 0.12D. At this point in the sequence as percent impingement is increased, new oblique shock structure becomes visible. This new shock structure is tangent to and downstream of the original reflected shocks. This new shock structure has its own intercepting shocks which are faintly visible in the shadowgraphs (figure 22 at 8 percent impingement). The remnant of the original normal shock disc begins to recede

towards the nozzle exit. The emergence of the new shock structure coincides closely with the peak acoustic radiation from the interacting jet flow.* The emerged shock structure moves downstream with increasing percent impingement and a regular repetitive pattern of oblique shock waves is eventually established (figure 22 at 18 percent impingement). The establishment of this regular shock pattern spans the percent impingement range in which the total acoustic power radiated achieves the relative minimum discussed earlier. The occurrence of the relative minimum power level for annular jet impingement at $x/D = 0.4$ and 0.8 takes place at significantly different values of percent impingement, but for all x/D values the relative minimum power radiation occurs at percent impingement conditions where the shock structure is qualitatively similar and exhibits the repetitive pattern indicated above. At the high percent impingement conditions, annular eddies are evident near the nozzle exit, and with further increase in percent impingement, these eddies grow in prominence and are the source of an optically observed discrete sound signal. These eddies are clearly evident in figure 22 at 35 percent impingement and characterize the flow up to 50 percent impingement, the highest value investigated for nozzle arrangement I.

The acoustic field generated by the interacting jet flows was also examined from the shadowgraphs. The main characteristics of the optically visible acoustic field will be reported under Discussion, p. 59.

---

*For impingement of the annular jet at $x/D = 0.4$ and 0.8 at which the values of percent impingement corresponding to the peak power radiation are slightly different, the shock structure is qualitatively similar. That is, the peak power radiation is closely associated with the emergence of the new oblique shock structure regardless of the value of percent impingement at which the peak power radiation occurs.

Nozzle Arrangement I: 45° Impingement

The total power level variations obtained with similar experiments as described above, but with the impinging jet flow inclined downstream at 45° are presented in figure 23. These results are qualitatively similar to those reported above, but span a greater percent impingement range. Shadowgraphs also indicated qualitatively similar flow and shock structure changes. Therefore it was concluded that the mechanisms in each case were intrinsically similar. In as much as it is desired to achieve a useful noise abatement effect with as little impinging flow as possible, and since in the arrangement of nozzles the phenomena of interest appeared at relatively higher values of percent impingement, further investigations with this arrangement were not pursued. However, for reference, the complete acoustical data obtained with this arrangement are included in Appendix C.

Nozzle Arrangement II

Basis of Design.- In nozzle arrangement I, no provision was made for entrainment by the interacting jets upstream of the impingement location. It is well established the the high shear flow region near the jet exit is an effective source of noise emission. If entrainment flow is enhanced into this region of a jet flow, the high shear may be reduced which may result in reduced noise emission. For this reason, nozzle arrangement II was fabricated to allow a relatively free entrainment by the interacting jets where previously in arrangement I it was obstructed. Nozzle arrangement II is shown in figure 13. The exit geometry of the nozzles is identical with that of nozzle arrangement I but the main nozzle block is modified to allow free passage of entrainment centrally through the annular buffer reservoir housing. The

acoustical investigations with nozzle arrangement I revealed the occurrence of a discrete tone at certain operating conditions. This was partly attributed to the truncated conical cavity formed by the impinging jet nozzle, and partly due to a resonant driving of the interior impinging jet cavity. It was also hoped that the geometric modifications incorporated into nozzle arrangement II for admitting entrainment would also serve to eliminate the discrete tone.

Acoustical Investigations.- The acoustic power level variations with percent impingement at various x/D values for nozzle arrangement II are presented in figure 24. Significantly, for all x/D values, the power levels at zero percent impingement are precisely the same and in fact agree with the power level of the main jet alone with the impinging jet nozzle removed. This rules out the existence of any obvious effect on the noise emission by the impinging jet nozzle assembly for these x/D conditions. Also, the effect of entrainment in nozzle arrangement II is to permit the use of x/D values as high as 1.3 without any nozzle housing effects, compared with $x/D = 0.8$ for nozzle arrangement I.

For x/D values between 0.6 and 1.0 the total power radiated exhibited qualitatively similar characteristics as were observed for the interacting jets with no entrainment provision. That is, with increasing percent impingement, the total acoustic power increased to a relative maximum, decreased to a relative minimum value close to the zero percent value, and then increased again. The values of percent impingement at which the relative maxima and minima occurred decreased with increasing values x/D.

Significantly, at $x/D = 1.2$ the power level at 18% impingement dropped well below the zero percent level. At $x/D = 1.3$ an immediate decrease

in power level with the addition of the impinging flow occurred and reached an absolute minimum value 2 1/2 dB below the zero percent value at 16% impingement.

Thus, the noise emission from the interacting and mixing jet flows was caused to decrease continuously below the level of the emission of the main jet flow alone with the increasing addition and mixing of the impinging flow. A 2 1/2 dB decrease represents an acoustic power reduction* of about 44% in spite of an 18% increase in mass flow.

At $x/D = 1.4$ (not shown in figure 24), the power level variation is qualitatively similar to that at $x/D = 1.3$, but the minimum power level occurs at 14% impingement and the acoustic power reduction is not as great as for $x/D = 1.3$. The power level data for $x/D = 1.4$ are tabulated in Appendix C.

The directivity index of the interacting jet noise emission for the case of zero percent impingement and for conditions of maximum and minimum power level for various x/d values are given in figure 25. Since nozzle arrangement II yielded a desirable noise reduction, these directivity data were obtained with a 5^{o} increment angle. For all x/D values at zero percent impingement the directivity index variations with azimuth angle are in close agreement. The only difference is in a slight gradual increase (indicating a greater acoustic emission) with x/D for azimuth angles greater than 60 of 70 degrees. At zero percent impingement, the maximum difference between

---

* For an abatement technique to be truly successful, the noise must be reduced by about 90% or 10 dB. This is what makes engine jet noise suppression so difficult as a noise reduction of 90% must be achieved while affecting thrust by not more than a fraction of a percent or so.

directivity index at $x/D = 0.6$ and $x/D = 1.3$ is about 1 1/2 dB at $\theta = 120^{o}$. The directivity index curves for all conditions of x/D and percent impingement, with minor variation, characteristically demonstrate a peak at 30^{o} and a lesser peak near 90^{o}. At conditions of maximum power level for all x/D, a third minor peak is indicated near 60^{o}.

Comparing the directivity index curves for the zero percent, peak power level, and minimum power level conditions at fixed x/D, it is seen that at $x/D = 0.6$ and 0.8 the effect of impinging flow is to make the acoustic emission less directional since the directivity index curves for peak and minimum power level conditions are flatter than for the zero percent condition. Comparatively the directivity index is most attenuated at the condition of peak power level particularly at the higher azimuth angles.

At the higher x/D values (1.0 - 1.3) corresponding to conditions of improved power level reduction with the addition of impinging flow, the sound emission becomes progressively less directional with increasing percent impingement. At the conditions corresponding to minimum power level the emission is less directional than at the other conditions at the same x/D. This is desirable, since in addition to having an overall power level decrease, there occurs also an attenuation of the directivity of the radiation which contributes to the noise emission attenuation in the direction of the peak. The actual sound level reduction achieved at $x/D = 1.3$ at $\theta = 30^{o}$ was 3 1/2 dB at 16% impingement indicating a better noise attenuation for practical purposes than a comparison of power levels would indicate, since the singularly important aspect to an observer of the emission of source is the intensity at the observer rather than the integrated power radiated in all directions.

The 1/3 octave band power spectra for x/D values of 1.0 and 1.3 are presented in figure 26. These are typical of the data at all x/D values. For the condition of zero percent impingement, the spectra are very nearly identical displaying a slightly triple peaked character with dips in the 20 and 50 kHz center frequency bands. For all other conditions, this character is more or less preserved. The effect of the impinging flow is primarily to alter the level of the spectra without radically affecting their basic form. However, comparing the frequency of the peak noise at the conditions of zero percent impingement with that at the condition of minimum power level, it is seen that whereas at zero percent the peak noise occurred in the 8 or 10 kHz center frequency band, at minimum power level, the peak occurred in the 25 or 31.5 kHz center frequency band effecting a slight emphasis on higher frequency emission at conditions of minimum power level. However, the spectra are still reasonably flat at these conditions so that the peak frequencies are not dominant, and the frequency shift would probably not contribute to effective noise abatement in the manner described earlier. The discrete tone in the 1/3 octave bands mentioned earlier in relation to nozzle arrangement I was largely absent except at maximum acoustic power conditions between x/D of 0.8 and 1.2. A tabulation of acoustic power dependence on frequency is included in Appendix D.

Shadowgraphic Investigations.- Shadowgraphs of the flows from nozzle arrangement II for x/D values of 0.6 and 0.8 indicated the same qualitative behavior of the shock structure as for the nozzle arrangement I. That is, with increasing percent impingement, the reflected shocks increased in length,

the intercepting shocks moved toward the jet axis diminishing the extent of the Mach disc, and a new oblique shock structure emerged coinciding approximately with the conditions of peak power level. A typical sequence of shadowgraphs for x/D = 0.8 is presented in figure 27.

For the higher x/D values, the impinging jet nozzle was located farther downstream and little of the first cell of the main jet flow at zero percent impingement was in view. The impinging flow, as usual, caused the Mach disc to recede towards the jet exit and at fairly low values of percent impingement all the shock structure was within the impinging jet nozzles with only shock-free turbulent flow visible in the shadowgraphs. At x/D of 1.0 and 1.2, where the shock structure was visible for the conditions of peak power radiation, it was observed that no new shock structure emerged at the maximum acoustic power condition and the normal shock disc diminished in size only slightly before receding into the nozzle shadow. This observation based on impingement at higher x/D values does not confirm the earlier conclusion deduced from data at lower x/D values that the peak power emission is attributable to flow properties characterized by the emergence of new oblique shock structure.

Nozzle Arrangement III

Basis of Design.- Since the enhancement of entrainment upstream of the impingement location improved the noise reduction achieved with the interacting jets, the attempt was made to optimize entrainment by the interacting jet flows by virtually eliminating all obstruction to it. To accomplish this, nozzle arrangement III, shown in figure 14, was fabricated in which the annular housing

is kept to a minimum physical size by elimination of the buffer reservoir. Wire screens were carefully installed to distribute tangentially the annular jet supply air, and the assembly was calibrated to ensure uniform axisymmetric annular impinging jet flow.

Acoustical Investigations.- The power level variations with percent impingement for nozzle arrangement III are given in figure 28. For $0.6 \leq x/D \leq 1.1$ the curves display the same qualitative character described for the previous two nozzle arrangements. That is, the power level undergoes an increase to a maximum, followed by a decrease to a minimum (or relative minimum), followed by still another increase. Also, the percent impingement value for minimum noise varies inversely with x/D, and there is a mid-range value of x/D at which the minimum power level is achieved. From $x/D = 1.1$ to $x/D = 1.2$, the character of the power level variation changed radically. This seemingly erratic power level curve will be discussed later. The best power level reduction for this nozzle arrangement occurred for $x/D = 1.0$ at 20% impingement, and amounted to a 1 1/2 dB reduction below the zero percent level. This is less of a reduction than that obtained with nozzle arrangement II.

Thus the effect of minimized obstruction to entrainment did not improve further the power level reduction as originally expected. If it is assumed that in fact the entrainment and not some other factor is responsible for this result, it may be explained, reasonably with the following argument. Returning again to the engine suppressor as an example, reduced noise is brought about by accelerating the surrounding air to form essentially a surrounding coaxial flow of intermediate velocity. This reduces the high shear otherwise present in the mixing region, and consequently may reduce the turbulence levels. In the

present investigations, for very low percent impingement values the power level is observed to increase, and this is tentatively attributed to increased turbulence levels induced by the shear created in the momentum exchange between the radial impinging flow and the axial main jet flow. Radially induced entrainment flow would be expected to have a similar but lesser effect. In nozzle arrangement II, the entrainment flow is constrained to accelerate into the main jet flow in an essentially axial direction, and this is known to reduce shear. However, nozzle arrangement III offers no such axial alignment of the entrainment air and the induced flow will have a significant radial velocity component. This radial component may possibly be responsible for some increase in turbulence level of the main jet and thus the noise reduction is not that pronounced as in arrangement II. Therefore it is theorized that a nozzle arrangement for interacting jet flows similar to that of nozzle arrangement II but with enhanced axial flow entrainment may very well offer the best possibilities for noise reduction.

Tabulations of the complete acoustical data for nozzle arrangement III may be found in Appendices C and D.

Shadowgraphic Investigations.- The shock structure development with percent impingement for nozzle arrangement III is shown in figure 29. The similarity with the results for the other nozzle arrangement is clearly apparant and therefore discussion of these shadowgraphs is omitted.

Effect of Main Jet Pressure

From all the preceding results, it is observed that nozzle arrangement II possesses somewhat optimum qualities, and this arrangement is examined further. Using this arrangement, power level data were obtained as functions of percent impingement for main jet total pressures of 75, 150, and 200 psig for various values of x/D. These data are presented in figure 30.

The resulting power level variations with percent impingement all demonstrated the same qualitative behavior discussed previously. However, for different main jet pressures at the same x/D value, the power level variations were dissimilar. This was expected since as the main jet pressure increases, the cell length increases and the jet expansion angle is greater so that the same x/D value in two different cases does not represent a geometrically similar impingement location. If however, comparison is made of tests for which the ratio of main jet pressure to x/D is a fixed value (i.e., geometric similarity is preserved approximately), the maximum and minimum power levels of each curve occur at approximately the same values of percent impingement.

DISCUSSION

The acoustic power level variations and reductions with percent impingement observed under many operating conditions of interacting jet flow are the most interesting results of these investigations (see figs. 18, 24 and 28). The noise generating mechanisms which may be acting in the interacting jet flows are

a) convected turbulence, including the associated Mach wave radiation

b) shock-turbulence interaction

c) flow induced oscillations of shocks

d) resonance phenomena

e) contributions from the impinging jet flow to the total acoustic power radiated from the interacting jet flows.

The observed total power level variations conceivably could be the result of modification in the strength of some or all of these sources. However the contributions by some of these sources to the total acoustic power level may be so minor that the effectiveness of these sources can be discounted. For example, for the impinging jet flow to add say 1 dB to the total acoustic power radiated by the two interacting jets, the noise level of the impinging jet must be within 6 dB of the level from the main jet.* This is highly unlikely at the low values of percent impingement (i.e., at low operating total pressures of the impinging jet).** Therefore noise contributions from impinging jet flow to the total acoustic power radiated may be neglected.

---

*See Appendix B.

**See figure 16 showing the variation of total acoustic power from the main jet alone with main jet total pressure. Since the main jet and the annular impinging jet have equal exit areas, at low operating total pressures of the impingement jet the total acoustic power radiated by the impinging jet is considerably less than that from the main jet alone. This was experimentally verified.

Some di crete acoustic radiation has been observed in the power spectra (figure 26) and in the shadowgraphs. This has been tentatively attributed to an acoustic driving of a cavity formed by the interacting jets. It is possible that such discrete acoustic radiation could be sustained by the resonance phenomena. However, it was demonstrated that the discrete radiation occurred only for selected nozzle arrangements and a limited range of operating conditions of the interacting jets. Furthermore it was not a dominant effect and it did not account for the observed wideband acoustic power level variations. Therefore resonance phenomena are not examined here in any detail. Flow fluctuations may induce shock oscillations. However no time-sequence of shadowgraphs was recorded and therefore the oscillations of the shocks and the possible noise contribution from source (c) could not be ascertained. The nature and the apparent strength of the acoustic emission evident in the shadowgraphs underline the importance of sources (a) and (b).

A careful examination of the shadowgraphs for emitted acoustic wave fronts is helpful in fixing some of the dominant sources of the observed noise field. For example in the shadowgraph of the main jet alone (figure 15) it is evident that spherical acoustic wave fronts emanate from an apparent source just downstream of the oblique shock tip or end. Using the shadowgraph and a transparent overlay with finely ruled concentric circles, the positions of the apparent center of the acoustic source in the main jet flow alone (figure 15) is determined to be situated at 2.4D downstream and 0.6D off the jet axis. This locates the source, 0.25D directly downstream of the oblique shock end. A similar acoustic source is located further downstream at 4.4D and 0.7D off axis. From original glossy enlargements of various shadowgraphs of interest,

additional downstream sources have also been located. In addition to the shock-tip flow region as the source of spherical acoustic emission, a directional emission is also observed to originate from near the nozzle exit. For a sketch illustrating these sources and their emissions see figure 31. Both of these acoustic sources have been recently examined by Ollerhead[37] in a shadowgraphic investigation of high speed jet flows issuing from converging-diverging nozzles. They tentatively identified the directional emission with Mach waves although their direction of propagation implied a greater eddy convection velocity than might be expected. However the nature of actual acoustic sources responsible for these emissions is still an unresolved problem. The apparent shock-tip sources of spherical acoustic emissions are tentatively attributed to the portions of the flow where the shock waves penetrate supersonic turbulence shear regions. It is not the intent here to examine in depth the fundamental nature of these sources and their emissions as these investigations were not planned to consider this phenomenon. However, some of the observations made in the course of the interacting jet noise investigations suggest an alternate (or perhaps supplementary) tentative explanation for the source of the shock-end emission.

The apparently spherical emission suggests a monopole source. Such a source near an oblique shock-end is physically plausible. In an interferometric investigation by Ladenburg et al[39] of converging underexpanded air jets operated at moderately high pressure ratios corresponding approximately to those used in this investigation, a localized small circular "island" of maximum density (compression region) situated just downstream of the oblique shock end is present. It is suggested that this type of localized high density region may

act as a monopole source if the flow region is driven by the turbulent eddies convected through it and if its physical dimensions are small compared to the average eddy size. Moreover the shock front may be disturbed due to the passage of eddies through it. This in turn may also disturb the localized high density region.

Regardless of the basic cause and the nature of the shock-end emission, it appears that the emission itself is spherical in nature. From the experimental evidence, a source of such emission is identified with each oblique-shock end. The typical progression of the shock structure with percent impingement is illustrated in the following sketch.

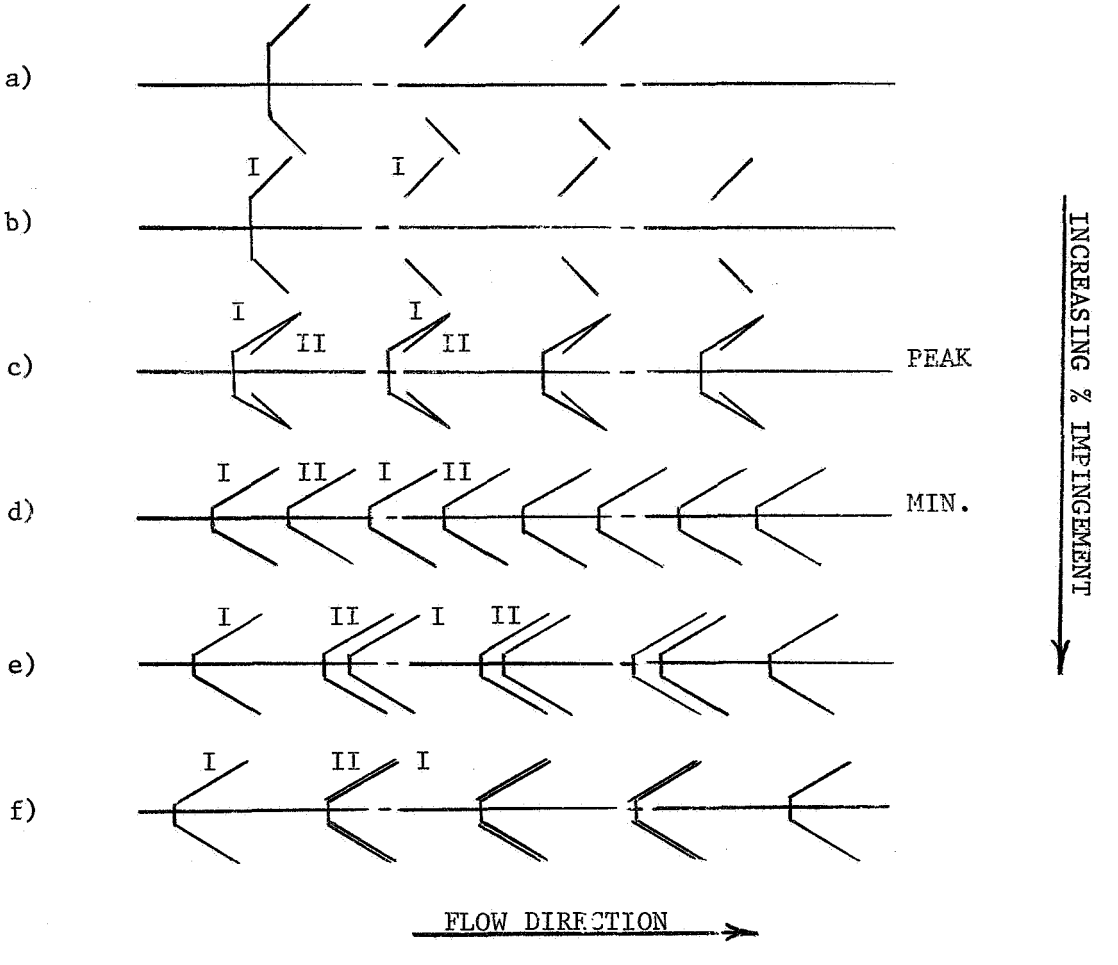

(a) At zero percent impingement there exists only the typical shock structure of the underexpanded axisymmetric converging main jet flow. (b) With increasing percent impingement, the length of the intercepting and reflected shocks and the diameter of the Mach disc but the geometric form of the shock structure essentially remains the same. Simultaneously, downstream shock structure (labelled I in the sketch) begins to consolidate and fairly regular shock pattern of approximate equal spacing is established. (c) At somewhat higher percent impingement, new oblique shock structure (labelled II in the sketch) emerges. In almost every case the emergence of this structure coincides with the peak acoustic power emission. Typical shadowgraphs recorded at his operating condition for the nozzle arrangements I, II and III are reproduced in figures 32a, b, and c. (d) Further increase in percent impingement causes the new shock structure to migrate downstream relative to the original shock structure in the main jet flow, which recedes upstream. Eventually, the newly emerged shocks become equally spaced between the original shocks and a regular shock pattern with approximately equal spacing is established. This condition generally corresponds to minimum acoustic power emission. Typical shadowgraphs recorded at this operating condition for the respective nozzle arrangements I, II and III and showing the acoustic emission are reproduced as figures 33a, b and c. (e) Still further increase in percent impingement causes the continued downstream migration of the emerged shocks, until once again a regular shock spacing is achieved.

The new shock structure comprises the intercepting shocks, the Mach disc and the reflected shock. A careful examination of the shadowgraphic data reveals that the new intercepting shock structure originates somewhat

downstream of the impingement location of the interacting jet flows. It is surmised that its origin is dependent upon the expansion of the interacted jet flows and the reflection of the associated expansion waves from the free boundary of the interacted flows as compression waves and their coalescence. The emergence of similar secondary shock structure has been observed earlier by Sheeran and Dosanjh in an investigation of transversely impinging two-dimensional jet flows.[40]

As the impingement ratio is increased the stand-off distance of the Mach disc associated with the new shock structure increases. The pressure changes in the subsonic flow region downstream of the Mach disc of the main jet flow as well as the pressure adjustments in the interaction region cause the Mach disc in the main jet to recede towards the jet exit. Thus the spacing between the original and the new shock cells changes with percent impingement.

It is noted that the acoustic emission from a stationary multipole source is always less than that of a single monopole source of the same strength because of cancellation effects. In the present investigations, the total noise generated varies with percent impingement. The same is true of the shock spacings. The small flow regions localized near shock-ends were identified as the apparent sources of spherical acoustic emission, and the spacing between the apparent sources also changes with percent impingement. Knowing that a dipole, for example, is constructed from two out-of-phase monopoles which are closely spaced compared to the emitted wavelength, and noting that, in the jet flow, convected turbulence might generate phase related sound from successive local noise generating flow regions, a cancellation mechanism acting in the interacting jet flows is plausible. On the basis of these

observations a simple acoustical model of the flow is proposed as a line distribution of phase related acoustic sources among which the spacing changes.

In reality, the shock-end source is in the shape of a torus, but because of the random nature of turbulence there is no correlation between the acoustic emission from different portions of the torus. Since for uncorrelated acoustic sources intensities add, cancellation effects among the random signals from the various portions of the toroidal source do not come into play. Therefore, for far field acoustic radiation, the toroidal source may be represented by a single monopole source of appropriate strength.

Essentially, the noise generating flow regions located just downstream of the shock-ends will be treated as acoustic sources driven in some manner by the turbulent eddies convected through them. Turbulent eddies decay as they are convected downstream. However, in their interaction with shock waves or high density flow regions, they may be amplified. It will be assumed in this case that the amplification gained in the interaction process is sufficient to preserve the character of the eddy until it reaches the next shock and acoustic source region, and so on. In this way a certain coherence of the eddy is assumed as it is convected downstream through various shock-end flow regions, and consequently the emission from each of these sources may be assumed to be phase-related.

Analysis

The sound generation by a distribution of arbitrarily spaced phase related acoustic monopole sources on a line will be derived from acoustical theory. The geometry of the problem is chosen as illustrated in figure 34.

The complex acoustic pressure from a simple monopole (spherical) source is

$$\underline{p} = \underline{j} \frac{\rho_o a_o \nu Q}{4\pi r} e^{\underline{j}(\omega t - \nu r)} \tag{23}$$

where an underbar denotes a complex quality; $\underline{j} = \sqrt{-1}$, the wave number ν is defined by

$$\nu = \frac{\omega}{a_o} ,$$

and ω is the radian frequency. The source strength is denoted by Q and represents the product of the velocity amplitude and the area of the source surface. This relation for acoustic pressure is valid for sources of arbitrary shape as long as the emitted wavelength is greater than the typical source dimension. In the present case, the emitting sources i.e., localized flow regions at shock-ends are assumed to be sufficiently small for the shortest emitted wavelength.

Let Q_i be the strength of the i^{th} source, and let s_i be the distance from the first to the i^{th} source. Also let r_i denote the distance from the i^{th} source to a point in the acoustic field. Referring to figure 34, the combined acoustic pressure $\underline{p_\Sigma}$ at a point from all the sources becomes

$$\underline{p_\Sigma} = \underline{j} \frac{\rho_o a_o \nu}{4\pi} \sum_{i=1}^{n} \frac{Q_i}{r_i} e^{\underline{j}(\omega[t-\Delta_i t]-\nu r_i)} \tag{24}$$

where $\Delta_i t$ is the time delay of the acoustic emission of the i^{th} source

from that of the first source, such that $\Delta_1 t \equiv 0$. If $r_1 >> s_i$ for all i's r_i may be approximated as

$$r_i = r_1 [1 - (s_i/r_1) \cos \theta] \quad i = 1,2,\ldots, n. \tag{25}$$

Substituting equation 25 into equation 24, and factoring out the constant terms it yields

$$\underline{p}_\Sigma = \underline{j} \frac{\rho_o a_o \nu}{4\pi r_1} e^{\underline{j}[\omega t - \nu r_1]} \sum_{i=1}^{n} \frac{Q_i}{1-(s_i/r_1)\cos\theta} e^{\underline{j}(\nu s_i \cos\theta - \omega\Delta_i t)}. \tag{26}$$

or,

$$\underline{p}_\Sigma = \underline{j} \frac{\rho_o a_o \nu}{4\pi r_1} e^{\underline{j}[\omega t - \nu r_1]} \sum_{i=1}^{n} Q_i \frac{\cos(\nu s_i \cos\theta - \omega\Delta_i t) + \underline{j} \sin(\nu s_i \cos\theta - \omega\Delta_i t)}{1 - (s_i/r_1) \cos\theta} \tag{27}$$

From equation 27 the magnitude of the acoustic pressure from the line multipole is obtained as

$$p_\Sigma = \frac{\rho_o a_o \nu}{4\pi r_1} \left[\left\{ \sum_{i=1}^{n} \frac{Q_i}{1-(s_i/r_1)\cos\theta} \cdot \cos(\nu s_i \cos\theta - \omega\Delta_i t) \right\}^2 + \left\{ \sum_{i=1}^{n} \frac{Q_i}{1-(s_i/r_1)\cos\theta} \cdot \sin(\nu s_i \cos\theta - \omega\Delta_i t) \right\}^2 \right]^{1/2}. \tag{28}$$

As a simple first approximation, it is assumed that the emission delay from the i^{th} source is proportional to its distance s_i from the first source.

We may write then

$$\Delta_i t \propto s_i \tag{29}$$

or

$$\Delta_i t = \frac{s_i}{a_o M_c}$$

Where M_c is an eddy mean convection Mach number. Therefore

$$\omega \Delta_i t = \frac{\nu s_i}{M_c} \quad . \tag{30}$$

Substituting this into equation 28, yields

$$p_\Sigma = \frac{\rho_o a_o \nu}{4\, r_1} \left[\left\{ \sum_{i=1}^{n} \frac{Q_i \cos[\nu s_i(\cos\theta - 1/M_c)]}{1-(s_i/r_1)\cos\theta} \right\}^2 + \left\{ \sum_{i=1}^{n} \frac{Q_i \sin[\nu s_i(\cos\theta - 1/M_c)]}{1-(s_i/r_1)\cos\theta} \right\}^2 \right]^{1/2} \tag{31}$$

Finally, choosing $r_1 = R$ sufficiently large compared to s_i so that the term containing s_i/r_1 may be neglected for all i, and noting that $s_1 \equiv 0$, we obtain from equation 31 the amplitude of the combined acoustic pressure from n phase-related monopole sources positioned on a line as a function of the azimuth angle θ as

$$p_\Sigma = \frac{\rho_o a_o \nu}{4\pi R} \left[\left(\sum_{i=1}^{n} Q_i \cos \Omega_i \right)^2 + \left(\sum_{i=1}^{n} Q_i \sin \Omega_i \right)^2 \right]^{1/2} \tag{32}$$

where

$$\Omega_i = \nu s_i(\cos\theta - 1/M_c) \quad .$$

Since the actual jet flow emits sound of continuous spectrum, the analytical model is extended to represent such a case. Each single source considered above is replaced with a superposition of independent sources at the same point, all emitting at a different individual frequency and strength necessary to establish a prescribed far field spectrum. Such a superposition is termed here as a "wideband monopole." For far field acoustic radiation, the intensity is given by

$$I_j = \frac{P_j^2}{2\rho_o a_o} \tag{33}$$

where j denotes the property of the sources of a particular frequency at a point.

The source strength and pressure amplitude from equation 1 is related as

$$P_{ij} = \frac{\rho_o a_o \nu_j (Q_i)_j}{4\pi R} \tag{34}$$

From equations 33 and 34

$$(Q_i)_j = \frac{4\pi R}{\nu_j} \sqrt{\frac{2I_{ij}}{\rho_o a_o}} \tag{35}$$

combining equations 32 and 35 we get

$$P_\Sigma^2 = 2\rho_o a_o \sum_j \left[\left\{ \sum_{i=1}^{n} I_{ij} \cos \Omega_{ij} \right\}^2 + \left\{ \sum_{i=1}^{n} I_{ij} \sin \Omega_{ij} \right\}^2 \right] \tag{36}$$

where

$$\Omega_{ij} = \nu_j s_i \ (\cos\theta - 1/M_c)$$

Let W_Σ denote the total acoustic power radiated, where

$$W_\Sigma = \int_A \frac{P_\Sigma^2}{2\rho_o a_o} \ dA \tag{37}$$

The surface integral is carried over the entire surface of an enclosing sphere with radius R.

Recalling that we are modeling the interacting jet flows, W_Σ is thus also a function of percent impingement. At 0% impingement, only a single well-defined shock cell is present. This is now to be considered as a reference condition and interpreted as a single wideband monopole source. Denoting the acoustic power from the first source alone at 0% impingement as W_{1o} where

$$W_{1o} = \int_A \sum_j I_{1j}(0) \ dA \tag{38}$$

Let $\overline{R}$ be the ratio of the total acoustic power emitted by all the monopole sources distributed along a line at a certain percent impingement to W_{1o}, then

$$\overline{R} = \frac{\int_A \frac{P_\Sigma^2}{2\rho_o a_o} \ dA}{\int_A \sum_j I_{1j}(0) \ dA}$$

or

$$\overline{R} = \frac{1}{\sum_j I_{1j(0)} \int_A dA} \int_A \sum_j \left[\left\{ \sum_{i=1}^{n} \sqrt{I_{ij}} \cos \Omega_{ij} \right\}^2 + \left\{ \sum_{i=1}^{n} \sqrt{I_{ij}} \sin \Omega_{ij} \right\}^2 \right] \tag{39}$$

To determine I_{ij} from the experimental data, the following assumptions were made. (1) The intensity of the radiation from a shock-end region is proportional to the surface area of the reflected oblique shock. (2) Each shock-end source emits sound of an identical spectrum so that the set of I_j for each source are identical.

Thus

$$I_{ij} = KG_i F_j \tag{40}$$

where

$$G_i = \frac{A_i}{A_{1(0)}}$$
$$F_j = \frac{I_j}{(I_j)_{max.}} \tag{41}$$

K is a proportionality constant, $A_1(0)$ is the surface area of the first reflected oblique shock at 0% impingement and $(I_j)_{max.}$ is the peak value of I_j obtained from spectrum.

Substituting equation 40 into equation 39, obtain

$$\overline{R} = \frac{1}{\Sigma_j F_j \int_A dA} \int_A \left[\sum_j F_j \sum_{i=1}^{n} \left\{ \sqrt{G_i} \cos \Omega_{ij} \right\}^2 + \left\{ \sum_{i=1}^{n} \sqrt{G_i} \sin \Omega_{ij} \right\}^2 \right] dA \ . \tag{42}$$

Since actual measurements were taken only at discrete number of stations, the surface integral was approximated by a finite sum. A typical elementary area is given by

$$\Delta A_k = 4\pi R^2 \sin k\Delta\theta \sin \Delta\theta/2 \tag{43}$$

where k denotes the k^{th} measuring station and $\Delta\theta$ is the incremental azimuth angle between two successive measuring stations.

Therefore finally the expression for $\overline{R}$ takes the form

$$\overline{R} = \frac{1}{\Sigma F_j \; \Sigma \sin k\Delta\theta \sin \Delta\theta/2} \cdot \sum_k \left\{ \sum_j F_j \right.$$

$$\times \left[\left\{ \sum_{i=1}^{n} \sqrt{G_i} \cos \Omega_{ij} \right\}^2 \right.$$

$$\left. \left. + \left\{ \sum_{i=1}^{n} \sqrt{G_i} \sin \Omega_{ij} \right\}^2 \right] \sin k\Delta\theta \sin \Delta\theta/2 \right\} \tag{44}$$

This equation yields the ratio of the acoustic power generated by n phase related wideband acoustic monopole sources to the wideband acoustic power emitted by a single such monopole source.

Let ΔPWL be the power level difference from the reference value

$$\Delta PWL = 10 \log_{10} \overline{R} \quad . \tag{45}$$

The variation of ΔPWL may then be readily compared on a relative basis with the experimental power level variation previously described.

ANALYTICAL RESULTS

Before passing on to a discussion of the fruitful application of the analytical result, equation 45, to the interacting jet noise investigations, it is informative to review a principal attempt which failed, and which led to the re-examination of the idea of direct shock-turbulence interaction as the likely source of the observed spherical acoustic emission.

The analysis was attempted originally on the implicit assumption that shock-turbulence interaction was the fundamental sound source. The measurable quantities A_i, equation 41, were initially taken to be the areas of the oblique shock waves which were in the form of truncated conical surfaces. From shadowgraphic evidence, these areas were computed for the visible shock waves, and the shock-wave spacings were measured for nozzle arrangement II at $x/D = 0.8$ from zero to 30 percent impingement. Since the actual eddy convection velocities were not known, various reasonable values of eddy convection Mach number were assumed. These data were substituted into equation 44 and the results compared with the measured power level variation from zero to 30 percent impingement. No strong correlation was observed between the computed and measured acoustical data.

Since the measurements and use of the actual geometry and spacing of the shock structure in equation 45 yielded inconclusive comparison with the experimental results, it was further assumed that (1) All the shock-end sources were of equal strength, i.e., $G_i = A_i/A_1(0) = 1$ for all i at each frequency. (2) Only the spacing variation among a set of established sources was considered. (3) At peak power conditions spacing between sources was 0.9", which was considered to be representative of all the data.

(4) There were eight sources which varied progressively in spacing according to the following sketch.

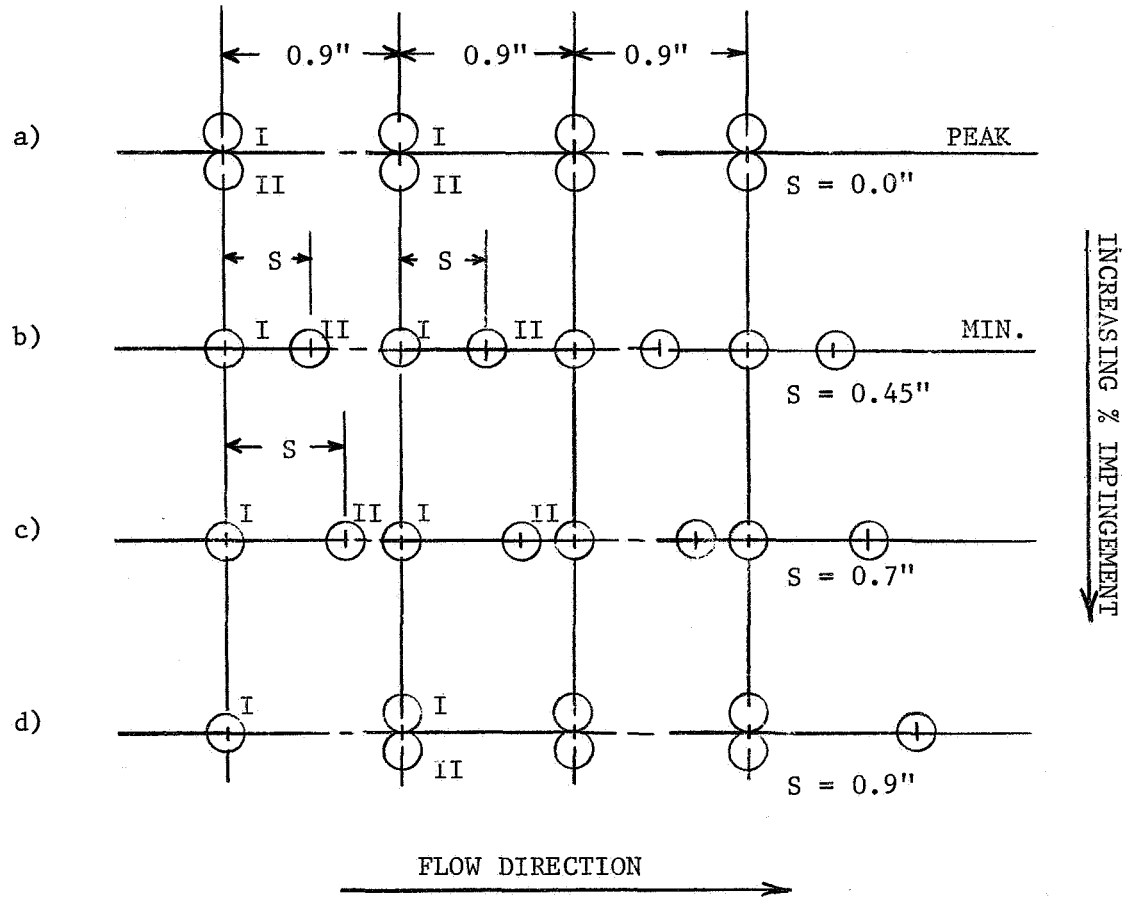

The premise is that the source distribution (a) corresponds with peak power emission. Further changes in spacing result in a minimum emission at source distribution (b). A range of eddy mean convection Mach number was assumed. The relative wideband power levels (ΔPWL) are calculated from equations 44 and 45 as functions of source spacing and the results are

presented in Figure 35 with the eddy convection Mach number as a parameter. The overall qualitative agreement of these analytical results with the experimentally observed decrease in the total acoustic power level with percent impingement is encouraging. For $M_c = 0.8$ and 0.6, which are reasonable values, the magnitude of the power level decrease, predicted analytically (Figure 35) is of the order of those observed experimentally (Figures 18, 24 and 28).

The analytical model takes no account of the observed directional emission originating at the nozzle exit (Figure 31) and the contribution of this emission to the observed acoustic power variations from interacting jet flows is yet unresolved. However it was noted previously that the nozzle edge emission, in spite of its apparent strength, does not necessarily contribute significantly to the total power because of its confinement to a small solid angle. Moreover, the radially impinging flow may act to reflect or refract the nozzle edge emission.

The observed acoustic power variations and reduction is most likely a complex combination of all the possible acoustic sources such as turbulence, Mach wave radiation, shock-turbulence interaction, shock oscillations, and emergence of the new shock structure leading to possible cancellation effects on which the acoustic model analyzed above was based. The preceding analysis is admittedly based on rather crude assumptions. A more refined model should take into account:

a) variations of eddy convection velocity with downstream distance;

b) the relative strength of the shock-end acoustic sources;

c) variations of emitted noise spectra with downstream distance.

A yet unresolved question is the nature of the initial increase in power level with percent impingement. Tentatively it may be attributed to increased turbulence levels created in the mixing process and its interaction with the shock structure.

As a final consideration, these results suggest a possible method of rocket noise reduction. The mixing of the impinging flow with the main jet flow probably resulted in an increase in turbulence level. It certainly caused the emergence of a new set of shock structure. However, when the new shock structure was disposed evenly between the original shock structure, the proposed cancellation effects were apparently sufficient to bring about an overall noise reduction. Therefore given a supersonic flow with a repetitive shock pattern, noise reduction may be effected by using auxiliary flows to contrive to interpose a shock pattern similar to and midway between the original shock pattern. Discarding the concept of radially impinging flow which carries with it the practical problem of weight and thrust penalty, it may be possible to accomplish a shock structure interposition using an annular axial flow which is fully thrust producing. That is, by replacing a single rocket nozzle with a double concentric nozzle, comprising a smaller central nozzle and a surrounding annular nozzle designed and operated such that the flows from each create mutually interposed shock patterns, a noise reduction may be effected. Certainly the feasibility of such a scheme is worth examining.

CONCLUSIONS

1. Under certain operating conditions the total acoustic power emitted by a high-speed converging axisymmetric main jet flow can be reduced using radially impinging annular jet flow.

2. One of the effects of the impinging flow is to cause radical alterations of the shock structure in the main jet flow. These are principally characterized by the emergence of new repetitive shock waves which, with increasing impingement, migrate downstream with respect to the original main jet flow shock waves.

3. Either directly or indirectly, the shock waves play an important role in the emission of the spherical acoustic waves originating from apparent monopole sources situated just downstream of each reflected oblique shock-end.

4. A simplified analytical model is developed which qualitatively explains the noise reduction in terms of the cancellation effects among the phase-related spherical acoustic emissions generated by monopole sources.

5. This cancellation mechanism, if valid, suggests a possible approach for accomplishing supersonic jet noise reduction. A single jet nozzle may be replaced by two coaxial thrust producing nozzles comprising a central nozzle and a surrounding annular nozzle. If the operating conditions were such that the flows from both nozzles create mutually interposed shock pattern, a noise reduction may be effected.

APPENDIX A

DESIGN DETAILS, MICROPHONE POSITIONING MECHANISM

In light of the excessive amount of experimental data that were to be obtained with the microphone, it was necessary that its mechanism could be positioned rapidly and precisely. Furthermore, the ability to select a small, variable increment angle $\Delta\theta$ was desirable. To meet these requirements, a basic positioning assembly was constructed as shown in Figure 36. The assembly comprises a vertical main shaft to which is fastened a support block for the microphone boom which is rotated in a horizontal plane. The main shaft is driven through 45^{o} bevel gears by a horizontal cross shaft which in turn is driven directly by a small reversible gearmotor with a rated output torque of 120 in-oz at 1.0 rpm. A 2:1 gear ratio results in a 1/2 rpm horizontal rotation rate of the microphone boom. Supported in an added-on bearing block is a second vertical shaft driven by the main shaft through a 3:1 ratio. This shaft makes three revolutions for every one of the microphone boom and supports a 120 tooth 24 pitch gear so that for each revolution of the microphone boom, 360 gear teeth pass a given point. The bearing block allows slight lateral positioning adjustment enabling the center spacing of the gearset to be held to a minimum, effectively eliminating backlash. Thus a count of the number of 24 pitch gear teeth passing a given point is an accurate indicator, with a precision on the order of the backlash, of the microphone boom position. Backlash in the gearmotor and cross-shaft drive has no effect on accurate position indication, and all shafts rotate on ball bearings for friction free motion.

The obvious simple approach to make a gear tooth count is to use a make-break electrical contact set cycled by the passage of a single gear tooth, and to electrically add or subtract these cycles depending on direction of gear motion. Choice of addition or subtraction can be simply accomplished by selecting the route of the count pulse using the forward/reverse switch of the gearmotor. However, critical evaluation reveals this approach has two inherent difficulties: a) if the count contacts complete a make-break cycle completing a positive count after which the gear tooth immediately comes to rest, a subsequent elemental reversal of gear motion will immediately remake the contact, instituting a negative count without detectable reverse motion, and a full degree readout error would result; b) a further count error could be introduced during reversal of the gearmotor through inertia of the system which would temporarily continue the boom in the original direction and cycle the contacts after switch reversal, resulting in the incorrect algebraic accumulation of one or more counts. Movement of the boom directly by hand, through the angle allowed by the backlash in the gearmotor drive, would also result in this type error. To forestall these difficulties, a counting system was devised incorporating an unusual make-break contact assembly in conjunction with a modified standard commercial electromagnetic counter.

The contact assembly is illustrated in Figure 37. In an ordinary manner, a set of counting contacts is utilized, actuated by the passage of the gear teeth through the detent motion of a spring loaded leflon actuator. However, the contact set and actuator as a unit are assembled on a slider block which may move slightly back and forth in the tangential direction of gear tooth motion. Assembled on each end of this block is another set of electrical

contacts comprising a single pole double throw switch. Extreme position of the slider block in either direction closes one side or the other of the switch. Uniquely, the sliding block is coupled by friction to the face of the 24 pitch gear so that motion of the gear in either direction will move the sliding block tangentially a fraction of an inch in that direction, alternating the throw of the switch prior to instituting detent action. Friction of the gear holds the contacts so disposed, without impeding gear motion, until the motion is reversed. Now, importantly, the double throw switch determines the route of the count pulse rather than the motor control switch which was suggested earlier. Thus, the actual motion of the gear itself determines the algebraic sign of the count pulse, eliminating one significant source of error.

The count pulses are transmitted by three wires (add, subtract, common) to a count register assembly on a panel in the control room. The assembly is illustrated in Figure 38. The basis of the assembly is a standard electro-mechanical ratchet-type increment/decrement digital counter modified to suit the present application. The modifications were necessary to prevent overheating of the intermittent-duty ratchet solenoids in the event the boom was stopped for any length of time with the count cycle current on. This was accomplished by interrupting the count current the instant the ratchet assembly registered the count. To activate the ratchet solenoid, the pulse current passed through the normally closed contacts of a continuous-duty relay. At the end of the ratchet stroke, insuring the register of the count, the ratchet mechanism actuated a pushrod which in turn closed a microswitch in turn energizing the relay and interrupting the ratchet solenoid current. The relay remained energized until the count current was interrupted.

To eliminate the other problem cited above of a error upon boom reversal, an elemental portion of the one-degree on-off count cycle was made identifiable as the place at which the discrete count would occur. This was simply done as follows. The detent electrical contacts were adjusted to make the current-on part of the on-off count cycle as long as possible, reducing the off part to a small fraction of a degree of boom angle. Care was taken then to readout the counter angle only when the count cycle was off, denoting a discrete angular position, and this was indicated by a deactivated relay at the control panel.

The final system provided rapid accurate microphone positioning with a precision well within 1/2 degree. Backlash or coasting properties of the drive, or hand movement of the boom, had no effect on the accurate boom position indication in the control room.

The positioning mechanism was suspended overhead in the anechoic chamber as close to the wedge tips as possible from four instrumentation hangers. A support-bar assembly allowed the vertical axis of boom rotation to be precisely positioned laterally. The entire unit may be easily relocated at any overhead position in the anechoic chamber. The boom itself was made from a length of electrical metalic tubing (EMT) held straight by a loop of turnbuckle-tensioned steel cable passing through it and forming a triangle with the boom support block on the vertical main shaft. To maintain invariable horizontal plane motion of the boom, and to eliminate friction producing moment bearing loads in the positioning mechanism, the microphone and boom were balanced by a counterweight which may be seen in Figure 7. The small gearmotor was sufficient for the reliable operation of the positioning mechanism.

For a continual check of the readout accuracy of the boom position, two electrical contacts were installed in the anechoic chamber ceiling (at precisely 15^{o} and 90^{o} from the jet axis) which were brushed by a contact carried by the microphone boom. The closing of these contacts by the boom lighted indicators on the control panel where a check was readily made with the counter indication.

APPENDIX B

COMBINED SOUND LEVELS

Because of the logarithmic basis of acoustic levels, the combined level from a number of sources is not a simple sum of the levels from the individual sources. By definition, sound pressure level SPL is given as

$$SPL = 20 \log_{10} \frac{p}{p_{ref}} , \tag{B1}$$

where p is the rms acoustic pressure and p_{ref} is a reference pressure. Intensity level IL is defined as

$$IL = 10 \log_{10} \frac{I}{I_{ref}} \tag{B2}$$

where I is the acoustic intensity, and I_{ref} is a reference intensity. For far field radiation, the intensity and the sound pressure are related by

$$I = \frac{p^2}{\rho_o a_o} \tag{B3}$$

If the acoustic emissions from two different sources combine at a point, provided the signals are of different frequencies, the intensities of the two emissions add.

$$I_c = I_1 + I_2 \tag{B4}$$

where the subscript c denotes the combined sound signal. Using equation B3, equation B4 yields

$$p_c^2 = p_1^2 + p_2^2 . \tag{B5}$$

If the signals are of the same frequency, the instantaneous sound pressures are additive, and phase relationships become important resulting in a combined acoustic pressure squared given by

$$p_c^2 = p_1^2 + p_2^2 + 2p_1p_2 \cos(\theta_1-\theta_2) \qquad \text{(B6)}$$

where θ are the phase angles of the different emissions. Equations B5 and B6 are used to determine the levels from combined acoustic sources. Equation B5 is used when the frequencies differ by 1 Hz or more.

If equation B1 is rewritten as

$$SPL = 10 \log \frac{p^2}{p_{ref}^2},$$

this may be solved for p^2 which may be substituted in general into equation B5 yielding

$$p_{ref}^2 \, 10^{SPL_c/10} = p_{ref}^2 \, 10^{SPL_1/10} + p_{ref}^2 \, 10^{SPL_2/10}$$

from which,

$$10^{SPL_c/10} = 10^{SPL_1/10} + 10^{SPL_2/10}.$$

Taking 10 times the logarithm to the base 10 of this result yields,

$$SPL_c = 10 \log_{10} (10^{SPL_1/10} + 10^{SPL_2/10}).$$

This result can be extended in general to the combined sound pressure level from any number of sources as

$$SPL_c = 10 \log_{10} (10^{SPL_1/10} + 10^{SPL_2/10} + \ldots + 10^{SPL_n/10}). \qquad \text{(B7)}$$

In a like manner, the similar result may be obtained for acoustic power levels.

In relation to the 1/3 octave band atat obtained in these investigations, the sound pressure level or power level in all the frequency bands may be combined according to equation B7 to yield the wideband sound pressure level or power level. The wideband sound pressure levels from different sources also combine according to equation B7.

APPENDIX C

TABULATED ACOUSTICAL DATA - DIRECTIVITY INDEX, MEAN SOUND PRESSURE LEVEL; WIDEBAND POWER LEVEL

This appendix contains a tabulation of the most significant data obtained in the investigation. Only part of these data are discussed or used in the text. The data are arranged in sequential order of nozzle arrangement, main jet total pressure, x/D ratio, and percent impingement. The main table entries are DIRECTIVITY INDEX DI(θ) as functions of azimuth angle THETA for various values of impinging jet total gage pressure P(TI) in psig. For each value of impinging jet total pressure, the mean sound pressure level SPL(R) is listed. By adding the directivity index to the mean sound pressure level, the measured sound pressure level (re 2×10^{-4} μbar) at the corresponding azimuth angle, 6 feet from the jets, is obtained. Also listed for each value of impinging jet total pressure is the wideband power level PWL re 10^{-12} watt. The ambient pressure is denoted by P AMB.

NOZZLE ARRANGEMENT I: 45 DEGREE IMPINGEMENT

P(TM) = 100 PSIG P ATM = 14.4 PSIA X/D = 0.2

THETA	15	30	45	60	75	90	105	120		
P(TI)			- DIRECTIVITY INDEX -						SPL(R)	PWL
0.0	2.6	6.9	2.0	-2.4	-4.0	-3.4	-3.7	-4.3	118.6	133.7
2.00	2.4	6.8	1.7	-2.4	-4.1	-2.6	-3.4	-4.0	119.1	134.2
4.00	2.3	6.9	1.5	-2.5	-3.9	-2.5	-3.5	-3.8	119.5	134.6
8.00	2.8	6.7	1.2	-2.4	-3.9	-2.8	-2.7	-2.8	119.7	134.8
10.00	2.7	7.1	1.0	-2.5	-4.3	-2.6	-3.8	-4.0	120.8	135.9
12.00	2.5	7.2	0.9	-3.1	-4.2	-2.3	-4.0	-3.7	121.5	136.6
14.00	0.2	7.4	0.7	-2.7	-4.1	-1.9	-4.1	-2.6	123.6	138.8
14.00	0.9	7.7	0.5	-2.9	-4.4	-2.7	-4.4	-3.1	122.9	138.1
16.00	-0.1	7.6	0.6	-2.7	-4.4	-2.4	-4.5	-2.8	123.9	139.1
18.00	-0.1	7.5	0.6	-2.8	-4.2	-2.3	-4.5	-2.3	123.8	139.0
20.00	0.1	7.4	1.0	-2.7	-4.2	-2.4	-4.5	-2.4	123.7	138.9
22.00	0.2	7.4	0.9	-2.6	-4.1	-2.2	-4.4	-3.3	123.6	138.7
24.00	-0.1	7.5	0.8	-2.5	-4.0	-2.3	-4.2	-3.3	123.5	138.7
26.00	0.0	7.5	0.7	-2.5	-4.0	-2.4	-4.1	-3.7	123.3	138.4
28.00	0.4	7.4	1.0	-2.5	-3.9	-2.6	-4.0	-3.0	123.0	138.2
30.00	0.1	7.7	0.8	-2.7	-4.3	-2.9	-4.4	-3.5	123.1	138.3
32.00	0.7	7.6	0.7	-2.4	-3.9	-2.8	-4.0	-3.5	122.5	137.7
34.00	1.2	7.3	1.0	-2.4	-3.8	-3.0	-3.6	-3.6	122.1	137.3
36.00	1.8	6.9	1.2	-2.2	-3.6	-2.9	-3.2	-3.2	121.6	136.7
38.00	1.4	6.9	1.3	-2.1	-3.8	-2.9	-3.1	-3.1	121.3	136.4
40.00	1.8	6.8	1.3	-2.2	-3.7	-3.1	-2.9	-3.1	120.7	135.8
42.00	1.7	6.8	1.1	-2.3	-3.6	-3.0	-2.8	-2.9	120.3	135.4
44.00	1.7	6.8	1.6	-2.3	-3.7	-3.0	-2.8	-3.0	120.1	135.3
46.00	1.7	6.7	1.8	-2.4	-3.5	-3.0	-2.8	-3.0	120.0	135.2
48.00	1.5	6.6	1.7	-2.4	-3.6	-2.9	-2.9	-2.9	120.0	135.1
50.00	1.5	6.5	1.8	-2.2	-2.7	-2.9	-2.9	-3.0	120.2	135.4

NOZZLE ARRANGEMENT I: 45 DEGREE IMPINGEMENT

P(TM) = 100 PSIG P ATM = 14.5 PSIA X/D = 0.4

THETA	15	30	45	60	75	90	105	120		
P(TI)			- DIRECTIVITY INDEX -						SPL(R)	PWL
0.0	3.0	7.0	2.2	-2.3	-4.3	-3.8	-4.0	-4.6	118.2	133.4
2.00	2.8	6.9	1.8	-2.3	-4.2	-3.1	-4.0	-4.5	118.7	133.8
4.00	2.4	7.1	1.5	-2.5	-4.0	-2.9	-3.9	-4.7	119.4	134.5
6.00	2.4	7.0	1.4	-2.3	-4.0	-2.2	-3.9	-4.7	120.0	135.2
8.00	2.0	7.0	1.2	-2.3	-4.0	-1.8	-3.4	-4.2	120.3	135.5
10.00	3.0	6.8	0.8	-2.0	-4.0	-2.7	-2.7	-3.0	120.2	135.4
12.00	2.6	6.9	0.6	-1.9	-3.9	-2.4	-3.0	-3.3	120.9	136.1
14.00	2.6	6.9	0.2	-1.9	-3.4	-2.0	-3.4	-2.9	122.3	137.4
16.00	2.1	6.9	0.0	-2.0	-3.5	-2.0	-3.4	-2.5	122.9	138.0
18.00	2.1	6.8	0.0	-1.7	-3.4	-2.1	-3.5	-2.4	122.7	137.8
20.00	2.3	6.7	0.1	-1.5	-3.4	-2.0	-3.4	-2.6	122.6	137.7
22.00	2.5	6.7	-0.0	-1.4	-3.3	-1.8	-3.1	-2.8	122.3	137.4
24.00	2.4	6.6	0.4	-1.4	-3.6	-2.2	-3.0	-2.7	122.1	137.2
26.00	2.0	6.4	0.4	-1.3	-3.4	-2.3	-2.4	-2.4	121.6	136.7
28.00	1.9	6.2	0.5	-1.3	-3.2	-2.3	-2.1	-2.1	121.1	136.2
30.00	1.6	6.0	0.6	-1.2	-3.1	-2.1	-1.9	-1.8	120.6	135.7
32.00	1.4	6.2	0.6	-1.5	-3.2	-2.3	-1.9	-1.9	120.3	135.4
34.00	1.6	6.3	1.1	-1.6	-3.3	-2.4	-2.0	-2.0	120.0	135.2
36.00	1.6	6.2	1.6	-1.7	-3.3	-2.3	-2.5	-2.4	119.8	134.9

NOZZLE ARRANGEMENT I: 45 DEGREE IMPINGEMENT
P(TM) = 100 PSIG P ATM = 14.5 PSIA X/D = 0.4, CONT'D.

38.00	1.6	6.3	1.6	-1.7	-3.4	-1.9	-2.6	-2.7	119.6	134.8
40.00	1.7	6.5	1.9	-2.2	-3.5	-2.5	-3.0	-3.0	119.4	134.5
42.00	1.7	6.6	2.2	-2.5	-3.5	-2.6	-3.1	-3.2	119.3	134.5
44.00	1.8	6.6	2.3	-2.3	-3.5	-2.8	-3.4	-3.5	119.3	134.4
46.00	1.7	6.6	2.3	-2.4	-3.4	-2.9	-3.5	-3.5	119.3	134.4
48.00	1.7	6.8	2.1	-2.5	-3.4	-3.0	-3.5	-3.6	119.3	134.4
50.00	1.7	6.6	2.4	-2.6	-3.6	-3.2	-3.5	-3.6	119.5	134.6

NOZZLE ARRANGEMENT I: 45 DEGREE IMPINGEMENT
P(TM) = 100 PSIG P ATM = 14.5 PSIA X/D = 0.6

THETA	15	30	45	60	75	90	105	120		
P(TI)			- DIRECTIVITY INDEX -						SPL(R)	PWL
0.0	3.3	6.7	1.8	-2.0	-3.9	-3.5	-3.4	-3.7	117.8	133.0
2.00	3.3	6.7	1.9	-2.1	-3.7	-3.1	-3.6	-4.1	118.4	133.6
4.00	2.9	6.9	1.4	-2.3	-3.9	-2.6	-3.9	-4.5	119.3	134.4
6.00	2.8	6.8	1.3	-1.9	-3.6	-2.3	-3.6	-4.2	119.9	135.0
8.00	1.6	6.7	1.0	-1.7	-3.4	-1.4	-3.1	-4.2	120.7	135.9
10.00	1.5	6.3	0.9	-1.6	-3.2	-1.2	-2.7	-3.6	121.2	136.3
12.00	0.9	4.9	0.6	0.6	-2.9	-1.9	-1.5	-1.5	120.9	136.1
14.00	0.6	4.0	0.3	2.1	-2.9	-2.1	-1.5	-1.6	121.8	137.0
16.00	-0.3	3.4	-0.2	3.1	-2.6	-2.2	-1.6	-1.9	122.4	137.6
18.00	-1.0	3.2	-0.0	3.3	-2.3	-2.3	-1.7	-2.1	122.5	137.7
20.00	-1.3	2.9	-0.5	3.9	-2.0	-2.8	-2.1	-2.3	122.8	138.0
22.00	-1.5	2.7	-0.0	3.7	-1.3	-2.6	-2.3	-2.7	122.8	138.0
24.00	-1.1	2.9	0.3	3.2	-1.2	-2.7	-1.9	-2.5	122.6	137.7
26.00	-1.3	3.1	0.9	2.6	-0.7	-2.4	-1.7	-2.6	122.6	137.7
28.15	-1.4	3.0	0.8	2.8	-0.8	-2.4	-1.9	-3.0	122.7	137.7
30.00	-1.4	3.1	1.0	2.9	-1.0	-2.2	-2.1	-3.1	122.6	137.7
32.00	-1.4	3.4	1.1	2.6	-0.8	-2.0	-2.1	-3.4	122.4	137.5
34.20	-1.0	3.7	1.6	1.5	-0.7	-1.8	-2.2	-3.5	122.0	137.0
36.00	-1.1	3.8	1.6	2.1	-0.6	-2.3	-2.4	-3.9	121.9	137.0
38.00	-1.1	3.8	1.7	2.0	-0.1	-2.2	-2.7	-4.6	121.8	136.9
40.00	-0.5	4.0	1.6	2.0	-0.1	-2.3	-3.0	-4.9	121.7	136.8
42.00	-1.1	4.1	1.6	2.1	0.1	-2.3	-3.4	-5.1	121.6	136.7
44.00	-0.7	4.2	1.6	1.8	0.0	-2.2	-3.7	-5.2	121.5	136.6
46.00	-0.4	4.4	1.8	1.3	0.0	-2.1	-3.7	-5.2	121.4	136.5
48.00	-0.4	4.4	1.9	1.5	-0.3	-1.8	-3.8	-5.1	121.3	136.4
50.00	-0.7	4.4	1.8	1.1	-0.1	-1.3	-3.6	-4.8	121.4	136.5

NOZZLE ARRANGEMENT I: 45 DEGREE IMPINGEMENT
P(TM) = 100 PSIG P ATM = 14.5 PSIA X/D = 0.8

THETA	15	30	45	60	75	90	105	120		
P(TI)			- DIRECTIVITY INDEX -						SPL(R)	PWL
0.0	3.1	6.5	2.1	-1.9	-3.9	-3.6	-3.3	-3.4	117.1	132.2
2.00	3.0	6.3	1.8	-1.7	-3.8	-3.3	-2.9	-3.0	117.0	132.1
4.00	3.1	6.1	1.8	-1.6	-3.6	-3.2	-2.7	-2.9	117.4	132.5
6.00	2.7	5.9	1.7	-1.3	-3.1	-2.8	-2.3	-2.5	118.3	133.4
8.00	2.6	5.5	1.6	-0.2	-3.1	-2.7	-2.4	-2.7	118.9	134.0
10.00	2.6	5.4	1.2	0.1	-2.9	-2.2	-2.7	-2.9	119.4	134.5
12.00	2.8	5.4	0.9	0.4	-3.1	-1.6	-2.6	-3.2	120.1	135.2
14.00	2.5	5.5	0.5	0.5	-3.0	-1.2	-3.0	-3.8	121.0	136.1

NOZZLE ARRANGEMENT I: 45 DEGREE IMPINGEMENT
P(TM) = 100 PSIG P ATM = 14.5 PSIA X/D = 0.8, CONT'D.

16.00	1.8	5.9	0.3	0.4	-3.0	-0.9	-3.2	-4.2	121.7	136.8
18.00	1.2	5.9	-0.1	0.2	-2.7	-0.6	-3.1	-4.4	122.3	137.4
20.00	1.0	6.0	-0.3	0.2	-2.7	-0.3	-3.4	-4.3	122.5	137.6
22.00	1.0	6.2	-0.2	0.0	-2.7	-0.4	-3.5	-4.5	122.5	137.6
24.00	1.2	6.0	0.0	0.0	-2.5	-0.8	-3.2	-4.1	122.3	137.3
26.00	1.2	5.9	0.5	-0.1	-2.5	-1.1	-3.2	-3.9	121.8	136.8
28.00	1.5	5.6	1.0	0.1	-2.3	-1.4	-2.8	-3.7	121.2	136.3
30.00	1.4	5.3	1.2	0.2	-2.1	-1.7	-2.5	-3.0	120.6	135.7
32.00	1.1	5.0	1.3	0.3	-1.8	-1.9	-2.0	-2.7	120.2	135.3
34.00	0.8	4.8	1.5	0.2	-1.6	-1.8	-2.2	-2.7	120.0	135.1
36.00	1.0	5.0	1.6	-0.2	-1.8	-1.6	-2.3	-3.1	119.7	134.8
38.00	1.0	5.2	1.8	-1.0	-1.7	-1.4	-2.4	-3.3	119.5	134.6
40.00	1.3	5.4	1.9	-1.1	-2.1	-1.2	-2.6	-3.6	119.4	134.5
42.00	1.4	5.5	1.9	-1.1	-2.1	-1.4	-2.6	-3.5	119.3	134.4
44.00	1.1	5.4	1.8	-0.9	-1.8	-1.8	-2.2	-3.4	119.4	134.5
46.00	0.8	5.1	1.5	-0.4	-1.7	-1.5	-2.0	-3.1	119.7	134.8
48.00	1.0	4.8	1.2	-0.1	-1.5	-1.5	-1.8	-3.0	120.0	135.1
50.00	0.7	4.6	1.1	-0.0	-1.3	-1.1	-1.8	-2.5	120.3	135.4

NOZZLE ARRANGEMENT I: 45 DEGREE IMPINGEMENT
P(TM) = 100 PSIG P ATM = 14.5 PSIA X/D = 1.0

THETA	15	30	45	60	75	90	105	120		
P(TI)			- DIRECTIVITY INDEX -						SPL(R)	PWL
0.0	1.3	3.6	2.4	-0.8	-2.1	-1.7	-0.8	-1.2	112.5	127.6
2.00	1.3	3.3	1.4	-1.0	-2.0	-1.2	-0.5	-0.6	113.2	128.3
4.00	1.0	3.8	2.5	-1.2	-1.9	-1.7	-1.4	-1.3	113.5	128.6
6.00	0.4	4.2	3.4	-1.5	-1.8	-1.7	-2.5	-2.7	114.1	129.2
8.00	1.4	4.6	3.1	-1.7	-2.1	-1.8	-2.3	-2.9	114.4	129.5
10.00	2.1	4.4	2.3	-1.5	-2.0	-1.1	-2.0	-2.8	114.4	129.5
12.00	2.6	4.7	1.6	-0.9	-2.1	-1.7	-1.7	-2.2	114.9	130.0
14.00	2.7	5.2	1.4	-1.1	-1.9	-2.1	-2.0	-2.5	115.8	130.9
16.00	2.7	5.7	1.3	-1.0	-2.3	-2.6	-2.6	-2.8	116.5	131.6
18.00	2.4	5.8	1.1	-0.5	-2.3	-2.1	-2.6	-3.1	116.9	132.0
20.00	2.0	5.9	1.0	-0.8	-2.1	-2.0	-2.6	-2.8	117.3	132.4
22.00	1.0	6.3	-0.0	-1.0	-2.0	-1.7	-2.5	-2.7	118.0	133.1
24.00	1.0	6.3	-0.2	-1.3	-2.0	-1.5	-2.8	-2.2	118.5	133.6
26.00	0.9	6.2	-0.3	-1.1	-2.1	-1.1	-2.9	-2.4	118.6	133.7
28.00	2.5	5.7	-0.5	-1.1	-1.9	-0.8	-3.1	-2.0	118.8	133.9
30.00	2.9	5.7	-0.5	-0.9	-1.7	-1.1	-2.8	-2.1	118.6	133.7
32.00	2.3	5.5	-0.4	-0.9	-1.7	-1.0	-2.7	-1.8	118.2	133.3
34.00	3.0	5.2	0.2	-1.0	-1.8	-1.0	-2.4	-2.2	117.5	132.6
36.00	4.2	4.7	0.2	-0.9	-1.7	-1.1	-2.1	-2.1	116.8	131.9
40.00	2.6	6.1	1.4	-1.7	-2.5	-2.2	-2.5	-3.1	117.9	133.1
42.00	3.2	5.7	1.2	-1.6	-2.4	-2.1	-2.3	-2.9	118.1	133.2
44.00	2.4	5.8	1.1	-1.4	-2.4	-2.1	-2.3	-2.6	118.4	133.5
46.00	2.4	5.6	0.9	-1.1	-1.9	-1.8	-2.1	-2.3	118.6	133.8
48.00	2.0	5.4	0.7	-1.0	-2.1	-1.6	-1.8	-2.0	119.0	134.1
50.00	2.2	5.2	0.5	-0.8	-1.8	-1.4	-1.8	-1.8	119.3	134.5

NOZZLE ARRANGEMENT I: 90 DEGREE IMPINGEMENT

P(TM) = 100 PSIG P ATM = 14.6 PSIA X/D = 0.2

THETA	15	30	45	60	75	90	105	120		
P(TI)				- DIRECTIVITY INDEX -					SPL(R)	PWL
0.0	5.2	7.2	1.4	-3.0	-4.7	-4.5	-4.9	-5.3	116.8	132.0
2.15	1.7	7.4	3.0	-2.8	-5.3	-5.3	-5.3	-5.5	117.8	132.9
4.00	4.6	7.5	0.8	-3.4	-4.9	-4.4	-4.4	-4.5	117.7	132.9
6.00	4.3	7.5	0.6	-3.1	-4.9	-4.1	-4.0	-3.9	118.2	133.4
8.00	4.6	7.5	-0.2	-3.2	-4.2	-3.2	-4.5	-4.0	120.7	135.9
10.00	3.6	7.6	-0.9	-3.2	-4.4	-2.9	-4.9	-2.9	122.4	137.5
12.00	3.2	7.2	0.2	-2.1	-3.8	-2.7	-4.3	-3.5	121.8	137.0
14.00	3.4	6.2	0.5	-1.0	-2.7	-2.6	-3.1	-3.0	120.8	136.0
16.00	2.6	6.0	1.0	-0.7	-2.4	-2.6	-2.7	-3.0	120.2	135.4
18.00	1.8	5.8	1.3	-0.4	-2.5	-2.4	-2.7	-3.2	120.2	135.4
20.00	1.7	5.5	0.9	0.2	-1.7	-2.0	-3.1	-3.6	120.2	135.3
22.00	1.2	5.4	1.8	-0.8	-1.3	-1.8	-2.8	-3.5	120.1	135.3
24.00	1.0	5.1	1.8	0.8	-1.3	-2.3	-3.2	-3.6	120.2	135.4
26.00	1.1	5.0	1.6	0.3	-0.9	-2.4	-2.9	-3.1	120.2	135.4
28.00	2.0	5.3	0.8	0.0	-1.3	-2.6	-2.7	-2.7	120.2	135.4
30.00	0.9	5.0	1.2	0.3	-1.0	-2.5	-2.6	-2.8	120.5	135.7
32.00	-0.3	4.5	0.8	0.0	-0.9	-1.2	-2.0	-2.0	121.7	136.8
34.00	-0.3	5.0	1.1	0.1	-1.3	-1.6	-2.1	-2.1	122.2	137.4
36.00	-0.1	5.4	0.7	-0.1	-1.5	-1.7	-2.5	-2.3	122.6	137.7
38.00	-0.2	5.6	0.6	-0.3	-1.4	-1.5	-2.7	-2.6	122.9	138.0
40.00	-0.2	5.5	0.8	-0.0	-1.5	-1.5	-2.6	-2.2	123.0	138.2
42.00	-0.3	5.5	0.7	-0.1	-1.6	-1.6	-2.5	-2.2	123.2	138.4
44.00	-0.9	5.2	0.1	0.1	-1.3	-1.3	-2.1	-2.0	123.8	138.9
46.00	-0.6	4.9	0.4	0.4	-1.1	-1.5	-1.7	-1.7	123.6	138.8
48.00	-0.8	4.4	0.1	0.6	-1.0	-1.4	-1.6	-1.4	123.5	138.6
50.00	-1.3	3.6	-0.0	2.4	-1.4	-1.7	-1.8	-1.5	123.7	138.8

NOZZLE ARRANGEMENT I: 90 DEGREE IMPINGEMENT

P(TM) = 100 PSIG P ATM = 14.5 PSIA X/D = 0.4

THETA	15	30	45	60	75	90	105	120		
P(TI)				- DIRECTIVITY INDEX -					SPL(R)	PWL
0.0	5.2	7.2	1.4	-3.0	-5.0	-4.8	-5.2	-5.5	116.5	131.6
2.00	5.3	7.3	1.1	-3.1	-4.8	-4.2	-5.3	-5.5	117.5	132.7
4.00	5.9	7.0	0.7	-3.1	-4.5	-4.2	-4.3	-4.3	117.8	133.0
6.00	5.0	7.5	0.0	-3.5	-5.0	-3.7	-4.7	-4.5	120.0	135.2
8.00	3.7	7.7	-0.5	-3.5	-4.7	-2.8	-4.8	-2.8	122.3	137.5
10.00	4.0	7.5	-0.5	-3.0	-4.5	-3.0	-4.7	-3.0	122.0	137.2
12.00	3.8	7.8	-0.2	-3.5	-4.9	-3.5	-4.9	-4.4	121.7	136.9
14.00	3.6	7.6	0.8	-3.2	-4.7	-4.2	-4.5	-4.2	120.7	135.9
16.00	2.9	7.4	1.3	-3.2	-4.5	-4.0	-4.1	-4.1	120.0	135.2
18.00	3.8	7.5	0.9	-3.4	-4.6	-4.2	-4.1	-4.2	119.4	134.6
20.00	3.7	7.5	1.5	-3.4	-4.8	-4.5	-4.5	-4.5	118.8	134.0
22.00	3.6	7.6	1.4	-3.6	-4.8	-4.7	-4.4	-4.5	118.3	133.5
24.00	3.3	7.5	1.5	-3.5	-4.8	-4.6	-4.4	-4.7	118.5	133.6
26.00	2.8	7.5	2.0	-3.5	-4.5	-4.5	-4.7	-4.5	119.0	134.2
28.00	4.3	7.6	0.6	-3.2	-4.3	-4.0	-4.6	-4.5	119.7	134.9
30.00	3.7	7.9	0.7	-3.6	-4.3	-4.3	-5.5	-4.9	120.8	136.0
32.10	0.7	7.7	0.9	-2.7	-3.8	-2.8	-4.3	-4.3	122.8	138.0
34.00	-0.3	7.5	0.9	-2.6	-3.6	-2.3	-4.3	-3.8	123.3	138.5
36.00	0.5	6.5	0.3	-1.5	-1.8	-2.0	-3.2	-2.8	123.0	138.1

NOZZLE ARRANGEMENT I: 90 DEGREE IMPINGEMENT
P(TM) = 100 PSIG P ATM = 14.5 PSIA X/D = 0.4, CONT'D.

38.00	2.2	6.2	-0.3	-1.2	-1.8	-1.6	-2.9	-2.5	123.3	138.5
40.00	-0.0	6.3	0.1	-0.6	-1.6	-1.8	-2.7	-2.7	123.5	138.7
42.00	-0.2	6.2	0.2	-0.5	-1.8	-1.8	-2.7	-2.7	123.7	138.9
44.00	0.0	6.0	-0.1	-0.2	-1.9	-1.8	-2.4	-2.3	123.8	139.0
46.00	1.0	5.7	-0.4	-0.1	-1.9	-1.7	-2.4	-2.1	123.8	138.9
48.00	-0.2	5.3	-0.3	0.4	-1.6	-1.5	-2.1	-1.5	123.7	138.9
50.00	1.6	4.8	-0.0	0.6	-1.8	-1.5	-2.0	-1.2	123.7	138.9

NOZZLE ARRANGEMENT I: 90 DEGREE IMPINGEMENT
P(TM) = 100 PSIG P ATM = 14.4 PSIA X/D = 0.6

THETA	15	30	45	60	75	90	105	120		
P(TI)			- DIRECTIVITY INDEX -						SPL(R)	PWL
0.0	3.7	6.8	2.0	-2.1	-4.0	-4.0	-3.7	-4.1	117.2	132.4
2.00	4.7	7.0	1.2	-2.5	-4.5	-3.3	-4.5	-4.8	118.8	134.0
4.00	4.0	7.2	0.2	-3.3	-4.3	-1.8	-4.3	-5.1	120.8	135.9
6.00	3.8	7.1	0.3	-2.4	-3.9	-2.6	-4.0	-3.6	121.9	137.1
8.00	1.9	7.4	0.2	-2.6	-4.1	-2.8	-4.3	-2.8	122.6	137.8
10.00	3.0	7.4	0.5	-2.5	-4.3	-2.9	-4.0	-3.8	121.8	137.0
12.00	2.2	7.2	1.1	-2.3	-4.3	-3.4	-3.4	-3.3	120.8	136.0
14.00	2.1	6.9	1.8	-2.5	-4.2	-3.3	-3.0	-3.0	119.2	134.4
16.00	2.2	6.9	2.5	-3.0	-4.5	-3.7	-3.7	-4.0	118.7	133.9
18.00	3.5	6.6	2.6	-3.2	-4.4	-3.8	-3.8	-4.0	118.0	133.1
20.00	3.0	7.1	2.5	-3.4	-4.6	-4.2	-4.2	-4.4	118.4	133.6
22.00	2.0	6.9	2.8	-3.3	-4.5	-3.7	-3.7	-3.8	118.8	134.0
24.00	3.1	7.0	1.1	-2.9	-3.8	-3.5	-3.5	-3.4	119.5	134.6
26.00	2.5	7.1	1.7	-2.4	-3.9	-3.6	-3.8	-3.8	120.4	135.6
28.00	2.6	7.4	0.7	-2.3	-3.8	-3.2	-3.9	-3.9	121.4	136.6
30.00	1.3	7.3	1.1	-2.2	-3.7	-2.9	-4.1	-4.0	122.2	137.4
32.00	0.1	7.4	0.8	-1.9	-3.3	-2.4	-4.4	-4.1	122.9	138.1
34.00	-0.2	7.5	0.3	-2.2	-3.4	-2.3	-4.5	-3.7	123.5	138.6
36.00	2.2	7.2	0.5	-2.0	-3.3	-2.1	-4.3	-3.9	123.8	139.0
38.00	0.2	7.2	0.2	-1.6	-2.9	-2.2	-4.2	-3.2	123.8	139.0
40.00	0.1	4.6	-0.1	2.1	-1.1	-2.4	-2.6	-2.8	123.4	138.6
42.00	-0.2	3.3	0.0	2.7	-0.7	-1.4	-3.0	-2.8	124.2	139.4
44.00	0.2	3.8	-0.5	2.0	-0.5	-0.9	-2.4	-2.5	123.8	139.0
46.00	1.3	5.4	0.1	-0.2	-1.5	-1.5	-2.5	-2.0	123.7	138.9
48.00	0.1	5.9	0.6	-1.0	-2.0	-1.7	-2.7	-1.5	123.7	138.9
50.00	0.7	5.7	0.6	-0.9	-1.6	-1.8	-2.4	-1.4	123.6	138.8

NOZZLE ARRANGEMENT I: 90 DEGREE IMPINGEMENT
P(TM) = 100 PSIG P ATM = 14.5 PSIA X/D = 0.8

THETA	15	30	45	60	75	90	105	120		
P(TI)			- DIRECTIVITY INDEX -						SPL(R)	PWL
0.0	3.4	6.4	1.6	-1.7	-3.5	-3.4	-3.0	-3.1	117.0	132.2
2.00	1.7	6.8	1.5	-1.8	-3.8	-3.3	-3.1	-3.3	119.0	134.1
4.00	1.9	7.4	0.4	-2.3	-4.1	-1.6	-4.1	-5.1	121.6	136.8
6.00	-0.2	7.1	0.8	-2.6	-4.2	-0.4	-3.8	-4.9	123.4	138.5
8.00	1.4	7.2	0.2	-3.0	-4.1	-0.4	-4.1	-4.8	123.3	138.4
10.00	1.9	7.3	0.4	-2.9	-3.9	-1.4	-4.1	-4.7	122.1	137.2
12.00	2.0	6.5	2.0	-2.3	-3.5	-3.2	-3.0	-3.0	119.5	134.7
14.00	1.8	6.9	2.6	-2.9	-4.1	-3.9	-3.6	-3.8	118.9	134.1

NOZZLE ARRANGEMENT I: 90 DEGREE IMPINGEMENT
P(TM) = 100 PSIG P ATM = 14.5 PSIA X/D = 0.8, CONT'D.

16.00	0.6	6.6	3.6	-3.0	-4.6	-4.4	-3.7	-4.4	118.9	134.0
18.00	0.4	6.4	3.6	-2.3	-4.5	-4.4	-2.0	-5.1	119.5	134.7
20.00	-0.0	6.1	3.0	-1.2	-4.4	-3.9	-1.0	-4.6	120.3	135.5
22.00	0.3	5.8	2.3	-0.2	-3.7	-3.4	-1.4	-3.8	120.7	135.9
24.00	0.4	5.5	2.1	1.1	-3.3	-2.8	-2.6	-4.0	121.5	136.7
26.00	0.5	5.2	1.9	1.6	-3.2	-2.6	-3.4	-4.1	122.4	137.5
28.00	0.9	5.2	1.5	1.6	-2.8	-2.2	-3.5	-3.8	122.7	137.9
30.00	0.8	5.3	1.0	1.3	-2.3	-1.8	-3.1	-3.1	123.0	138.2
32.00	1.6	5.3	0.3	0.9	-2.2	-1.6	-2.8	-2.7	123.1	138.3
34.00	1.2	5.0	0.1	1.3	-2.0	-1.4	-2.7	-2.5	123.3	138.5
36.00	0.4	3.9	0.2	2.6	-0.9	-1.8	-3.4	-3.1	124.1	139.3
38.00	0.5	4.0	-0.0	1.7	-1.0	-1.1	-2.1	-2.2	123.2	138.4
40.00	0.9	4.1	-0.3	1.9	-1.6	-1.4	-2.2	-2.0	123.4	138.6
42.00	0.4	2.7	-0.3	2.1	-0.6	-1.0	-1.6	-2.1	123.9	139.1
44.00	-0.5	1.7	-0.4	2.6	-0.1	-1.1	-1.4	-2.6	124.1	139.2
46.00	-0.8	1.4	-0.5	2.9	-0.3	-0.7	-1.3	-2.6	124.1	139.3
48.00	-0.8	1.5	-0.8	3.0	-0.5	-1.1	-1.3	-2.6	124.3	139.4
50.00	-0.4	1.7	-1.0	3.3	-0.7	-1.3	-1.1	-2.4	124.2	139.4

NOZZLE ARRANGEMENT I: 90 DEGREE IMPINGEMENT
P(TM) = 100 PSIG P ATM = 14.6 PSIA X/D = 0.9

THETA	15	30	45	60	75	90	105	120		
P(TI)			- DIRECTIVITY INDEX -						SPL(R)	PWL
0.0	1.1	2.9	2.3	-1.1	-2.4	-1.4	-0.6	-0.3	110.6	125.7
2.00	1.8	3.4	1.4	-0.5	-2.0	-1.4	-0.6	-0.4	111.8	126.9
4.00	1.7	4.0	2.4	-1.2	-2.1	-1.9	-1.5	-1.2	112.8	127.9
6.00	2.3	4.5	1.6	-1.2	-2.5	-2.4	-1.2	-1.0	113.7	128.7
8.00	2.7	5.5	1.5	-1.5	-3.0	-2.0	-2.0	-2.0	115.5	130.6
10.00	2.1	5.6	0.1	-1.1	-2.5	-1.1	-2.1	-2.2	117.4	132.4
12.00	2.5	5.8	-0.5	-1.5	-2.5	-0.5	-1.9	-2.1	119.0	134.1
14.00	1.4	6.6	2.7	-2.5	-3.8	-3.8	-3.7	-3.2	119.8	134.9
16.00	0.9	6.7	3.0	-2.2	-3.9	-3.9	-3.8	-3.8	120.1	135.2
18.00	0.2	6.0	3.2	-1.1	-3.9	-3.9	-3.0	-3.7	120.8	135.8
20.00	0.5	5.5	3.0	-0.1	-3.1	-3.1	-3.1	-3.8	121.3	136.4
22.00	0.3	4.9	2.6	0.3	-2.9	-2.8	-1.8	-3.5	121.9	137.0
24.00	0.1	4.9	2.4	0.9	-2.5	-2.4	-2.3	-3.5	122.6	137.7
26.00	0.4	4.3	2.0	1.0	-0.9	-2.0	-3.1	-3.7	123.4	138.5
28.00	-0.3	3.8	1.8	1.4	0.0	-1.9	-3.7	-3.5	124.0	139.1
30.00	0.5	4.1	1.1	1.4	-0.2	-1.8	-3.2	-3.2	124.2	139.3
32.00	0.0	3.6	0.9	1.7	-0.2	-1.6	-3.2	-3.0	124.3	139.3
34.00	-0.6	3.0	1.2	0.7	-0.7	-0.8	-1.6	-1.8	123.1	138.1
36.00	-0.7	2.2	1.1	0.9	-0.7	-0.5	-1.3	-1.3	122.6	137.7
38.00	-0.7	3.0	0.5	0.5	-0.7	-0.3	-1.2	-1.2	122.5	137.6
40.00	-1.2	1.8	-0.1	2.9	-0.8	-0.8	-1.8	-2.4	124.5	139.6
42.00	-1.2	1.5	-0.2	3.3	-1.1	-1.0	-1.5	-2.4	124.4	139.5
44.00	-0.7	1.7	-0.5	3.2	-1.3	-0.9	-1.4	-2.1	124.2	139.3
46.00	-0.7	1.8	-0.6	2.8	-1.5	-0.7	-0.8	-2.1	124.2	139.3
48.00	-0.5	1.8	-0.4	2.8	-1.7	-0.9	-1.0	-2.0	124.2	139.2
50.00	-0.8	2.0	0.3	2.2	-0.8	-1.2	-1.1	-1.8	124.0	139.1

NOZZLE ARRANGEMENT I: 90 DEGREE IMPINGEMENT

P(TM) = 100 PSIG P ATM = 14.6 PSIA X/D = 1.0

THETA	15	30	45	60	75	90	105	120		
P(TI)			- DIRECTIVITY INDEX -						SPL(R)	PWL
0.0	1.1	3.6	2.5	-0.4	-1.9	-1.7	-1.1	-1.6	111.3	126.5
2.00	2.0	3.8	1.8	-0.8	-2.0	-1.7	-1.2	-1.2	112.2	127.3
4.00	1.9	4.4	1.9	-0.6	-2.1	-2.1	-1.4	-1.3	112.6	127.8
6.00	2.2	4.7	1.4	-1.0	-2.0	-1.9	-1.5	-1.5	114.8	129.9
8.00	2.8	5.9	1.1	-1.2	-2.5	-2.4	-2.3	-2.4	116.2	131.4
10.00	2.3	6.1	0.1	-1.1	-3.0	-1.5	-2.2	-2.3	117.7	132.9
12.00	2.2	5.9	-0.2	-1.3	-2.3	-0.8	-2.5	-2.3	118.3	133.5
14.00	2.5	5.3	0.2	-1.0	-2.1	-1.1	-1.8	-1.8	117.3	132.5
16.00	2.2	4.2	0.6	-1.0	-1.9	-1.5	-0.6	-0.6	115.7	130.9
18.00	0.5	5.9	2.7	-1.1	-2.3	-3.0	-3.3	-3.3	120.5	135.6
20.00	0.3	5.6	2.3	-0.6	-1.3	-2.8	-3.5	-3.6	121.6	136.7
22.00	0.0	5.0	2.0	-0.1	-1.0	-2.2	-2.9	-3.1	121.9	137.0
24.00	0.8	4.2	1.7	0.7	-1.3	-1.4	-2.3	-2.7	122.0	137.1
26.00	0.5	3.4	1.6	0.5	-0.1	-1.3	-2.4	-2.4	122.8	137.9
28.00	-1.3	3.9	1.7	0.7	-0.4	-1.4	-2.1	-2.3	123.1	138.3
30.00	0.2	3.6	1.2	0.8	-0.7	-1.2	-1.5	-2.1	122.8	138.0
32.00	0.1	3.4	0.9	0.6	-0.5	-1.2	-1.5	-2.0	122.8	137.9
34.00	-0.5	3.0	0.7	0.7	-0.5	-0.8	-1.0	-1.6	122.3	137.4
36.00	0.3	2.8	0.3	1.0	-0.8	-0.6	-1.0	-1.5	122.2	137.3
38.00	-0.9	2.8	0.3	0.8	-0.5	-0.4	-1.1	-1.2	122.4	137.5
40.00	-1.5	2.8	0.2	1.9	-0.5	-0.8	-1.5	-1.6	123.0	138.2
42.00	-2.0	2.3	0.0	2.1	-0.4	-1.0	-1.4	-1.7	123.4	138.5
44.00	-2.0	2.0	0.7	1.9	0.2	-1.3	-1.5	-2.0	123.5	138.6
46.00	-1.8	1.8	0.7	1.7	1.0	-1.6	-1.5	-2.1	123.8	138.9
48.00	-1.7	1.9	0.8	1.8	0.8	-1.9	-1.5	-2.0	123.9	139.0
50.00	-1.7	2.0	0.9	1.9	0.7	-1.7	-1.8	-2.1	124.0	139.1

NOZZLE ARRANGEMENT I: 90 DEGREE IMPINGEMENT

P(TM) = 150 PSIG P ATM = 14.5 PSIA X/D = 0.6

THETA	15	30	45	60	75	90	105	120		
P(TI)			- DIRECTIVITY INDEX -						SPL(R)	PWL
0.0	1.8	5.0	2.1	-0.7	-2.5	-2.4	-2.0	-2.4	118.7	133.8
3.00	2.1	6.9	2.3	-2.1	-4.0	-3.8	-3.9	-4.4	120.9	136.0
6.00	1.8	6.8	2.8	-2.3	-4.1	-3.8	-3.9	-4.4	121.7	136.8
9.00	1.1	6.3	2.1	-1.9	-3.2	-2.8	-2.8	-2.8	122.9	138.0
12.00	-0.3	6.3	0.9	-1.6	-2.8	-1.6	-2.6	-2.5	125.1	140.2
15.00	-0.0	6.4	1.5	-1.5	-3.0	-1.9	-2.7	-2.5	124.8	140.0
18.00	0.3	6.2	0.8	-1.2	-2.8	-2.1	-2.2	-2.4	124.2	139.3
21.00	0.2	5.8	2.2	-1.3	-2.8	-2.4	-2.4	-2.6	123.6	138.7
24.00	1.2	6.1	2.7	-1.7	-3.2	-3.0	-2.9	-3.2	123.1	138.2
27.00	0.6	6.1	2.9	-1.9	-3.3	-2.9	-3.0	-3.5	122.7	137.8
30.00	1.0	6.3	2.7	-1.9	-3.2	-2.9	-3.2	-3.5	122.7	137.8
33.00	0.7	5.9	2.9	-1.9	-3.1	-2.8	-2.9	-3.1	122.9	138.0
36.00	0.3	5.5	2.8	-1.3	-2.9	-2.5	-2.5	-3.0	123.5	138.6
39.00	0.1	5.3	2.1	-0.2	-2.5	-2.3	-2.1	-2.4	123.9	139.0
42.00	-0.1	5.0	1.9	0.6	-2.5	-2.4	-2.4	-2.5	124.7	139.7
45.00	0.2	5.4	1.7	-0.1	-2.5	-1.8	-2.2	-2.4	124.8	139.9
48.00	-0.1	5.4	1.4	-0.3	-2.4	-1.7	-2.3	-2.4	125.1	140.1
50.00	0.3	5.5	1.3	-0.4	-2.2	-1.4	-2.2	-2.3	125.2	140.3

NOZZLE ARRANGEMENT II: 90 DEGREE IMPINGEMENT
P(TM) = 75 PSIG P ATM = 14.6 PSIA X/D = 0.4

THETA	15	30	45	60	75	90	105	120		
P(TI)			- DIRECTIVITY INDEX -						SPL(R)	PWL
0.0	0.3	7.8	1.0	-2.8	-4.4	-2.7	-4.6	-5.7	118.0	133.1
1.50	1.1	6.9	0.6	-2.1	-3.6	-2.2	-2.4	-3.2	117.9	133.0
3.00	1.3	5.4	1.0	-1.3	-2.6	-2.0	-1.3	-1.3	117.8	132.9
4.50	0.7	5.1	0.1	-1.0	-2.5	-1.8	-0.9	-0.6	119.1	134.2
6.00	0.7	4.7	0.6	-0.6	-2.1	-1.6	-0.8	-0.6	119.1	134.2
7.50	0.6	4.9	0.7	-0.6	-2.4	-1.8	-1.1	-0.8	119.1	134.2
9.00	0.8	5.0	1.2	-0.6	-2.2	-1.8	-2.3	-1.0	118.8	133.9
10.50	1.1	5.5	1.5	-0.7	-2.5	-2.1	-1.6	-2.3	118.6	133.7
12.00	0.9	5.3	2.0	-0.9	-2.6	-2.3	-1.9	-1.8	118.5	133.6
13.50	1.7	5.4	2.0	-0.9	-2.8	-2.4	-2.3	-2.1	118.3	133.4
15.00	1.1	5.6	2.6	-0.9	-2.9	-3.0	-2.6	-2.7	118.4	133.5
16.50	0.8	6.0	2.5	-0.8	-2.9	-3.1	-3.1	-3.4	118.6	133.7
18.00	1.0	5.7	3.5	0.4	-2.9	-4.1	-4.6	-5.9	121.1	136.2
19.50	0.5	5.2	3.2	1.0	-2.8	-3.5	-3.6	-5.7	122.8	137.9
21.00	1.5	4.3	4.1	0.8	-2.5	-3.9	-3.7	-6.5	122.5	137.6
22.50	-0.5	5.4	2.6	1.7	-3.4	-3.9	-2.8	-6.1	122.6	137.7

NOZZLE ARRANGEMENT II: 90 DEGREE IMPINGEMENT
P(TM) = 75 PSIG P ATM = 14.6 PSIA X/D = 0.6

THETA	15	30	45	60	75	90	105	120		
P(TI)			- DIRECTIVITY INDEX -						SPL(R)	PWL
0.0	-0.3	8.1	1.5	-3.3	-4.2	-3.7	-5.5	-6.3	118.0	133.1
1.50	0.5	7.5	0.9	-2.5	-3.9	-2.6	-3.8	-4.6	118.1	133.2
3.00	0.7	6.7	1.0	-2.1	-3.3	-2.1	-2.3	-2.8	118.3	133.4
4.50	1.2	5.5	1.0	-1.2	-2.7	-2.0	-1.5	-1.8	118.5	133.5
6.00	1.6	5.2	0.6	-0.8	-2.5	-1.9	-1.0	-1.1	118.6	133.7
7.50	1.0	5.1	0.4	-0.9	-2.4	-1.7	-1.0	-1.1	118.7	133.8
9.00	0.9	5.0	0.8	-0.7	-2.2	-1.4	-1.4	-1.5	118.7	133.8
10.50	0.9	5.2	1.4	-0.9	-2.2	-1.1	-2.4	-2.4	119.1	134.1
12.00	-0.0	5.3	1.9	-0.3	-2.0	-1.0	-2.7	-3.2	119.5	134.6
13.50	0.4	5.3	2.4	-0.3	-1.8	-1.8	-3.3	-4.1	120.1	135.2
15.00	0.3	5.3	2.5	0.0	-1.9	-2.4	-3.2	-4.3	120.0	135.0
16.50	1.0	5.3	2.3	-0.1	-2.2	-2.0	-2.7	-3.7	119.2	134.3
18.00	1.3	5.3	2.6	-0.1	-2.4	-2.4	-3.2	-3.8	118.4	133.5
19.50	1.0	5.6	2.2	-0.3	-2.1	-2.6	-3.0	-4.0	117.6	132.7
21.00	1.3	5.3	2.8	-0.4	-2.2	-2.9	-3.0	-3.8	116.7	131.8
22.50	1.2	5.4	2.9	-0.3	-2.2	-2.8	-3.1	-3.9	116.6	131.7

NOZZLE ARRANGEMENT II: 90 DEGREE IMPINGEMENT
P(TM) = 75 PSIG P ATM = 14.6 PSIA X/D = 0.8

THETA	15	30	45	60	75	90	105	120		
P(TI)			- DIRECTIVITY INDEX -						SPL(R)	PWL
0.0	1.4	7.5	1.4	-2.7	-3.7	-3.4	-4.3	-5.5	117.9	132.9
1.50	-0.6	7.7	0.9	-2.7	-3.2	-2.7	-4.3	-5.2	118.6	133.7
3.00	-0.8	7.6	1.1	-2.9	-3.0	-2.9	-4.0	-5.2	119.0	134.1
4.50	-0.6	7.5	1.1	-2.5	-3.0	-2.1	-4.0	-4.9	119.1	134.2
6.00	-0.6	7.3	0.9	-2.6	-2.8	-2.1	-3.7	-4.6	119.2	134.3
7.50	-0.5	7.1	1.0	-2.2	-2.5	-1.9	-3.2	-4.1	119.0	134.1
9.00	-2.5	6.7	1.1	-1.5	-2.4	-1.4	-3.4	-4.1	119.4	134.4
10.50	-1.6	6.9	0.7	-2.2	-2.6	-1.2	-3.3	-3.8	119.2	134.2

NOZZLE ARRANGEMENT II: 90 DEGREE IMPINGEMENT
P(TM) = 75 PSIG P ATM = 14.6 PSIA X/D = 0.8, CONT'D.

12.00	-0.7	6.3	1.3	-1.7	-2.2	-1.8	-2.5	-2.9	118.1	133.2
13.50	0.9	5.2	1.3	-0.9	-1.7	-1.9	-1.6	-2.0	116.6	131.7
15.00	1.6	4.7	1.6	-0.9	-1.7	-1.9	-1.6	-2.0	115.8	130.9
16.50	1.8	4.8	1.7	-0.7	-1.6	-2.1	-2.0	-2.1	115.4	130.5
18.00	1.5	4.5	1.7	-0.4	-1.2	-1.9	-2.0	-2.1	115.5	130.6
19.50	1.2	4.2	1.1	-0.0	-1.3	-1.6	-1.4	-1.5	115.8	130.9
21.00	1.1	3.8	0.8	-0.3	-1.0	-1.5	-1.3	-1.0	116.4	131.4
22.50	1.2	3.6	0.7	-0.2	-1.2	-1.4	-1.0	-0.8	116.7	131.8

NOZZLE ARRANGEMENT II: 90 DEGREE IMPINGEMENT
P(TM) = 75 PSIG P ATM = 14.6 PSIA X/D = 1.0

THETA	15	30	45	60	75	90	105	120		
P(TI)			- DIRECTIVITY INDEX -						SPL(R)	PWL
0.0	2.3	7.3	1.1	-2.6	-3.5	-3.7	-3.6	-4.0	117.3	132.4
1.50	2.5	7.0	1.4	-2.4	-3.1	-3.6	-3.3	-3.7	117.5	132.6
3.00	2.5	6.9	1.1	-2.2	-3.1	-3.6	-3.0	-4.0	117.3	132.3
4.50	2.2	6.4	1.6	-1.7	-3.0	-3.1	-2.3	-3.0	116.9	132.0
6.00	2.5	6.0	1.8	-1.7	-2.6	-3.0	-2.5	-2.6	116.7	131.8
7.50	1.9	5.6	1.7	-1.4	-2.8	-2.7	-2.1	-2.0	116.3	131.3
9.00	1.7	5.5	1.7	-1.3	-2.3	-2.6	-2.1	-1.9	115.9	131.0
10.50	2.0	5.3	1.9	-1.1	-2.2	-2.5	-2.0	-2.0	115.2	130.3
12.00	2.4	5.4	2.1	-1.0	-2.3	-2.6	-2.6	-2.5	114.6	129.7
13.50	2.1	5.4	2.1	-0.9	-2.2	-2.7	-2.4	-2.9	114.5	129.6
15.00	1.9	4.9	1.9	-0.6	-2.4	-2.2	-1.9	-1.8	114.7	129.8
16.50	1.5	4.5	1.6	-0.7	-1.7	-1.9	-1.6	-1.7	115.1	130.2
18.00	1.4	4.2	1.7	-0.5	-1.7	-1.9	-1.4	-1.6	115.1	130.2
19.50	1.1	4.1	1.7	-0.4	-1.6	-1.8	-1.5	-1.6	115.4	130.4
21.00	0.7	3.9	1.5	-0.2	-1.4	-1.7	-1.2	-1.4	115.9	131.0
22.50	1.3	3.4	1.7	-0.0	-1.2	-1.5	-1.3	-1.1	116.2	131.3

NOZZLE ARRANGEMENT II: 90 DEGREE IMPINGEMENT
P(TM) = 75 PSIG P ATM = 14.4 PSIA X/D = 1.2

THETA	15	30	45	60	75	90	105	120		
P(TI)			- DIRECTIVITY INDEX -						SPL(R)	PWL
0.0	2.4	6.8	1.2	-2.3	-3.2	-3.4	-2.8	-3.1	116.9	132.1
1.50	2.1	6.2	2.0	-1.9	-3.2	-3.1	-2.3	-2.5	116.6	131.8
3.00	2.4	6.0	1.7	-1.7	-3.1	-2.8	-2.3	-2.5	116.1	131.3
4.50	2.5	5.9	1.7	-1.5	-2.9	-3.1	-2.2	-2.3	115.7	130.9
6.00	2.7	5.4	2.2	-1.3	-2.8	-2.9	-2.3	-2.6	115.2	130.3
7.50	2.7	5.5	2.1	-1.2	-2.7	-2.6	-2.3	-2.8	114.8	130.0
9.00	2.7	5.4	2.2	-1.2	-2.4	-2.8	-2.3	-2.6	114.6	129.8
10.50	2.2	5.7	1.8	-1.3	-2.6	-2.6	-2.5	-2.8	114.9	130.0
12.00	1.9	5.0	2.1	-0.9	-1.9	-2.0	-2.1	-2.8	114.6	129.8
13.50	3.2	4.7	2.1	-0.7	-1.7	-2.1	-2.2	-3.2	114.5	129.7
15.00	1.9	4.7	2.6	-0.3	-1.7	-2.1	-2.5	-3.8	114.5	129.7
16.50	2.0	4.3	2.4	0.2	-1.4	-1.9	-2.5	-3.7	114.6	129.8
18.00	1.3	4.2	2.5	0.2	-1.3	-1.9	-2.0	-3.4	115.2	130.4
19.50	1.4	3.8	2.6	0.1	-1.5	-1.7	-2.2	-3.2	115.8	130.9
21.00	1.2	3.5	2.5	0.1	-1.0	-1.4	-2.2	-2.8	116.1	131.2
22.50	0.3	3.6	2.5	0.2	-0.9	-1.3	-2.2	-2.8	116.5	131.7

NOZZLE ARRANGEMENT II: 90 DEGREE IMPINGEMENT

P(TM) = 100 PSIG P ATM = 14.6 PSIA X/D = 0.4

THETA	15	30	45	60	75	90	105	120		
P(TI)			- DIRECTIVITY INDEX -						SPL(R)	PWL
0.0	2.0	7.2	2.5	-2.1	-4.0	-4.4	-4.5	-5.2	118.0	133.2
2.00	2.4	6.8	2.1	-2.1	-4.0	-3.9	-3.4	-3.9	118.1	133.2
4.00	2.7	6.5	2.1	-1.9	-4.0	-3.8	-3.2	-3.3	118.5	133.6
6.00	2.0	6.1	1.7	-1.0	-3.3	-3.0	-2.7	-2.3	119.3	134.5
8.00	1.5	5.2	0.9	-0.4	-2.6	-2.0	-1.4	-1.4	121.0	136.2
10.00	1.7	5.1	0.9	-0.5	-2.7	-1.9	-1.4	-1.4	121.0	136.2
12.00	0.9	5.2	1.3	-0.5	-2.6	-2.2	-1.6	-1.2	121.4	136.6
14.00	0.9	5.3	1.7	-0.9	-2.8	-2.4	-1.8	-1.7	121.4	136.5
16.00	1.1	5.4	1.7	-0.8	-2.9	-2.5	-2.0	-1.7	121.1	136.2
18.00	1.5	5.5	2.1	-0.9	-3.1	-2.8	-2.3	-2.2	121.0	136.1
20.00	1.4	5.7	2.2	-1.1	-3.2	-2.8	-2.3	-2.3	120.8	136.0
22.00	1.2	5.9	2.0	-0.9	-3.1	-2.8	-2.3	-2.4	120.8	136.0
24.00	0.8	5.5	2.4	-0.8	-2.8	-2.5	-2.3	-2.3	121.0	136.2
26.00	0.8	5.4	2.3	-0.7	-2.8	-2.7	-2.5	-2.4	121.5	136.6
28.00	0.6	5.4	2.3	-0.5	-2.6	-2.3	-2.6	-2.5	122.0	137.1
30.00	0.6	5.2	2.3	-0.3	-2.3	-2.1	-2.6	-2.7	122.4	137.5
32.00	0.5	5.3	2.0	-0.3	-2.0	-2.2	-2.7	-2.7	122.8	137.9
34.00	0.7	5.4	2.2	-0.4	-1.9	-2.3	-2.8	-2.9	123.1	138.3
36.00	0.9	5.5	1.8	-0.5	-1.7	-2.6	-2.8	-2.8	123.3	138.4
38.00	1.3	5.1	2.0	-0.7	-1.4	-2.1	-2.7	-2.7	123.2	138.3
40.00	1.4	4.9	2.2	-0.7	-1.3	-2.3	-2.6	-2.5	123.3	138.4
42.00	1.4	4.7	1.7	-0.5	-1.1	-2.2	-2.2	-2.5	123.2	138.3
44.00	1.4	4.8	1.5	-0.5	-1.0	-2.0	-2.0	-2.0	123.0	138.2
46.00	1.3	4.4	1.7	-0.5	-1.1	-2.0	-1.9	-1.9	123.1	138.2
48.00	1.2	4.3	1.5	-0.2	-1.2	-1.8	-1.7	-1.8	123.0	138.1
50.00	1.2	4.3	1.6	-0.5	-1.2	-1.9	-1.8	-1.7	123.1	138.2

NOZZLE ARRANGEMENT II: 90 DEGREE IMPINGEMENT

P(TM) = 100 PSIG P ATM = 14.6 PSIA X/D = 0.6

THETA	15	30	45	60	75	90	105	120		
P(TI)			- DIRECTIVITY INDEX -						SPL(R)	PWL
0.0	3.1	7.1	1.9	-2.1	-4.2	-4.2	-3.9	-4.3	117.5	132.7
2.00	2.5	6.6	2.1	-1.6	-3.9	-3.7	-3.2	-3.8	118.0	133.2
4.00	2.2	6.2	1.7	-1.6	-3.4	-2.9	-2.7	-2.9	118.5	133.6
6.00	1.9	5.9	1.6	-1.1	-2.9	-2.7	-2.3	-2.4	119.0	134.1
8.00	1.5	5.6	1.1	-0.7	-2.6	-2.2	-1.7	-2.0	119.6	134.8
10.00	1.3	5.1	0.9	-0.4	-2.4	-2.1	-1.5	-1.4	120.3	135.4
12.00	0.8	4.9	0.7	-0.1	-2.0	-1.8	-1.6	-1.5	120.9	136.0
14.00	1.1	4.9	1.3	-0.2	-2.0	-2.2	-1.4	-1.4	121.0	136.2
16.00	0.9	4.8	0.6	-0.2	-2.1	-2.0	-1.3	-1.1	120.8	135.9
18.00	1.0	4.9	0.7	-0.5	-2.4	-1.9	-1.3	-0.9	120.4	135.5
20.00	1.1	4.9	0.9	-0.6	-2.2	-1.9	-1.2	-1.0	120.0	135.1
22.00	1.0	5.1	1.2	-0.8	-2.5	-2.1	-1.4	-1.2	119.7	134.8
24.00	1.8	5.2	1.3	-0.8	-2.5	-2.3	-1.9	-1.6	119.3	134.4
26.00	1.5	5.4	1.8	-0.8	-2.5	-2.6	-2.1	-2.3	118.9	134.0
28.00	1.6	5.6	2.0	-1.2	-2.6	-2.6	-2.4	-2.5	118.6	133.7
30.00	1.9	5.5	2.3	-0.8	-2.6	-2.7	-2.6	-2.8	118.4	133.5
32.00	1.8	5.4	2.5	-0.8	-2.6	-2.7	-2.8	-3.2	118.4	133.5
34.00	1.7	5.4	2.5	-0.7	-2.1	-2.6	-2.7	-3.2	118.4	133.6
36.00	1.5	5.5	2.2	-0.7	-2.1	-2.5	-2.5	-3.2	118.6	133.8

NOZZLE ARRANGEMENT II: 90 DEGREE IMPINGEMENT
P(TM) = 100 PSIG P ATM = 14.6 PSIA X/D = 0.6, CONT'D.

38.00	1.2	5.2	2.4	-0.4	-2.2	-2.4	-2.4	-2.9	119.0	134.2
40.00	0.8	4.8	2.3	-0.4	-1.8	-2.3	-2.2	-2.9	119.5	134.6
42.00	0.9	4.7	1.5	-0.1	-1.4	-1.9	-2.0	-2.3	119.6	134.7
44.00	1.0	4.5	2.1	-0.1	-1.4	-1.8	-1.9	-2.5	120.2	135.4
46.00	0.6	4.1	2.0	0.1	-1.3	-1.8	-1.9	-2.2	120.5	135.6
48.00	0.6	4.0	2.0	-0.0	-1.1	-1.5	-1.7	-2.3	120.8	136.0
50.00	0.2	3.8	2.3	0.1	-0.9	-1.5	-1.8	-2.3	121.3	136.5

NOZZLE ARRANGEMENT II: 90 DEGREE IMPINGEMENT
P(TM) = 100 PSIG P ATM = 14.4 PSIA X/D = 0.8

THETA	15	30	45	60	75	90	105	120		
P(TI)			- DIRECTIVITY INDEX -						SPL(R)	PWL
0.0	2.9	7.1	2.0	-2.2	-4.3	-4.2	-3.8	-4.1	117.5	132.7
2.00	2.7	6.7	2.1	-1.7	-3.7	-3.7	-3.4	-3.9	117.7	132.9
4.00	2.5	6.4	1.7	-1.3	-3.3	-3.2	-2.8	-3.3	117.8	133.0
6.00	2.0	6.2	1.8	-1.2	-3.1	-3.1	-2.6	-3.2	118.3	133.5
8.00	1.4	6.0	1.4	-0.9	-2.8	-2.5	-2.5	-2.8	118.8	134.0
10.00	1.2	5.8	0.9	-0.8	-2.1	-2.0	-2.1	-2.4	119.4	134.6
12.00	0.7	5.4	0.2	-0.7	-1.6	-1.3	-1.8	-2.3	120.4	135.6
14.00	0.6	5.5	0.6	-0.9	-1.7	-1.3	-1.9	-2.6	120.9	136.1
16.00	1.2	5.4	0.4	-0.8	-2.0	-1.5	-1.3	-1.8	119.8	135.0
18.00	1.6	5.5	1.1	-1.3	-2.4	-2.2	-1.8	-1.8	118.8	134.0
20.00	2.1	5.8	1.4	-1.4	-2.5	-2.4	-2.2	-2.4	117.9	133.1
22.00	2.2	6.1	2.1	-1.6	-2.8	-3.1	-2.8	-3.3	117.2	132.4
24.00	2.4	6.2	2.2	-1.6	-2.6	-3.0	-3.1	-3.7	116.8	132.0
26.00	2.1	6.0	2.1	-1.4	-2.5	-2.9	-2.9	-3.4	117.1	132.3
28.00	2.3	5.7	1.7	-1.3	-2.2	-2.6	-2.3	-2.9	117.5	132.7
30.00	1.3	5.2	2.5	-1.1	-2.2	-2.5	-2.2	-2.4	118.2	133.4
32.00	1.9	5.1	1.2	-0.8	-2.1	-2.1	-1.8	-1.7	118.3	133.5
34.00	1.8	4.9	1.3	-0.6	-1.8	-1.8	-1.6	-1.7	118.8	134.0
36.00	1.7	4.9	0.8	-0.6	-1.7	-1.7	-1.4	-1.4	119.0	134.2
38.00	1.3	4.6	1.2	-0.5	-1.7	-1.8	-1.5	-1.3	119.3	134.5
40.00	1.7	4.4	0.7	-0.3	-1.7	-1.6	-1.3	-1.2	119.3	134.5
42.00	1.4	4.2	0.7	-0.2	-1.7	-1.6	-1.2	-1.2	119.6	134.8
44.00	1.3	4.3	0.6	-0.2	-1.6	-1.3	-1.3	-1.1	119.7	134.9
46.00	1.2	4.1	0.5	-0.1	-1.6	-1.5	-1.1	-1.0	120.0	135.2
48.00	1.5	4.0	0.5	0.0	-1.4	-1.4	-1.3	-1.3	120.1	135.3
50.00	1.4	3.9	0.6	0.0	-1.5	-1.5	-1.1	-1.1	120.2	135.4

NOZZLE ARRANGEMENT II: 90 DEGREE IMPINGEMENT
P(TM) = 100 PSIG P ATM = 14.6 PSIA X/D = 1.0

THETA	15	30	45	60	75	90	105	120		
P(TI)			- DIRECTIVITY INDEX -						SPL(R)	PWL
0.0	2.5	6.9	1.9	-2.0	-4.1	-4.1	-3.6	-4.2	117.7	132.8
2.00	2.2	6.9	1.9	-1.6	-3.7	-3.8	-3.5	-4.0	118.2	133.4
4.00	2.3	6.1	2.3	-1.4	-3.4	-3.1	-2.9	-3.6	118.2	133.3
6.00	1.4	6.6	1.9	-1.4	-3.2	-3.4	-3.4	-3.2	119.0	134.1
8.00	0.3	6.8	1.6	-1.0	-2.9	-3.0	-3.3	-4.4	119.6	134.7
10.00	-0.2	6.6	1.6	-0.4	-2.3	-2.7	-3.6	-4.5	120.1	135.3
12.00	-0.1	6.3	1.4	-0.4	-1.9	-2.4	-3.4	-4.2	120.3	135.4
14.00	0.2	6.3	1.4	-0.6	-2.3	-2.5	-3.2	-3.9	119.8	134.9

NOZZLE ARRANGEMENT II: 90 DEGREE IMPINGEMENT
P(TM) = 100 PSIG P ATM = 14.6 PSIA X/D = 1.0, CONT'D.

16.00	1.1	5.9	1.4	-0.5	-2.3	-2.6	-2.5	-2.9	118.7	133.8
18.00	2.2	5.1	1.6	-0.7	-2.1	-2.1	-1.9	-2.2	117.6	132.8
20.00	1.9	5.2	1.9	-0.8	-2.2	-2.2	-2.1	-2.7	117.0	132.1
22.00	2.1	5.1	2.1	-0.6	-2.0	-2.3	-2.3	-2.9	116.6	131.8
24.00	1.8	4.8	1.7	-0.5	-1.5	-1.9	-1.8	-3.5	116.9	132.0
26.00	1.5	4.2	1.8	-0.5	-1.6	-1.7	-1.6	-2.0	117.6	132.7
28.00	1.3	4.3	1.6	-0.3	-1.6	-1.6	-1.4	-2.0	117.9	133.0
30.00	1.5	4.0	1.9	-0.2	-1.6	-1.4	-1.4	-1.9	118.4	133.6
32.00	1.6	3.6	1.7	0.3	-1.5	-1.4	-1.3	-1.9	118.9	134.1
34.00	0.7	3.5	1.7	0.2	-1.4	-1.3	-1.1	-1.8	119.1	134.3
36.00	0.7	3.2	1.8	1.1	-1.6	-1.4	-1.5	-2.0	119.7	134.9
38.00	0.4	3.4	2.0	0.5	-1.5	-1.4	-1.6	-2.1	119.9	135.0
40.00	0.6	3.4	2.1	0.5	-1.4	-1.4	-1.6	-2.1	120.2	135.3
42.00	0.5	3.3	2.2	0.5	-1.4	-1.5	-1.7	-2.3	120.5	135.6
44.00	0.4	3.4	2.3	0.5	-1.5	-1.4	-1.6	-2.3	120.8	136.0
46.00	-0.1	3.4	2.4	0.6	-1.6	-1.5	-1.7	-2.6	121.2	136.3
48.00	-0.6	3.1	2.6	1.1	-1.4	-1.5	-1.9	-2.8	121.4	136.6
50.00	-0.7	3.3	2.6	1.0	-1.3	-1.6	-2.0	-3.0	121.8	136.9

NOZZLE ARRANGEMENT II: 90 DEGREE IMPINGEMENT
P(TM) = 100 PSIG P ATM = 14.6 PSIA X/D = 1.2

THETA	15	30	45	60	75	90	105	120		
P(TI)			- DIRECTIVITY INDEX -						SPL(R)	PWL
0.0	2.9	6.8	1.7	-1.9	-4.0	-3.7	-3.5	-3.7	117.8	132.9
2.00	2.8	6.8	2.3	-1.9	-3.9	-4.0	-3.8	-4.4	118.3	133.5
4.00	2.4	6.4	2.6	-1.8	-3.4	-3.9	-3.8	-4.1	118.5	133.6
6.00	2.8	6.5	1.8	-1.5	-3.2	-3.4	-3.2	-3.6	118.1	133.3
8.00	2.6	6.0	2.3	-1.2	-3.1	-3.1	-2.9	-3.2	117.8	133.0
10.00	2.7	5.9	2.1	-1.2	-3.0	-3.0	-2.7	-3.0	117.4	132.6
12.00	2.9	5.6	2.3	-0.8	-2.5	-3.0	-3.6	-3.1	116.7	131.9
14.00	2.9	5.4	2.2	-0.9	-2.1	-2.8	-2.9	-3.8	116.2	131.3
16.00	2.8	5.4	2.4	-0.6	-2.2	-3.0	-3.2	-4.3	115.8	130.9
18.00	2.7	5.0	2.4	-0.5	-1.6	-2.5	-2.9	-4.5	115.7	130.8
20.00	2.5	4.5	2.3	-0.4	-1.4	-2.0	-2.3	-3.8	116.1	131.2
22.00	1.7	4.1	2.1	-0.4	-1.1	-1.5	-1.8	-3.3	116.5	131.6
24.00	1.5	3.8	2.0	-0.4	-0.7	-1.4	-1.5	-3.3	117.1	132.2
26.00	1.3	3.5	2.1	0.1	-0.6	-1.4	-2.4	-2.8	117.5	132.6
28.00	2.6	3.4	1.9	-0.3	-0.8	-1.6	-1.6	-2.8	118.2	133.3
30.00	1.0	3.2	1.9	0.1	-0.7	-1.5	-1.1	-2.4	118.4	133.6
32.00	0.6	3.4	2.2	0.1	-0.6	-1.4	-1.3	-2.8	118.9	134.1
34.00	0.3	3.6	2.6	0.0	-1.0	-1.4	-1.7	-3.4	120.0	135.1
36.00	0.3	3.6	2.9	-0.0	-1.1	-1.6	-1.7	-3.5	120.3	135.5
38.00	-0.0	3.6	3.1	0.3	-1.4	-1.5	-1.8	-3.6	120.9	136.1
40.00	-0.7	3.5	3.3	0.7	-1.9	-1.4	-2.1	-3.9	121.4	136.6
42.00	-0.6	3.4	3.5	0.7	-2.1	-1.5	-2.4	-4.2	121.8	136.9
44.00	-1.0	3.1	3.7	0.7	-2.1	-2.0	-1.8	-4.4	122.1	137.2
46.00	-1.7	3.5	3.4	1.0	-2.1	-1.9	-1.7	-4.3	122.2	137.4
48.00	-1.6	3.5	2.8	1.9	-2.1	-2.1	-1.5	-4.4	122.6	137.8
50.00	-1.8	2.5	3.4	2.3	-2.4	-2.8	-1.6	-4.3	123.3	138.5

NOZZLE ARRANGEMENT II: 90 DEGREE IMPINGEMENT

P(TM) = 100 PSIG P ATM = 14.5 PSIA X/D = 1.3

THETA	15	30	45	60	75	90	105	120		
P(TI)			- DIRECTIVITY INDEX -						SPL(R)	PWL
0.0	3.0	6.8	1.8	-2.1	-4.1	-3.8	-3.3	-4.3	117.7	132.8
2.00	3.0	6.7	2.0	-1.8	-3.7	-3.8	-3.2	-4.0	117.5	132.7
4.00	2.9	6.6	2.1	-1.6	-3.6	-3.8	-3.5	-3.9	117.3	132.5
6.00	3.2	6.3	1.8	-1.8	-2.8	-3.1	-3.0	-4.5	117.3	132.4
8.00	3.1	6.5	2.0	-1.3	-3.4	-3.7	-3.9	-4.5	116.5	131.6
10.00	3.5	6.3	2.5	-1.7	-3.4	-3.7	-3.9	-5.2	116.2	131.3
12.00	3.6	6.0	2.6	-1.4	-2.9	-3.4	-4.0	-5.7	115.8	130.9
14.00	3.5	5.9	2.7	-1.0	-2.4	-3.0	-4.0	-5.8	115.3	130.5
16.00	3.1	5.4	2.8	-0.8	-1.8	-2.6	-3.7	-5.7	115.2	130.4
18.00	2.7	5.2	2.6	-0.7	-1.9	-2.0	-3.3	-5.2	115.3	130.4
20.00	2.6	4.9	2.5	-0.3	-1.6	-1.8	-2.9	-5.3	115.3	130.5
22.00	2.2	4.7	2.1	0.2	-1.1	-1.7	-2.9	-5.1	115.3	130.4
24.00	2.1	4.2	1.9	0.3	-1.0	-1.2	-2.4	-4.5	115.7	130.8
26.00	1.9	4.2	1.9	0.0	-1.1	-1.3	-2.3	-4.1	116.3	131.4
28.00	1.4	3.8	1.7	0.3	-0.7	-0.9	-2.4	-3.9	116.7	131.8
30.00	1.2	3.6	1.8	0.4	-1.0	-0.5	-1.9	-3.5	117.0	132.2
32.00	0.8	3.7	2.0	0.3	-1.0	-0.8	-2.0	-3.3	117.5	132.6
34.00	0.8	3.6	2.1	0.3	-1.2	-0.7	-1.8	-3.2	117.7	132.9
36.00	0.3	3.5	2.2	0.4	-1.3	-0.8	-1.9	-3.3	118.3	133.4
38.00	0.3	3.5	2.1	0.3	-1.0	-0.8	-2.2	-3.2	118.7	133.8
40.00	0.0	3.6	2.4	0.6	-1.4	-1.0	-2.0	-3.5	119.2	134.3
42.00	-0.9	3.8	2.9	0.4	-1.6	-1.5	-1.4	-4.3	120.4	135.5
44.00	-3.0	4.1	3.0	0.6	-1.7	-1.7	-1.0	-4.9	121.5	136.7
46.00	-2.3	3.9	2.9	0.6	-1.9	-1.7	-0.8	-4.6	121.9	137.0
48.00	-2.4	3.8	3.0	1.0	-1.7	-2.4	-1.0	-4.4	122.2	137.4
50.00	-1.9	3.5	3.2	1.2	-1.8	-2.2	-1.5	-4.6	122.2	137.3

NOZZLE ARRANGEMENT II: 90 DEGREE IMPINGEMENT

P(TM) = 100 PSIG P ATM = 14.4 PSIA X/D = 1.4

THETA	15	30	45	60	75	90	105	120		
P(TI)			- DIRECTIVITY INDEX -						SPL(R)	PWL
0.0	1.5	6.6	2.3	-1.8	-3.6	-3.4	-3.1	-3.3	117.8	133.1
2.00	3.6	6.5	1.4	-1.8	-3.6	-3.4	-3.2	-3.4	117.7	132.9
4.00	3.9	6.5	1.3	-1.6	-3.6	-3.7	-3.3	-3.1	117.2	132.4
6.00	3.6	6.6	2.1	-1.8	-3.8	-4.3	-3.8	-3.6	117.0	132.2
8.00	3.6	6.6	2.3	-1.7	-3.6	-3.9	-3.7	-4.7	116.3	131.5
10.00	3.6	6.3	2.4	-1.6	-3.4	-3.7	-3.6	-4.9	116.0	131.2
12.00	3.8	5.8	2.4	-1.2	-2.9	-3.1	-3.3	-4.8	115.5	130.7
14.00	3.5	5.6	1.8	-1.2	-2.2	-2.5	-2.8	-4.3	115.4	130.6
16.00	3.1	5.1	2.0	-0.8	-2.0	-2.2	-2.1	-3.9	115.5	130.7
18.00	3.0	4.8	2.1	-0.1	-2.0	-2.1	-2.4	-4.3	115.7	130.9
20.00	2.9	4.7	2.1	-0.2	-1.4	-2.0	-2.4	-4.4	115.6	130.8
22.00	2.5	4.4	2.2	-0.0	-1.4	-1.8	-2.2	-4.3	115.8	131.0
24.00	2.0	4.1	1.7	0.1	-0.9	-1.4	-2.0	-3.9	116.3	131.5
26.00	1.3	3.0	1.2	1.1	-0.1	-0.5	-2.0	-3.8	117.6	132.8
28.00	0.4	2.2	1.2	1.4	0.1	-0.5	-1.8	-3.5	118.7	133.9
30.00	0.5	2.4	1.1	2.0	-0.5	-0.9	-2.0	-3.3	118.8	134.0
32.00	1.9	3.9	1.5	0.1	-1.2	-1.0	-1.8	-3.1	117.1	132.3
34.00	1.8	3.9	1.7	-0.0	-1.3	-0.8	-1.8	-3.0	117.3	132.5
36.00	1.6	3.8	1.7	0.3	-1.4	-0.9	-1.9	-3.0	117.7	132.9

NOZZLE ARRANGEMENT II: 90 DEGREE IMPINGEMENT
P(TM) = 100 PSIG P ATM = 14.4 PSIA X/D = 1.4, CONT'D.

38.00	1.7	3.8	1.7	0.2	-1.5	-0.8	-1.6	-3.0	118.0	133.2
40.00	1.3	3.7	1.8	-0.1	-1.4	-0.8	-1.6	-3.1	118.5	133.6
42.00	0.9	3.8	1.9	0.1	-1.2	-0.9	-1.7	-3.3	118.9	134.1
44.00	1.4	3.8	2.1	0.2	-1.6	-1.0	-1.4	-3.5	119.5	134.7
46.00	2.3	3.7	3.8	0.5	-2.8	-3.0	-2.3	-4.2	122.0	137.2
48.00	3.5	3.1	4.0	0.7	-3.2	-3.0	-3.0	-5.5	123.2	138.3
50.00	2.4	3.0	4.2	0.9	-2.6	-3.5	-2.6	-5.5	123.1	138.3

NOZZLE ARRANGEMENT II: 90 DEGREE IMPINGEMENT
P(TM) = 100 PSIG P ATM = 14.5 PSIA X/D = 1.6

THETA	15	30	45	60	75	90	105	120		
P(TI)			- DIRECTIVITY INDEX -						SPL(R)	PWL
0.0	2.8	6.7	2.1	-2.1	-4.0	-3.7	-3.5	-4.1	117.3	132.4
2.00	3.3	6.7	2.0	-2.2	-3.8	-3.8	-3.6	-4.1	117.1	132.3
4.00	3.3	6.9	2.1	-2.2	-4.1	-3.9	-3.9	-4.8	116.7	131.9
6.00	3.4	6.7	2.2	-2.2	-3.9	-3.8	-4.0	-4.9	116.3	131.4
8.00	3.5	6.4	2.3	-2.2	-3.2	-3.2	-3.7	-4.5	116.0	131.2
10.00	3.5	6.2	2.0	-2.0	-2.9	-2.8	-3.2	-4.3	116.0	131.2
12.00	3.3	5.9	1.8	-1.7	-2.5	-2.5	-3.0	-4.3	116.0	131.1
14.00	3.3	5.9	1.6	-0.9	-2.5	-2.3	-2.8	-4.2	115.7	130.9
16.00	2.8	5.5	1.8	-0.8	-1.9	-2.3	-3.0	-4.5	115.5	130.6
18.00	3.1	5.5	2.0	-0.6	-1.4	-2.3	-3.2	-5.1	115.2	130.4
20.00	2.3	5.4	2.0	-0.3	-1.2	-2.1	-3.1	-5.6	115.4	130.6
22.00	2.0	4.7	2.0	0.2	-0.9	-1.8	-2.4	-5.0	115.7	130.9
24.00	1.4	4.6	1.4	0.1	-0.9	-1.1	-2.1	-4.2	115.9	131.1
26.00	2.2	4.2	1.8	0.2	-1.1	-0.7	-2.6	-4.2	115.8	131.0
28.00	2.1	4.8	2.0	0.1	-1.3	-0.9	-3.5	-5.0	115.7	130.9
30.00	1.8	4.6	2.1	0.3	-1.3	-1.8	-2.0	-5.3	116.0	131.2
32.00	1.9	4.6	1.9	0.0	-1.2	-0.7	-3.2	-5.4	116.2	131.4
34.00	1.7	4.5	2.0	0.0	-1.0	-0.6	-3.1	-5.8	116.5	131.7
36.00	1.5	4.2	1.9	0.1	-0.9	-0.4	-3.1	-5.5	116.9	132.1
38.00	1.2	4.2	2.2	0.2	-0.9	-0.4	-3.0	-5.9	117.3	132.5
40.00	1.0	4.1	1.7	0.1	-0.6	0.2	-2.8	-5.7	117.6	132.8
42.00	1.1	3.8	1.9	0.3	-0.6	0.2	-2.6	-6.0	118.2	133.5
44.00	0.9	3.6	1.6	0.4	-0.4	0.4	-2.8	-6.3	118.8	134.0
46.00	0.6	3.4	1.8	0.2	-0.4	0.5	-2.6	-6.5	119.1	134.3
48.00	0.7	3.2	2.0	0.3	-0.2	0.3	-3.0	-6.5	119.3	134.5
50.00	1.1	3.7	1.7	0.3	-0.2	0.1	-2.9	-6.3	119.6	134.8

NOZZLE ARRANGEMENT II: 90 DEGREE IMPINGEMENT
P(TM) = 150 PSIG P ATM = 14.7 PSIA X/D = 1.2

THETA	15	30	45	60	75	90	105	120		
P(TI)			- DIRECTIVITY INDEX -						SPL(R)	PWL
0.0	2.8	5.7	1.7	-1.4	-3.1	-2.7	-2.1	-2.8	117.3	132.4
3.00	1.7	7.9	1.0	-3.2	-4.5	-4.6	-4.3	-5.0	119.1	134.1
6.00	1.4	7.7	1.0	-2.7	-4.3	-4.1	-4.0	-4.8	119.3	134.3
9.00	1.4	7.9	0.5	-3.5	-3.8	-3.4	-4.2	-5.1	119.9	135.0
12.00	-1.7	6.8	1.4	-1.6	-3.0	-1.9	-1.8	-6.7	122.3	137.4
15.00	-3.1	6.5	1.4	-1.1	-2.5	-0.9	-3.5	-4.4	122.7	137.8
18.00	-2.2	6.4	1.4	-1.3	-2.2	-1.0	-3.6	-4.1	122.4	137.4
21.00	-0.3	6.4	1.3	-1.4	-2.4	-1.3	-3.1	-4.5	121.5	136.5

NOZZLE ARRANGEMENT II: 90 DEGREE IMPINGEMENT
P(TM) = 150 PSIG P ATM = 14.7 PSIA X/D = 1.2, CONT'D.

24.00	2.1	6.1	1.5	-1.7	-2.5	-2.0	-2.6	-3.4	120.0	135.1
27.00	3.6	5.8	1.4	-1.8	-2.8	-2.5	-2.4	-3.3	119.1	134.1
30.00	2.9	5.7	1.3	-1.4	-2.3	-2.2	-2.4	-3.0	118.9	134.0
33.00	2.9	5.3	0.6	-1.2	-2.0	-1.7	-1.5	-2.0	119.3	134.4
36.00	2.2	4.5	0.4	-0.6	-1.7	-1.4	-1.0	-1.4	120.0	135.1
39.00	2.0	3.8	-0.2	-0.5	-1.5	-1.0	-0.6	-0.7	120.4	135.5
42.00	1.0	3.7	-0.1	0.2	-1.4	-0.9	-0.6	-0.7	120.9	136.0
45.00	1.1	3.9	-0.0	-0.1	-1.5	-0.9	-0.6	-0.7	121.3	136.4
48.00	0.9	3.6	0.0	0.2	-1.3	-0.9	-0.8	-0.9	121.7	136.8

NOZZLE ARRANGEMENT II: 90 DEGREE IMPINGEMENT
P(TM) = 200 PSIG P ATM = 14.6 PSIA X/D = 1.2

THETA	15	30	45	60	75	90	105	120		
P(TI)			- DIRECTIVITY INDEX -						SPL(R)	PWL
0.0	2.6	6.1	1.3	-1.4	-2.9	-2.4	-2.4	-3.1	120.4	135.5
4.00	0.8	6.5	1.8	-1.5	-3.1	-2.7	-2.6	-3.1	121.6	136.8
8.00	1.0	6.1	1.3	-1.2	-3.1	-2.3	-2.2	-2.6	122.5	137.6
12.00	0.8	5.6	0.1	-0.7	-2.4	-1.5	-1.4	-1.7	123.7	138.8
16.00	0.7	6.2	-0.1	-1.3	-3.0	-0.0	-2.5	-3.1	125.3	140.4
20.00	1.5	6.2	-0.0	-1.3	-3.0	-0.5	-2.2	-3.0	124.0	139.2
24.00	2.3	6.5	0.4	-1.7	-2.9	-2.7	-2.2	-2.7	122.2	137.3
28.00	2.5	7.0	1.0	-2.4	-3.3	-2.8	-3.1	-3.7	120.8	135.9
32.00	2.7	7.1	1.2	-2.7	-3.3	-3.2	-3.5	-4.1	120.6	135.7
36.00	2.6	6.5	0.9	-2.0	-2.6	-2.5	-2.6	-3.0	120.6	135.8
40.00	1.6	5.9	0.2	-1.2	-2.4	-1.8	-1.6	-1.9	121.6	136.7
44.00	1.5	5.1	-0.4	-0.9	-1.9	-1.4	-0.9	-1.2	122.2	137.3
48.00	1.9	5.0	-0.5	-0.7	-1.8	-1.4	-0.9	-1.2	122.7	137.8

NOZZLE ARRANGEMENT III: 90 DEGREE IMPINGEMENT
P(TM) = 100 PSIG P ATM = 14.4 PSIA X/D = 0.6

THETA	15	30	45	60	75	90	105	120		
P(TI)			- DIRECTIVITY INDEX -						SPL(R)	PWL
0.0	2.2	6.6	2.2	-1.8	-4.1	-3.6	-3.4	-3.6	118.1	133.2
2.00	1.8	5.9	2.1	-1.5	-3.4	-2.9	-2.5	-2.5	118.5	133.6
4.00	1.3	5.6	1.9	-1.2	-2.9	-2.5	-1.8	-2.0	119.2	134.3
6.00	0.6	4.8	1.6	-0.8	-2.3	-2.1	-1.3	-1.2	120.4	135.5
8.00	-0.4	4.5	1.4	-0.4	-2.0	-1.8	-1.2	-0.9	121.8	136.9
10.00	-0.1	4.4	2.8	0.0	-2.3	-2.6	-2.1	-1.9	122.7	137.8
12.00	1.4	4.2	3.0	1.1	-2.1	-3.3	-3.2	-3.0	123.7	138.9
14.00	1.5	3.4	3.0	2.0	-2.9	-3.5	-3.4	-3.0	124.0	139.1
16.00	1.2	3.7	3.0	1.4	-2.5	-2.2	-3.4	-3.0	123.6	138.7
18.00	1.7	4.1	3.0	0.9	-2.5	-1.8	-3.6	-3.4	123.1	138.3
20.00	0.8	4.4	3.2	0.8	-2.7	-1.9	-3.5	-3.7	122.4	137.6
22.00	-0.2	4.9	3.3	0.6	-2.6	-2.6	-4.0	-4.0	122.4	137.5
24.00	-0.7	5.0	3.6	0.6	-2.6	-3.1	-3.9	-3.9	122.2	137.4
26.00	-1.0	4.7	3.7	0.8	-2.1	-3.0	-4.2	-3.9	122.3	137.5
28.00	-0.6	4.7	3.0	0.2	-1.8	-2.3	-3.5	-3.5	122.3	137.4
30.00	-1.2	4.4	3.0	0.4	-1.5	-2.2	-3.0	-3.6	122.7	137.8

NOZZLE ARRANGEMENT III: 90 DEGREE IMPINGEMENT
P(TM) = 100 PSIG P ATM = 14.4 PSIA X/D = 0.8

THETA	15	30	45	60	75	90	105	120		
P(TI)				- DIRECTIVITY INDEX -					SPL(R)	PWL
0.0	2.2	6.6	2.5	-1.8	-4.1	-3.8	-3.3	-3.6	118.1	133.3
2.00	2.0	6.1	1.8	-1.6	-3.3	-3.0	-2.5	-2.7	118.5	133.6
4.00	1.8	5.9	2.1	-1.1	-3.3	-2.7	-2.4	-2.5	119.2	134.4
6.00	1.3	5.7	1.9	-0.7	-3.5	-2.0	-2.2	-2.6	120.2	135.4
8.00	0.3	5.4	2.3	-0.5	-3.5	-1.9	-2.2	-2.8	121.4	136.5
10.00	-0.4	5.5	2.0	-0.5	-3.8	-1.3	-2.2	-2.9	122.0	137.1
12.00	-0.6	5.2	2.4	-0.3	-3.8	-1.1	-2.0	-2.7	121.8	137.0
14.00	0.1	5.6	1.9	-0.6	-3.3	-1.5	-2.0	-2.5	121.1	136.3
16.00	0.7	5.0	2.1	-0.2	-2.9	-1.8	-2.0	-2.1	120.4	135.6
18.00	1.4	5.2	2.3	-0.9	-2.8	-2.0	-2.0	-2.1	119.6	134.8
20.00	1.8	5.1	2.5	-0.7	-2.7	-1.7	-2.6	-2.7	119.2	134.4
22.00	1.4	5.4	2.3	-0.7	-2.7	-2.1	-2.8	-3.0	118.9	134.0
24.00	0.9	5.5	2.6	-0.7	-2.4	-2.2	-2.9	-3.2	118.9	134.1
26.00	0.9	5.1	2.3	-0.3	-2.4	-2.0	-2.6	-3.0	119.1	134.2
28.00	0.5	4.7	2.4	-0.4	-2.1	-1.5	-2.6	-2.6	119.6	134.7
30.00	0.2	4.6	1.4	-0.1	-1.7	-1.3	-2.2	-1.9	119.9	135.0

NOZZLE ARRANGEMENT III: 90 DEGREE IMPINGEMENT
P(TM) = 100 PSIG P ATM = 14.4 PSIA X/D = 1.0

THETA	15	30	45	60	75	90	105	120		
P(TI)				- DIRECTIVITY INDEX -					SPL(R)	PWL
0.0	2.3	5.6	2.3	0.3	-1.9	-4.4	-3.9	-3.9	118.7	133.8
2.00	2.2	6.2	2.4	-1.8	-3.5	-3.2	-2.6	-2.9	118.1	133.3
4.00	1.9	6.2	2.0	-1.1	-3.2	-3.3	-2.8	-3.3	118.6	133.7
6.00	0.7	6.4	2.3	-0.9	-3.3	-3.5	-3.3	-4.0	119.6	134.7
8.00	-0.4	6.2	2.1	0.0	-3.2	-3.1	-3.5	-3.9	120.1	135.2
10.00	-1.3	6.0	2.6	0.2	-3.0	-2.8	-3.8	-4.3	120.8	135.9
12.00	-1.0	5.8	2.5	0.5	-3.4	-2.2	-4.0	-4.4	120.7	135.8
14.00	-0.2	5.9	2.5	0.1	-3.2	-2.5	-3.8	-4.2	120.2	135.3
16.00	1.0	5.9	2.3	-0.6	-2.9	-2.8	-2.9	-2.9	118.7	133.9
18.00	1.9	5.3	2.0	-1.2	-2.3	-2.5	-2.3	-2.3	117.6	132.7
20.00	2.3	5.0	1.9	-1.2	-2.0	-2.1	-2.0	-1.9	117.1	132.3
22.00	2.1	4.8	1.6	-1.0	-2.0	-2.0	-1.7	-1.5	117.3	132.5
24.00	2.0	4.6	1.0	-0.6	-1.8	-1.6	-1.5	-1.0	117.5	132.7
26.00	1.5	4.2	0.9	0.3	-2.1	-1.8	-1.3	-0.9	118.1	133.3
28.00	1.8	4.2	0.6	-0.4	-1.9	-1.6	-1.0	-0.7	118.2	133.4
30.00	1.4	4.1	0.7	-0.3	-2.0	-1.7	-1.0	-0.5	118.6	133.7

NOZZLE ARRANGEMENT III: 90 DEGREE IMPINGEMENT
P(TM) = 100 PSIG P ATM = 14.3 PSIA X/D = 1.1

THETA	15	30	45	60	75	90	105	120		
P(TI)				- DIRECTIVITY INDEX -					SPL(R)	PWL
0.0	2.3	6.3	2.4	-1.7	-3.6	-3.5	-3.0	-3.3	118.0	133.2
2.00	2.2	6.1	2.1	-1.2	-3.1	-3.0	-2.6	-3.1	118.4	133.6
4.00	2.1	6.1	2.1	-1.3	-3.1	-3.0	-2.6	-3.0	118.7	133.9
6.00	1.1	6.2	2.5	-0.9	-3.2	-3.3	-3.0	-3.3	119.2	134.4
8.00	0.5	6.2	2.5	-0.6	-3.1	-3.3	-3.2	-3.5	119.8	135.0
10.00	0.2	6.2	2.5	-0.4	-2.9	-3.4	-3.6	-4.2	120.1	135.3
12.00	0.1	6.1	2.7	-0.3	-3.2	-3.1	-3.4	-4.0	119.9	135.1
14.00	1.3	5.6	2.2	-0.3	-2.8	-2.6	-2.7	-2.8	118.8	134.0

NOZZLE ARRANGEMENT III: 90 DEGREE IMPINGEMENT
P(TM) = 100 PSIG P ATM = 14.3 PSIA X/D = 1.1, CONT'D.

16.00	1.9	4.5	2.2	-1.1	-1.7	-2.1	-1.9	-2.2	117.8	132.9
18.00	2.0	4.6	1.9	-0.8	-1.7	-2.0	-2.1	-2.1	117.5	132.6
20.00	1.4	4.3	1.8	-0.6	-1.8	-1.9	-1.6	-1.5	117.9	133.1
22.00	1.8	4.2	1.2	-0.5	-1.7	-1.7	-1.2	-0.8	118.1	133.3
24.00	1.2	3.9	1.1	-0.4	-1.6	-1.7	-0.9	-0.5	118.4	133.6
26.00	0.9	3.6	1.0	-0.6	-1.5	-1.5	-1.0	-0.3	118.7	133.8
28.00	1.0	3.5	0.8	-0.3	-1.5	-1.5	-0.9	-0.2	119.0	134.2
30.00	1.2	3.5	0.6	-0.2	-1.5	-1.5	-0.6	-0.0	119.1	134.3

NOZZLE ARRANGEMENT III: 90 DEGREE IMPINGEMENT
P(TM) = 100 PSIG P ATM = 14.3 PSIA X/D = 1.2

THETA	15	30	45	60	75	90	105	120		
P(TI)			- DIRECTIVITY INDEX -						SPL(R)	PWL
0.0	2.3	6.1	2.3	-1.1	-3.8	-3.2	-3.3	-3.5	118.5	133.6
2.00	2.3	5.6	2.7	-0.7	-3.5	-3.1	-2.8	-3.4	118.9	134.1
4.00	1.9	6.0	1.7	-1.3	-2.9	-2.7	-2.4	-2.7	118.6	133.8
6.00	1.9	5.9	2.1	-1.5	-3.0	-2.8	-2.5	-2.8	118.8	134.0
8.00	1.8	5.6	2.0	-1.0	-2.8	-2.7	-2.4	-2.6	118.6	133.8
10.00	2.0	5.3	2.2	-1.0	-2.7	-2.4	-2.4	-2.5	118.4	133.6
12.00	2.0	4.9	2.1	-0.9	-2.2	-2.2	-2.2	-2.0	117.7	132.9
14.00	1.7	5.0	2.9	-0.9	-1.4	-3.1	-3.0	-3.4	117.9	133.1
16.00	1.3	4.5	3.5	-0.5	-1.8	-2.0	-3.8	-3.7	118.3	133.5
18.00	0.7	4.2	3.2	0.7	-2.2	-2.4	-3.1	-3.1	119.0	134.2
20.00	1.0	4.0	2.5	0.2	-1.4	-1.8	-2.8	-2.8	118.8	133.9
22.00	1.8	3.9	1.6	0.1	-1.5	-1.7	-1.7	-1.6	118.0	133.2
24.00	1.3	3.5	1.3	0.4	-0.9	-1.8	-1.6	-1.4	119.0	134.2
26.00	0.9	3.2	1.4	0.4	-0.8	-1.6	-1.6	-1.3	119.8	135.0
28.00	1.0	3.1	1.0	0.4	-1.0	-1.4	-1.2	-1.2	119.7	134.8
30.00	0.8	3.4	0.8	-0.1	-1.2	-1.5	-0.7	-0.5	119.5	134.7

NOZZLE ARRANGEMENT III: 90 DEGREE IMPINGEMENT
P(TM) = 100 PSIG P ATM = 14.4 PSIA X/D = 1.3

THETA	15	30	45	60	75	90	105	120		
P(TI)			- DIRECTIVITY INDEX -						SPL(R)	PWL
0.0	1.8	5.2	0.8	1.3	-1.6	-1.3	-4.4	-5.0	120.1	135.2
2.00	0.6	5.0	1.6	1.1	-2.4	-0.7	-4.1	-3.7	120.3	135.5
4.00	1.0	4.4	2.0	1.3	-2.9	-0.8	-3.7	-3.8	120.1	135.2
6.00	0.5	5.2	1.9	0.1	-2.9	-1.2	-2.9	-3.5	119.5	134.6
8.00	2.5	4.2	1.6	0.0	-1.8	-1.6	-2.3	-2.3	118.7	133.8
10.00	2.0	4.7	1.7	0.3	-1.8	-1.7	-2.7	-2.7	117.9	133.1
12.00	2.7	4.9	1.8	-0.4	-1.9	-1.3	-3.3	-3.5	117.7	132.8
14.00	2.7	4.5	2.1	-0.0	-1.6	-1.4	-3.2	-3.0	117.8	133.0
16.00	2.2	4.2	1.4	1.0	-1.3	-1.7	-2.8	-2.6	118.2	133.4
18.00	2.3	3.5	1.6	0.4	-0.8	-1.3	-2.7	-2.5	118.4	133.5
20.00	2.4	3.5	1.9	0.2	-0.6	-1.6	-2.7	-2.3	118.7	133.8
22.00	2.1	3.6	1.6	0.3	-0.5	-1.7	-2.3	-1.9	119.3	134.5
24.00	1.5	3.0	2.2	0.7	-0.4	-1.6	-2.5	-2.3	120.4	135.6
26.00	1.6	3.0	1.9	0.9	-0.4	-1.7	-2.7	-2.3	120.9	136.0
28.00	0.5	2.9	1.6	0.9	-0.8	-0.8	-2.2	-1.8	120.7	135.8
30.00	0.7	3.3	1.5	0.5	-0.6	-1.5	-2.1	-1.8	121.1	136.2

NOZZLE ARRANGEMENT III: 90 DEGREE IMPINGEMENT

P(TM) = 100 PSIG P ATM = 14.4 PSIA X/D = 1.4

THETA	15	30	45	60	75	90	105	120		
P(TI)				- DIRECTIVITY INDEX -					SPL(R)	PWL
0.0	2.4	5.5	2.1	-0.7	-2.7	-1.6	-4.0	-2.5	119.2	134.5
1.00	3.7	5.7	1.5	-1.4	-2.4	-2.0	-3.1	-3.2	118.7	133.9
2.00	3.3	5.6	1.7	-1.6	-2.2	-1.4	-3.4	-3.2	118.9	134.1
3.10	2.6	5.4	1.1	-1.9	-1.5	-1.2	-2.8	-2.9	119.0	134.1
4.30	2.7	5.4	1.6	-1.3	-1.4	-2.0	-2.8	-2.7	118.5	133.7
5.60	3.2	5.2	1.7	-1.6	-1.9	-1.6	-3.0	-2.9	118.2	133.3
6.90	2.8	4.9	2.3	-1.8	-1.3	-1.6	-2.7	-2.9	118.2	133.4
8.30	2.2	4.6	2.7	-1.1	-2.0	-1.0	-3.5	-3.7	118.0	133.1
9.70	3.0	4.2	2.8	-1.2	-0.8	-1.1	-3.7	-4.3	118.0	133.1
11.20	2.1	4.8	2.2	-0.4	-0.9	-1.7	-3.6	-3.7	118.0	133.1
12.72	1.4	4.6	1.7	1.6	-1.9	-2.2	-4.1	-3.7	118.5	133.6
14.28	2.2	4.1	1.4	1.5	-1.0	-1.8	-3.8	-3.3	118.4	133.5
15.86	2.1	3.6	1.6	1.1	0.4	-2.2	-3.8	-3.6	118.5	133.6
17.41	2.1	4.2	1.9	-0.0	-0.6	-1.7	-3.2	-2.8	118.2	133.3
18.98	1.6	3.6	2.1	0.1	0.4	-2.1	-3.2	-2.6	118.5	133.7
20.54	1.9	2.8	1.1	1.6	0.3	-2.3	-3.2	-2.2	119.8	134.9
22.00	1.5	2.9	1.1	1.5	0.5	-2.4	-3.3	-2.6	120.2	135.3
24.00	1.4	2.9	0.8	1.5	-0.1	-1.8	-2.8	-2.0	120.4	135.5
26.00	1.8	2.8	1.5	0.5	0.5	-2.0	-2.7	-2.2	120.6	135.7
28.00	1.4	2.8	1.7	0.9	0.3	-1.8	-2.5	-2.2	120.9	136.1
30.00	1.8	3.1	1.7	0.5	-0.2	-1.8	-2.5	-2.0	121.1	136.2

APPENDIX D

TABULATED ACOUSTICAL DATA - 1/3 OCTAVE BAND SPECTRA

This appendix contains a representative sample of the 1/3 octave band spectra obtained in the interacting-jet noise investigations with main jet operated at 100 psig. The data are arranged in order of nozzle arrangement, x/D, and percent impingement. For each jet operating conditions, the sound pressure level dependence on frequency and azimuth angle, SPL(F,THETA) re 2 x 10^{-4} μbar, is tabulated. For each spectrum band, the power radiated in all directions is listed as PWL(F) in dB re 10^{-12} watt. For each azimuth angle, the wideband sound pressure level is computed from the 1/3 octave band data and entered as COMPUTED SPL(THETA), re 2 x 10^{-12} μbar. From these data is computed the total acoustic power which is denoted as a power level, PWL re 10^{-12} watt, and is noted also in watts.

In addition to the 1/3 octave band power spectra, and the directivity, which were discussed in the text, these tabulations permit examination of the spectrum dependence on azimuth angle and the directivity dependence on frequency.

MAIN JET ALONE

(OF NOZZLE ARRANGEMENT II AND III)

P(TM) = 100 PSIG P ATM = 14.6 PSIA

THETA	15	30	45	60	75	90	105	120	
FREQUENCY				- SPL(F,THETA) -					PWL(F)
315	82.0	0.0	0.0	0.0	0.0	0.0	0.0	0.0	83.4
400	85.4	81.4	0.0	0.0	0.0	0.0	0.0	0.0	89.3
500	88.8	84.8	0.0	0.0	0.0	0.0	0.0	0.0	92.7
630	91.7	88.6	81.7	0.0	0.0	0.0	0.0	0.0	96.5
800	95.1	91.8	85.0	0.0	0.0	0.0	0.0	0.0	99.8
1000	98.2	95.4	88.0	82.0	81.5	0.0	0.0	0.0	103.4
1250	101.3	98.9	92.0	85.4	84.3	82.6	81.3	0.0	107.0
1600	103.2	102.5	95.0	87.4	86.1	84.6	82.8	81.4	109.8
2000	104.9	105.8	98.3	89.9	88.0	86.8	85.2	83.9	112.6
2500	106.3	108.5	101.6	92.0	90.2	88.6	87.3	85.8	115.1
3150	107.6	111.0	104.7	94.2	92.1	90.6	88.7	87.8	117.5
4000	108.9	112.6	107.2	96.3	93.7	92.0	90.8	89.4	119.2
5000	109.7	113.8	109.1	98.0	95.1	93.3	92.0	90.9	120.6
6300	110.6	114.9	110.2	99.8	96.3	94.8	92.3	92.4	121.7
8000	111.9	115.2	110.3	101.1	97.6	95.8	93.8	95.3	122.1
10000	111.8	115.4	110.2	102.1	98.6	97.1	97.0	103.2	122.5
12500	111.4	114.5	109.2	102.6	99.2	99.3	104.8	106.7	122.5
16000	110.0	113.8	108.5	102.7	100.2	105.0	106.7	106.7	122.6
20000	107.3	112.3	107.8	103.0	102.3	105.8	105.4	105.0	121.6
25000	106.9	112.6	109.2	105.5	106.7	106.1	105.5	106.0	122.7
31500	105.2	111.5	109.4	107.1	107.0	105.3	106.4	106.6	122.7
40000	102.6	109.1	108.3	108.5	105.0	105.3	106.2	105.9	121.9
50000	100.2	107.1	107.0	107.4	104.1	104.9	105.4	104.3	120.7
63000	99.7	106.8	107.2	107.3	105.4	105.9	105.7	104.5	121.1
80000	96.1	104.0	104.6	104.8	104.0	104.1	103.5	101.9	118.9
100000	92.0	100.6	100.9	100.9	100.6	100.7	99.9	98.2	115.3

- COMPUTED SPL(THETA) -

THETA	15	30	45	60	75	90	105	120
	120.7	124.6	120.4	116.2	114.6	114.9	115.4	115.5

TOTAL ACOUSTIC POWER

PWL	WATTS
133.4	22.0

NOZZLE ARRANGEMENT I: 90 DEGREE IMPINGEMENT

P(TM) = 100 PSIG
P(TI) = 5 PSIG
P ATM = 14.6 PSIA
X/D = 0.6

THETA	15	30	45	60	75	90	105	120	
FREQUENCY				- SPL(F,THETA) -					PWL(F)
400	86.0	81.9	0.0	0.0	0.0	0.0	0.0	0.0	89.8
500	89.0	85.8	0.0	0.0	0.0	0.0	0.0	0.0	93.2
630	92.2	89.0	82.0	0.0	0.0	0.0	0.0	0.0	97.0
800	95.9	92.6	85.3	81.2	80.6	0.0	0.0	0.0	101.0
1000	99.9	97.3	89.3	84.2	84.0	82.2	0.0	0.0	105.3
1250	102.9	101.0	93.0	88.0	86.5	84.9	83.0	81.3	108.8
1600	104.4	104.1	96.1	89.4	88.5	86.8	85.0	83.4	111.3
2000	106.0	107.6	99.9	92.1	90.9	89.0	87.4	85.8	114.3
2500	108.0	111.0	103.6	94.8	93.5	91.5	89.8	88.0	117.4
3150	109.5	113.8	107.2	97.4	95.2	93.4	91.4	90.3	120.1
4000	111.0	115.9	110.2	100.0	97.2	95.1	93.5	92.4	122.3
5000	111.5	116.7	112.0	101.7	98.5	96.4	94.9	93.7	123.4
6300	112.2	117.3	113.0	103.6	100.3	98.2	96.6	96.3	124.2
8000	121.4	124.5	113.5	112.2	109.0	108.0	105.0	108.3	130.9
10000	113.0	117.8	113.0	105.3	102.7	101.7	104.8	109.2	125.4
12500	111.0	116.6	112.3	105.2	102.7	105.7	110.6	111.2	125.6
16000	110.1	116.5	111.2	106.0	105.1	115.1	111.9	109.9	127.1
20000	107.3	114.9	110.2	106.4	108.5	110.3	108.5	108.4	124.9
25000	106.2	114.0	110.0	108.5	111.0	108.1	109.0	108.8	125.0
31500	104.5	112.4	109.7	110.4	108.6	108.7	108.2	107.6	124.3
40000	103.7	110.9	109.2	111.8	107.5	107.8	107.7	106.6	123.9
50000	101.1	109.3	108.1	110.8	107.0	106.8	106.3	105.2	122.8
63000	100.0	107.5	107.8	108.9	106.5	106.5	105.9	104.2	121.8
80000	97.8	105.3	105.3	106.2	104.8	104.3	103.5	102.1	119.6
100000	96.1	104.1	104.3	105.2	104.1	103.6	102.6	101.1	118.6

- COMPUTED SPL(THETA) -

THETA	15	30	45	60	75	90	105	120
	124.3	128.6	122.7	119.9	118.2	119.6	118.7	118.6

TOTAL ACOUSTIC POWER

PWL	WATTS
137.0	49.6

NOZZLE ARRANGEMENT I: 90 DEGREE IMPINGEMENT

P(TM) = 100 PSIG
P(TI) = 8 PSIG
P ATM = 14.7 PSIA
X/D = 0.6

THETA	15	30	45	60	75	90	105	120	
FREQUENCY				- SPL(F,THETA) -					PWL(F)
400	85.9	0.0	0.0	0.0	0.0	0.0	0.0	0.0	87.2
500	89.2	85.8	0.0	0.0	0.0	0.0	0.0	0.0	93.3
630	92.0	89.0	0.0	0.0	0.0	0.0	0.0	0.0	96.3
800	95.5	92.7	86.0	82.2	82.0	0.0	0.0	0.0	101.1
1000	99.1	97.0	90.0	85.2	84.6	83.3	0.0	0.0	105.1
1250	102.6	101.0	94.2	88.4	87.8	86.1	84.3	0.0	108.9
1600	104.0	104.2	97.5	91.0	89.8	88.5	86.4	84.4	111.5
2000	105.5	107.5	100.8	93.6	92.3	90.6	88.8	87.2	114.3
2500	107.3	111.1	104.5	96.4	94.8	93.1	91.0	89.1	117.6
3150	108.8	113.8	108.0	99.0	97.0	95.1	93.2	92.0	120.3
4000	109.6	116.0	111.0	101.6	99.0	96.9	95.1	93.8	122.5
5000	110.5	116.2	112.8	103.1	100.1	98.0	96.2	95.2	123.4
6300	111.5	117.8	114.2	105.5	102.5	100.0	98.3	99.7	125.0
8000	123.2	128.6	116.5	114.5	114.0	112.0	109.0	115.0	134.6
10000	111.8	117.7	114.2	106.8	104.2	103.5	107.6	111.3	126.1
12500	109.9	116.5	113.0	106.7	104.5	108.0	113.0	112.8	126.6
16000	111.3	119.3	112.3	108.0	107.9	117.9	113.5	111.2	129.4
20000	106.5	115.3	111.0	108.3	110.5	111.4	110.2	110.3	126.1
25000	106.0	115.6	111.0	110.5	112.1	109.9	110.8	110.0	126.4
31500	104.2	113.4	110.2	112.2	109.9	110.5	109.5	108.6	125.6
40000	103.2	111.7	110.1	112.7	109.1	108.8	108.4	107.4	124.9
50000	100.6	110.2	109.0	111.4	108.3	107.8	107.0	105.8	123.6
63000	99.5	109.0	108.3	110.5	107.3	107.2	106.5	105.0	122.8
80000	96.3	106.6	106.1	106.9	105.5	105.1	104.1	102.5	120.3
100000	95.1	105.3	105.1	106.1	104.7	104.2	102.9	101.2	119.3

- COMPUTED SPL(THETA) -

THETA	15	30	45	60	75	90	105	120
	125.1	130.9	123.9	121.5	120.2	121.7	120.4	120.9

TOTAL ACOUSTIC POWER

PWL	WATTS
138.8	76.7

NOZZLE ARRANGEMENT I: 90 DEGREE IMPINGEMENT

P(TM) = 100 PSIG
P(TI) = 10 PSIG

P ATM = 14.5 PSIA
X/D = 0.6

THETA	15	30	45	60	75	90	105	120	
FREQUENCY				- SPL(F,THETA) -					PWL(F)
400	86.8	82.0	0.0	0.0	0.0	0.0	0.0	0.0	90.4
500	90.0	86.0	80.1	0.0	0.0	0.0	0.0	0.0	94.5
630	93.0	89.8	82.6	0.0	0.0	0.0	0.0	0.0	97.8
800	96.2	93.3	86.5	82.0	81.2	0.0	0.0	0.0	101.7
1000	100.0	97.5	89.6	85.0	84.0	82.6	81.0	0.0	105.7
1250	103.2	101.5	94.0	87.7	87.4	86.0	83.8	81.8	109.4
1600	104.8	104.5	96.8	90.1	89.2	88.0	86.0	84.2	111.8
2000	106.0	108.0	100.9	92.9	91.8	90.0	88.0	86.6	114.8
2500	108.0	111.4	104.8	95.5	94.4	92.0	90.2	89.0	117.9
3150	109.9	114.2	108.1	97.9	96.0	94.0	92.2	91.0	120.7
4000	110.8	116.5	111.2	100.8	98.0	96.1	94.2	93.2	123.0
5000	111.0	117.0	112.6	102.0	99.1	97.3	95.6	94.7	123.8
6300	112.2	118.0	113.9	104.4	101.8	99.1	97.2	99.0	125.0
8000	122.2	126.0	114.5	112.8	110.0	109.0	103.5	112.8	132.3
10000	111.3	117.9	113.9	105.8	103.1	102.5	106.9	111.0	126.0
12500	109.0	117.0	113.0	105.8	103.5	107.5	112.0	111.6	126.3
16000	109.6	117.5	112.1	106.7	106.5	115.9	112.1	109.5	127.8
20000	106.8	114.8	110.5	107.1	109.5	110.3	108.4	108.5	125.1
25000	105.5	114.0	110.5	109.0	111.0	108.0	109.3	108.0	125.1
31500	103.2	112.4	109.7	111.2	108.6	108.7	108.1	107.1	124.5
40000	101.7	110.7	109.1	112.0	107.7	107.3	106.8	106.1	123.8
50000	99.8	109.3	108.7	110.8	106.9	106.7	105.7	104.7	122.8
63000	97.0	107.5	107.8	108.8	106.2	106.0	105.0	103.2	121.6
80000	95.3	104.8	105.3	105.9	104.3	104.0	102.4	101.3	119.2
100000	92.8	103.7	104.1	104.9	103.6	103.1	101.7	100.3	118.2

- COMPUTED SPL(THETA) -

THETA	15	30	45	60	75	90	105	120
	124.4	129.4	123.3	120.3	118.5	120.0	118.9	119.4

TOTAL ACOUSTIC POWER

PWL	WATTS
137.6	57.8

NOZZLE ARRANGEMENT I: 90 DEGREE IMPINGEMENT

P(TM) = 100 PSIG
P(TI) = 15 PSIG

P ATM = 14.5 PSIA
X/D = 0.6

THETA	15	30	45	60	75	90	105	120	
FREQUENCY				- SPL(F,THETA) -					PWL(F)
400	87.8	82.8	0.0	0.0	0.0	0.0	0.0	0.0	91.3
500	91.6	86.7	80.4	0.0	0.0	0.0	0.0	0.0	95.7
630	94.5	90.2	83.0	0.0	0.0	0.0	0.0	0.0	98.7
800	98.0	94.0	86.6	81.8	81.0	0.0	0.0	0.0	102.7
1000	100.6	98.0	89.9	84.1	83.2	82.0	80.1	0.0	106.1
1250	104.0	101.2	93.0	86.7	86.0	84.0	82.2	81.2	109.3
1600	106.0	104.8	96.1	89.0	88.0	86.0	84.4	83.0	112.1
2000	107.6	108.2	99.7	91.5	90.2	88.0	86.8	85.2	114.9
2500	109.0	111.0	102.8	93.7	92.0	90.2	88.9	87.1	117.4
3150	110.0	113.2	106.0	96.0	93.8	92.0	90.3	89.6	119.5
4000	110.8	115.1	108.6	98.1	95.4	93.9	92.2	91.1	121.4
5000	111.2	116.0	110.3	99.2	96.5	95.0	93.9	92.7	122.5
6300	112.0	117.0	112.3	101.2	98.8	96.6	95.2	94.6	123.7
8000	113.0	118.0	113.0	103.2	101.0	98.8	97.7	99.2	124.8
10000	111.6	117.8	112.9	103.8	101.0	99.9	102.3	106.8	124.9
12500	110.4	117.0	112.0	104.0	101.1	102.9	108.5	109.0	125.0
16000	109.1	115.9	111.1	104.9	102.7	108.1	108.9	108.1	124.7
20000	106.1	113.8	110.2	105.3	105.6	108.3	106.8	108.1	123.7
25000	105.0	112.3	109.9	106.5	108.0	107.0	108.2	108.0	123.6
31500	103.2	110.2	109.0	108.1	106.4	107.2	107.3	106.7	122.8
40000	101.7	108.7	108.4	109.2	106.0	107.2	106.7	105.7	122.5
50000	98.3	106.3	108.8	108.8	106.3	106.1	105.1	104.6	121.8
63000	96.2	104.7	106.8	106.8	106.1	105.3	105.0	103.2	120.6
80000	92.8	101.5	103.8	104.3	104.0	103.9	102.7	101.0	118.3
100000	91.9	100.9	103.1	103.3	103.3	103.0	101.5	99.7	117.4

- COMPUTED SPL(THETA) -

THETA	15	30	45	60	75	90	105	120
	121.4	126.5	122.1	117.3	115.9	116.6	116.9	116.9

TOTAL ACOUSTIC POWER

PWL	WATTS
135.1	32.0

NOZZLE ARRANGEMENT I: 90 DEGREE IMPINGEMENT

P(TM) = 100 PSIG P ATM = 14.5 PSIA
P(TI) = 18 PSIG X/D = 0.6

THETA	15	30	45	60	75	90	105	120	
FREQUENCY				- SPL(F,THETA) -					PWL(F)
400	88.2	83.5	0.0	0.0	0.0	0.0	0.0	0.0	91.8
500	91.5	87.5	80.8	0.0	0.0	0.0	0.0	0.0	95.9
630	95.0	91.2	83.5	0.0	0.0	0.0	0.0	0.0	99.4
800	98.1	94.6	87.0	82.0	81.2	0.0	0.0	0.0	103.0
1000	101.0	98.2	90.0	84.6	83.6	82.0	0.0	0.0	106.2
1250	104.0	102.1	93.6	87.0	86.2	84.5	82.8	81.5	109.7
1600	106.0	105.6	96.9	89.5	88.1	86.5	84.8	83.0	112.6
2000	107.6	108.6	100.1	91.8	90.2	88.4	87.0	85.8	115.2
2500	108.8	111.3	103.3	94.0	92.0	90.3	89.0	87.4	117.6
3150	109.8	113.3	106.0	96.1	93.8	92.1	90.5	89.5	119.6
4000	110.3	115.0	108.9	98.3	95.6	94.0	92.5	91.6	121.3
5000	110.6	115.8	110.7	99.7	96.7	95.0	94.0	92.9	122.4
6300	111.0	116.5	112.4	101.5	98.3	96.5	95.5	94.7	123.4
8000	111.0	117.0	113.3	102.8	99.7	97.9	96.8	96.6	124.0
10000	110.8	117.5	113.2	103.8	100.5	98.9	98.9	101.1	124.4
12500	109.8	117.1	112.7	104.5	101.1	100.5	102.9	103.2	124.2
16000	109.1	115.8	111.8	105.3	102.1	103.1	103.9	104.8	123.6
20000	106.8	113.8	110.6	105.3	103.2	103.5	105.1	108.6	123.1
25000	105.5	112.3	110.4	106.0	104.9	105.0	109.8	109.0	123.6
31500	104.7	110.7	109.4	106.5	105.2	108.7	108.9	106.9	123.2
40000	101.7	108.8	109.0	107.0	106.2	108.8	106.9	106.2	122.6
50000	99.7	106.5	110.6	107.1	107.4	106.5	106.4	106.0	122.4
63000	97.6	104.5	107.2	106.2	107.0	106.0	105.6	103.7	120.9
80000	94.3	102.0	104.3	104.6	104.3	104.3	103.3	101.3	118.7
100000	92.6	100.6	103.7	104.1	104.0	103.5	102.1	100.1	117.9

- COMPUTED SPL(THETA) -

THETA	15	30	45	60	75	90	105	120
	120.9	126.3	122.6	116.6	115.5	116.0	116.4	116.1

TOTAL ACOUSTIC POWER

PWL	WATTS
134.8	30.2

NOZZLE ARRANGEMENT I: 90 DEGREE IMPINGEMENT

P(TM) = 100 PSIG
P(TI) = 20 PSIG

P ATM = 14.5 PSIA
X/D = 0.6

THETA	15	30	45	60	75	90	105	120	
FREQUENCY				- SPL(F,THETA) -					PWL(F)
400	88.5	83.0	0.0	0.0	0.0	0.0	0.0	0.0	91.8
500	91.5	87.2	80.2	0.0	0.0	0.0	0.0	0.0	95.8
630	94.5	90.3	83.0	0.0	0.0	0.0	0.0	0.0	98.8
800	98.0	94.0	86.5	81.8	81.0	0.0	0.0	0.0	102.7
1000	100.7	98.0	89.9	84.3	83.5	82.0	80.5	0.0	106.1
1250	103.7	101.8	93.2	87.2	85.8	84.2	82.8	81.3	109.5
1600	106.0	105.0	96.6	89.2	88.0	86.2	84.8	83.0	112.3
2000	107.6	107.4	99.6	91.7	90.0	88.3	87.0	85.5	114.5
2500	108.6	110.9	102.8	94.0	92.0	90.6	89.0	87.6	117.3
3150	109.7	113.0	105.5	96.0	93.6	92.1	90.6	89.8	119.3
4000	110.3	114.8	109.4	98.1	95.3	93.9	92.5	91.4	121.4
5000	110.5	115.5	110.2	99.5	96.5	95.0	93.8	92.8	122.1
6300	111.0	116.1	112.0	101.3	98.0	96.7	95.0	94.4	123.1
8000	111.2	116.8	112.5	102.5	99.2	97.5	96.2	96.0	123.7
10000	110.8	117.0	112.9	103.5	100.2	98.7	98.0	100.0	124.0
12500	109.8	116.3	111.9	104.0	100.5	99.8	101.0	102.0	123.5
16000	109.1	115.6	111.0	104.4	101.1	102.1	102.1	103.3	123.1
20000	106.3	113.2	109.8	104.4	101.9	102.3	103.9	107.6	122.3
25000	105.0	112.0	109.3	105.1	103.2	104.1	108.8	108.2	122.8
31500	103.2	109.7	108.2	105.2	103.4	107.7	107.4	105.8	122.0
40000	100.7	107.9	107.8	105.5	105.0	107.7	105.7	104.9	121.4
50000	98.8	105.8	110.3	105.8	106.0	105.8	104.9	103.8	121.4
63000	96.5	104.0	105.9	104.9	105.9	104.9	104.0	102.6	119.8
80000	92.8	101.2	103.2	103.4	103.3	103.3	101.9	100.1	117.6
100000	91.6	99.6	102.4	102.8	102.5	102.1	100.8	98.6	116.6

- COMPUTED SPL(THETA) -

THETA	15	30	45	60	75	90	105	120
	120.8	125.9	122.0	115.7	114.3	115.1	115.1	114.9

TOTAL ACOUSTIC POWER

PWL	WATTS
134.2	26.0

NOZZLE ARRANGEMENT I: 90 DEGREE IMPINGEMENT

P(TM) = 100 PSIG
P(TI) = 25 PSIG

P ATM = 14.5 PSIA
X/D = 0.6

THETA	15	30	45	60	75	90	105	120	
FREQUENCY				- SPL(F,THETA) -					PWL(F)
400	88.6	83.5	0.0	0.0	0.0	0.0	0.0	0.0	92.1
500	92.0	87.2	81.0	0.0	0.0	0.0	0.0	0.0	96.1
630	95.2	91.3	84.0	0.0	0.0	0.0	0.0	0.0	99.6
800	98.5	94.8	87.8	82.5	81.7	0.0	0.0	0.0	103.4
1000	101.5	98.9	91.8	84.5	84.0	82.5	81.0	0.0	107.0
1250	104.5	102.8	94.0	87.5	86.9	85.3	83.2	82.0	110.4
1600	106.5	105.7	97.8	90.1	89.0	87.0	85.2	83.6	113.0
2000	108.0	109.0	101.0	92.6	91.1	89.0	87.8	86.0	115.7
2500	109.2	111.8	104.2	94.8	93.0	91.0	89.8	88.0	118.2
3150	110.8	114.2	107.2	97.0	94.5	93.0	91.4	90.2	120.5
4000	111.5	115.6	109.8	99.0	96.5	95.0	93.2	92.0	122.1
5000	111.7	116.0	111.6	100.5	97.5	95.9	94.2	93.6	122.9
6300	115.2	119.5	113.7	105.3	105.5	101.0	97.3	99.2	126.3
8000	115.0	119.7	113.8	106.0	104.8	101.5	99.3	102.6	126.4
10000	111.0	117.1	113.8	104.5	101.9	100.9	104.0	108.0	125.0
12500	109.0	116.6	112.5	105.0	102.0	105.0	108.9	108.9	125.0
16000	108.9	115.6	111.6	105.9	104.1	109.1	108.3	107.6	124.8
20000	106.3	113.5	110.4	106.3	107.0	107.8	106.5	108.2	123.8
25000	106.0	112.5	110.2	108.1	108.2	106.8	108.9	108.2	124.1
31500	104.7	110.2	109.4	109.7	106.7	107.4	107.4	107.2	123.3
40000	102.0	108.7	108.3	109.3	106.3	107.4	106.7	105.7	122.6
50000	100.6	106.4	109.4	108.6	106.7	107.1	105.3	104.3	122.1
63000	98.0	105.0	106.5	106.6	106.0	105.5	104.5	103.2	120.5
80000	94.8	102.2	103.9	104.3	104.3	103.4	102.4	100.5	118.2
100000	93.1	101.1	102.6	103.7	103.3	103.0	101.1	99.7	117.4

- COMPUTED SPL(THETA) -

THETA	15	30	45	60	75	90	105	120
	122.4	127.1	122.8	118.2	116.8	117.1	117.1	117.2

TOTAL ACOUSTIC POWER

PWL	WATTS
135.7	37.0

NOZZLE ARRANGEMENT I: 90 DEGREE IMPINGEMENT

P(TM) = 100 PSIG
P(TI) = 30 PSIG

P ATM = 14.5 PSIA
X/D = 0.6

THETA	15	30	45	60	75	90	105	120	
FREQUENCY				- SPL(F,THETA) -					PWL(F)
400	88.2	84.0	0.0	0.0	0.0	0.0	0.0	0.0	92.0
500	91.8	88.0	81.8	0.0	0.0	0.0	0.0	0.0	96.4
630	94.5	91.7	85.0	81.4	0.0	0.0	0.0	0.0	99.8
800	97.8	94.9	88.3	84.0	0.0	0.0	0.0	0.0	103.1
1000	100.7	98.9	91.8	86.5	86.0	84.2	82.3	80.8	106.9
1250	103.5	103.0	95.6	89.5	88.5	86.8	85.0	83.0	110.4
1600	105.5	106.3	99.1	91.9	90.6	89.0	87.0	85.3	113.3
2000	106.8	109.6	102.7	94.5	93.0	91.3	89.6	87.8	116.2
2500	108.0	112.8	106.2	97.0	95.4	93.4	91.6	90.1	119.1
3150	109.2	115.0	109.6	99.5	97.0	95.3	93.4	92.2	121.5
4000	110.0	116.6	112.0	102.0	99.0	97.0	95.4	94.0	123.3
5000	110.2	117.0	113.5	103.3	100.2	98.2	96.6	95.8	124.1
6300	120.2	127.6	116.7	113.8	114.2	111.0	104.0	111.5	133.5
8000	115.6	122.5	115.2	109.5	108.7	106.0	103.0	108.8	129.0
10000	109.5	117.3	114.6	106.7	104.0	104.0	108.2	110.6	126.0
12500	110.0	117.8	113.8	107.3	105.0	115.0	113.0	111.0	128.0
16000	108.1	116.7	113.1	108.1	107.6	113.9	111.3	109.6	127.1
20000	105.3	114.9	111.9	108.9	110.5	109.3	109.3	109.8	125.7
25000	106.0	114.1	111.9	111.3	111.1	109.0	109.8	109.1	125.9
31500	106.2	113.2	111.7	113.6	109.3	109.4	109.1	108.5	125.9
40000	104.2	111.6	110.2	112.4	108.7	108.8	108.5	107.5	124.8
50000	101.0	109.3	108.8	110.8	108.0	108.2	107.0	105.8	123.4
63000	99.0	108.0	107.7	109.0	107.5	107.4	106.3	104.6	122.3
80000	96.3	105.7	105.3	106.7	105.9	105.3	104.0	102.3	120.1
100000	94.8	104.6	104.3	105.7	104.8	104.3	103.1	101.1	119.1

- COMPUTED SPL(THETA) -

THETA	15	30	45	60	75	90	105	120
	123.6	130.8	124.5	121.6	120.3	121.1	119.7	119.8

TOTAL ACOUSTIC POWER

PWL	WATTS
138.7	73.7

NOZZLE ARRANGEMENT II: 90 DEGREE IMPINGEMENT

P(TM) = 100 PSIG P ATM = 14.6 PSIA
P(TI) = 14 PSIG X/D = 0.6

THETA	15	30	45	60	75	90	105	120	
FREQUENCY				- SPL(F,THETA) -					PWL(F)
315	82.8	0.0	0.0	0.0	0.0	0.0	0.0	0.0	84.2
400	86.3	82.0	0.0	0.0	0.0	0.0	0.0	0.0	90.0
500	90.0	85.8	0.0	0.0	0.0	0.0	0.0	0.0	93.8
630	92.8	89.6	82.5	0.0	0.0	0.0	0.0	0.0	97.6
800	96.2	93.0	85.8	80.9	0.0	0.0	0.0	0.0	101.1
1000	99.0	96.7	89.0	83.6	82.6	81.1	0.0	0.0	104.6
1250	102.2	100.6	92.8	86.0	85.2	83.7	82.0	80.5	108.2
1600	104.5	104.1	95.9	88.5	86.9	85.5	83.8	82.1	111.2
2000	106.0	107.5	99.6	90.9	89.5	87.5	86.0	84.6	114.1
2500	107.3	110.1	102.8	93.0	91.3	89.9	88.3	86.6	116.5
3150	108.6	112.5	105.6	95.4	93.3	91.9	90.1	88.8	118.8
4000	109.6	114.0	108.0	97.7	94.8	93.6	92.0	90.5	120.4
5000	110.1	114.8	109.7	99.3	96.3	94.6	93.4	92.0	121.4
6300	110.8	115.9	111.0	101.6	98.9	96.9	95.1	95.0	122.6
8000	111.8	117.6	112.2	106.1	104.4	101.2	99.3	100.0	124.5
10000	112.9	117.0	111.9	105.3	102.9	102.3	105.8	110.5	125.1
12500	110.4	115.2	110.8	104.9	103.0	105.8	112.5	114.5	126.2
16000	109.0	113.7	109.4	106.0	105.2	111.8	113.6	111.9	126.1
20000	138.5	114.1	111.2	109.9	110.3	112.7	110.1	108.9	140.1
25000	109.3	113.5	111.9	112.6	113.6	110.7	110.3	110.4	127.0
31500	107.4	111.5	110.6	113.1	111.8	110.0	110.6	109.6	126.2
40000	105.0	109.6	109.4	113.6	109.6	109.5	109.0	107.7	125.2
50000	102.2	107.4	108.3	112.1	108.6	108.0	107.5	105.8	123.7
63000	102.3	107.2	108.7	110.9	108.9	108.4	107.4	105.6	123.5
80000	98.9	105.6	105.9	108.6	106.8	106.3	105.2	103.4	121.2
100000	95.3	100.7	102.3	104.8	103.4	102.8	101.5	99.5	117.5

- COMPUTED SPL(THETA) -

THETA	15	30	45	60	75	90	105	120
	138.6	125.8	122.0	121.1	119.6	119.6	120.1	120.0

TOTAL ACOUSTIC POWER

PWL	WATTS
141.5	140.3

NOZZLE ARRANGEMENT II: 90 DEGREE IMPINGEMENT

P(TM) = 100 PSIG
P(TI) = 32 PSIG

P ATM = 14.5 PSIA
X/D = 0.6

THETA	15	30	45	60	75	90	105	120	
FREQUENCY				- SPL(F,THETA) -					PWL(F)
250	80.6	0.0	0.0	0.0	0.0	0.0	0.0	0.0	82.0
315	84.0	0.0	0.0	0.0	0.0	0.0	0.0	0.0	85.4
400	87.4	83.0	0.0	0.0	0.0	0.0	0.0	0.0	91.1
500	90.8	87.0	80.5	0.0	0.0	0.0	0.0	0.0	95.4
630	93.6	90.6	83.5	0.0	0.0	0.0	0.0	0.0	98.5
800	97.2	94.0	87.0	82.1	80.9	0.0	0.0	0.0	102.4
1000	99.9	97.6	90.2	84.6	83.5	82.0	80.5	0.0	105.7
1250	102.8	101.1	93.7	87.5	86.2	84.6	82.9	81.4	108.9
1600	104.5	104.4	97.0	89.4	88.0	86.3	84.8	82.9	111.6
2000	106.2	107.6	100.1	92.1	90.4	88.5	86.9	85.4	114.4
2500	107.2	110.1	103.2	94.6	92.5	90.5	89.0	87.3	116.7
3150	108.1	112.0	105.6	96.7	94.7	92.4	90.8	89.8	118.5
4000	108.9	113.4	107.8	98.4	95.9	94.4	92.4	90.9	120.0
5000	109.1	114.0	109.6	100.0	96.8	95.2	93.7	92.1	121.0
6300	109.4	114.6	110.9	101.3	98.4	96.7	95.1	93.8	121.8
8000	109.3	114.8	111.3	103.0	100.1	98.1	96.4	95.1	122.2
10000	109.0	114.7	111.1	103.8	100.7	99.1	98.6	99.7	122.3
12500	107.6	113.7	110.3	104.3	101.0	100.0	101.7	103.3	121.9
16000	107.8	112.3	109.0	105.4	101.6	101.7	103.4	103.4	121.4
20000	107.5	111.5	109.6	106.9	104.3	104.1	104.4	105.2	122.1
25000	108.8	112.8	112.1	110.7	107.4	106.8	108.5	107.6	124.7
31500	106.1	110.1	109.5	109.0	106.1	107.9	108.4	106.1	123.3
40000	103.1	108.7	108.0	108.6	106.8	108.3	106.2	104.2	122.5
50000	101.5	106.5	106.3	107.3	106.6	106.4	105.1	102.5	121.1
63000	101.0	106.1	106.6	107.7	107.4	106.7	105.4	102.2	121.4
80000	98.0	103.6	104.4	105.7	105.4	104.3	102.8	99.6	119.1
100000	93.7	99.7	100.6	101.8	101.7	100.8	98.9	95.4	115.3

- COMPUTED SPL(THETA) -

THETA	15	30	45	60	75	90	105	120
	119.9	124.4	121.3	118.0	115.9	115.9	115.6	114.3

TOTAL ACOUSTIC POWER

PWL	WATTS
133.8	24.1

NOZZLE ARRANGEMENT II: 90 DEGREE IMPINGEMENT

P(TM) = 100 PSIG
P(TI) = 14 PSIG

P ATM = 14.5 PSIA
X/D = 0.8

THETA	15	30	45	60	75	90	105	120	
FREQUENCY				- SPL(F,THETA) -					PWL(F)
315	83.0	0.0	0.0	0.0	0.0	0.0	0.0	0.0	84.5
400	85.8	82.5	0.0	0.0	0.0	0.0	0.0	0.0	90.0
500	89.6	86.2	0.0	0.0	0.0	0.0	0.0	0.0	93.8
630	92.3	89.6	82.5	0.0	0.0	0.0	0.0	0.0	97.4
800	95.7	93.0	86.0	81.4	80.6	0.0	0.0	0.0	101.3
1000	98.7	96.5	89.0	83.9	83.3	81.9	0.0	0.0	104.6
1250	101.7	100.7	92.9	86.7	86.2	84.7	82.8	81.0	108.3
1600	103.7	104.0	96.0	88.8	88.1	86.6	84.4	82.5	111.1
2000	105.7	107.8	99.8	92.0	91.0	88.9	87.0	85.0	114.4
2500	107.1	110.9	103.4	94.4	93.0	91.0	89.0	87.1	117.2
3150	108.6	113.6	106.3	96.9	95.0	93.1	90.9	89.5	119.7
4000	109.6	114.9	108.7	99.2	96.3	94.8	93.0	91.2	121.3
5000	109.5	115.4	110.0	100.7	97.9	95.4	94.1	92.4	122.0
6300	110.9	117.8	111.0	105.8	106.1	100.5	97.0	95.3	124.4
8000	114.0	121.2	112.5	111.1	111.2	106.2	101.2	101.7	128.0
10000	111.3	116.0	110.5	104.4	101.7	101.5	107.1	111.3	124.6
12500	110.0	114.3	109.4	104.4	102.4	109.9	113.4	112.4	125.9
16000	108.4	113.3	108.3	105.2	105.8	114.5	112.1	108.4	126.0
20000	106.3	111.4	107.3	106.2	109.5	109.3	106.7	107.5	123.5
25000	105.9	111.3	108.5	109.1	110.8	107.4	108.6	107.7	124.2
31500	105.0	110.6	108.8	111.8	108.7	109.2	107.9	107.2	124.4
40000	102.4	108.3	108.3	112.4	107.3	107.2	106.9	105.3	123.5
50000	99.4	105.9	106.7	110.5	106.3	106.0	105.1	103.3	121.8
63000	99.6	106.1	107.1	109.2	106.7	106.4	105.2	102.9	121.6
80000	97.8	102.9	105.0	106.8	105.3	104.7	102.8	100.4	119.5
100000	93.8	99.1	101.1	103.2	102.2	100.9	99.0	96.5	115.9

- COMPUTED SPL(THETA) -

THETA	15	30	45	60	75	90	105	120
	120.9	126.5	120.9	120.0	118.7	119.3	118.9	118.2

TOTAL ACOUSTIC POWER

PWL	WATTS
135.9	38.8

NOZZLE ARRANGEMENT II: 90 DEGREE IMPINGEMENT

P(TM) = 100 PSIG
P(TI) = 24 PSIG

P ATM = 14.4 PSIA
X/D = 0.8

THETA	15	30	45	60	75	90	105	120	
FREQUENCY				- SPL(F,THETA) -					PWL(F)
315	83.0	0.0	0.0	0.0	0.0	0.0	0.0	0.0	84.5
400	86.7	82.3	0.0	0.0	0.0	0.0	0.0	0.0	90.5
500	90.2	86.4	0.0	0.0	0.0	0.0	0.0	0.0	94.3
630	93.1	89.5	82.8	0.0	0.0	0.0	0.0	0.0	97.8
800	96.5	93.0	86.2	81.6	80.5	0.0	0.0	0.0	101.6
1000	99.5	96.5	89.2	84.3	82.9	81.2	0.0	0.0	104.9
1250	102.2	100.7	92.8	86.8	85.7	84.1	82.0	80.5	108.4
1600	103.9	103.5	95.7	88.8	87.7	85.7	83.8	82.0	110.8
2000	105.6	106.8	98.9	91.4	89.9	87.8	86.1	84.6	113.6
2500	106.6	109.4	101.8	93.5	91.9	90.0	88.2	86.4	115.9
3150	107.9	111.4	104.3	95.8	93.8	92.5	90.3	88.6	117.9
4000	108.5	112.8	106.6	97.9	94.9	94.0	92.5	90.3	119.4
5000	108.8	113.2	107.9	99.1	96.6	94.5	93.7	91.7	120.0
6300	110.0	114.3	109.2	100.8	96.9	96.9	94.8	93.9	121.2
8000	110.1	114.4	109.3	102.2	99.5	97.4	95.8	94.3	121.5
10000	110.8	113.9	109.2	103.1	100.1	98.1	97.5	97.1	121.5
12500	109.9	113.4	108.6	103.6	100.3	98.6	98.7	98.7	121.1
16000	109.0	111.7	107.7	103.8	100.6	99.5	99.0	98.6	120.2
20000	106.5	110.4	107.0	103.9	101.2	99.7	100.0	101.4	119.6
25000	106.2	110.1	107.2	105.4	102.7	101.9	104.8	105.9	120.9
31500	104.4	108.8	107.5	105.8	103.9	105.0	107.0	105.1	121.3
40000	101.6	107.0	106.1	105.4	104.3	106.3	104.5	102.4	120.3
50000	99.4	104.3	104.2	104.2	104.3	104.5	102.9	100.8	118.8
63000	99.6	104.5	104.6	105.2	105.6	104.8	103.7	100.6	119.5
80000	97.0	101.9	102.9	104.4	105.6	104.0	101.8	98.1	118.4
100000	93.8	98.6	100.2	102.5	103.5	101.0	98.3	94.7	115.8

- COMPUTED SPL(THETA) -

THETA	15	30	45	60	75	90	105	120
	120.0	123.6	119.2	115.5	114.2	113.8	113.4	112.2

TOTAL ACOUSTIC POWER

PWL	WATTS
132.3	17.1

NOZZLE ARRANGEMENT II: 90 DEGREE IMPINGEMENT

P(TM) = 100 PSIG
P(TI) = 12 PSIG

P ATM = 14.4 PSIA
X/D = 1.0

THETA	15	30	45	60	75	90	105	120	
FREQUENCY				- SPL(F,THETA) -					PWL(F)
315	83.3	0.0	0.0	0.0	0.0	0.0	0.0	0.0	84.8
400	86.6	82.1	0.0	0.0	0.0	0.0	0.0	0.0	90.4
500	89.9	86.1	0.0	0.0	0.0	0.0	0.0	0.0	94.0
630	92.8	89.2	82.5	0.0	0.0	0.0	0.0	0.0	97.5
800	95.7	92.7	85.7	81.3	80.5	0.0	0.0	0.0	101.1
1000	98.3	96.0	89.0	84.0	83.4	81.7	0.0	0.0	104.2
1250	101.4	99.9	92.7	86.7	86.2	84.7	82.9	80.9	107.8
1600	103.5	103.5	96.1	89.1	88.3	86.8	84.7	82.6	110.8
2000	105.8	107.4	100.1	92.2	91.2	89.0	87.5	85.5	114.3
2500	107.1	110.6	103.5	94.7	93.2	91.2	89.3	87.5	117.1
3150	108.5	113.5	106.7	97.1	95.1	93.7	91.6	89.8	119.8
4000	109.8	114.8	109.0	99.5	96.5	95.0	93.2	91.7	121.3
5000	109.8	114.8	109.8	100.8	107.9	95.8	94.5	92.8	122.4
6300	110.1	114.9	110.6	104.3	111.9	99.1	96.2	94.9	123.9
8000	116.7	123.3	115.7	116.0	113.9	107.9	102.6	101.8	130.6
10000	110.3	114.0	110.7	104.7	102.2	100.4	104.0	108.2	123.0
12500	108.9	112.4	109.7	104.3	101.6	104.8	109.6	108.9	123.3
16000	108.1	112.3	108.7	104.7	104.6	112.0	109.2	105.8	124.2
20000	106.5	110.4	107.4	104.8	106.4	107.0	104.8	105.5	121.9
25000	106.3	110.7	108.5	107.1	108.5	105.6	106.9	106.2	122.8
31500	105.4	109.6	108.2	108.9	106.9	106.5	106.4	105.3	122.6
40000	102.5	107.8	107.1	109.7	105.7	105.5	105.3	104.0	121.8
50000	100.3	105.2	106.3	108.8	105.0	104.4	104.2	102.2	120.6
63000	99.7	105.2	106.6	108.8	105.8	105.2	104.5	102.0	120.9
80000	96.9	102.4	103.9	105.4	103.7	103.3	102.0	99.4	118.3
100000	93.0	98.4	100.0	101.7	100.2	99.4	98.2	95.5	114.5

- COMPUTED SPL(THETA) -

THETA	15	30	45	60	75	90	105	120
	121.4	126.6	121.5	120.0	119.2	117.3	116.7	115.9

TOTAL ACOUSTIC POWER

PWL	WATTS
135.6	36.0

NOZZLE ARRANGEMENT II: 90 DEGREE IMPINGEMENT

P(TM) = 100 PSIG
P(TI) = 22 PSIG

P ATM = 14.4 PSIA
X/D = 1.0

THETA	15	30	45	60	75	90	105	120	
FREQUENCY				- SPL(F,THETA) -					PWL(F)
315	82.8	0.0	0.0	0.0	0.0	0.0	0.0	0.0	84.3
400	86.2	81.5	0.0	0.0	0.0	0.0	0.0	0.0	89.9
500	89.8	85.6	0.0	0.0	0.0	0.0	0.0	0.0	93.7
630	92.5	88.9	81.9	0.0	0.0	0.0	0.0	0.0	97.2
800	95.9	92.3	85.4	80.4	0.0	0.0	0.0	0.0	100.8
1000	98.7	95.8	88.5	83.3	82.5	80.9	0.0	0.0	104.2
1250	101.4	99.5	91.9	85.8	85.0	83.7	81.9	80.4	107.5
1600	103.2	102.5	94.9	87.9	86.9	85.5	83.7	81.7	110.0
2000	104.7	106.0	98.3	90.7	89.3	87.4	86.0	84.3	112.8
2500	106.0	108.5	101.2	92.9	91.3	89.7	88.1	86.4	115.1
3150	106.9	110.5	103.8	95.0	93.5	92.0	90.2	88.5	117.1
4000	107.7	111.6	105.3	97.2	94.8	93.4	92.0	90.3	118.3
5000	107.8	111.8	106.6	98.4	96.3	94.3	93.2	92.0	118.8
6300	108.8	112.1	107.7	100.4	98.0	97.0	95.0	93.9	119.6
8000	108.9	112.1	108.5	103.0	100.7	98.3	96.7	95.4	120.2
10000	109.7	111.8	108.8	103.3	100.9	99.3	99.2	100.9	120.6
12500	109.7	111.0	108.5	104.1	100.8	100.1	103.4	94.8	120.5
16000	108.5	110.7	108.2	104.6	101.9	103.3	104.9	104.0	121.1
20000	107.7	109.8	107.3	104.4	103.6	104.5	103.6	102.5	120.6
25000	107.4	109.3	108.4	106.8	106.0	104.8	104.8	104.3	121.6
31500	105.9	108.6	107.6	107.0	105.2	104.1	105.0	104.4	121.2
40000	102.5	106.3	106.6	107.2	104.9	104.3	104.6	103.0	120.5
50000	100.2	103.9	105.4	105.5	104.5	104.4	103.5	101.1	119.3
63000	100.2	103.6	105.5	105.2	105.3	104.7	103.8	101.2	119.5
80000	96.6	101.1	102.6	103.1	103.5	102.7	101.4	98.5	117.3
100000	92.3	97.1	99.0	99.5	100.2	99.0	97.6	94.4	113.6

- COMPUTED SPL(THETA) -

THETA	15	30	45	60	75	90	105	120
	119.5	122.1	119.0	116.0	114.7	114.1	114.1	112.5

TOTAL ACOUSTIC POWER

PWL	WATTS
132.0	15.8

NOZZLE ARRANGEMENT II: 90 DEGREE IMPINGEMENT

P(TM) = 100 PSIG P ATM = 14.6 PSIA
P(TI) = 4 PSIG X/D = 1.2

THETA	15	30	45	60	75	90	105	120	
FREQUENCY				- SPL(F,THETA) -					PWL(F)
315	82.3	0.0	0.0	0.0	0.0	0.0	0.0	0.0	83.7
400	86.0	0.0	0.0	0.0	0.0	0.0	0.0	0.0	87.4
500	89.5	85.6	0.0	0.0	0.0	0.0	0.0	0.0	93.4
630	92.5	89.0	82.0	0.0	0.0	0.0	0.0	0.0	97.1
800	95.5	92.3	85.1	80.8	0.0	0.0	0.0	0.0	100.5
1000	98.5	96.4	88.6	83.6	83.1	81.5	0.0	0.0	104.3
1250	101.6	100.0	92.3	86.2	85.6	84.0	82.3	80.6	107.7
1600	103.7	103.4	95.5	88.7	87.6	86.0	84.2	82.4	110.6
2000	105.7	106.9	98.9	91.2	90.0	88.0	86.6	84.9	113.6
2500	107.1	110.0	102.7	93.5	92.0	90.2	88.6	87.0	116.4
3150	108.7	112.8	106.0	96.0	93.8	92.3	90.6	89.2	119.1
4000	109.7	114.3	108.5	98.3	95.6	93.8	92.3	91.2	120.7
5000	110.3	114.9	109.9	99.9	97.1	95.0	93.8	92.3	121.6
6300	110.8	115.3	110.3	101.7	98.8	96.6	95.1	93.9	122.1
8000	112.1	120.6	112.0	109.8	108.3	103.6	100.3	97.7	126.8
10000	111.8	115.7	110.9	104.1	101.2	99.5	100.2	104.3	123.1
12500	111.0	114.4	110.3	104.3	100.7	101.4	106.3	107.2	123.0
16000	109.4	113.5	109.4	104.3	101.8	107.8	107.9	106.6	123.2
20000	108.0	112.0	108.5	104.5	104.1	106.3	105.2	104.7	121.9
25000	108.1	112.4	109.9	106.7	107.4	106.3	105.8	106.0	123.0
31500	107.2	111.6	109.8	108.6	107.3	105.7	106.6	106.2	123.1
40000	104.5	109.7	108.9	109.3	105.5	105.4	106.3	105.4	122.3
50000	102.4	107.2	107.4	108.5	104.8	105.2	105.4	103.8	121.2
63000	102.1	106.8	107.6	108.7	106.3	106.2	105.9	103.7	121.6
80000	99.1	104.5	105.3	106.1	104.8	104.3	103.5	101.2	119.4
100000	94.9	100.8	101.6	102.2	101.6	101.0	99.8	97.3	115.8

- COMPUTED SPL(THETA) -

THETA	15	30	45	60	75	90	105	120
	121.2	126.0	121.2	118.1	116.2	115.9	116.0	115.4

TOTAL ACOUSTIC POWER

PWL	WATTS
134.5	28.2

NOZZLE ARRANGEMENT II: 90 DEGREE IMPINGEMENT

P(TM) = 100 PSIG
P(TI) = 17 PSIG

P ATM = 14.6 PSIA
X/D = 1.2

THETA	15	30	45	60	75	90	105	120	
FREQUENCY				- SPL(F,THETA) -					PWL(F)
315	82.6	0.0	0.0	0.0	0.0	0.0	0.0	0.0	84.0
400	86.5	81.5	0.0	0.0	0.0	0.0	0.0	0.0	89.9
500	89.5	85.5	0.0	0.0	0.0	0.0	0.0	0.0	93.3
630	92.3	88.6	82.4	0.0	0.0	0.0	0.0	0.0	96.9
800	95.6	92.1	85.6	80.5	0.0	0.0	0.0	0.0	100.5
1000	98.5	94.6	88.6	83.0	82.0	80.7	0.0	0.0	103.5
1250	101.3	99.4	92.3	85.7	84.5	83.1	81.6	0.0	107.2
1600	103.2	102.4	95.3	88.0	86.5	84.9	83.6	81.6	109.8
2000	104.7	105.5	98.7	90.2	88.7	87.0	86.0	84.1	112.5
2500	105.8	108.0	101.5	92.4	90.8	88.0	87.8	85.9	114.7
3150	107.0	110.1	104.0	94.5	92.5	91.4	89.8	88.1	116.7
4000	107.6	111.4	106.0	96.7	94.2	92.8	91.3	89.9	118.1
5000	108.1	111.8	107.0	98.0	95.9	93.9	92.9	91.3	118.8
6300	109.1	111.8	107.9	99.9	97.3	96.1	94.1	93.0	119.3
8000	108.7	111.3	108.3	101.5	99.1	97.2	96.1	94.5	119.4
10000	108.9	110.8	108.5	102.4	99.5	98.3	97.7	97.7	119.6
12500	108.6	110.1	108.4	103.2	99.9	99.1	100.4	101.3	119.7
16000	108.1	109.4	107.8	103.8	101.0	101.2	102.5	101.5	119.8
20000	107.7	108.8	107.8	104.5	104.7	103.0	102.7	101.3	120.2
25000	108.0	109.8	109.3	107.3	106.6	105.0	104.5	103.0	121.9
31500	106.6	109.1	108.8	107.1	105.0	104.6	104.7	103.7	121.4
40000	103.0	107.1	107.8	106.9	105.3	104.9	105.2	103.3	120.9
50000	101.0	104.5	106.2	106.3	105.1	104.7	104.8	101.8	120.0
63000	100.5	104.3	106.5	106.6	106.3	105.9	105.4	102.3	120.6
80000	97.7	102.2	104.2	104.3	104.5	104.4	103.4	99.8	118.6
100000	93.4	98.3	100.5	100.8	101.2	100.8	99.6	96.0	115.0

- COMPUTED SPL(THETA) -

THETA	15	30	45	60	75	90	105	120
	119.4	121.8	119.4	116.2	115.0	114.2	114.0	112.2

TOTAL ACOUSTIC POWER

PWL	WATTS
131.9	15.4

NOZZLE ARRANGEMENT II: 90 DEGREE IMPINGEMENT

P(TM) = 100 PSIG
P(TI) = 15 PSIG

P ATM = 14.6 PSIA
X/D = 1.3

THETA	15	30	45	60	75	90	105	120	
FREQUENCY				- SPL(F,THETA) -					PWL(F)
315	82.4	0.0	0.0	0.0	0.0	0.0	0.0	0.0	83.8
400	85.6	81.5	0.0	0.0	0.0	0.0	0.0	0.0	89.4
500	89.5	85.2	0.0	0.0	0.0	0.0	0.0	0.0	93.2
630	92.2	88.8	82.0	0.0	0.0	0.0	0.0	0.0	96.9
800	95.6	92.1	84.7	80.3	0.0	0.0	0.0	0.0	100.4
1000	98.4	95.6	88.2	83.0	82.4	80.6	0.0	0.0	103.8
1250	101.1	99.3	91.5	85.5	84.5	83.0	81.5	0.0	107.0
1600	103.2	102.4	94.6	87.8	86.6	84.9	83.3	81.7	109.7
2000	104.9	105.6	97.8	90.2	88.7	87.0	85.7	84.0	112.4
2500	105.9	108.2	100.9	92.3	90.5	89.1	87.8	85.9	114.7
3150	107.0	110.2	103.2	94.2	92.6	91.2	89.6	88.0	116.6
4000	107.9	111.8	105.2	96.6	94.2	92.4	91.1	89.9	118.2
5000	108.5	112.0	106.3	97.9	95.6	93.6	92.6	91.2	118.8
6300	109.0	111.9	107.2	99.7	97.0	95.6	93.9	92.7	119.2
8000	108.7	111.3	107.7	101.0	98.4	96.3	95.5	93.9	119.2
10000	108.6	110.4	107.9	102.1	99.1	97.5	96.5	96.0	119.1
12500	108.1	109.7	107.8	102.6	99.5	98.2	98.2	98.3	119.0
16000	107.8	109.1	107.3	103.2	100.4	99.2	99.7	99.2	118.9
20000	106.4	108.6	107.2	103.4	102.5	100.8	100.6	99.3	119.0
25000	107.3	109.5	108.6	106.3	104.4	103.6	102.9	101.9	120.8
31500	106.4	109.3	108.2	106.2	104.2	104.0	104.4	103.7	120.9
40000	103.0	106.9	107.0	105.7	104.4	104.5	104.9	103.0	120.2
50000	100.6	104.4	105.8	105.2	104.4	104.7	104.4	101.8	119.5
63000	100.4	103.5	106.1	105.8	106.0	105.6	105.4	102.0	120.2
80000	97.2	101.4	103.6	103.8	104.3	104.0	103.2	99.7	118.2
100000	93.0	97.9	100.1	100.4	100.9	100.5	99.5	95.8	114.7

- COMPUTED SPL(THETA) -

THETA	15	30	45	60	75	90	105	120
	119.2	121.7	118.8	115.4	114.1	113.5	113.3	111.4

TOTAL ACOUSTIC POWER

PWL	WATTS
131.4	13.8

NOZZLE ARRANGEMENT III: 90 DEGREE IMPINGEMENT

P(TM) = 100 PSIG
P(TI) = 12 PSIG

P ATM = 14.5 PSIA
X/D = 0.8

THETA	15	30	45	60	75	90	105	120	
FREQUENCY				- SPL(F,THETA) -					PWL(F)
315	82.5	0.0	0.0	0.0	0.0	0.0	0.0	0.0	83.9
400	85.5	82.4	0.0	0.0	0.0	0.0	0.0	0.0	89.8
500	88.7	86.4	0.0	0.0	0.0	0.0	0.0	0.0	93.4
630	91.7	89.6	83.0	0.0	0.0	0.0	0.0	0.0	97.2
800	95.4	93.1	86.7	81.4	80.6	0.0	0.0	0.0	101.2
1000	98.0	96.6	90.4	84.4	82.8	81.9	0.0	0.0	104.5
1250	101.4	100.6	94.2	87.4	85.9	84.5	82.8	81.0	108.3
1600	103.5	104.2	97.8	90.0	88.1	87.7	84.8	82.8	111.4
2000	105.4	107.7	101.7	93.0	90.8	88.9	87.5	85.4	114.5
2500	106.6	110.6	105.0	95.5	93.0	91.0	89.4	87.8	117.2
3150	108.4	113.0	108.5	98.1	95.0	93.0	91.1	90.0	119.8
4000	109.5	114.5	111.0	100.8	96.9	94.6	93.5	92.0	121.6
5000	109.6	114.6	111.7	102.1	98.1	96.0	94.5	93.5	122.0
6300	111.1	117.1	115.1	119.2	100.2	100.5	98.4	98.8	128.3
8000	115.7	122.6	121.3	117.2	104.3	107.0	105.2	107.3	131.3
10000	110.3	115.7	112.5	106.6	103.1	102.3	107.7	112.1	125.1
12500	109.4	115.0	111.9	107.2	104.2	110.0	113.0	112.2	126.3
16000	108.5	114.5	111.8	108.6	106.6	116.2	113.2	109.5	127.5
20000	109.5	114.5	113.3	110.4	110.0	111.5	108.9	109.5	126.3
25000	107.6	112.9	111.7	110.1	111.7	108.7	109.8	109.2	125.6
31500	108.0	112.2	111.5	112.0	111.0	111.0	109.9	109.4	126.0
40000	106.1	110.5	110.5	111.9	109.4	109.0	108.9	107.5	124.8
50000	103.6	108.3	108.9	110.5	108.2	108.0	107.5	105.9	123.3
63000	102.8	108.0	109.2	110.2	108.8	108.2	107.7	105.8	123.4
80000	100.4	105.5	106.8	107.8	106.7	106.4	105.8	103.5	121.3
100000	96.6	101.8	102.9	104.1	103.2	102.7	102.2	99.7	117.6

- COMPUTED SPL(THETA) -

THETA	15	30	45	60	75	90	105	120
	121.6	127.2	125.3	123.8	119.1	120.9	120.1	119.6

TOTAL ACOUSTIC POWER

PWL	WATTS
137.8	59.8

NOZZLE ARRANGEMENT III: 90 DEGREE IMPINGEMENT

P(TM) = 100 PSIG
P(TI) = 24 PSIG

P ATM = 14.5 PSIA
X/D = 0.8

THETA	15	30	45	60	75	90	105	120	
FREQUENCY				- SPL(F,THETA) -					PWL(F)
315	82.5	0.0	0.0	0.0	0.0	0.0	0.0	0.0	83.9
400	86.0	82.0	0.0	0.0	0.0	0.0	0.0	0.0	89.9
500	89.6	84.8	0.0	0.0	0.0	0.0	0.0	0.0	93.1
630	92.6	89.5	82.5	0.0	0.0	0.0	0.0	0.0	97.4
800	95.6	93.0	86.2	80.6	0.0	0.0	0.0	0.0	100.9
1000	98.5	96.3	89.0	83.5	82.2	81.5	0.0	0.0	104.3
1250	101.4	100.0	92.8	86.0	85.0	83.6	82.3	80.6	107.7
1600	103.6	103.3	95.7	88.5	87.1	85.8	84.3	82.5	110.5
2000	105.2	106.2	99.3	91.0	89.0	87.6	86.6	84.7	113.1
2500	106.5	109.0	102.0	93.1	91.3	90.0	88.5	87.0	115.6
3150	107.4	110.6	104.8	95.8	93.2	91.9	90.5	89.0	117.3
4000	108.0	112.0	107.0	98.0	95.4	93.8	92.6	91.3	118.9
5000	108.5	112.9	108.7	99.6	97.1	95.1	94.3	93.1	120.0
6300	109.4	113.7	110.1	101.5	98.8	97.1	96.3	95.4	121.1
8000	109.1	113.9	110.3	103.5	100.3	98.4	98.1	96.3	121.5
10000	109.3	113.8	110.3	105.0	101.6	100.0	99.8	98.5	121.8
12500	108.9	113.6	110.2	106.2	103.3	101.7	100.4	99.4	122.0
16000	111.0	116.5	113.2	110.5	107.1	107.1	102.1	103.8	125.3
20000	111.3	114.1	112.7	110.3	105.8	107.4	104.8	106.0	124.6
25000	109.1	111.2	110.3	108.5	105.2	106.1	107.9	98.2	122.8
31500	108.6	111.6	110.5	109.2	107.0	108.3	109.5	107.6	124.2
40000	107.0	110.1	109.5	108.5	107.3	109.1	108.0	105.9	123.4
50000	104.0	108.0	107.5	107.4	107.1	107.4	107.0	104.5	122.1
63000	103.8	108.2	107.8	107.7	107.8	107.6	107.8	104.3	122.4
80000	101.3	105.7	105.6	105.8	106.2	105.4	105.6	102.3	120.4
100000	97.3	102.0	102.0	102.3	102.4	102.2	102.2	98.3	116.8

- COMPUTED SPL(THETA) -

THETA	15	30	45	60	75	90	105	120
	120.7	124.5	121.7	118.7	116.7	117.0	116.6	114.4

TOTAL ACOUSTIC POWER

PWL	WATTS
134.3	26.8

NOZZLE ARRANGEMENT III: 90 DEGREE IMPINGEMENT

P(TM) = 100 PSIG P ATM = 14.6 PSIA
P(TI) = 10 PSIG X/D = 1.0

THETA	15	30	45	60	75	90	105	120	
FREQUENCY				- SPL(F,THETA) -					PWL(F)
315	81.9	0.0	0.0	0.0	0.0	0.0	0.0	0.0	83.3
400	85.0	81.0	0.0	0.0	0.0	0.0	0.0	0.0	88.8
500	88.4	84.6	0.0	0.0	0.0	0.0	0.0	0.0	92.3
630	91.0	88.0	82.0	0.0	0.0	0.0	0.0	0.0	96.0
800	94.2	91.4	85.6	81.5	80.7	0.0	0.0	0.0	99.9
1000	96.8	94.8	88.7	84.3	83.6	82.1	80.5	0.0	103.2
1250	99.8	98.8	92.5	87.4	86.0	85.0	83.5	81.5	106.8
1600	102.0	102.3	96.0	90.1	88.8	87.7	85.7	83.8	109.8
2000	103.8	107.1	99.8	92.9	91.7	89.9	88.4	86.5	113.6
2500	105.4	109.8	103.7	95.6	94.0	92.2	90.7	88.7	116.4
3150	106.6	112.5	107.2	98.3	96.2	94.3	92.4	91.0	119.1
4000	108.2	114.4	110.0	100.8	98.2	96.0	94.3	93.1	121.2
5000	107.5	114.3	110.9	102.2	99.4	97.2	96.0	94.9	121.5
6300	107.5	114.6	112.0	105.8	101.4	99.0	97.7	97.6	122.5
8000	115.1	125.3	120.2	118.5	111.9	106.4	107.3	108.8	132.6
10000	106.7	113.2	112.1	106.2	103.2	101.9	104.8	107.6	123.0
12500	105.4	112.8	110.7	106.2	103.5	106.3	109.0	109.2	123.6
16000	104.5	113.5	111.3	107.9	107.9	114.9	110.1	107.5	126.2
20000	104.0	111.0	109.5	106.9	107.1	107.8	107.0	107.4	123.0
25000	105.2	111.3	109.9	108.5	108.7	107.5	109.0	108.0	123.9
31500	105.6	111.4	109.9	110.5	109.0	109.0	108.6	107.8	124.4
40000	103.8	109.4	107.9	110.4	107.8	107.9	107.4	106.0	123.2
50000	101.0	107.5	108.0	109.4	106.8	106.6	106.4	104.5	122.1
63000	100.8	107.3	108.2	109.2	107.6	107.4	106.6	104.6	122.4
80000	98.6	104.8	105.8	106.7	105.9	105.6	104.4	102.2	120.2
100000	95.4	101.3	102.5	103.2	102.4	102.2	100.8	98.4	116.7

- COMPUTED SPL(THETA) -

THETA	15	30	45	60	75	90	105	120
	119.6	127.7	123.9	121.8	118.6	119.3	118.3	117.7

TOTAL ACOUSTIC POWER

PWL	WATTS
136.7	47.0

NOZZLE ARRANGEMENT III: 90 DEGREE IMPINGEMENT

P(TM) = 100 PSIG P ATM = 14.4 PSIA
P(TI) = 20 PSIG X/D = 1.0

THETA	15	30	45	60	75	90	105	120	
FREQUENCY				- SPL(F,THETA) -					PWL(F)
315	83.0	0.0	0.0	0.0	0.0	0.0	0.0	0.0	84.4
400	86.5	82.4	0.0	0.0	0.0	0.0	0.0	0.0	90.3
500	90.1	86.2	0.0	0.0	0.0	0.0	0.0	0.0	94.0
630	93.0	89.5	82.7	0.0	0.0	0.0	0.0	0.0	97.7
800	96.1	93.1	86.0	81.4	80.4	0.0	0.0	0.0	101.4
1000	99.0	96.6	89.0	83.8	82.8	81.5	0.0	0.0	104.6
1250	102.0	100.4	92.6	86.7	85.4	83.8	82.3	81.0	108.1
1600	104.1	103.8	95.9	88.6	87.1	85.9	84.4	82.7	110.9
2000	105.8	106.7	99.0	91.2	89.4	87.9	86.7	85.0	113.5
2500	106.8	109.3	101.9	93.4	91.4	89.9	88.6	87.2	115.8
3150	107.8	111.1	104.6	95.3	93.0	91.8	90.3	89.6	117.6
4000	108.6	112.5	106.8	97.5	95.0	93.4	92.3	91.7	119.2
5000	109.0	112.6	107.5	98.9	96.0	94.6	93.3	93.1	119.5
6300	109.3	112.9	108.5	100.9	97.5	96.0	95.3	95.1	120.2
8000	110.4	114.1	109.6	104.2	99.5	97.4	97.3	98.2	121.6
10000	110.3	112.8	109.2	103.4	100.4	99.0	99.8	103.7	121.2
12500	109.4	111.5	108.3	104.2	101.0	100.5	105.2	107.0	121.5
16000	108.7	111.4	107.9	104.4	101.8	104.8	106.7	106.9	121.9
20000	107.3	110.4	107.5	104.8	103.7	105.6	105.5	105.5	121.4
25000	107.7	110.5	108.6	106.5	106.3	105.7	105.8	106.8	122.3
31500	108.4	110.5	109.7	108.8	107.0	106.5	107.6	107.8	123.4
40000	106.0	108.3	108.5	108.3	106.0	106.9	107.0	106.5	122.4
50000	104.3	106.7	107.7	106.9	105.8	107.0	105.7	105.0	121.5
63000	104.4	107.0	108.8	107.7	108.6	107.5	106.9	105.6	122.6
80000	103.2	105.5	107.6	106.7	108.0	105.8	105.1	104.2	121.4
100000	99.3	101.4	102.9	102.4	102.7	101.8	100.8	100.4	116.9

- COMPUTED SPL(THETA) -

THETA	15	30	45	60	75	90	105	120
	120.5	123.3	120.2	117.2	116.2	116.0	116.2	116.3

TOTAL ACOUSTIC POWER

PWL	WATTS
133.4	22.0

NOZZLE ARRANGEMENT III: 90 DEGREE IMPINGEMENT

P(TM) = 100 PSIG
P(TI) = 10 PSIG

P ATM = 14.4 PSIA
X/D = 1.1

THETA	15	30	45	60	75	90	105	120	
FREQUENCY				- SPL(F,THETA) -					PWL(F)
315	83.0	0.0	0.0	0.0	0.0	0.0	0.0	0.0	84.4
400	86.7	82.0	0.0	0.0	0.0	0.0	0.0	0.0	90.3
500	89.4	86.0	0.0	0.0	0.0	0.0	0.0	0.0	93.6
630	92.5	89.4	83.0	0.0	0.0	0.0	0.0	0.0	97.4
800	95.6	92.6	86.2	81.8	0.0	0.0	0.0	0.0	100.8
1000	98.3	96.0	89.4	84.4	83.8	82.3	80.6	0.0	104.4
1250	101.2	99.9	93.3	87.8	86.7	85.1	83.5	81.7	107.9
1600	103.3	103.4	96.6	90.0	89.0	87.6	85.7	83.9	110.8
2000	105.3	107.2	100.6	93.0	91.9	90.0	88.3	86.2	114.1
2500	106.8	110.6	104.2	95.8	94.2	92.0	90.3	88.8	117.2
3150	108.3	113.4	107.9	98.1	96.2	94.0	92.2	90.9	120.0
4000	109.6	115.4	110.8	100.6	98.2	95.9	94.1	93.5	122.1
5000	109.5	115.1	111.3	102.1	99.3	97.1	95.7	95.0	122.2
6300	108.7	114.7	112.0	104.2	101.0	98.6	97.2	97.1	122.5
8000	117.8	124.3	119.1	116.8	110.7	105.1	104.1	107.2	131.6
10000	108.1	113.7	112.3	106.5	103.3	101.5	104.1	106.9	123.2
12500	106.4	113.2	111.0	106.5	103.5	104.7	108.3	108.6	123.5
16000	105.4	112.9	111.3	107.0	106.3	111.9	109.6	107.6	124.9
20000	105.6	110.7	110.4	106.9	106.4	107.5	106.6	106.9	123.0
25000	106.0	110.8	110.1	108.1	108.3	107.1	108.3	107.7	123.6
31500	106.8	111.0	110.6	110.0	108.9	108.3	108.8	107.6	124.3
40000	105.1	109.4	109.7	110.0	108.0	107.8	107.7	106.4	123.5
50000	102.5	107.4	108.3	109.3	107.0	106.8	106.5	104.7	122.3
63000	102.4	107.4	108.5	109.6	107.7	107.5	107.0	104.8	122.7
80000	100.2	104.8	106.0	107.0	106.4	105.8	104.7	102.8	120.6
100000	96.4	101.1	102.4	103.2	102.7	102.1	101.1	99.0	116.9

- COMPUTED SPL(THETA) -

THETA	15	30	45	60	75	90	105	120
	121.5	127.3	123.8	121.0	118.2	118.1	117.9	117.3

TOTAL ACOUSTIC POWER

PWL	WATTS
136.4	43.5

NOZZLE ARRANGEMENT III: 90 DEGREE IMPINGEMENT

P(TM) = 100 PSIG
P(TI) = 18 PSIG

P ATM = 14.4 PSIA
X/D = 1.1

THETA	15	30	45	60	75	90	105	120	
FREQUENCY				- SPL(F,THETA) -					PWL(F)
315	83.2	0.0	0.0	0.0	0.0	0.0	0.0	0.0	84.6
400	86.6	82.4	0.0	0.0	0.0	0.0	0.0	0.0	90.4
500	89.8	86.7	0.0	0.0	0.0	0.0	0.0	0.0	94.1
630	92.9	90.0	82.8	0.0	0.0	0.0	0.0	0.0	97.8
800	96.0	93.2	86.1	81.5	80.6	0.0	0.0	0.0	101.4
1000	98.8	96.7	89.2	84.0	82.9	81.8	0.0	0.0	104.6
1250	101.9	100.2	92.6	86.6	85.4	83.8	82.4	81.0	108.0
1600	103.8	103.5	95.8	88.9	87.5	85.9	84.2	82.6	110.7
2000	105.1	106.5	98.8	91.2	89.8	87.9	86.7	85.2	113.2
2500	106.1	109.0	101.9	93.4	91.5	89.9	88.7	87.2	115.5
3150	107.0	110.9	104.3	95.7	93.2	91.8	90.4	89.6	117.3
4000	107.6	111.8	106.0	97.9	95.3	93.3	92.3	91.8	118.5
5000	108.2	112.2	107.1	99.1	96.3	94.5	93.9	93.2	119.1
6300	108.7	112.5	108.0	100.8	97.8	96.1	95.5	95.3	119.8
8000	109.1	112.9	109.0	103.3	99.3	97.4	97.1	97.5	120.6
10000	109.1	112.2	109.0	103.9	100.7	99.0	100.2	103.2	120.9
12500	108.7	111.3	108.2	104.1	101.3	101.1	105.0	107.2	121.4
16000	107.3	110.9	107.8	104.4	102.4	104.5	107.2	107.2	121.8
20000	105.4	109.4	107.2	104.6	103.5	105.6	105.5	105.5	121.0
25000	106.2	109.6	108.3	106.3	106.5	105.8	105.2	105.7	121.8
31500	106.7	109.9	109.1	108.2	106.9	106.1	106.0	106.0	122.5
40000	105.1	108.3	108.4	108.4	105.9	106.3	105.6	105.1	121.9
50000	104.5	106.9	107.8	107.3	106.1	106.3	105.0	103.9	121.3
63000	108.8	110.4	114.6	111.2	112.0	110.5	110.4	109.2	126.5
80000	105.8	106.9	108.6	107.7	106.9	105.5	104.7	104.3	121.6
100000	100.7	102.2	103.7	102.6	102.3	101.5	100.0	99.7	116.9

- COMPUTED SPL(THETA) -

THETA	15	30	45	60	75	90	105	120
	119.9	122.9	120.8	117.8	116.9	116.3	116.4	116.3

TOTAL ACOUSTIC POWER

PWL	WATTS
133.6	22.9

REFERENCES

1. Hubbard, H. H. "A Survey of the Aircraft-Noise Problem with Special Reference to its Physical Aspects." NACA TN 2701, 1952.

2. Richards, E. J. "The Constraining Order of Airport Noise." Institute of Sound and Vibration Report No. 148, 1966.

3. Kupferman, T. R. "Noise: The Need for Legislation and Technology." Engineer, Vol. VII, No. 3, 1966.

4. Wilhold, G. A. "Aerospace Noise." Aeronautics and Astronautics, Vol. 5, No. 5, May, 1967.

5. Yaffee, M. L. "NASA Begins Major Engine Noise Project." Aviation Week and Space Technology, Vol. 87, No. 8, August 21, 1967.

6. Dosanjh, D. S. and Sheeran, W. J. "Experiments on Two-Dimensional, Transversely Impinging Jets." AIAA Journal, February, 1963.

7. Ingard, V. and Maling, G. C. "Noise Generated by Two Interacting Air Jets." JASA, Vol. 31, No. 7, July, 1959, p. 1031.

8. Lighthill, M. J. "On Sound Generated Aerodynamically. I - General Theory." Proc. Roy. Soc. A, Vol. 211, 1952.

9. Lighthill, M. J. "On Sound Generated Aerodynamically. II - Turbulence as a Source of Sound." Proc. Roy. Soc. A, Vol. 222, 1954.

10. Lighthill, M. J. "Sound Generated Aerodynamically." Proc. Roy. Soc. A, Vol. 267, 1962.

11. Corcos, G. M. "Some Measurements Bearing on the Principle of Operation of Jet Silencing Devices." Douglas Report No. SM-23114, March, 1958.

12. Chu, W. T. "Turbulence Measurements Relevant to Jet Noise." UTIAS Report No. 119, November, 1966.

13. Mollo-Christensen, E. "Jet Noise and Shear Flow Instability Seen from an Experimenters Viewpoint." ASME Paper No. 67-APM-C., 1967.

14. Lighthill, M. J. "Jet Noise." AGARD Report 448, April, 1963, p. 15.

15. Ribner, H. S. "The Generation of Sound by Turbulent Jets." Advances in Applied Mechanics, Volume 8, Academic Press, New York, 1964.

16. Phillips, O. M. "On the Generation of Sound by Supersonic Turbulent Shear Layers." J. Fluid Mech., 9, Part 1, 1960.

17. Ffowcs-Williams, J. E. "The Noise from Turbulence Convected at High Speed." Proc. Roy. Soc. A, Vol. 255, 1963.

18. Lowson, M. V. and Ollerhead, J. B. "Shadowgraph Visualization of Jet Noise." Wyle Laboratories Research Staff, Huntsville, Alabama. Abstract listed in JASA, V. 41, No. 6, June, 1967, p. 1610.

19. Mayes, W. H., Lanford, W. E., and Hubbard, H. H. "Near Field and Far Field Noise Surveys of Solid Fuel Rocket Engines for a Range of Nozzle Exit Pressures." NASA TN D-21, 1959.

20. Lighthill, M. J. "Jet Noise" AGARD Report 448, April, 1963, p. 14.

21. Kovasznay, L. "Turbulence in Supersonic Flow." J. Aeron. Sci. Vol. 20, No. 10, October, 1953.

22. Franklin, R. E. "Noise Measurements on Cold Jets Using Convergent-Divergent Nozzles." Aeronautical Quarterly, V. 8, November, 1957.

23. Howes, W. L. "Similarity of Far Noise Fields of Jets." NASA TR R-52, 1960.

24. Ribner, H. S. "Convection of a Pattern of Vorticity through a Shock Wave." NACA Report 1164, 1954.

25. Hollingsworth, M. A. and Richards, E. J. "On the Sound Generated by the Interaction of a Vortex and a Shock Wave." ARC 18257, FM 2371, 1956.

26. Dosanjh, D. S. and Weeks, T. M. "Sound Generated by Shock-Vortex Interaction." AIAA Journal, Vol. 5, No. 4, April, 1967.

27. Ribner, H. S. "Shock-Turbulence Interaction and the Generation of Noise." NACA Report 1233, 1955.

28. Ribner, H. S. "Acoustic Energy Flux from Shock-Turbulence Interaction." UTIAS Technical Note No. 108, July, 1967.

29. Powell, A. "On the Mechanism of Choked Jet Noise." Proc. Phys. Soc., Vol. B66, 1953.

30. Hammitt, A. G. "The Oscillation and Noise of an Overpressure Sonic Jet." GASL Technical Report No. 137, November, 1959.

31. Greatrex, F. B., Richards, E. J., et al "Aeronautical Acoustics - In Particular, Jet Noise." J. Roy. Aero. Soc. Vol. 58, No. 520, April, 1954.

32. Barnett, N. E. "Experimental Study of Sound Power Radiated from Cold Model Jets and Ground Silencing Arrangement." Air Force Aero Propulsion Laboratory, Wright-Patterson AFB, Technical Report AFAPL-TR-65-55, Volume I, 1965.

33. Morgan, W. V., Sutherland, L. C., and Young, K. J. "The Use of Acoustic Scale Models for Investigating Near Field Noise of Jet and Rocket Engines." WADD Technical Report 61-178, April, 1961.

34. Pernet, D. F. "Experimental Noise Investigation of Model Nozzles." Air Force Aero Propulsion Laboratory, Wright-Patterson AFB, Technical Report AFAPL-TR-64-138, December, 1964.

35. Harris, C. M. ed. "Handbook of Noise Control." McGraw-Hill Book Company, 1957, 20, p. 9.

36. Love, E. S., Grigsby, C. E., Lee, L. P., and Woodling, M. J. "Experimental and Theoretical Studies of Axisymmetric Free Jets." NASA TR R-6, 1959.

37. Ollerhead, J. "Some Shadowgraph Experiments with a Cold Supersonic Jet." Wyle Laboratories Research Staff Report No. WR 66-44, October, 1966.

38. Lassiter, L. W. and Hubbard, H. H. "The Near Noise Field of Static Jets and Some Model Studies of Devices for Noise Reduction." NACA TN 3187, 1954.

39. Ladenburg, R., VanVoorhis, C. C., and Winckler, J. "Interferometric Studies of Faster than Sound Phenomena. Part II. Analysis of Supersonic Air Jets." Physical Review, V. 76, No. 5, September 1, 1949.

40. Sheeran, W. J. and Dosanjh, D. S. "Transversely Impinging Two-Dimensional Jet Flows." Advances in Fluidics, ASME, 1967.

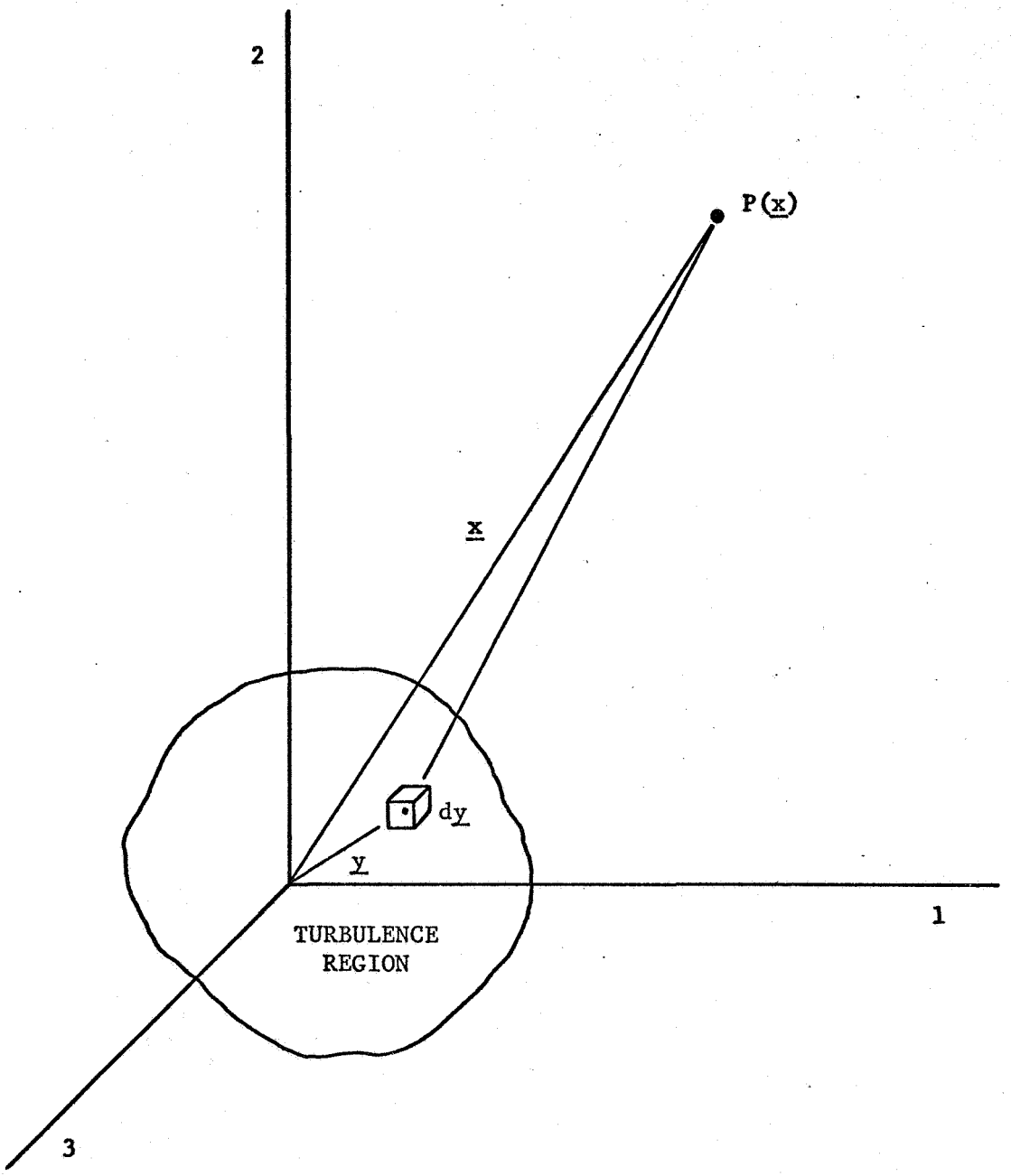

FIGURE 1. COORDINATE SYSTEM FOR LIGHTHILL THEORY OF AERODYNAMIC SOUND GENERATION.

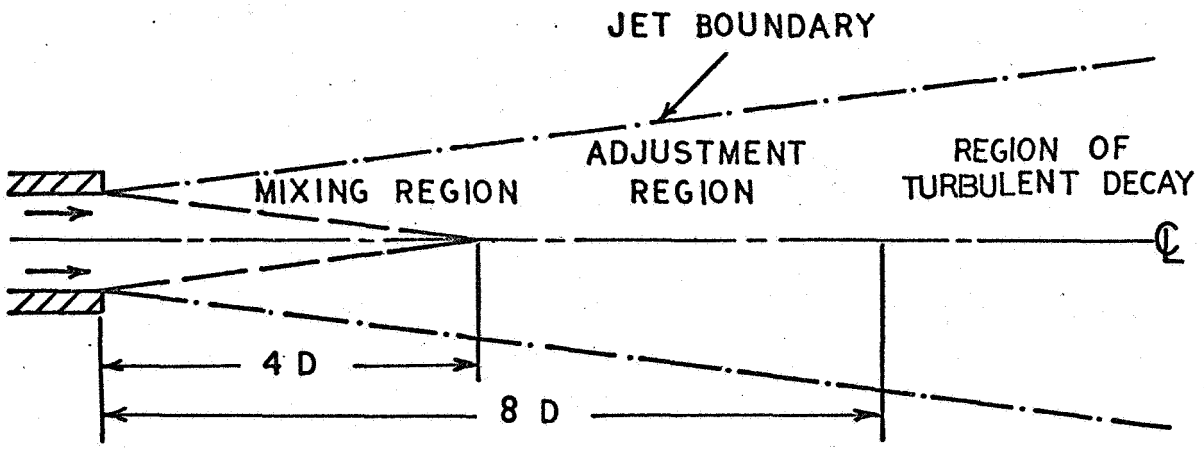

A) SUBSONIC JET FLOW.

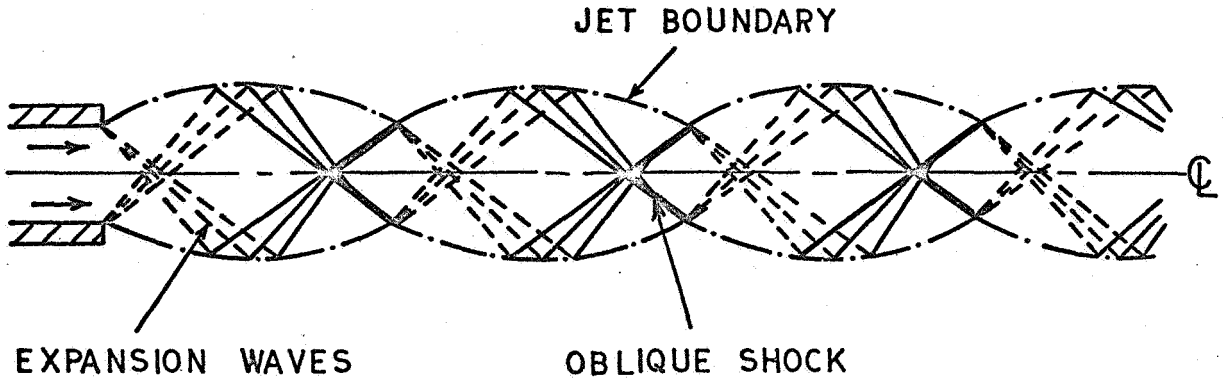

B) UNDEREXPANDED JET FLOW WITH REPETITIVE SHOCKS.

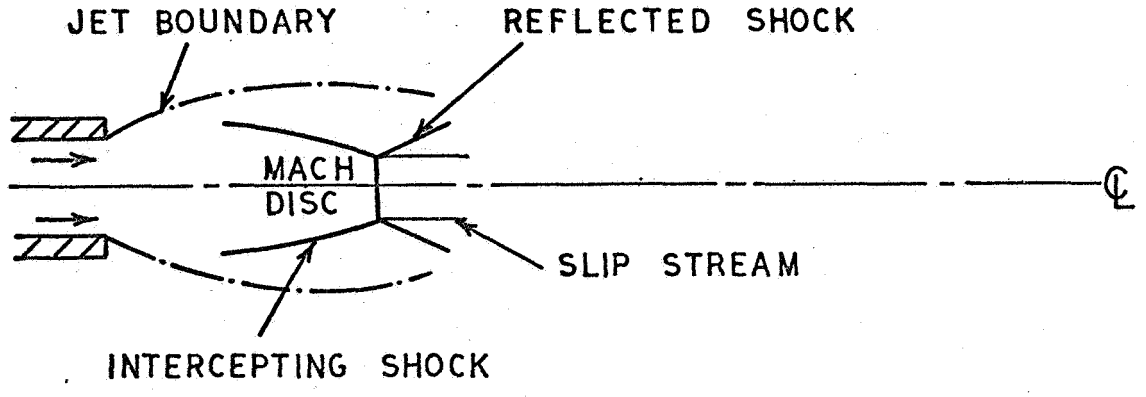

C) UNDEREXPANDED JET FLOW WITH MACH DISC.

FIG. 2. MAIN FEATURES OF AXISYMMETRIC JET FLOWS.

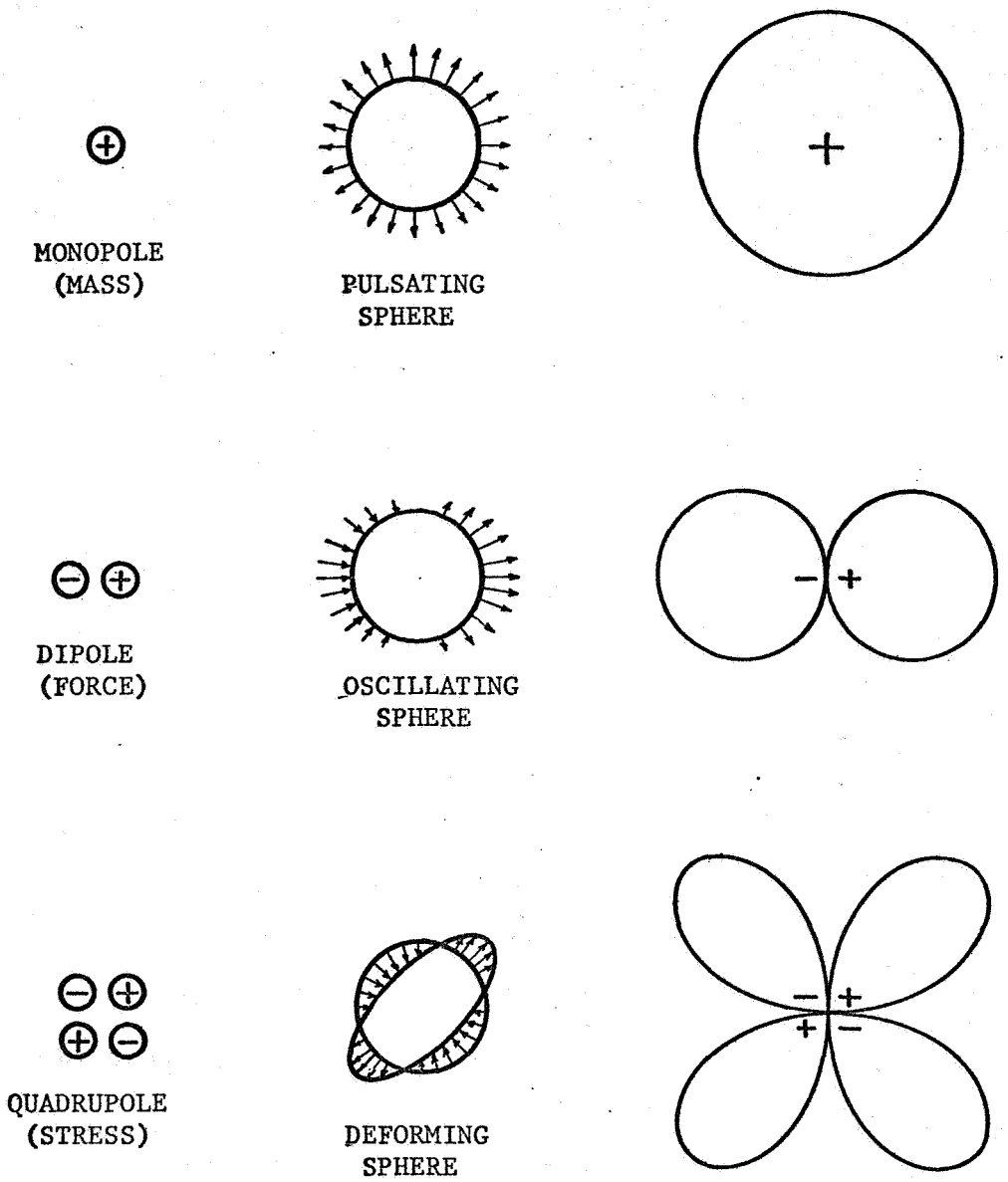

FIGURE 3. REPRESENTATIONS OF CLASSICAL ACOUSTIC SOURCES.

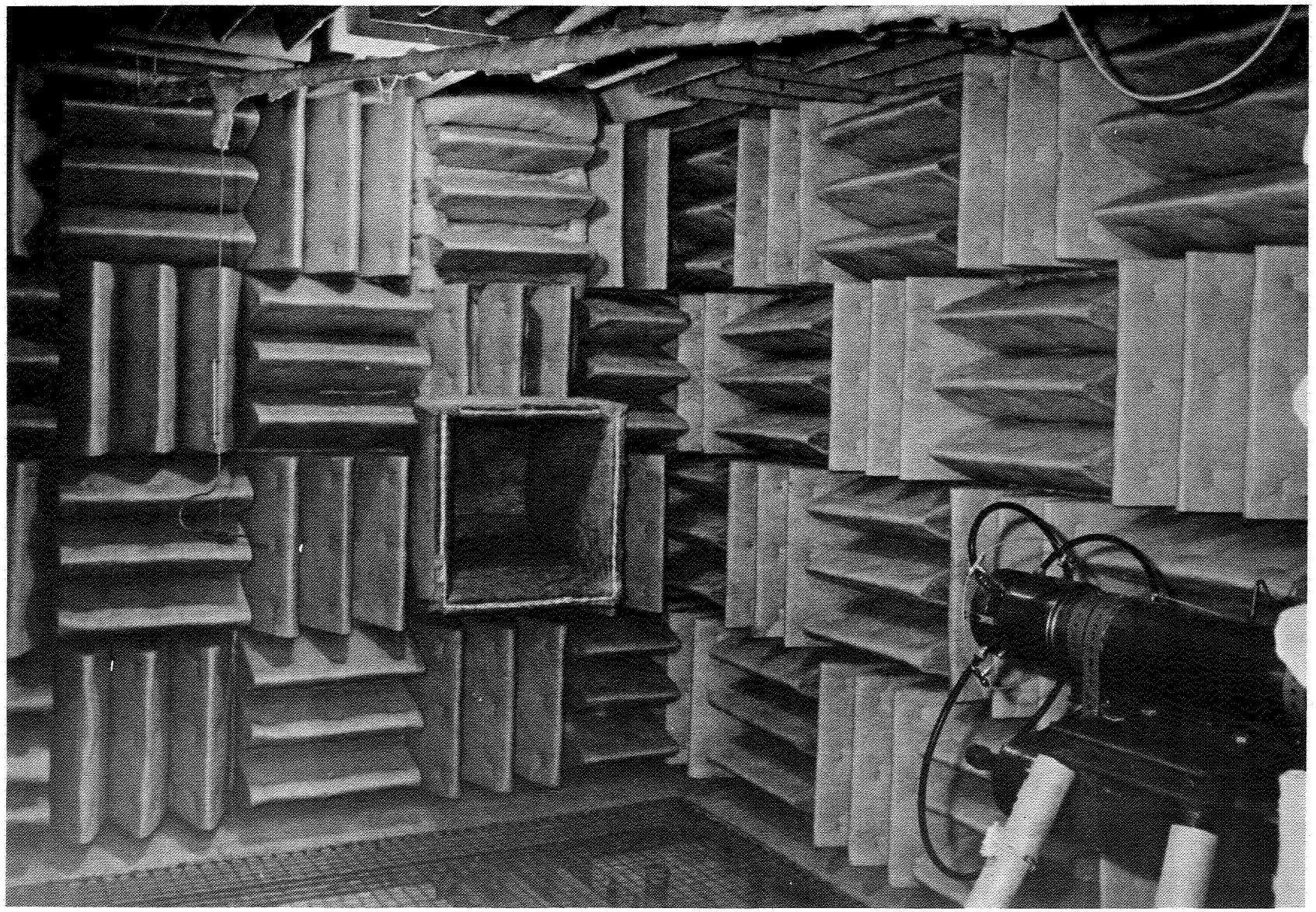

FIGURE 4. VIEW IN ANECHOIC CHAMBER SHOWING IMPINGEMENT FUNNEL, BOOM-SUSPENDED MICROPHONE, AND INSTALLED NOZZLE ASSEMBLY. COVERING FIBERGLASS IS REMOVED TO SHOW INSTALLATION DETAILS OF RESERVOIRS.

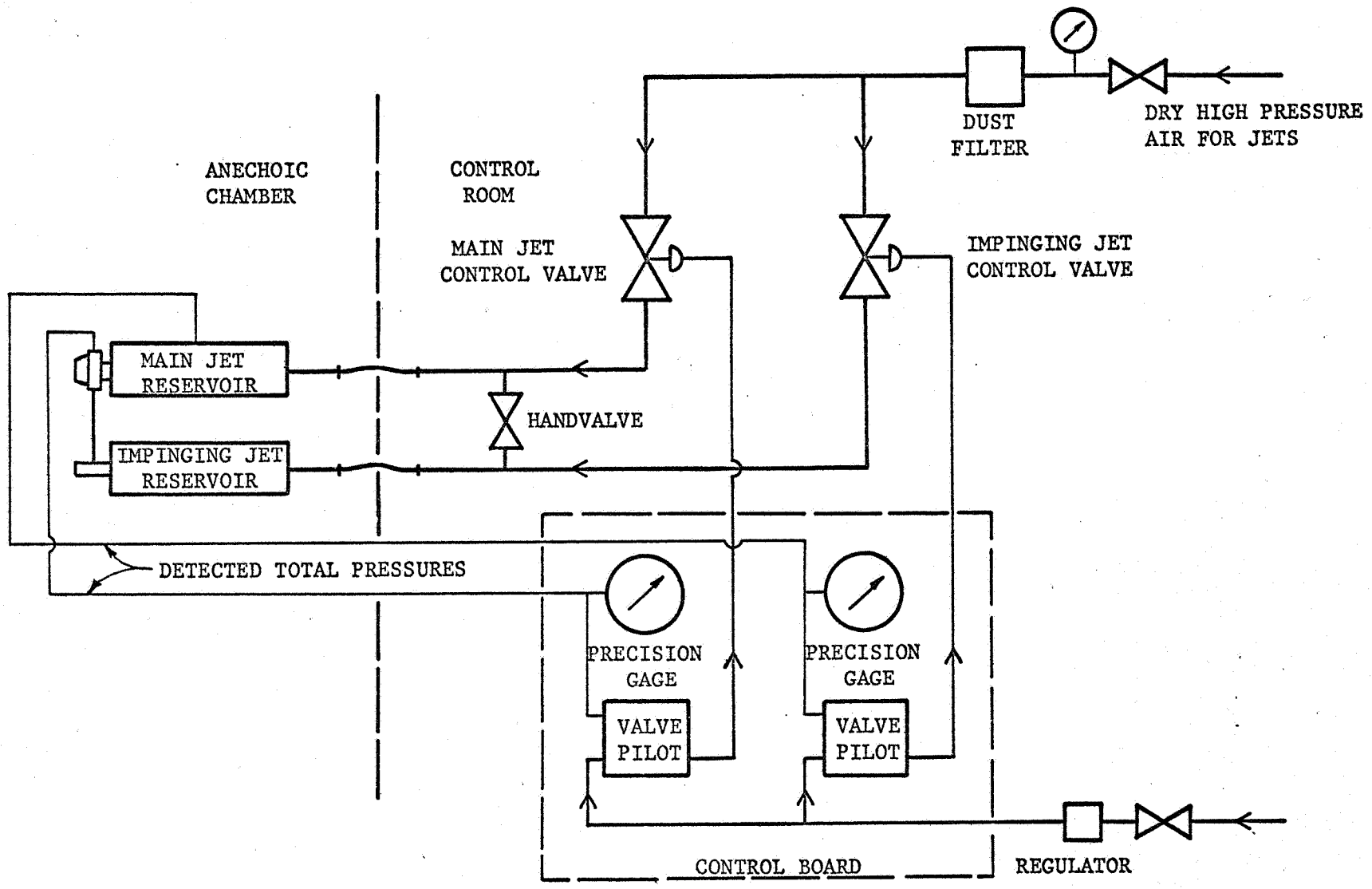

FIGURE 5. SCHEMATIC DIAGRAM OF AIR FLOW CONTROL SYSTEM.

FIGURE 6. VIEW IN CONTROL ROOM SHOWING AIR FLOW CONTROL SYSTEM AND ACOUSTICAL INSTRUMENTATION.

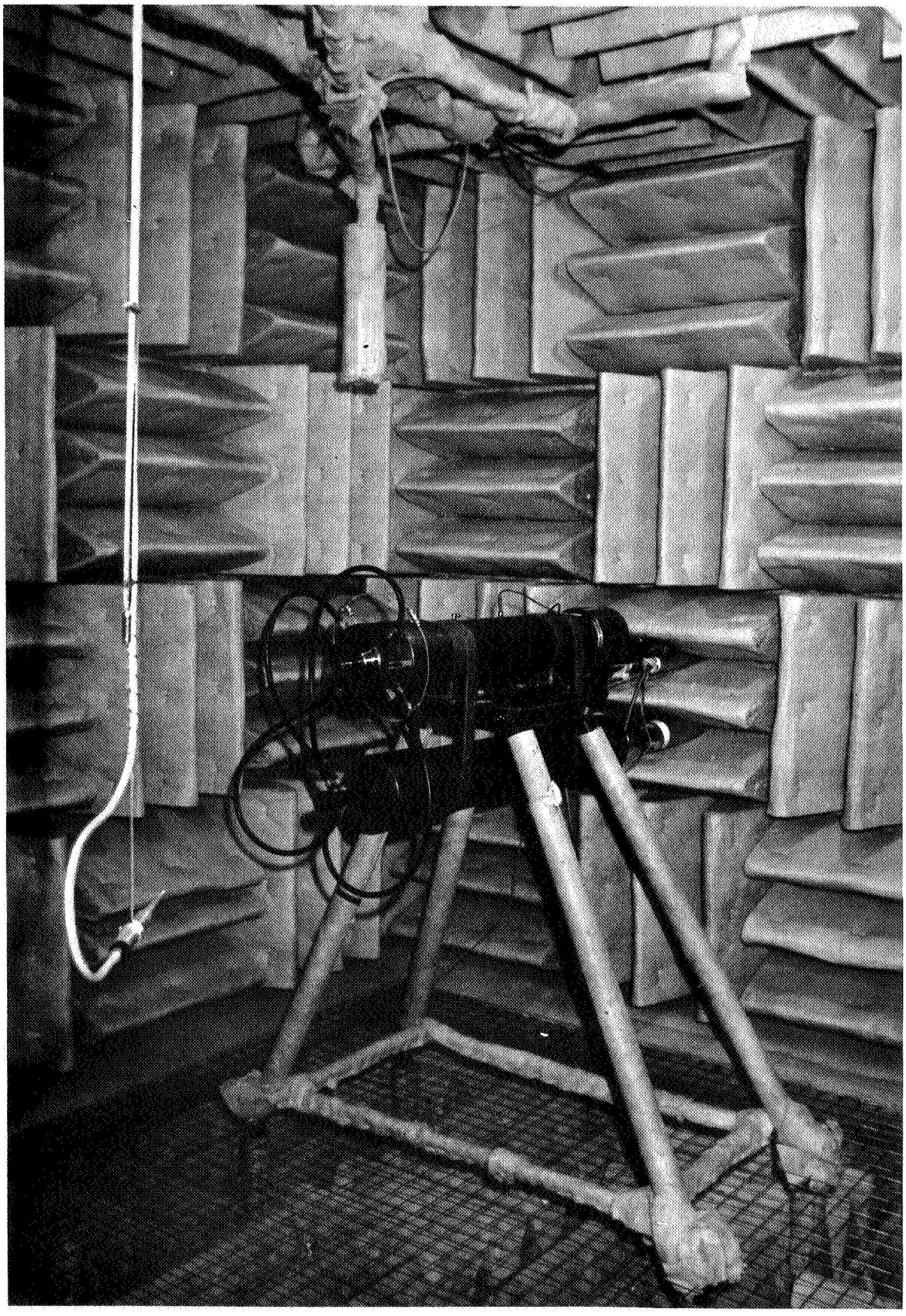

FIGURE 7. VIEW IN ANECHOIC CHAMBER SHOWING INSTALLED NOZZLE ASSEMBLY, RESERVOIRS, AND SUPPORTING STAND. FIBERGLASS COVERING OF RESERVOIRS IS REMOVED TO SHOW THE INSTALLATION DETAILS.

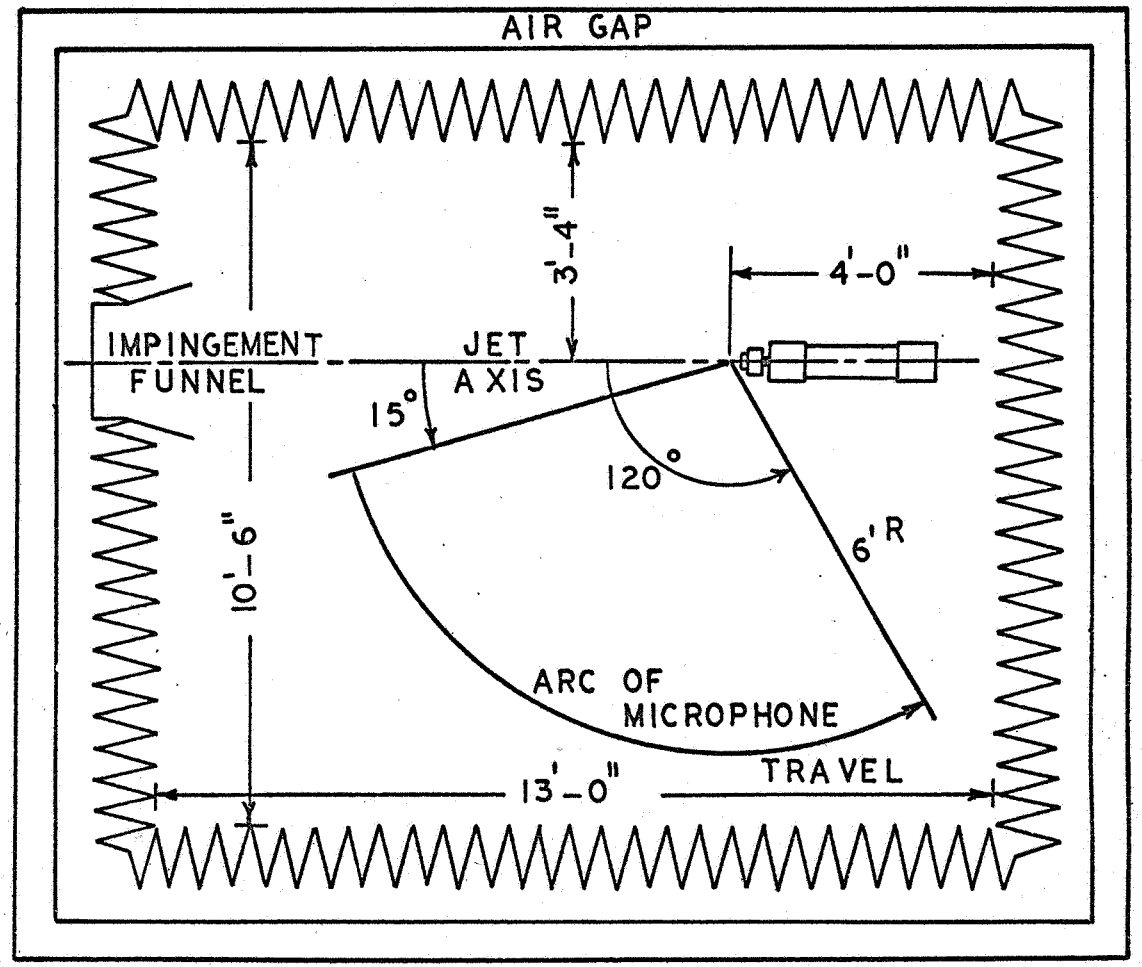

FIGURE 8. SCHEMATIC PLAN OF ANECHOIC CHAMBER.

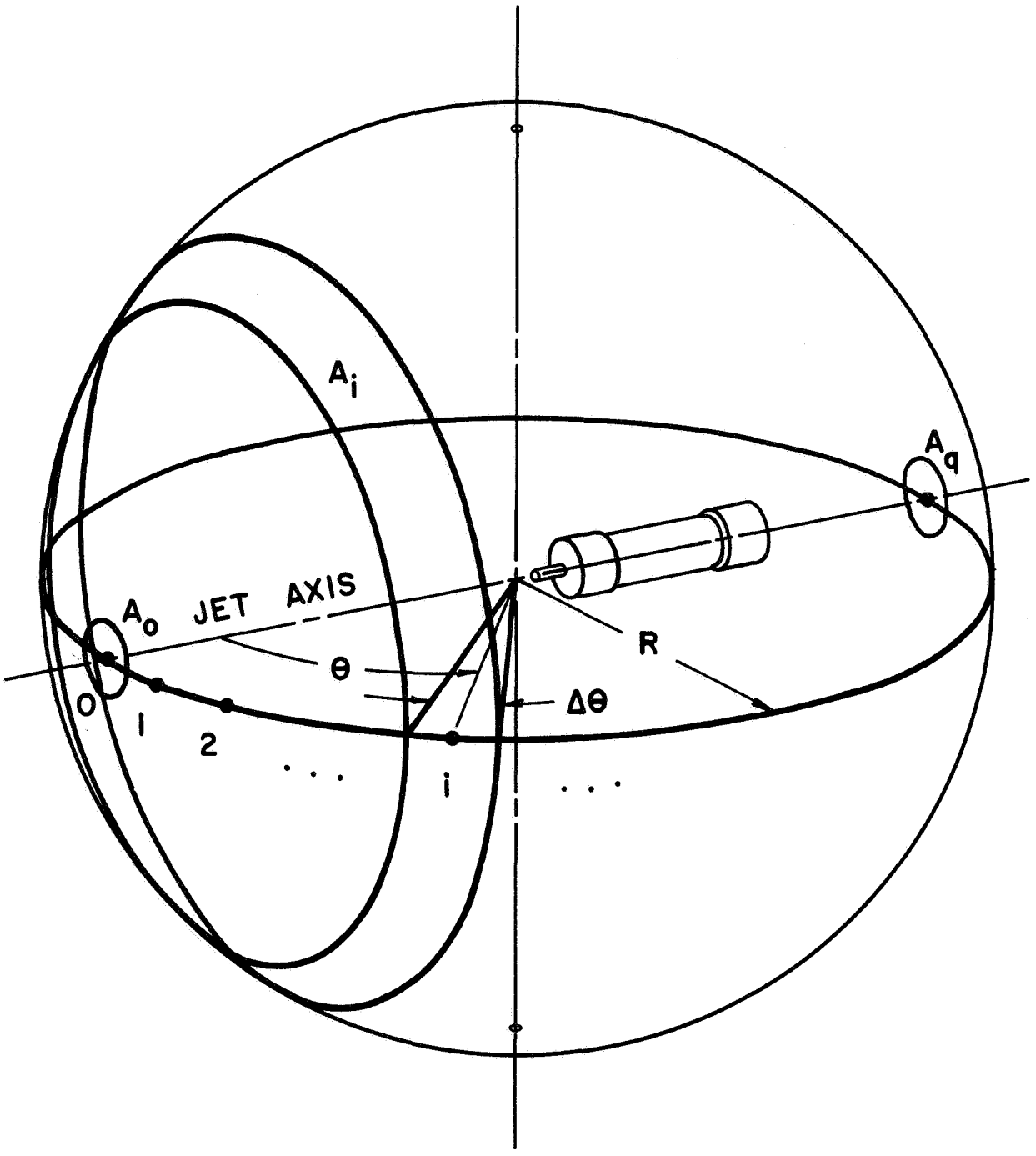

FIGURE 9. ENCLOSING SPHERE OF ACOUSTICAL MEASURMENTS AND ELEMENTAL AREAS AT MEASURING STATIONS.

a) SHADOWGRAPH APPARATUS INSTALLED IN ANECHOIC CHAMBER.

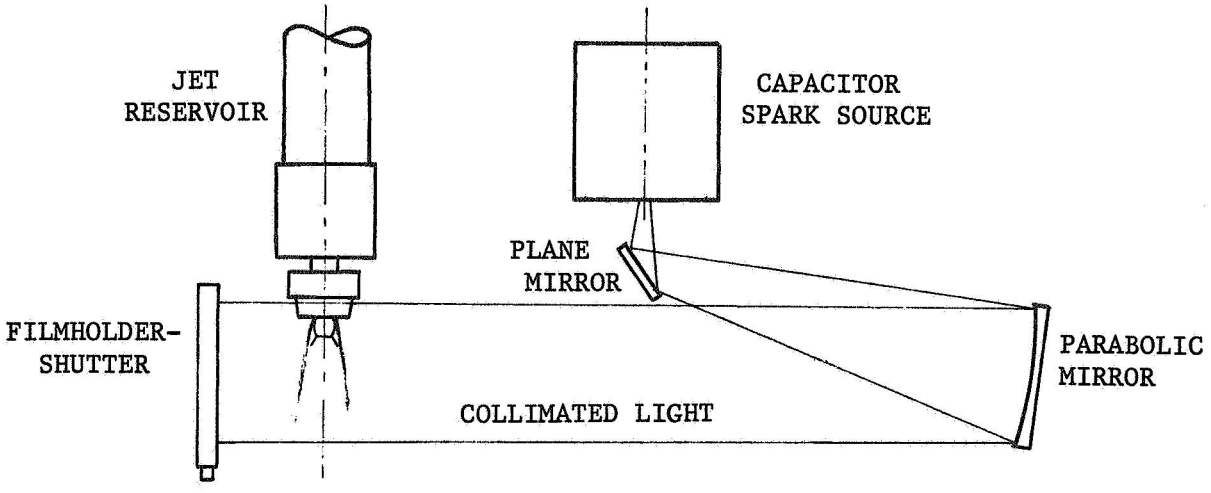

b) SCHEMATIC PLAN VIEW OF ARRANGEMENT.

FIGURE 10. PORTABLE SHADOWGRAPH APPARATUS.

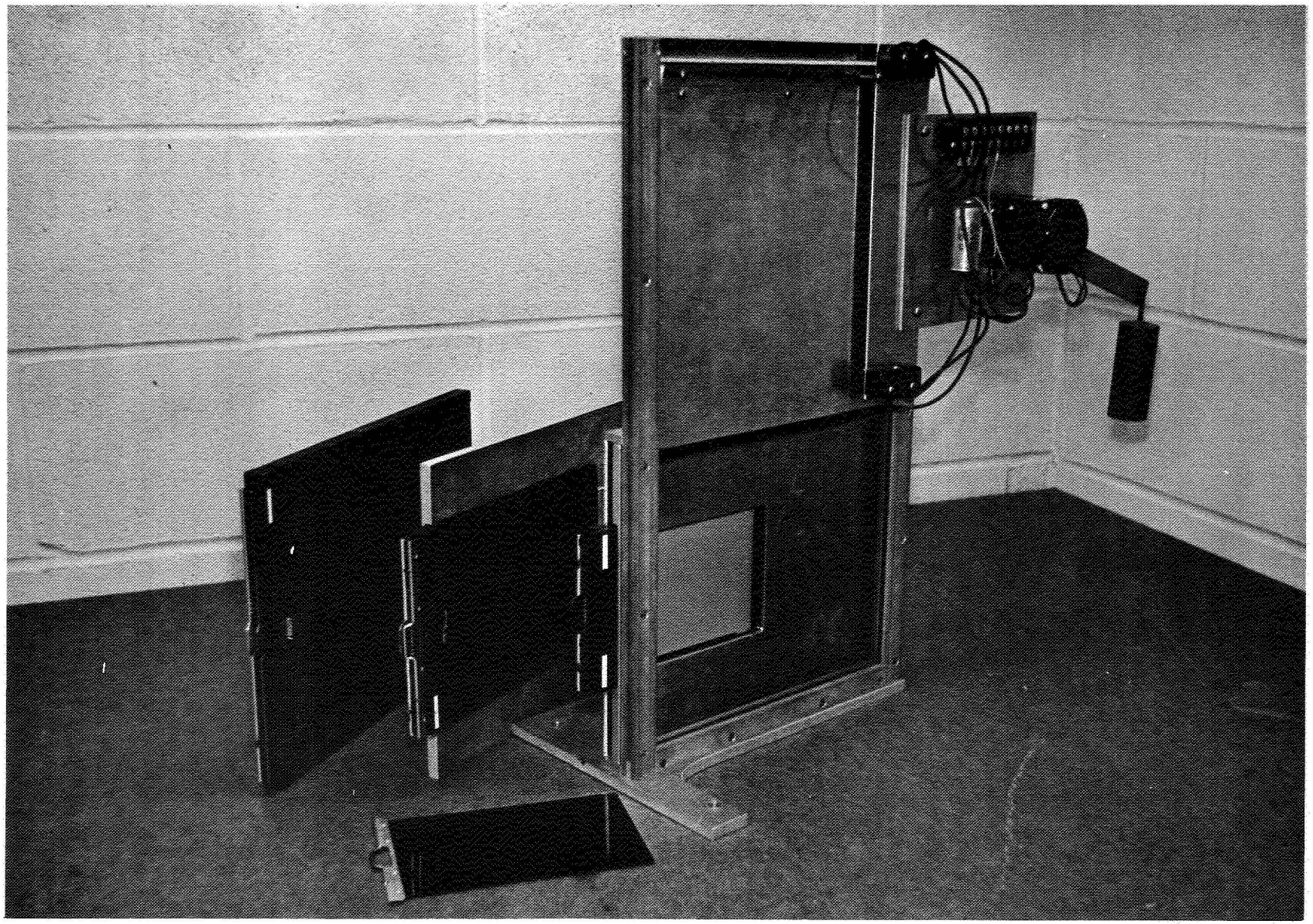

FIGURE 11. REMOTELY OPERATED FILMHOLDER/SHUTTER. UNIT ACCEPTS 4x5, 5x8, AND 8x10 INCH CUT FILM.

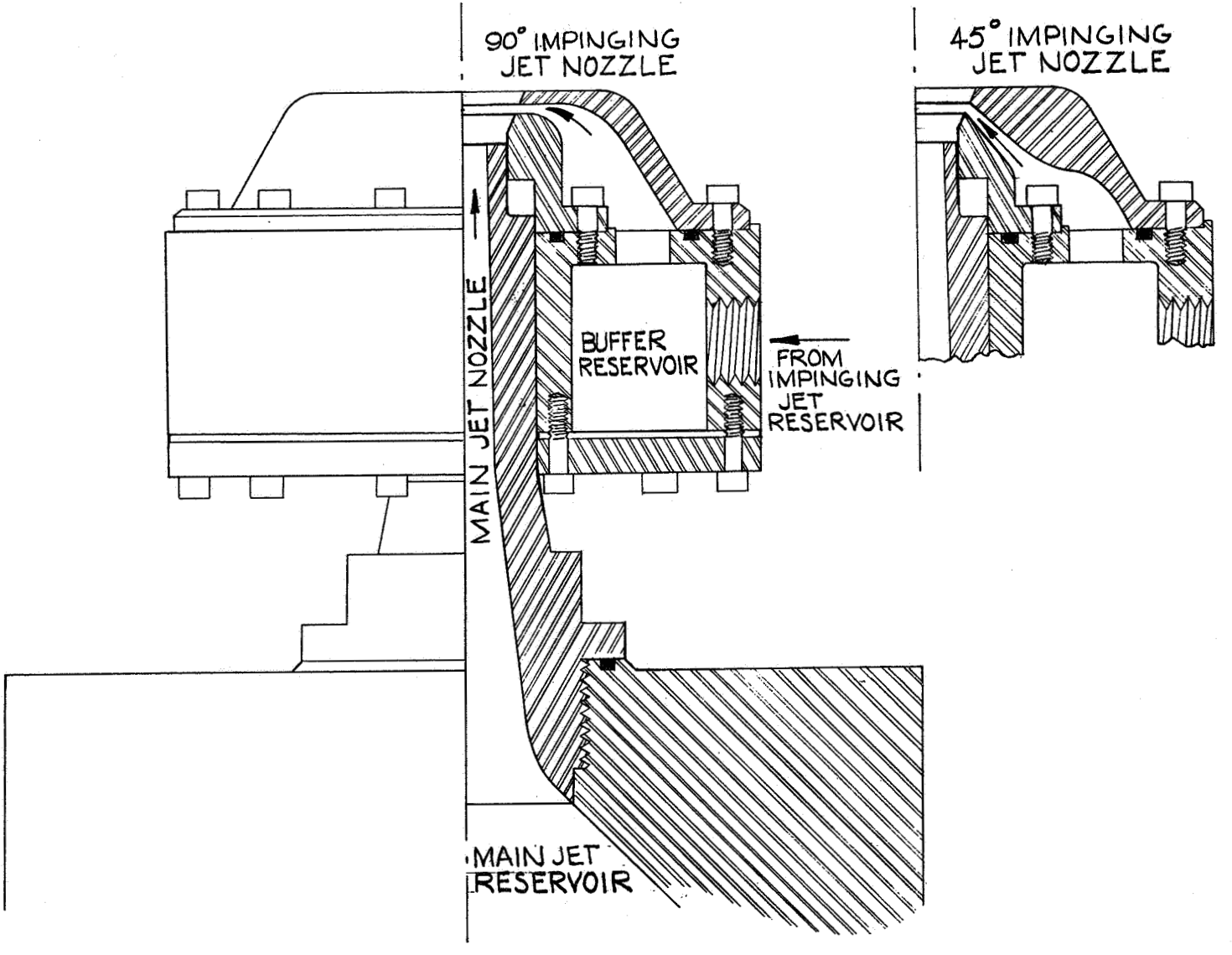

FIGURE 12. NOZZLE ARRANGEMENT I. BOTH 90° AND 45° IMPINGEMENT USED WITH NO ENTRAINMENT PROVISION MADE UPSTREAM OF THE IMPINGEMENT LOCATION. MAIN JET EXIT DIAMETER = 3/8 IN. IMPINGING JET ANNULUS EXIT: 3/4 IN. DIAM. X 3/64 IN. WIDE.

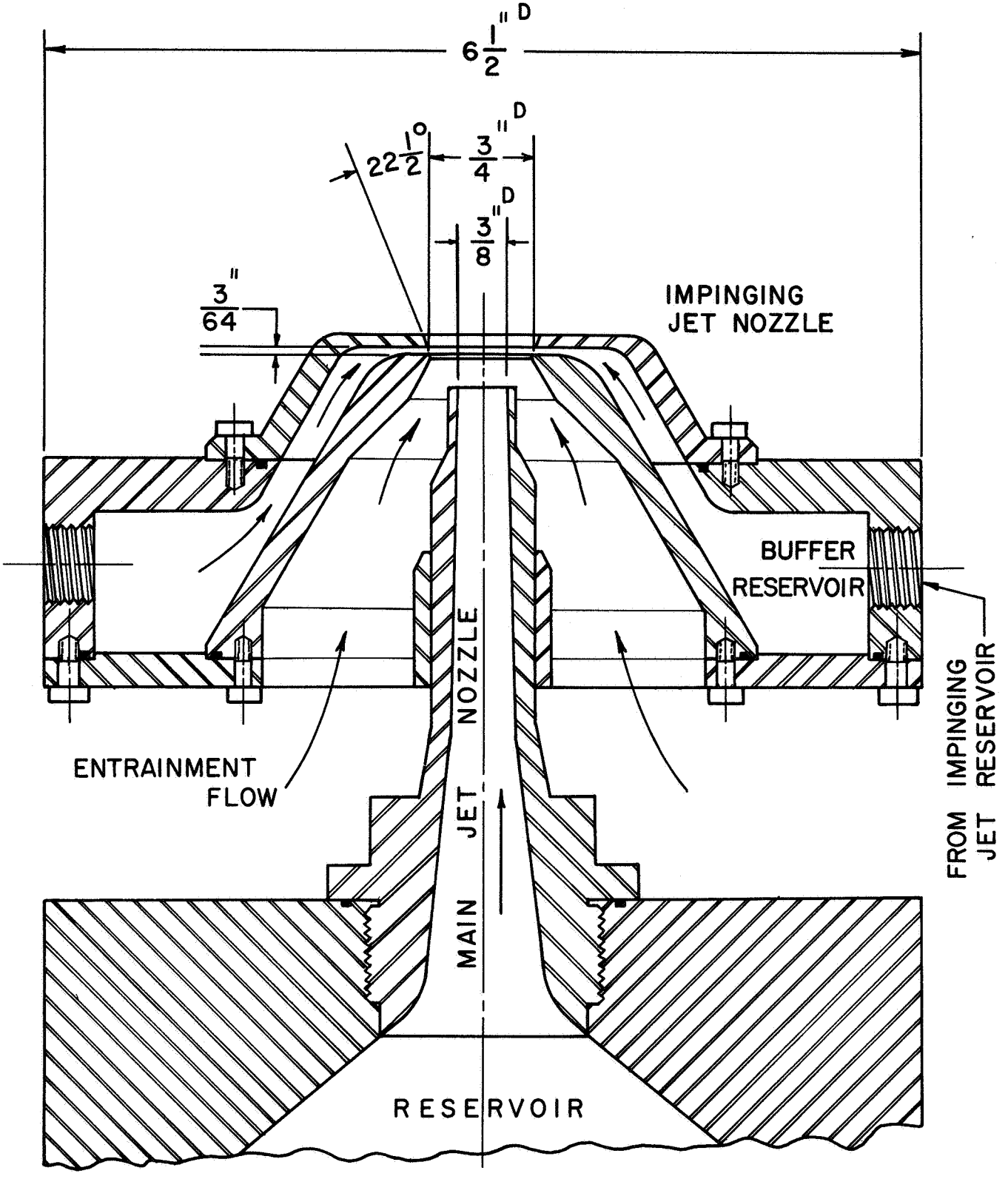

FIGURE 13. NOZZLE ARRANGEMENT II. PROVISION MADE FOR ENTRAINMENT BY INTERACTING JET FLOWS UPSTREAM OF IMPINGEMENT LOCATION. MAIN JET DIAMETER = 3/8 IN. IMPINGING JET ANNULUS EXIT: 3/4 IN. DIAM. X 3/64 IN. WIDE.

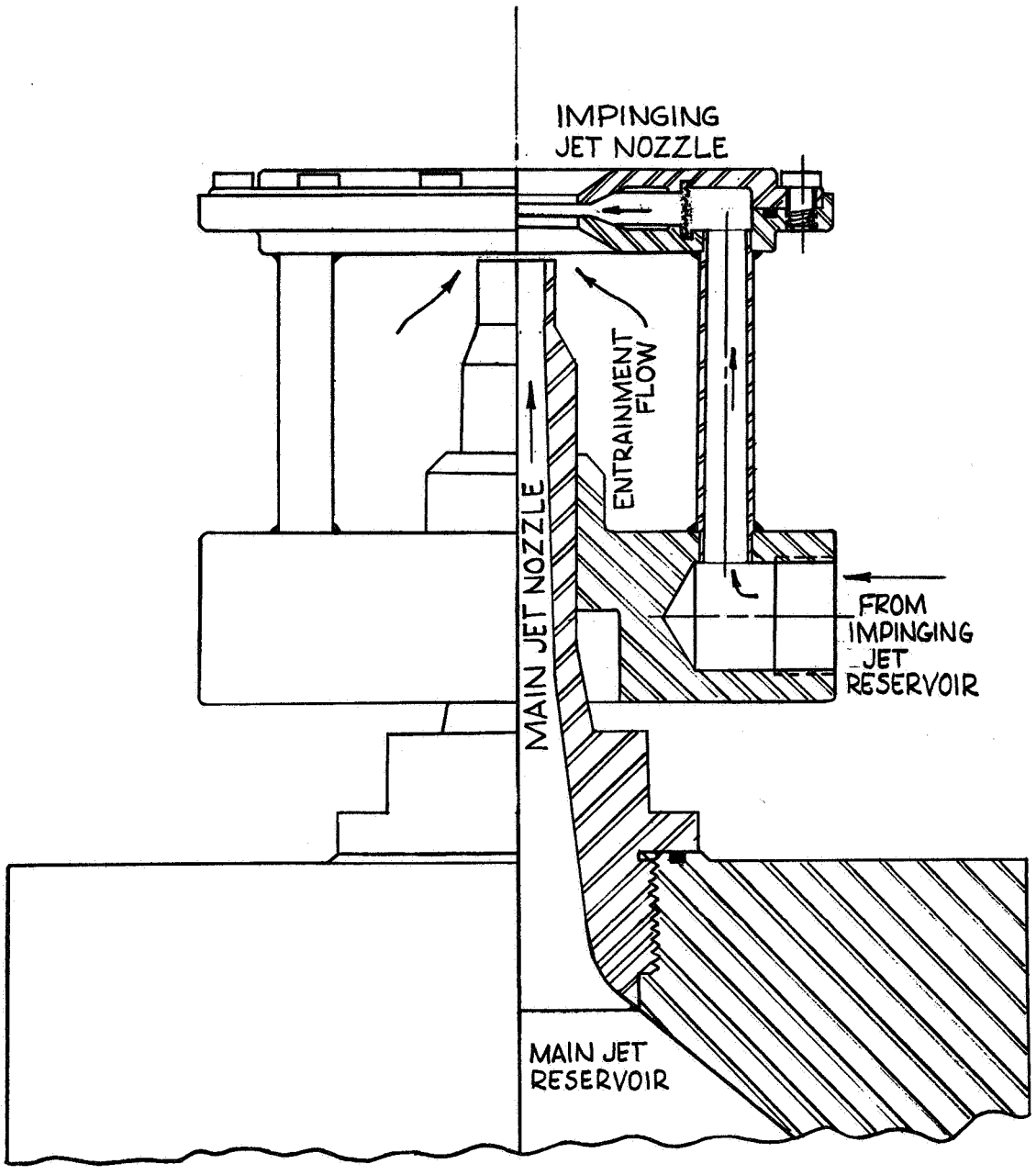

FIGURE 14. NOZZLE ARRANGEMENT III. MAXIMUM UNOBSTRUCTED PROVISION MADE FOR ENTRAINMENT BY INTERACTING JET FLOWS UPSTREAM OF IMPINGEMENT LOCATION. MAIN JET EXIT DIAMETER = 3/8 IN. IMPINGING JET ANNULUS EXIT: 3/4 IN. DIAM. X 3/64 IN. WIDE.

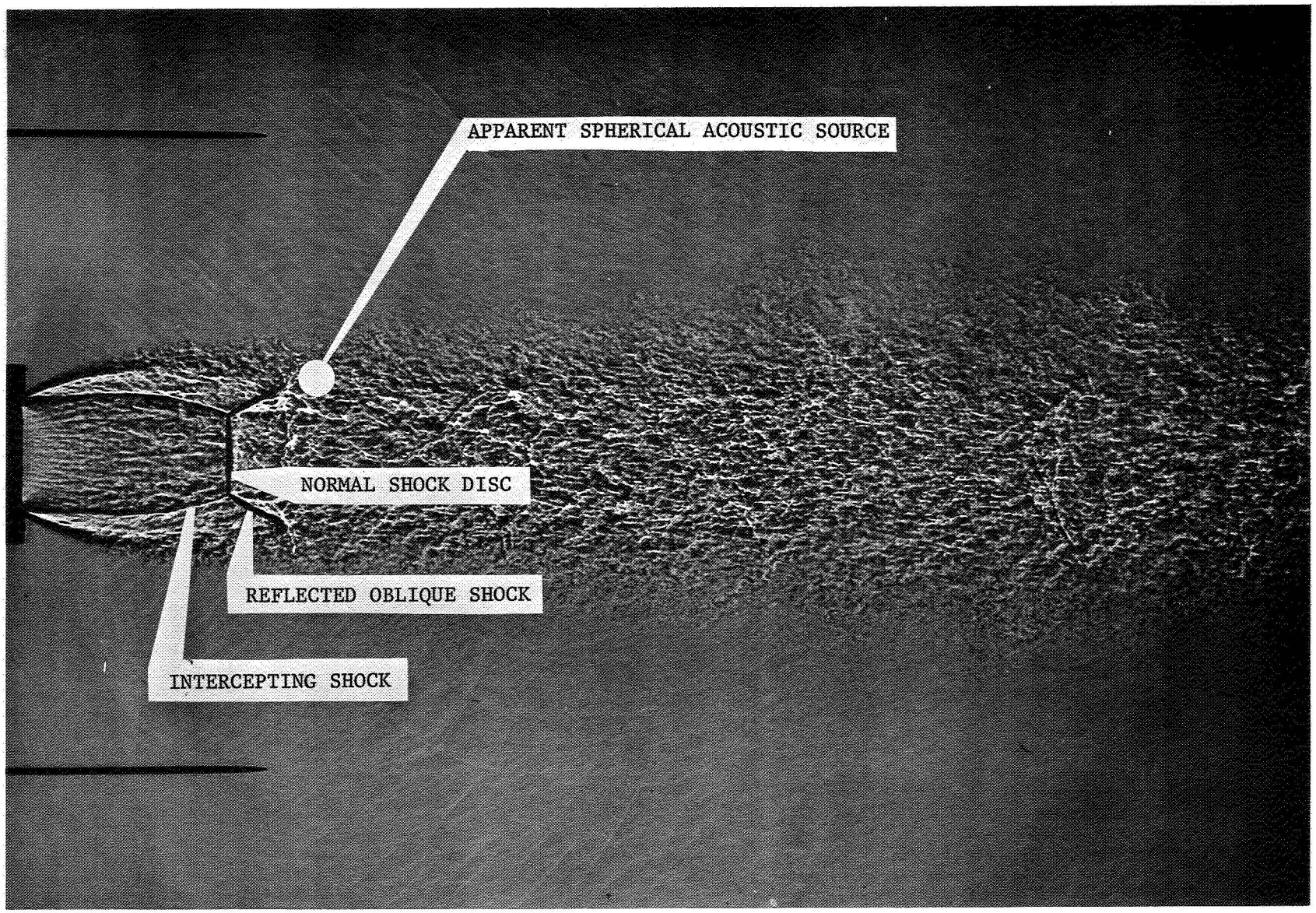

FIGURE 15. SHADOWGRAPH OF MAIN JET ALONE AT TOTAL PRESSURE OF 100 PSIG SHOWING CHARACTERISTIC SHOCK STRUCTURE AND ACOUSTIC EMISSIONS. THE SCALING NEEDLES ARE TWO INCHES APART.

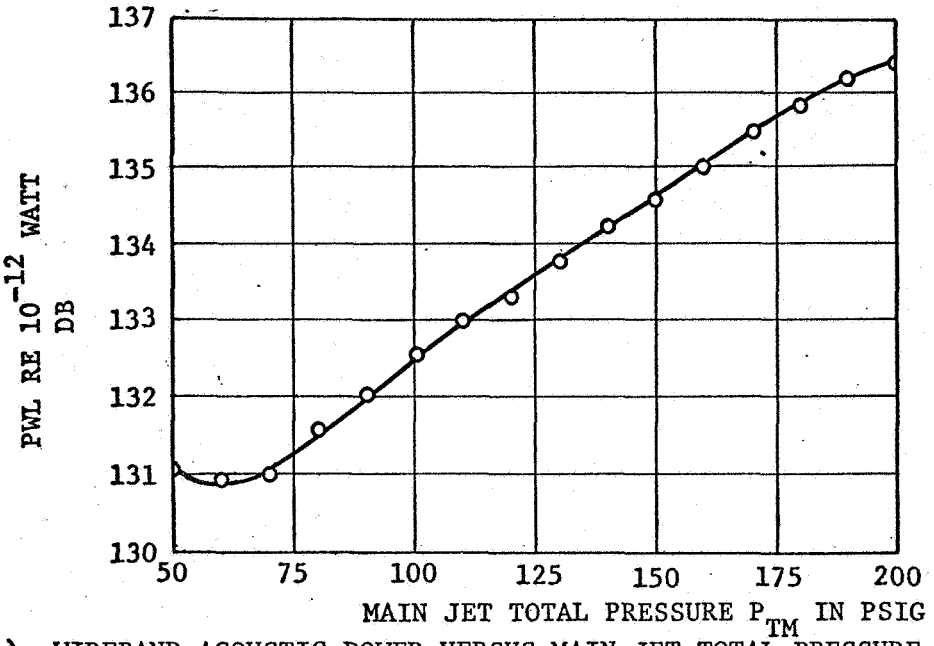

a) WIDEBAND ACOUSTIC POWER VERSUS MAIN JET TOTAL PRESSURE.

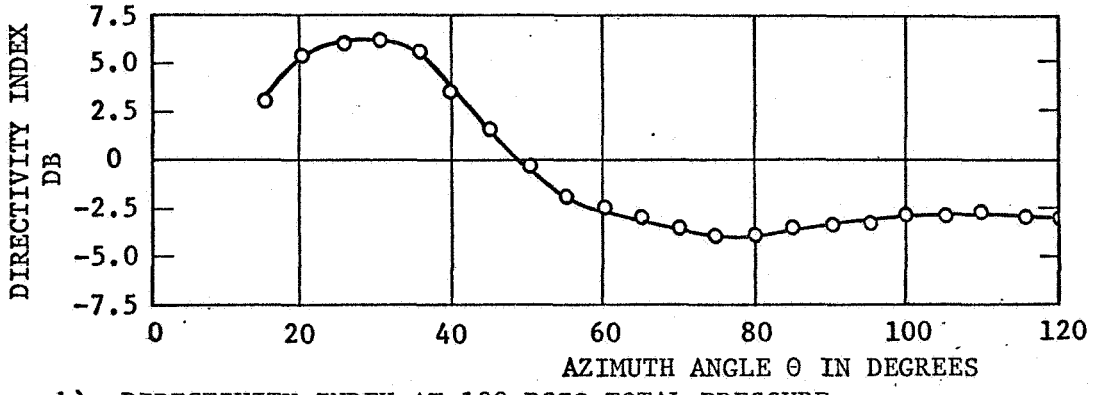

b) DIRECTIVITY INDEX AT 100 PSIG TOTAL PRESSURE.

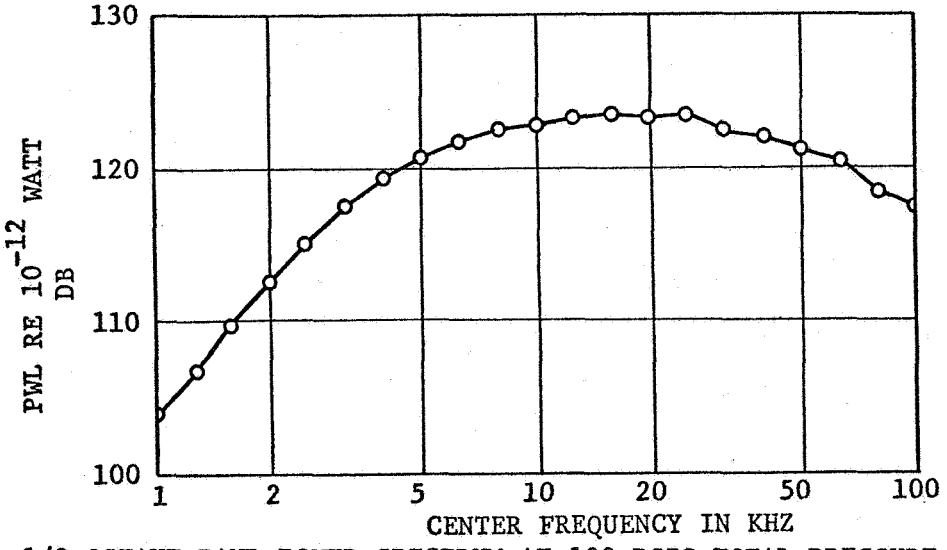

c) 1/3 OCTAVE BAND POWER SPECTRUM AT 100 PSIG TOTAL PRESSURE.

FIGURE 16. ACOUSTICAL DATA FOR MAIN JET ALONE.

MAIN JET ALONE

(OF NOZZLE ARRANGEMENT I)

P(TM) = 100 PSIG P ATM = 14.6 PSIA

THETA	15	30	45	60	75	90	105	120	
FREQUENCY				- SPL(F,THETA) -					PWL(F)
315	82.0	0.0	0.0	0.0	0.0	0.0	0.0	0.0	83.4
400	85.5	81.0	0.0	0.0	0.0	0.0	0.0	0.0	89.2
500	89.8	85.0	0.0	0.0	0.0	0.0	0.0	0.0	93.3
630	91.5	88.4	81.3	0.0	0.0	0.0	0.0	0.0	96.3
800	95.3	91.8	84.4	80.3	0.0	0.0	0.0	0.0	100.1
1000	98.3	95.5	87.5	82.6	81.6	80.3	0.0	0.0	103.6
1250	101.4	98.8	91.2	85.3	84.3	82.6	81.0	0.0	106.9
1600	103.5	102.4	94.5	87.5	86.3	84.6	83.0	81.3	109.8
2000	105.4	105.6	97.6	90.0	88.5	86.7	85.3	83.9	112.5
2500	108.0	108.7	100.9	92.0	90.5	88.6	87.3	85.7	115.5
3150	108.3	111.0	103.7	94.2	92.2	90.5	88.9	87.9	117.4
4000	109.5	113.1	106.5	96.5	93.9	92.2	90.6	89.8	119.5
5000	110.4	114.0	108.2	98.0	94.4	93.4	92.1	91.1	120.6
6300	111.1	115.2	109.5	99.6	96.7	94.9	93.5	92.8	121.8
8000	112.3	115.5	109.7	101.0	98.2	96.1	95.0	96.3	122.3
10000	112.5	115.7	109.8	102.0	98.9	97.3	98.5	103.9	122.8
12500	112.4	114.8	109.0	102.5	99.5	99.8	105.8	107.5	123.0
16000	111.5	114.3	108.6	103.4	100.7	106.1	107.9	107.6	123.3
20000	109.8	113.3	108.2	103.6	103.7	107.0	106.3	105.9	122.7
25000	108.2	112.8	108.7	105.1	107.2	106.3	105.6	106.1	122.8
31500	106.2	111.2	108.4	107.1	106.2	104.9	106.1	106.0	122.2
40000	104.2	109.7	107.9	108.9	105.0	105.2	106.0	105.4	122.0
50000	101.8	108.5	106.8	107.8	104.3	105.1	105.3	104.4	121.1
63000	100.5	106.5	106.2	106.9	105.0	105.3	104.9	103.5	120.5
80000	97.8	103.9	103.9	104.5	103.4	103.5	103.0	101.3	118.4
100000	96.1	103.1	103.1	103.3	102.9	102.8	102.0	100.1	117.5

- COMPUTED SPL(THETA) -

THETA	15	30	45	60	75	90	105	120
	121.7	125.0	120.0	116.4	114.7	115.2	115.8	115.8

TOTAL ACOUSTIC POWER

PWL	WATTS
133.6	23.1

FIGURE 17. 1/3 OCTAVE BAND SPECTRUM ANALYSIS FOR MAIN JET ALONE.

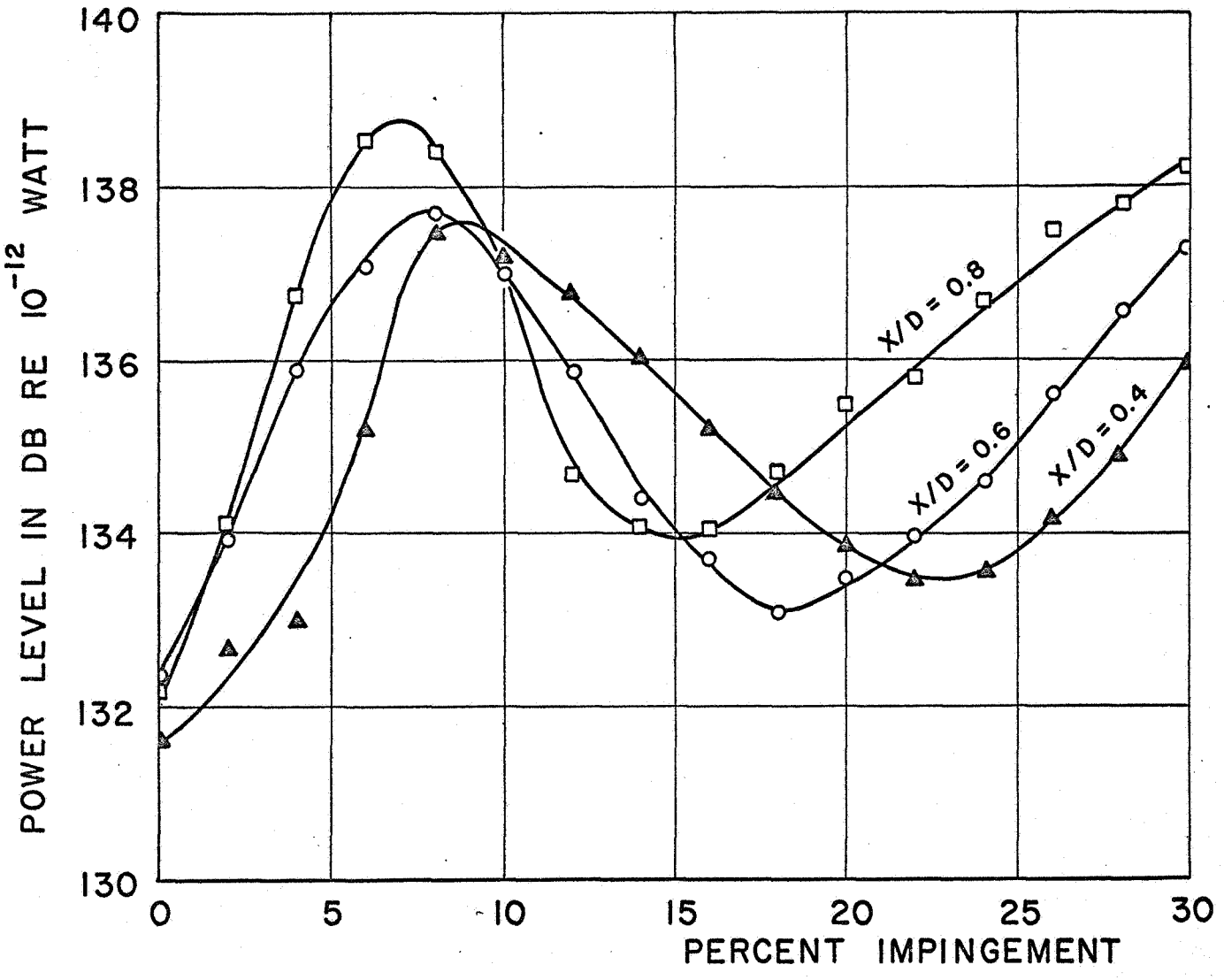

FIGURE 18. TOTAL ACOUSTIC POWER VERSUS PERCENT IMPINGEMENT FOR NOZZLE ARRANGEMENT I WITH 90° IMPINGING FLOW. MAIN JET TOTAL PRESSURE = 100 PSIG.

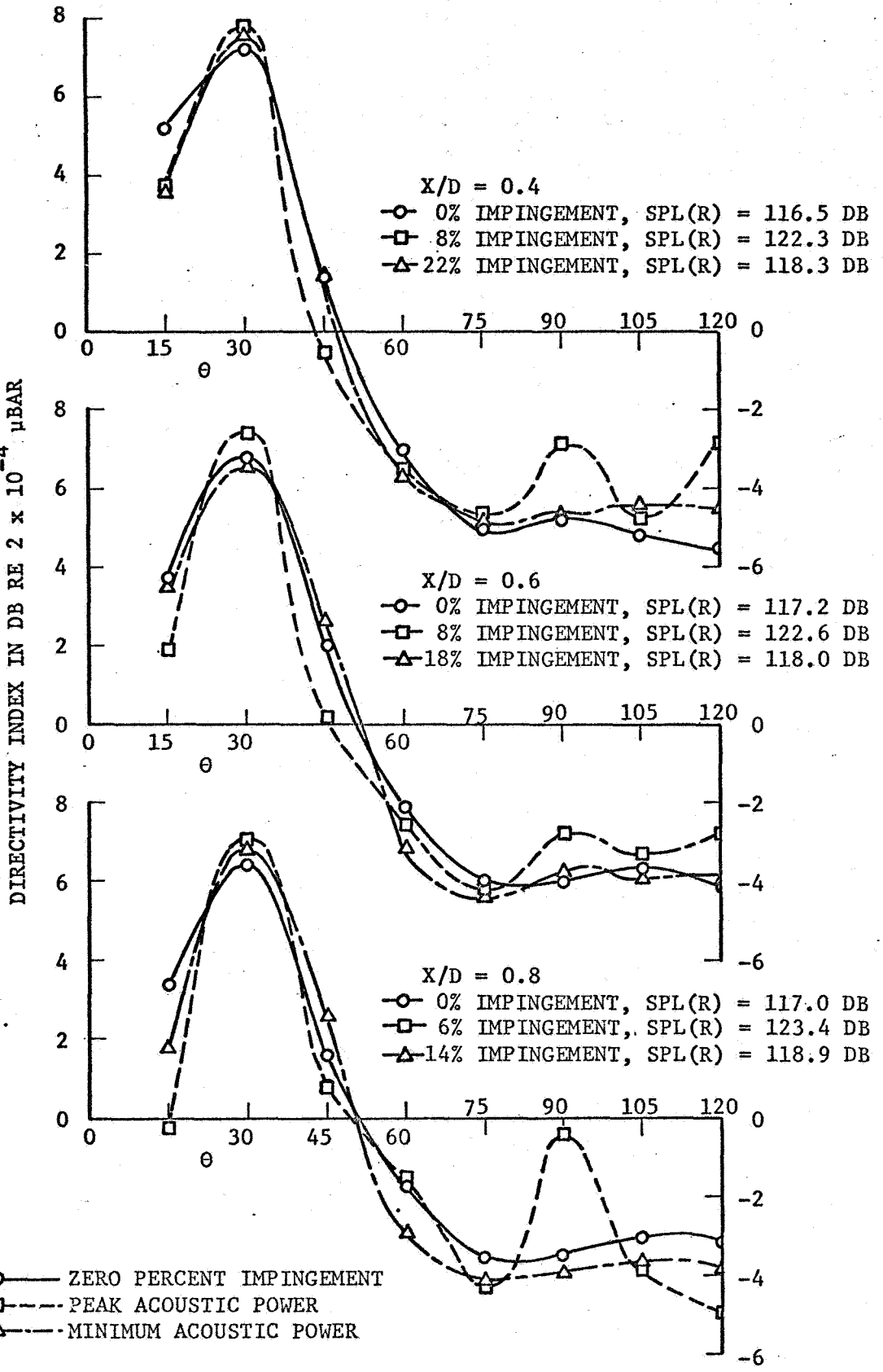

FIGURE 19. DIRECTIVITY INDEX AT ZERO PERCENT IMPINGEMENT AND CONDITIONS OF PEAK AND MINIMUM ACOUSTIC POWER. NOZZLE ARRANGEMENT I. MAIN JET TOTAL PRESSURE = 100 PSIG.

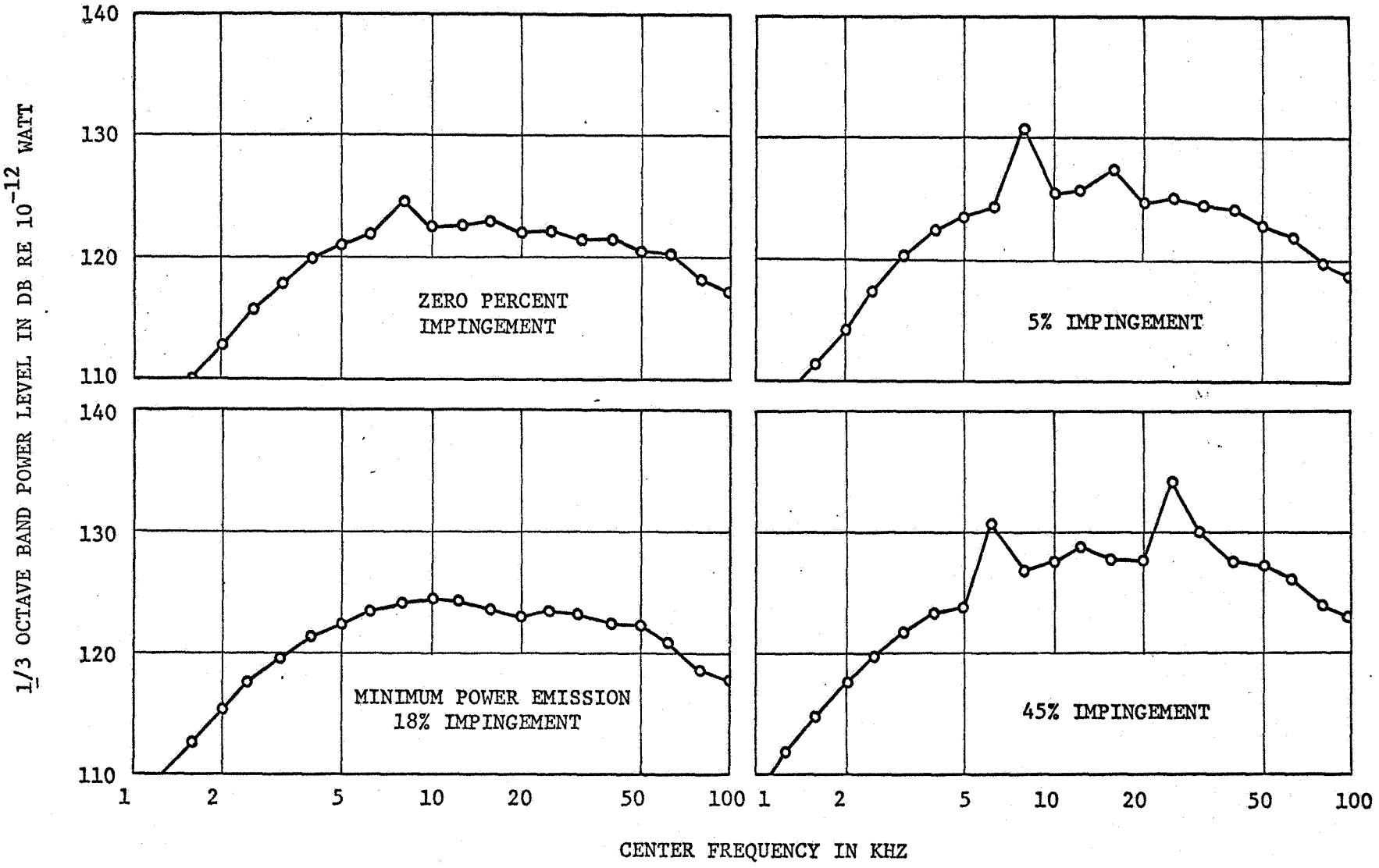

FIGURE 20. TYPICAL 1/3 OCTAVE BAND POWER SPECTRA FOR NOZZLE ARRANGEMENT I AT X/D = 0.6. MAIN JET TOTAL PRESSURE = 100 PSIG.

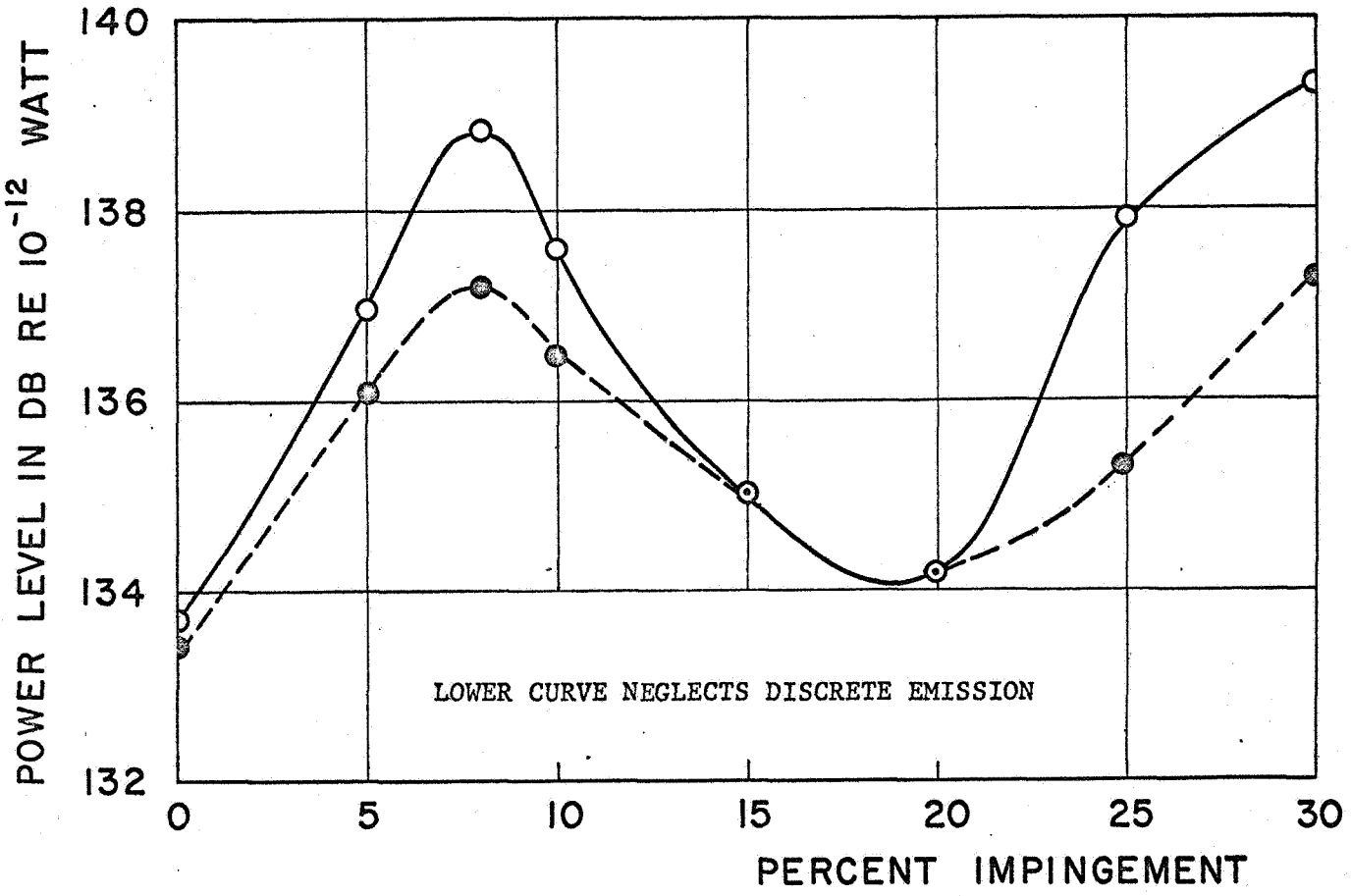

FIGURE 21. COMPARISON OF TOTAL POWER VARIATIONS COMPUTED FROM 1/3 OCTAVE BAND SPECTRA WITH AND WITHOUT DISCRETE EMISSION. NOZZLE ARRANGEMENT I, X/D = 0.6. MAIN JET TOTAL PRESSURE = 100 PSIG.

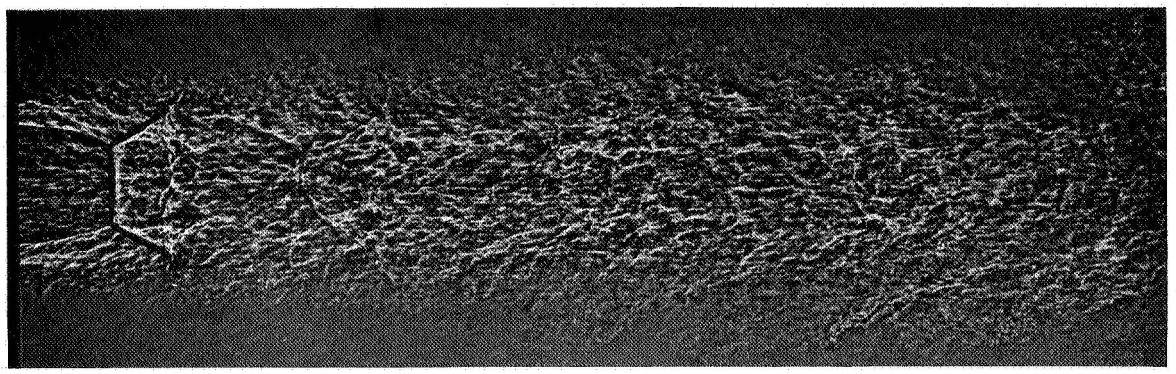

0% IMPINGEMENT

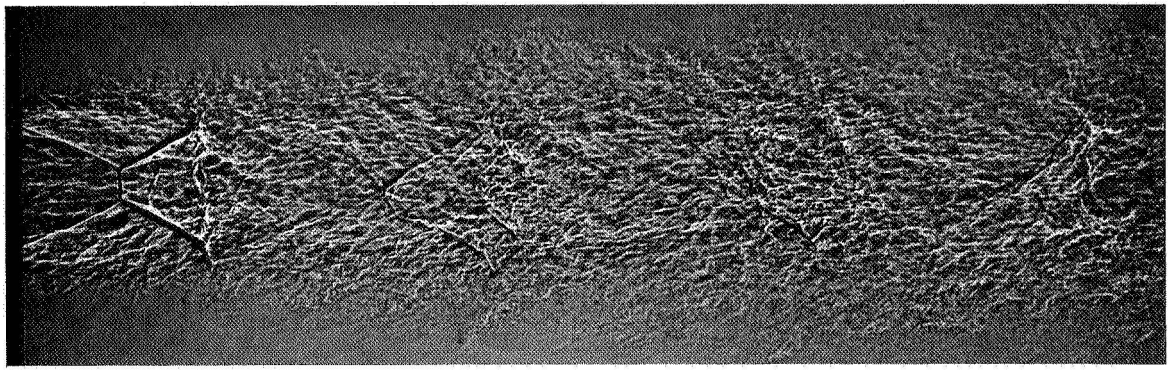

5% IMPINGEMENT

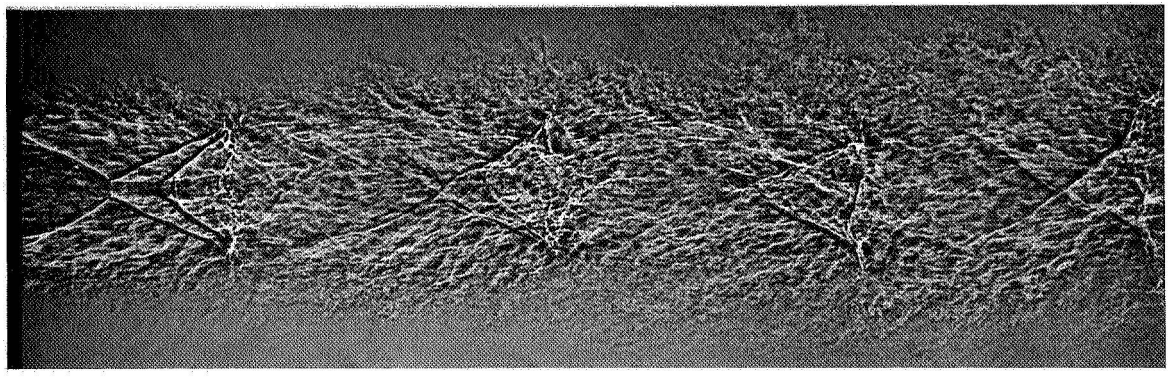

8% IMPINGEMENT, PEAK TOTAL ACOUSTIC POWER EMISSION

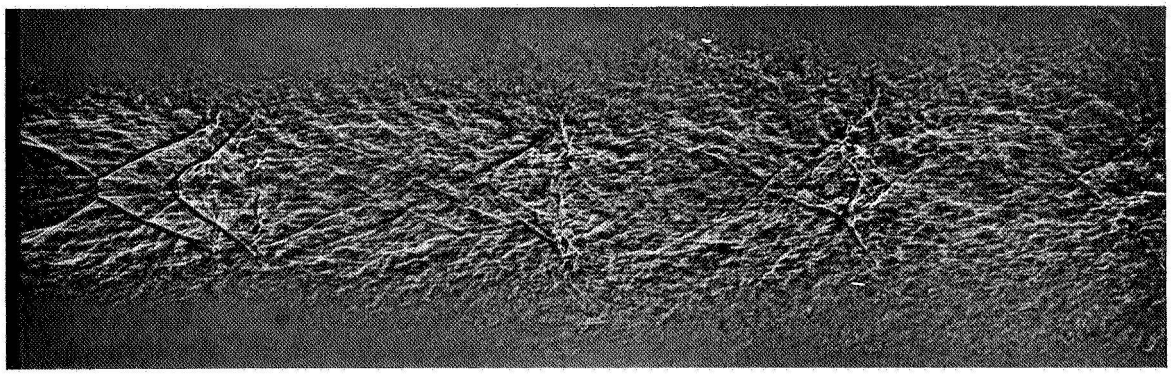

10% IMPINGEMENT

FIGURE 22. DEVELOPMENT OF SHOCK STRUCTURE WITH PERCENT IMPINGEMENT. NOZZLE ARRANGEMENT I, X/D = 0.6. MAIN JET TOTAL PRESSURE = 100 PSIG.

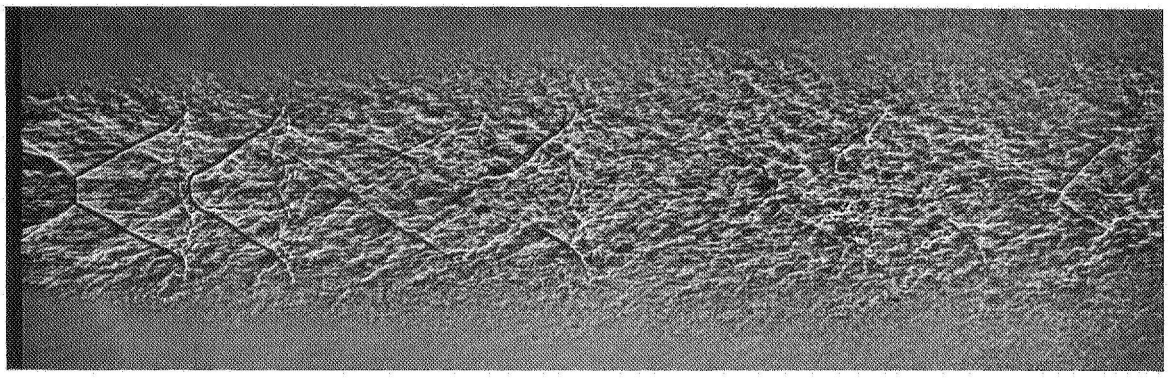

15% IMPINGEMENT

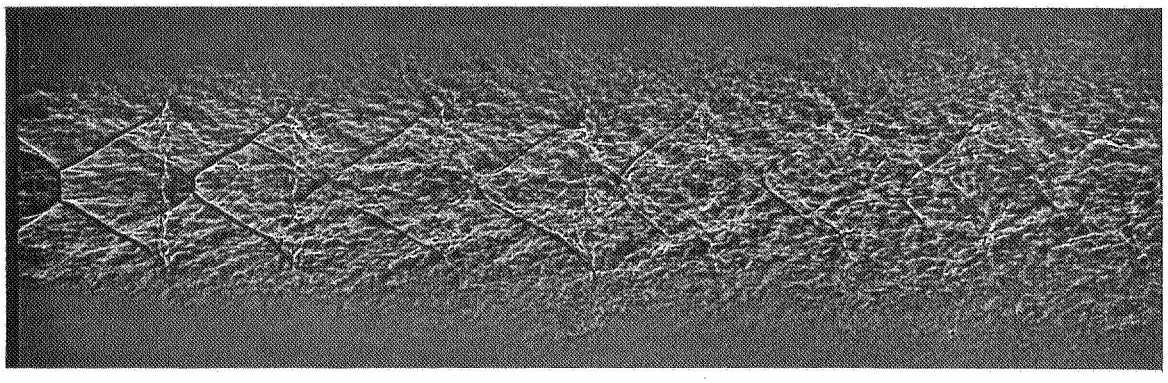

18% IMPINGEMENT, MINIMUM TOTAL ACOUSTIC POWER EMISSION

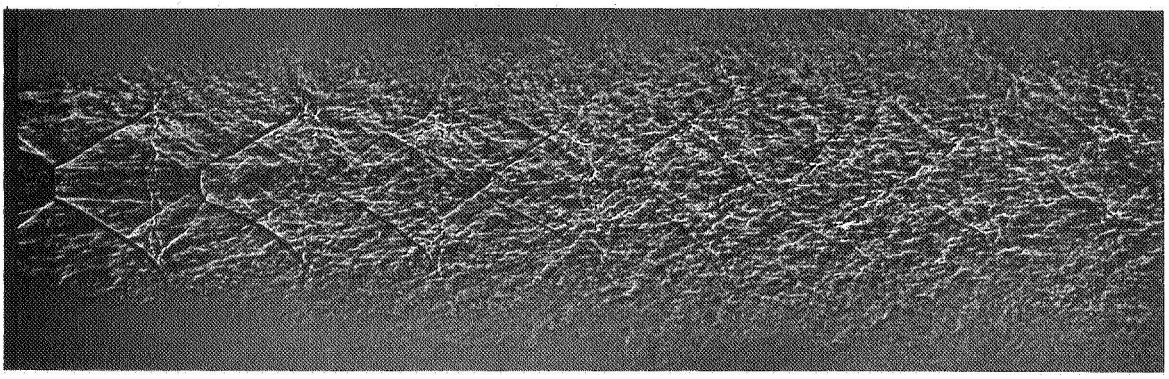

20% IMPINGEMENT

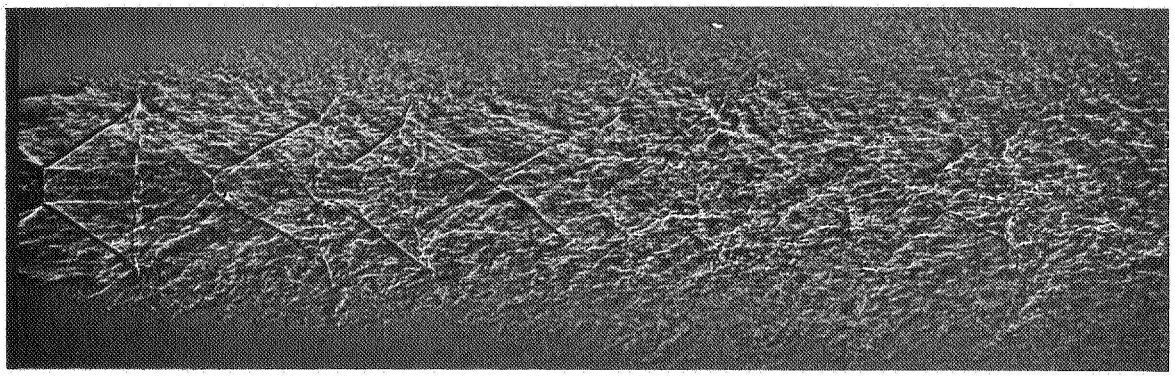

25% IMPINGEMENT

FIGURE 22, CONTINUED.

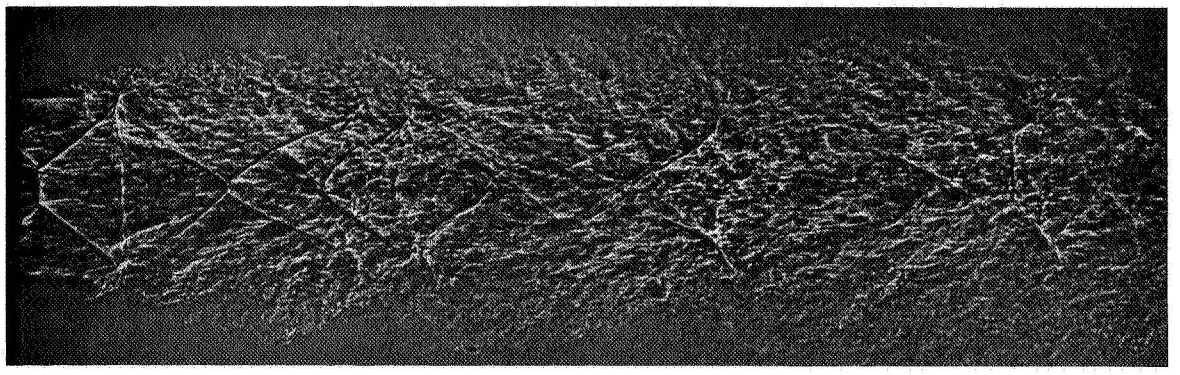

30% IMPINGEMENT

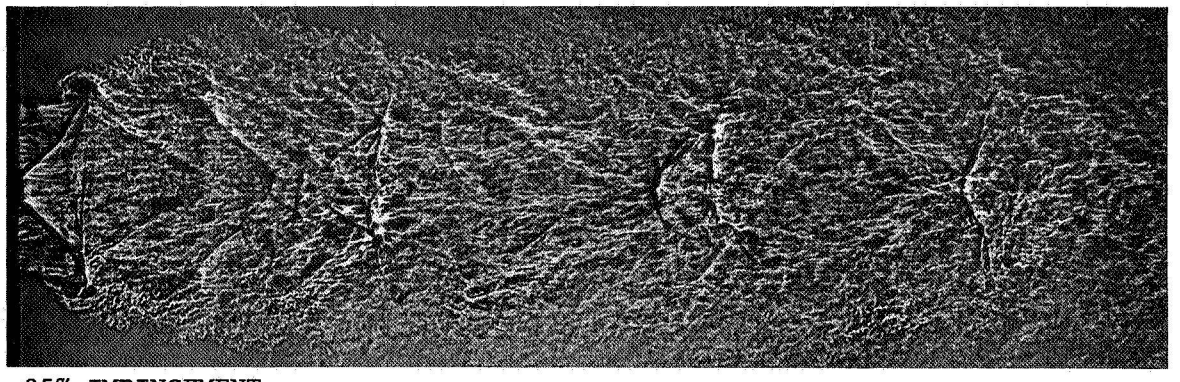

35% IMPINGEMENT

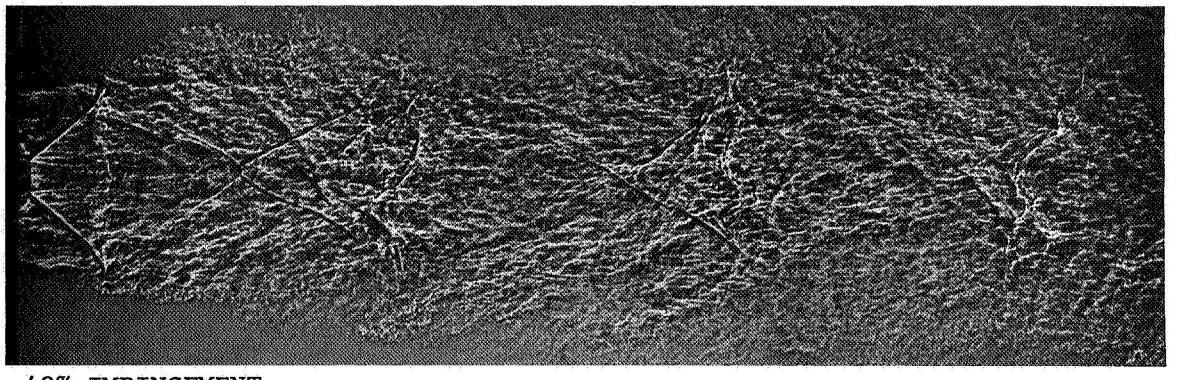

40% IMPINGEMENT

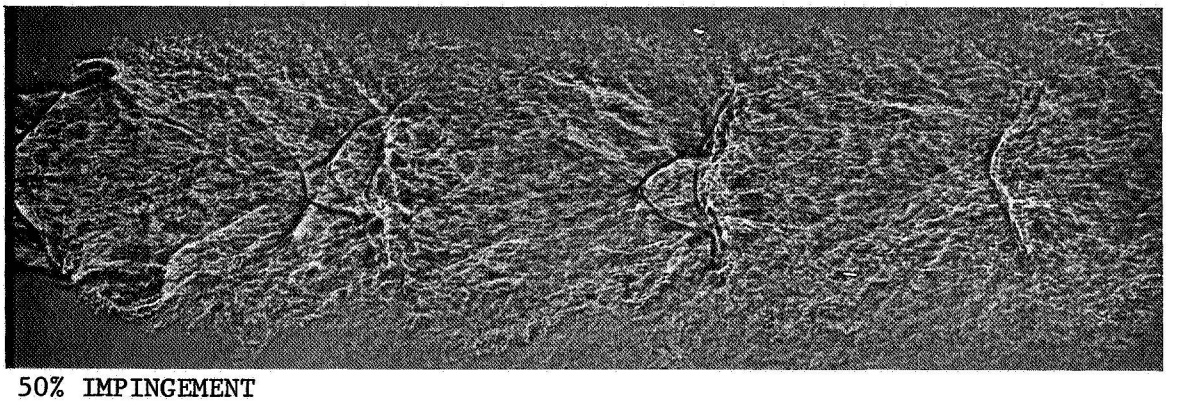

50% IMPINGEMENT

FIGURE 22, CONTINUED.

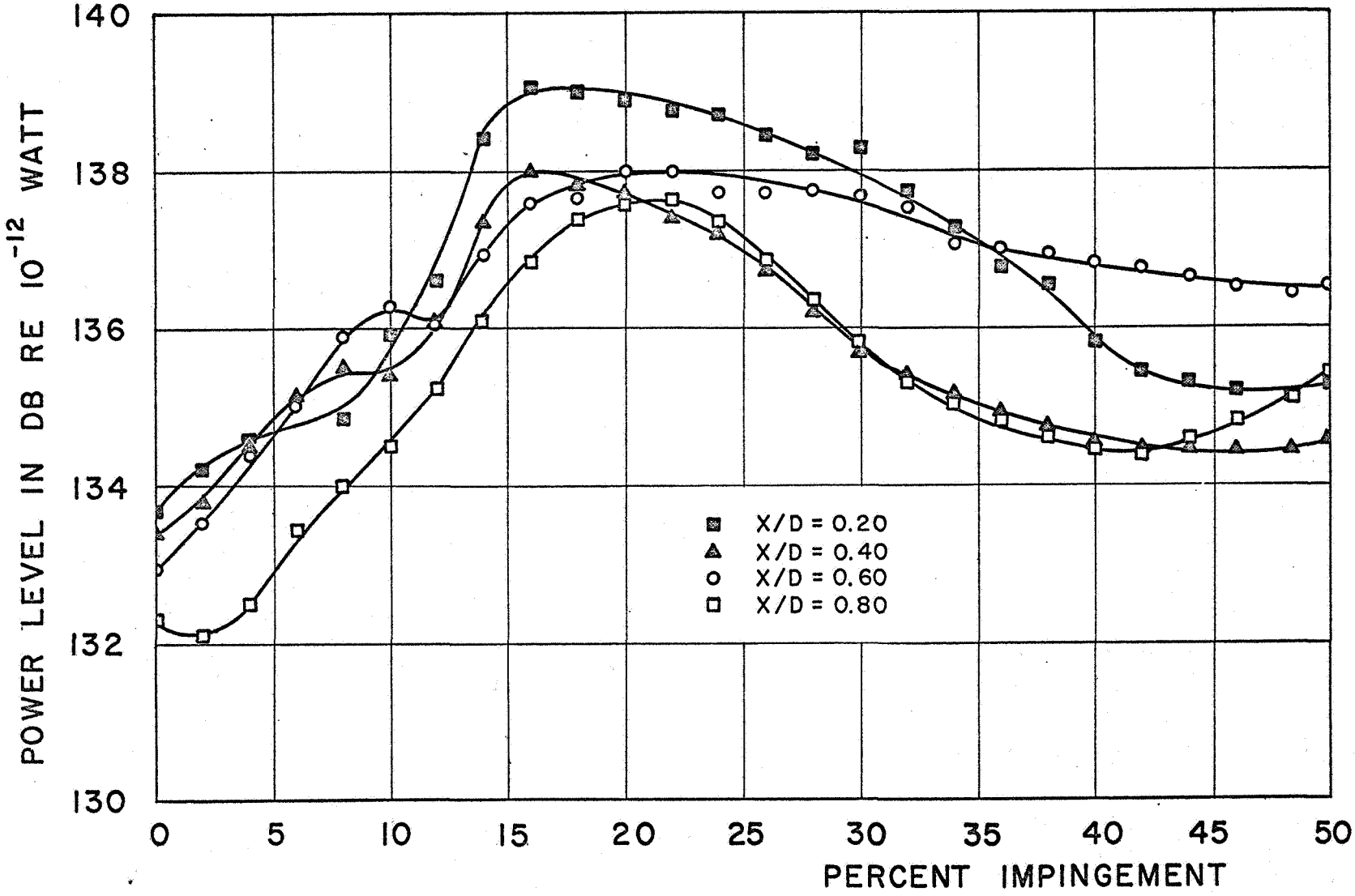

FIGURE 23. TOTAL ACOUSTIC POWER VERSUS PERCENT IMPINGEMENT FOR NOZZLE ARRANGEMENT I WITH 45° IMPINGING FLOW. MAIN JET TOTAL PRESSURE = 100 PSIG.

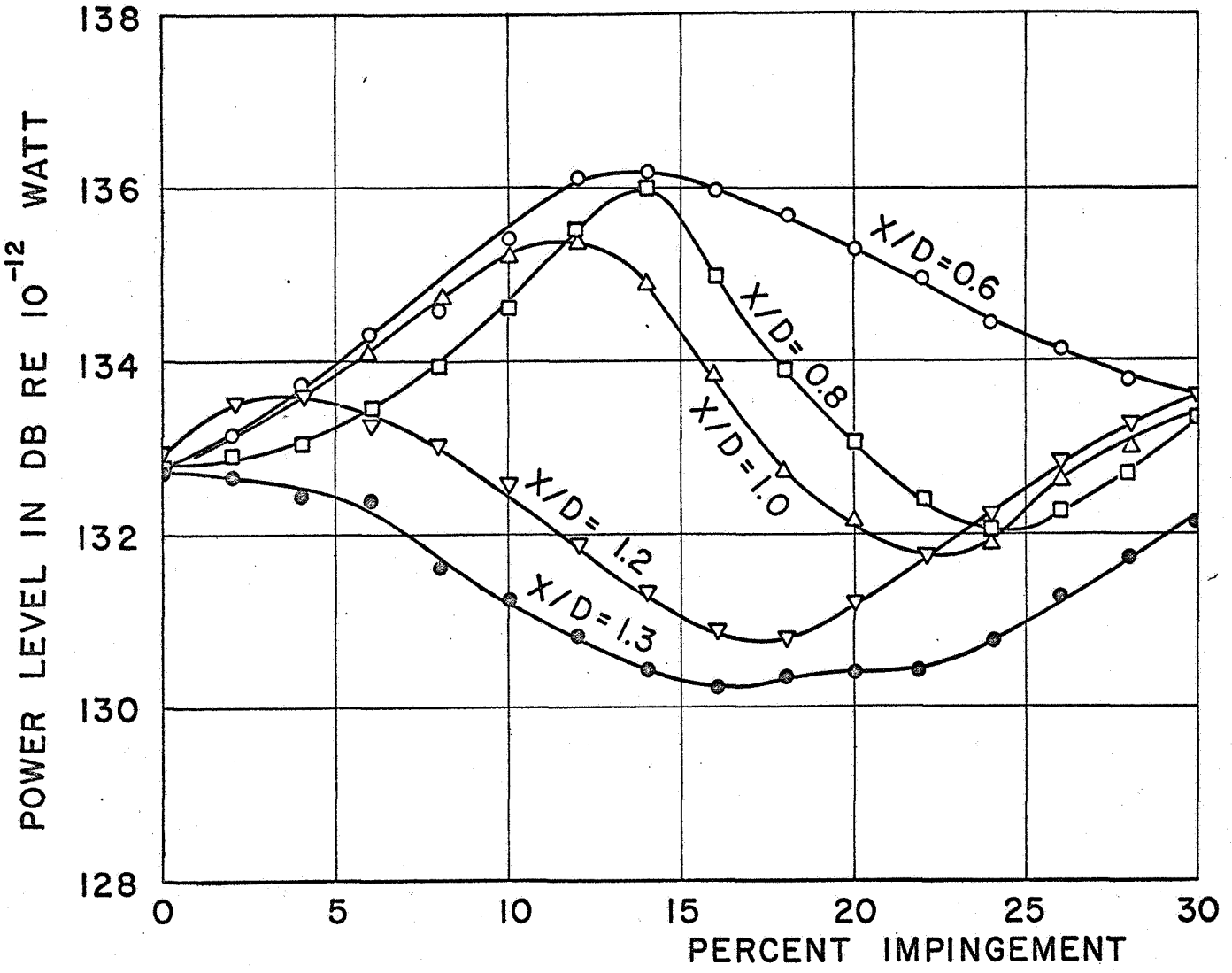

FIGURE 24. TOTAL ACOUSTIC POWER VERSUS PERCENT IMPINGEMENT FOR NOZZLE ARRANGEMENT II WITH 90° IMPINGING FLOW. MAIN JET TOTAL PRESSURE = 100 PSIG.

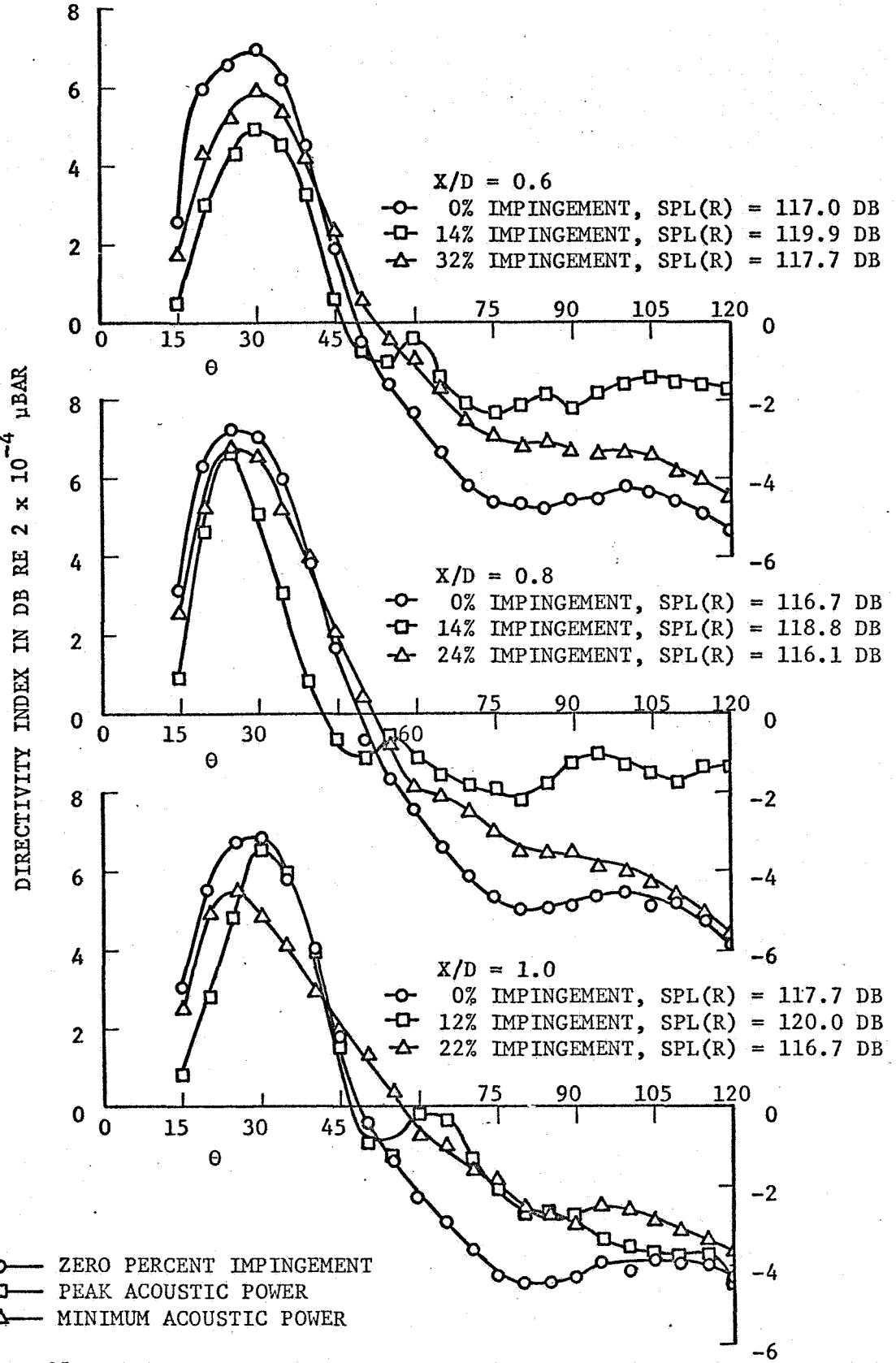

FIGURE 25. DIRECTIVITY INDEX AT ZERO PERCENT IMPINGEMENT AND CONDITIONS OF PEAK AND MINIMUM ACOUSTIC POWER. NOZZLE ARRANGEMENT II. MAIN JET TOTAL PRESSURE = 100 PSIG.

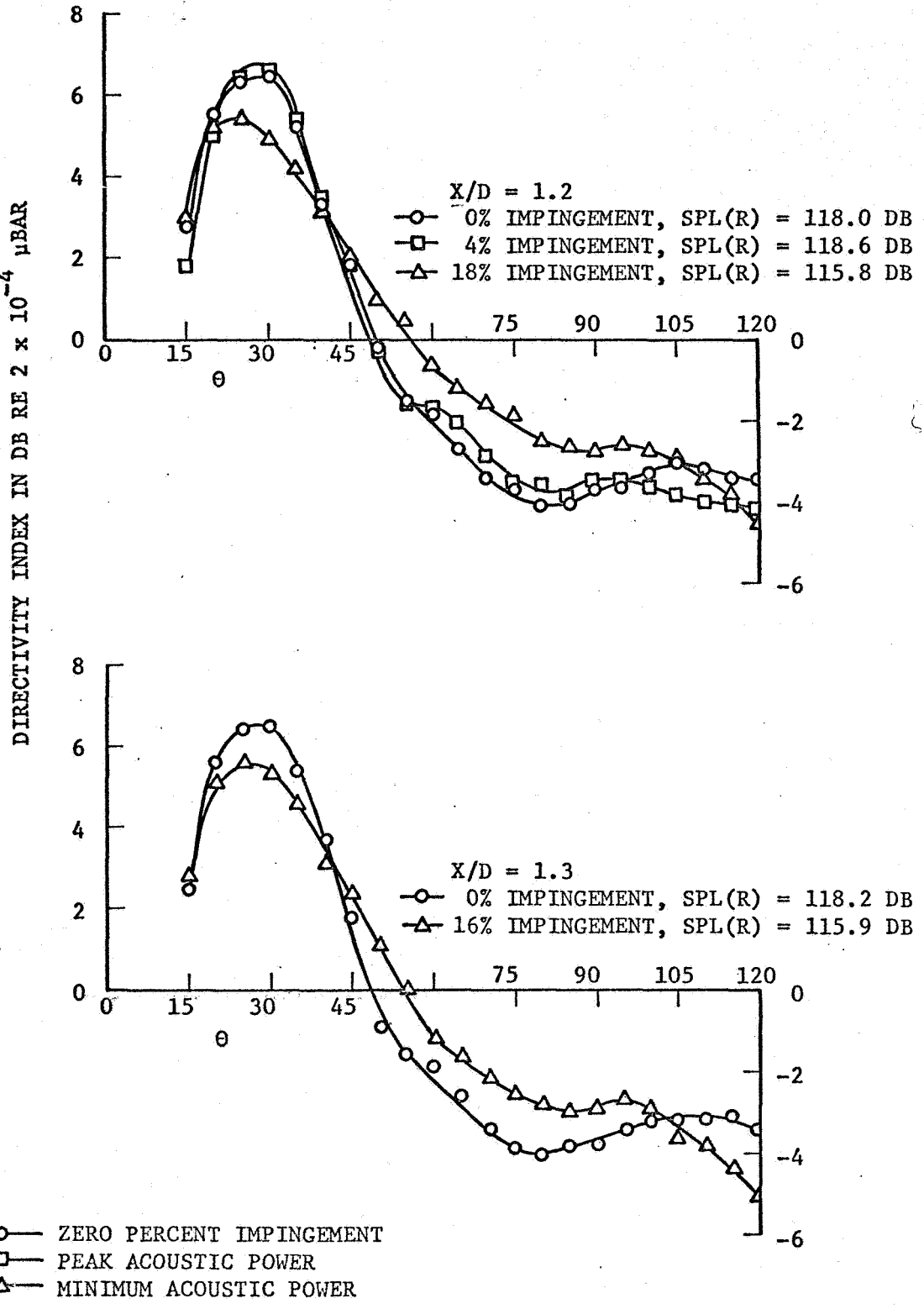

FIGURE 25, CONTINUED.

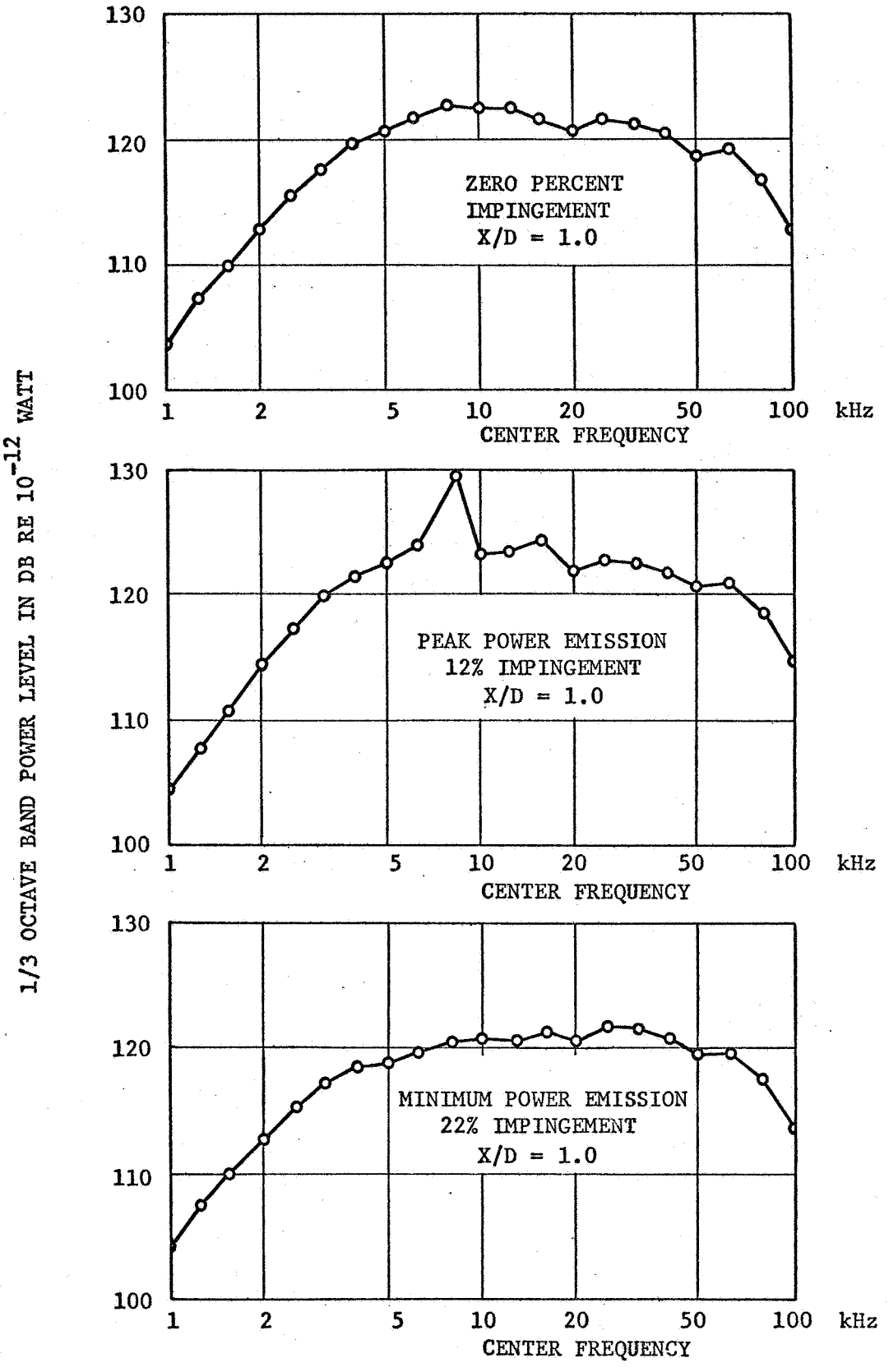

FIGURE 26. 1/3 OCTAVE BAND POWER SPECTRA FOR NOZZLE ARRANGEMENT II WITH 90^{o} IMPINGEMENT. MAIN JET TOTAL PRESSURE = 100 PSIG.

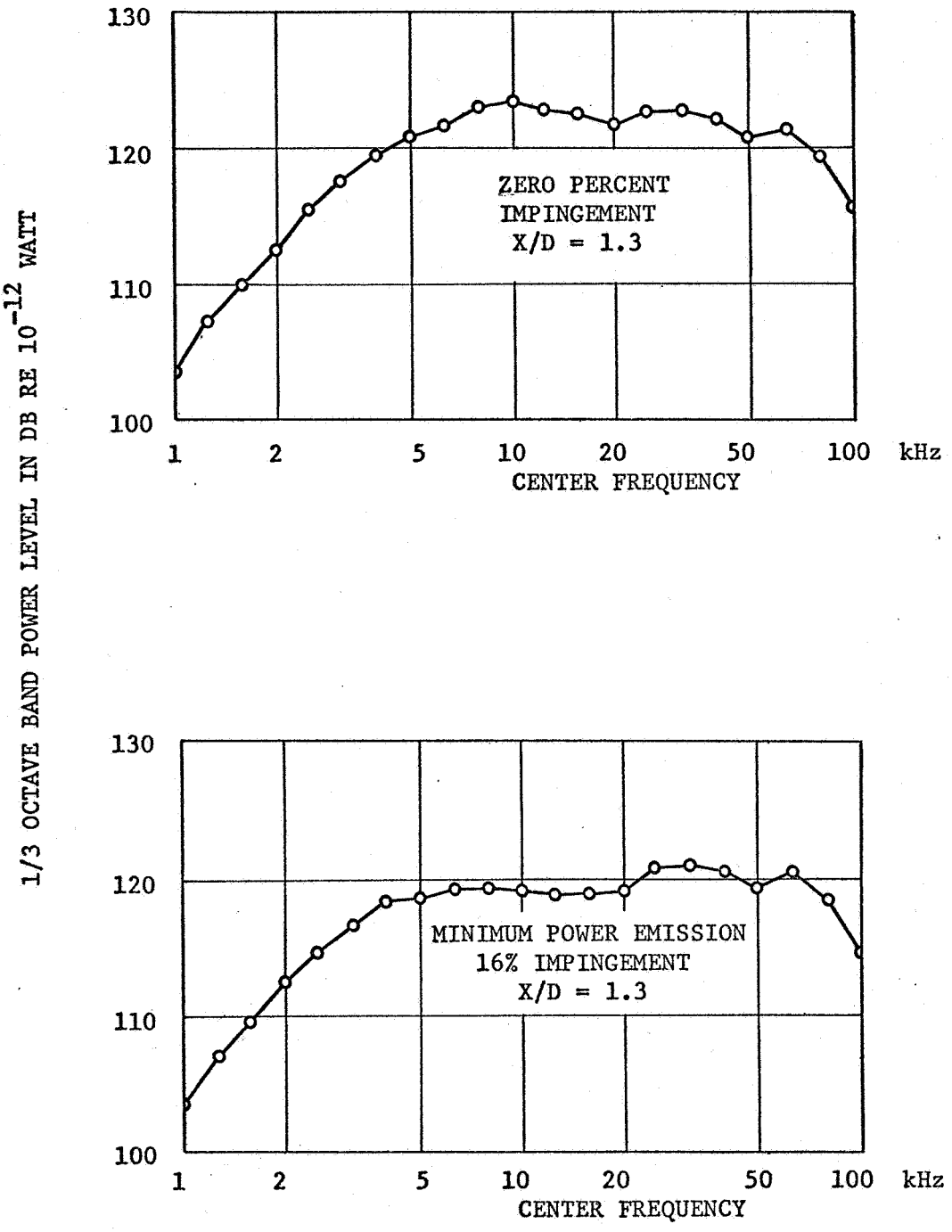

FIGURE 26, CONTINUED. MAIN JET TOTAL PRESSURE = 100 PSIG.

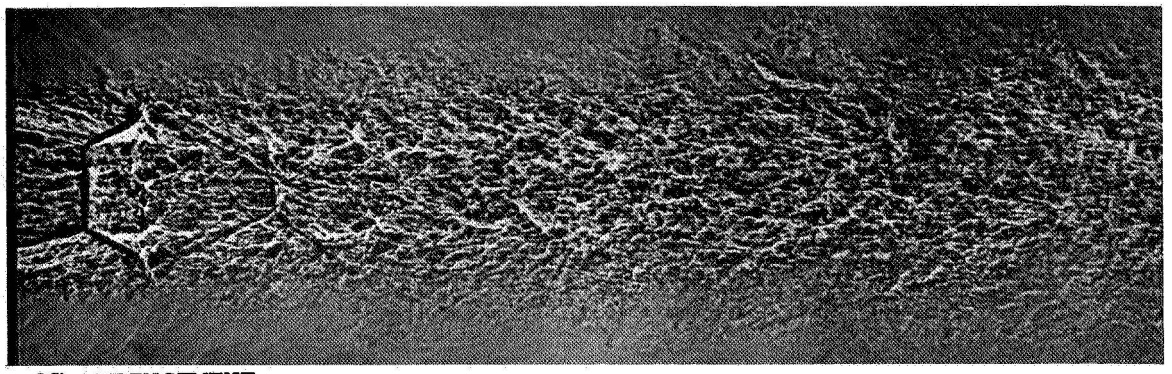

0% IMPINGEMENT

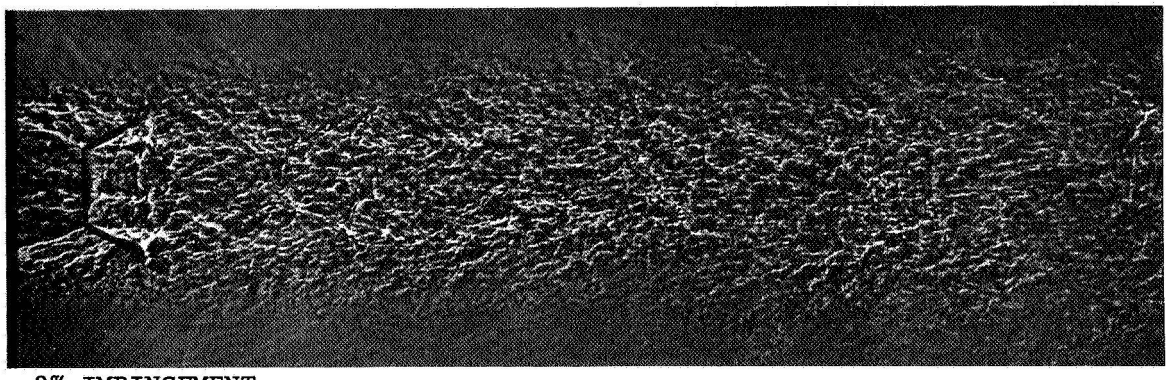

2% IMPINGEMENT

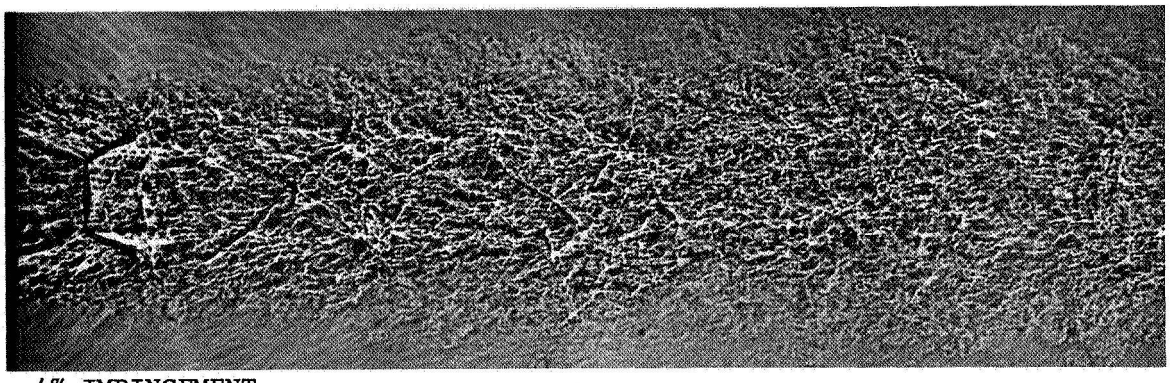

4% IMPINGEMENT

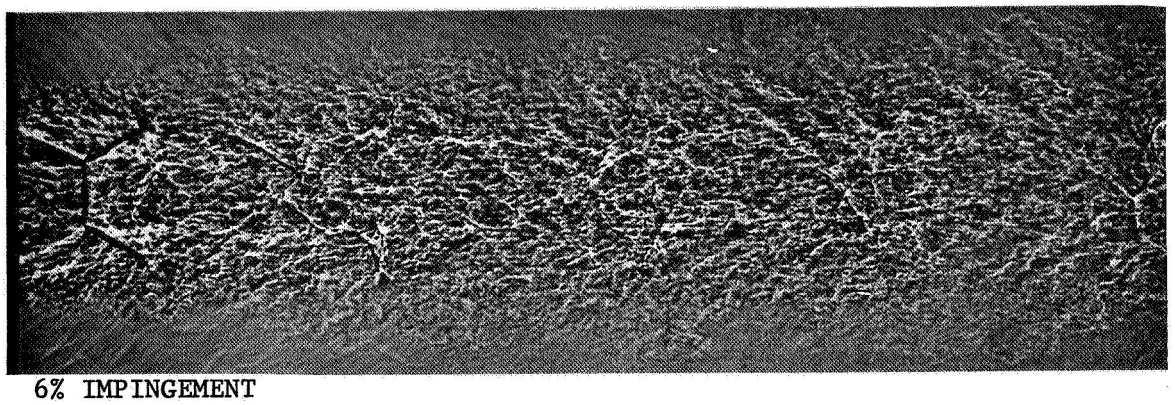

6% IMPINGEMENT

FIGURE 27. DEVELOPMENT OF SHOCK STRUCTURE WITH PERCENT IMPINGEMENT. NOZZLE ARRANGEMENT II, X/D = 0.8. MAIN JET TOTAL PRESSURE = 100 PSIG.

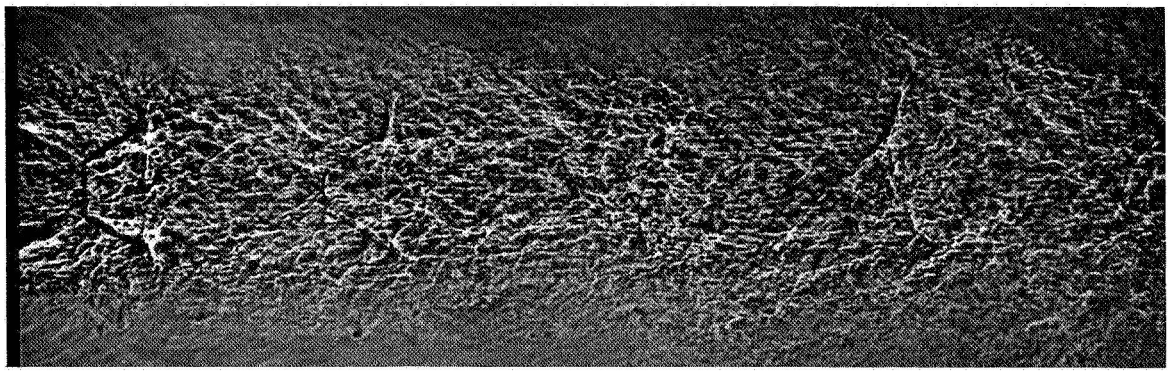

8% IMPINGEMENT

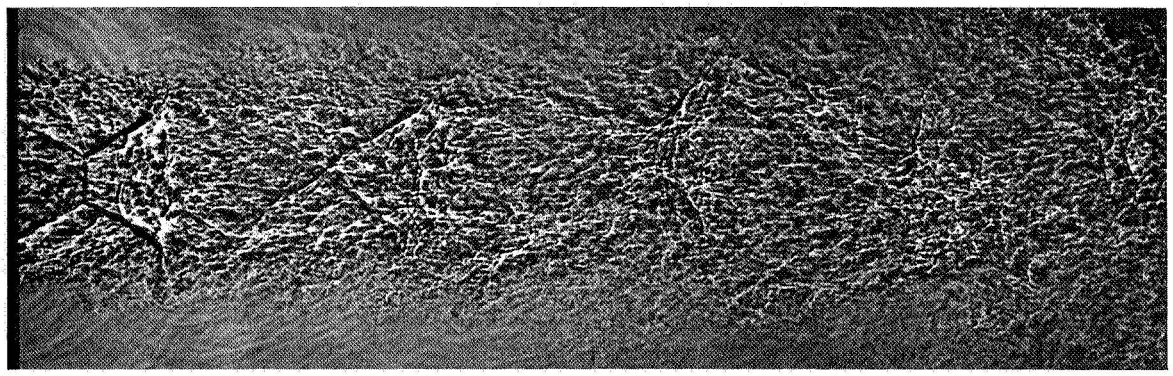

10% IMPINGEMENT

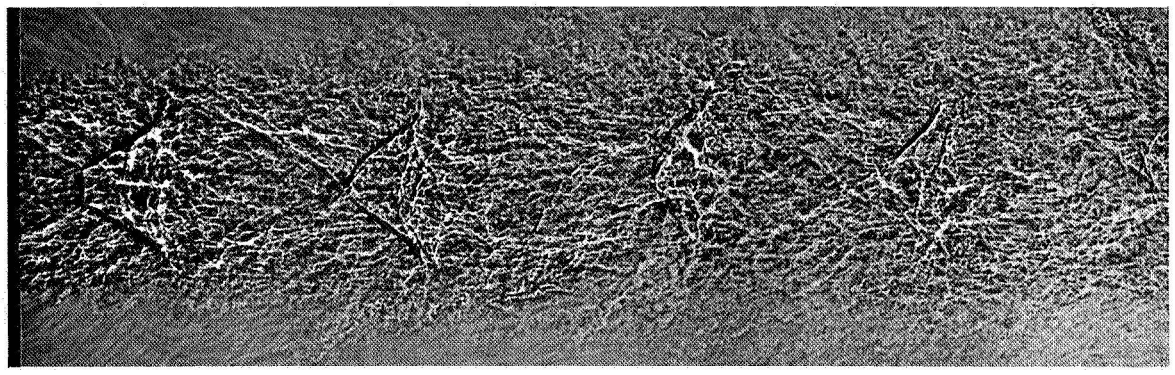

12% IMPINGEMENT

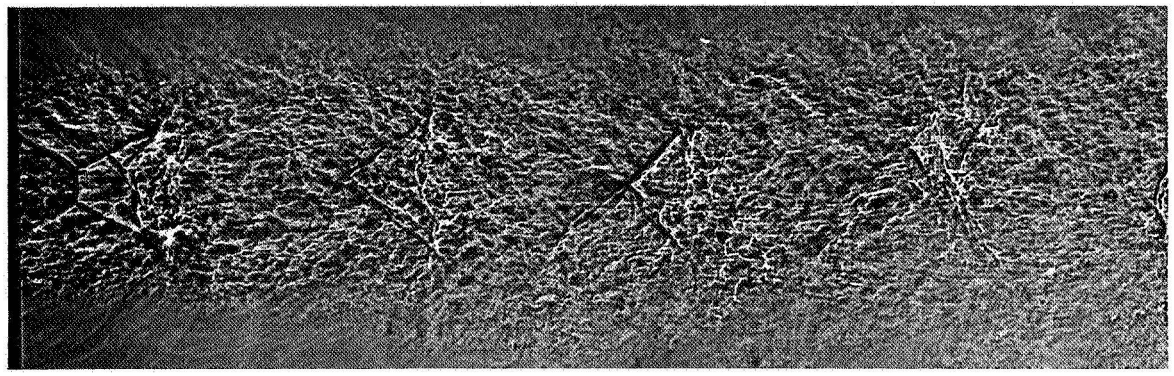

14% IMPINGEMENT, PEAK TOTAL ACOUSTIC POWER EMISSION

FIGURE 27, CONTINUED.

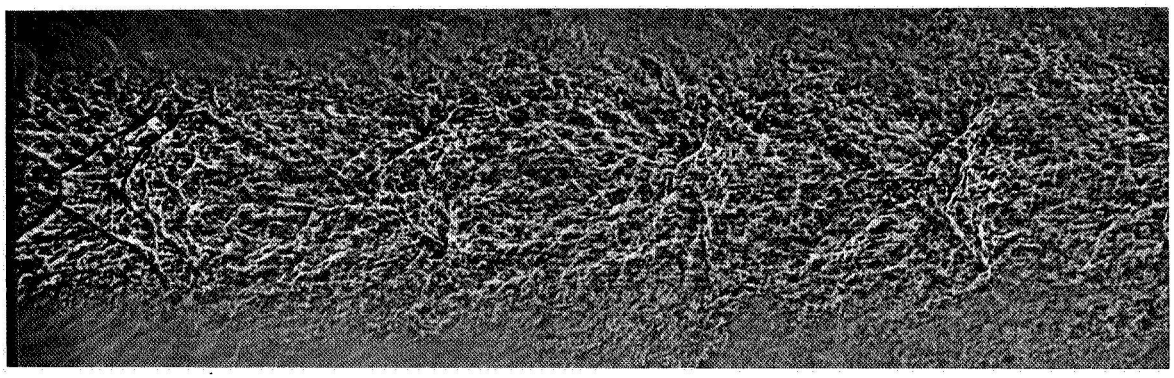

16% IMPINGEMENT

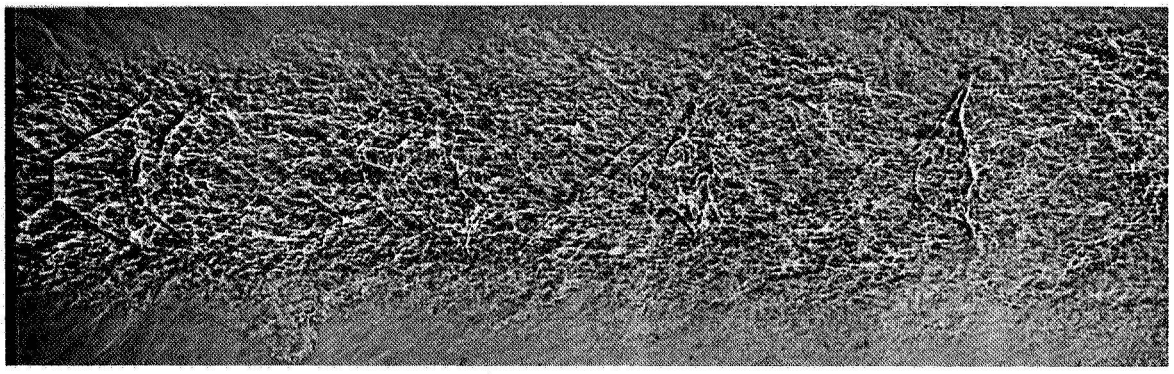

18% IMPINGEMENT

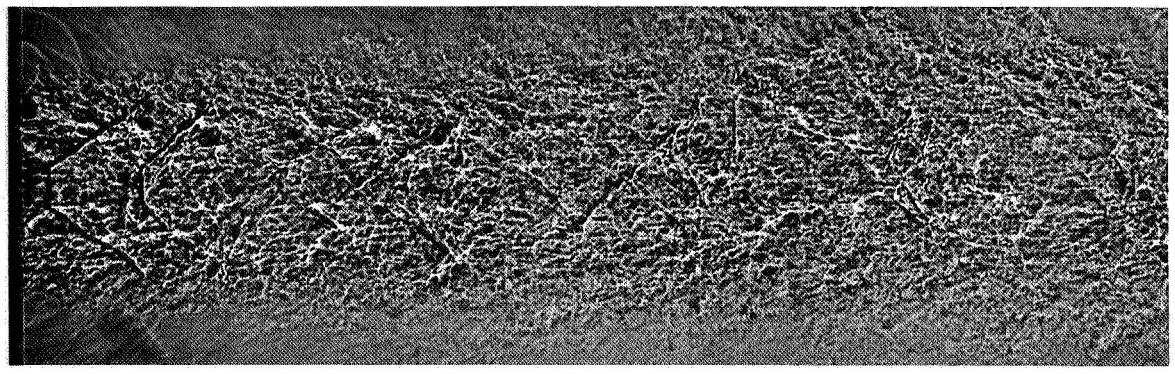

20% IMPINGEMENT

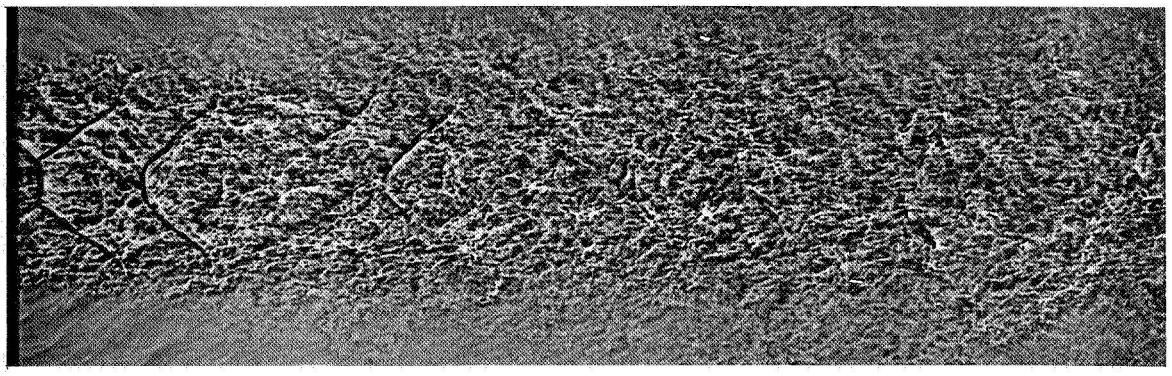

22% IMPINGEMENT

FIGURE 27, CONTINUED.

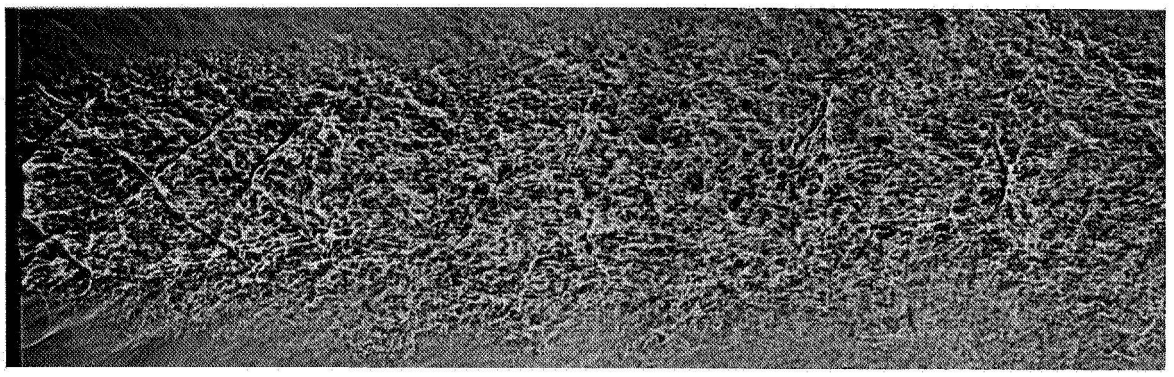

24% IMPINGEMENT, MINIMUM TOTAL ACOUSTIC POWER EMISSION

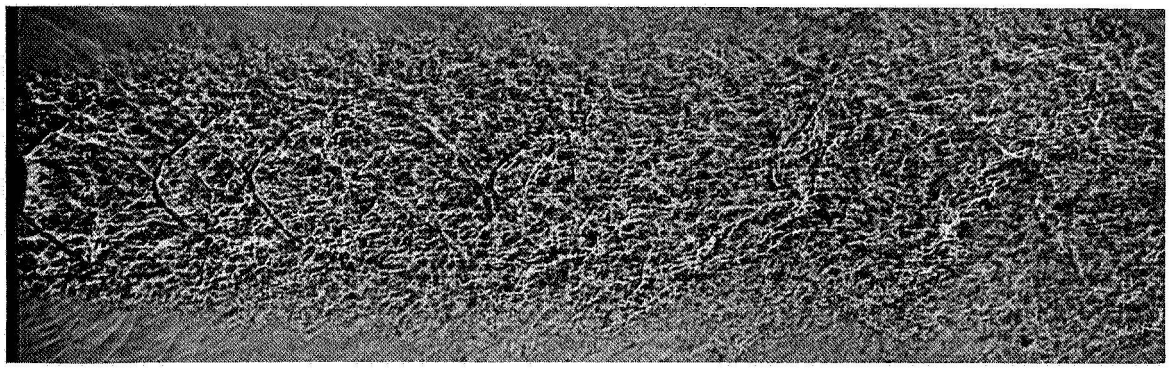

26% IMPINGEMENT

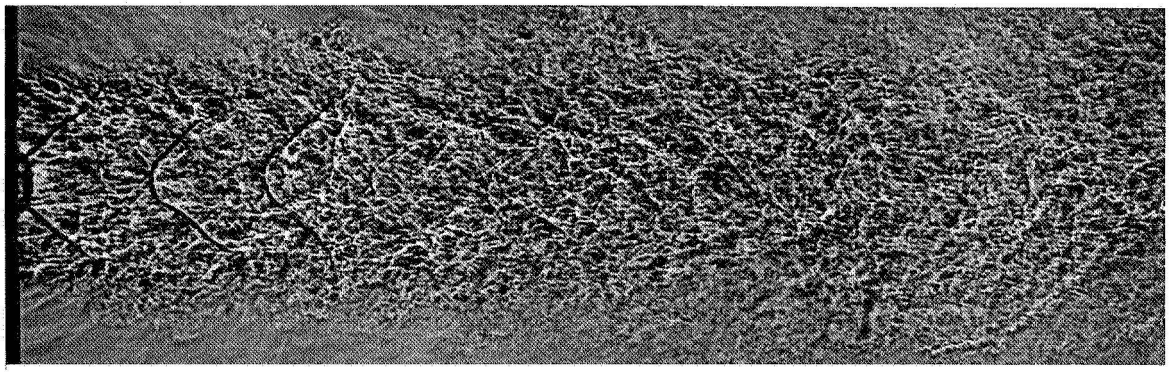

28% IMPINGEMENT

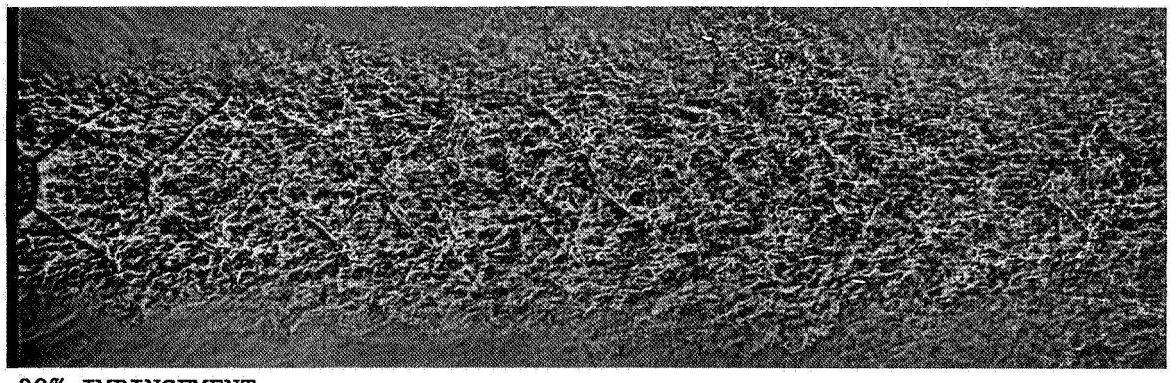

30% IMPINGEMENT

FIGURE 27, CONTINUED.

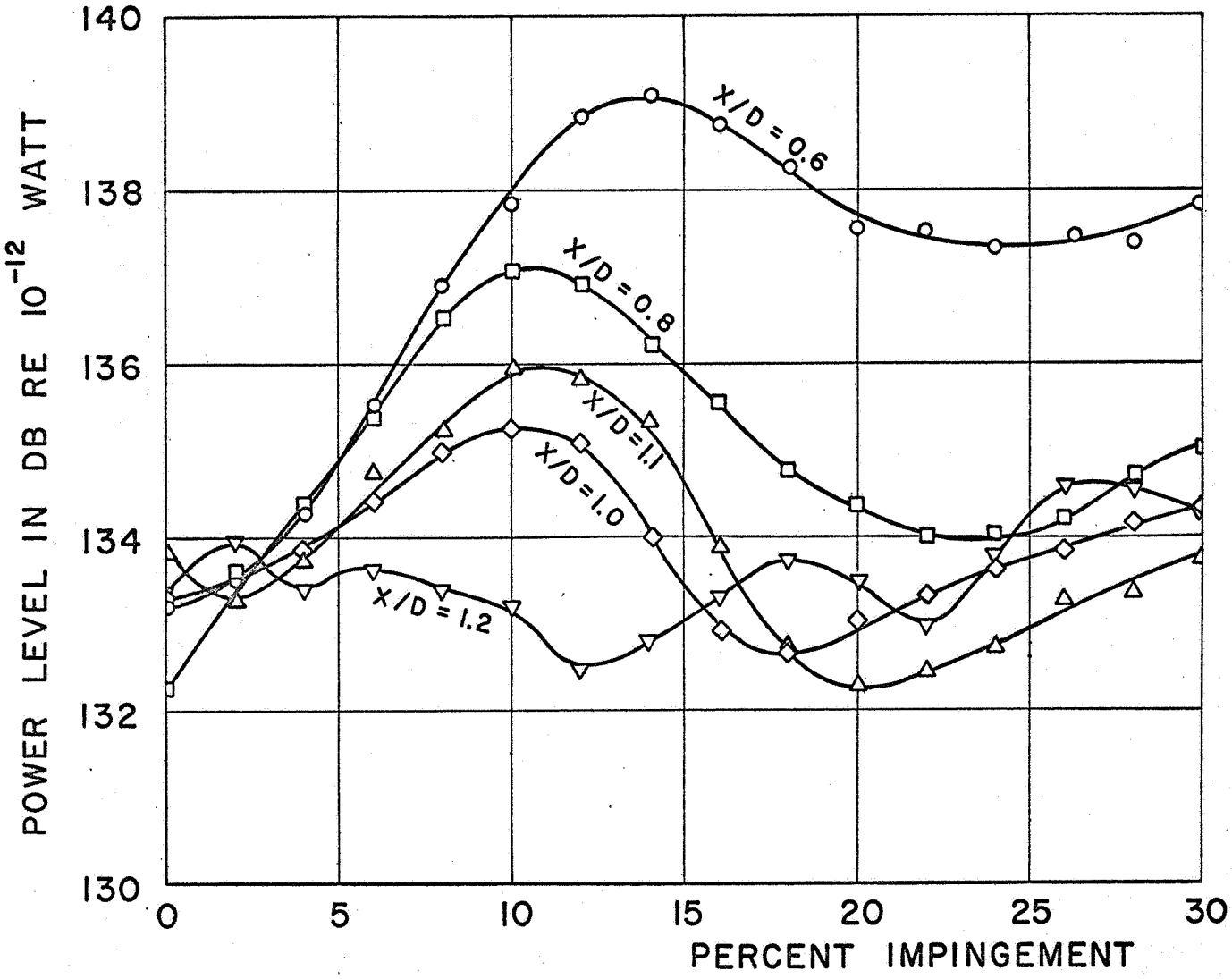

FIGURE 28. TOTAL ACOUSTIC POWER VERSUS PERCENT IMPINGEMENT FOR NOZZLE ARRANGEMENT III WITH 90° IMPINGING FLOW. MAIN JET TOTAL PRESSURE = 100 PSIG.

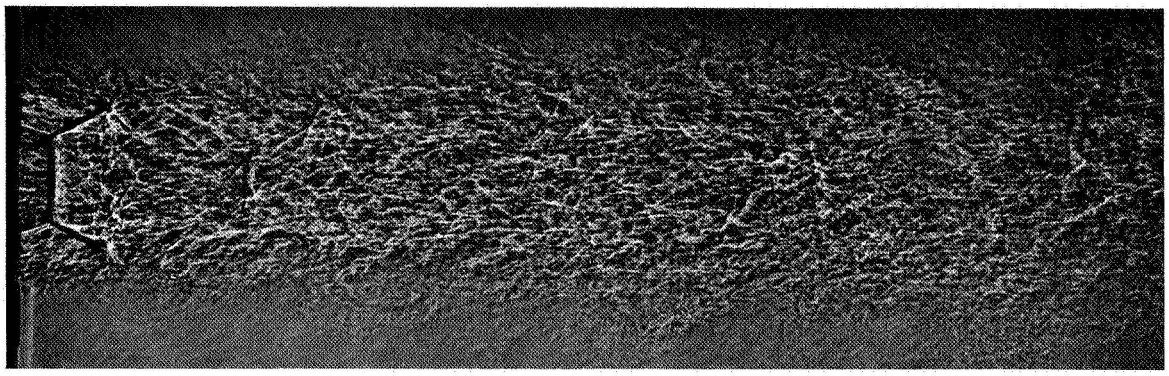

0% IMPINGEMENT

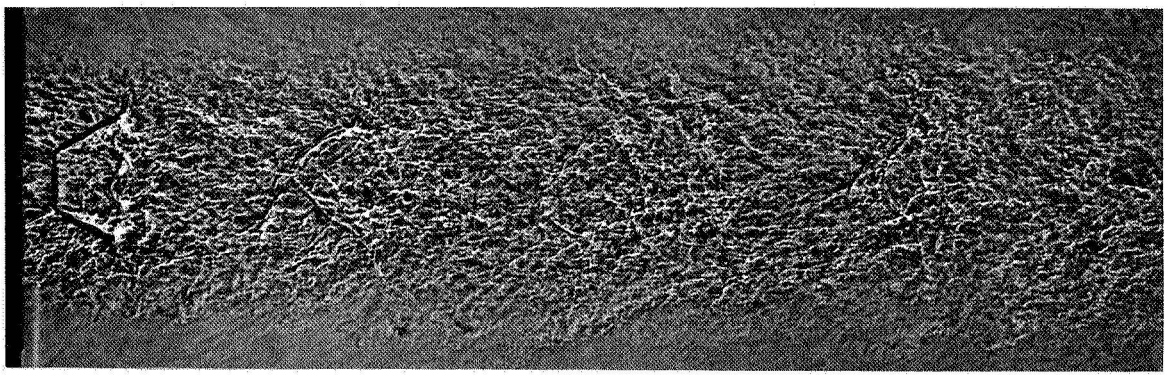

4% IMPINGEMENT

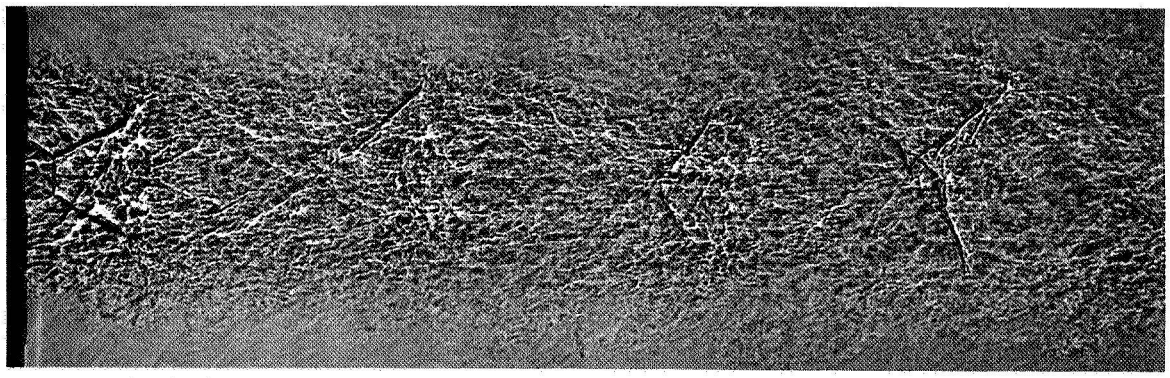

8% IMPINGEMENT

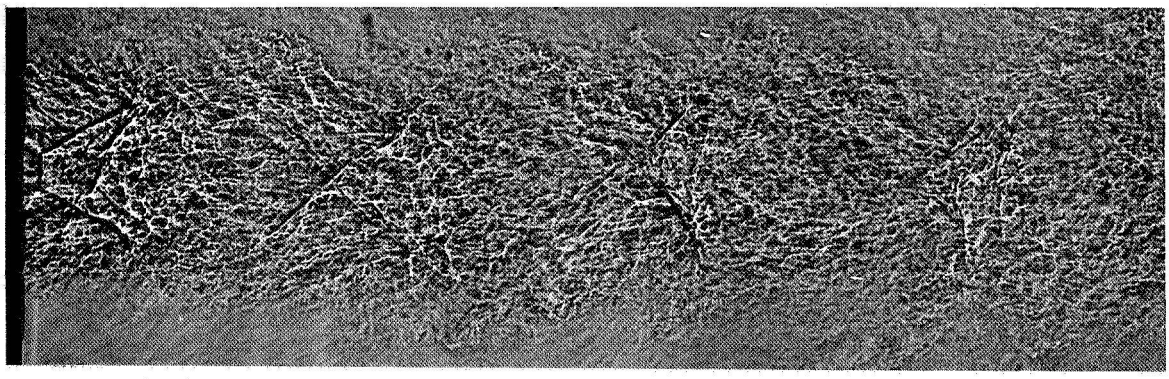

12% IMPINGEMENT, APPROXIMATELY PEAK TOTAL ACOUSTIC POWER EMISSION

FIGURE 29. DEVELOPMENT OF SHOCK STRUCTURE WITH PERCENT IMPINGEMENT. NOZZLE ARRANGEMENT III, X/D = 0.8. MAIN JET TOTAL PRESSURE = 100 PSIG.

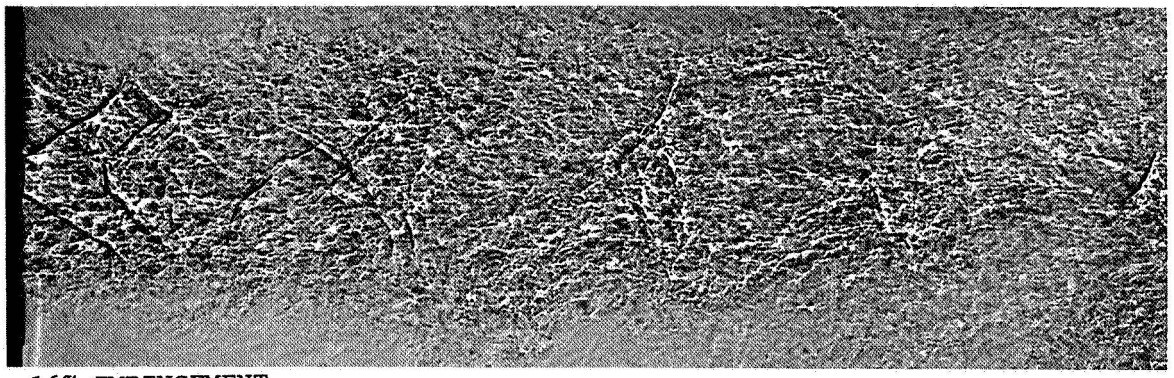

16% IMPINGEMENT

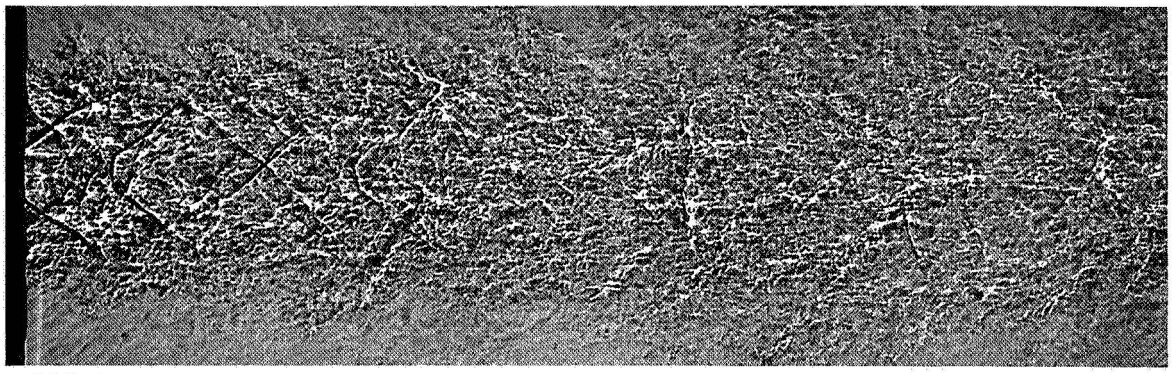

20% IMPINGEMENT

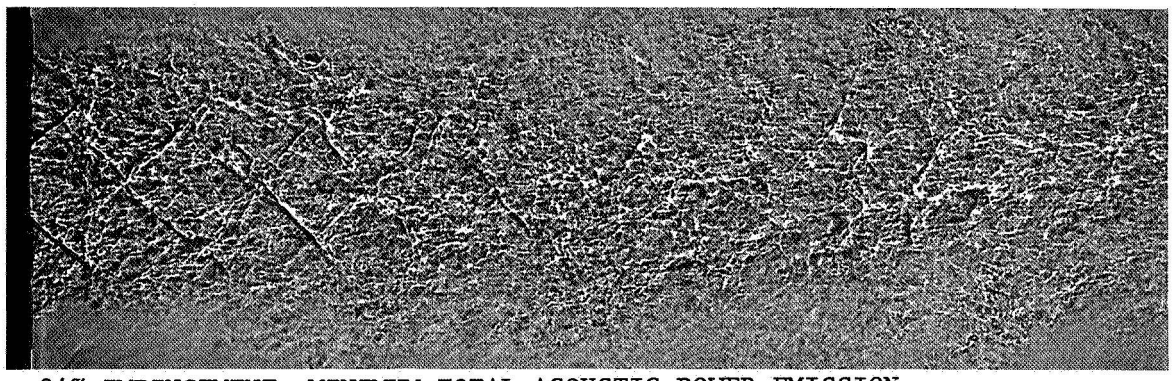

24% IMPINGEMENT, MINIMUM TOTAL ACOUSTIC POWER EMISSION

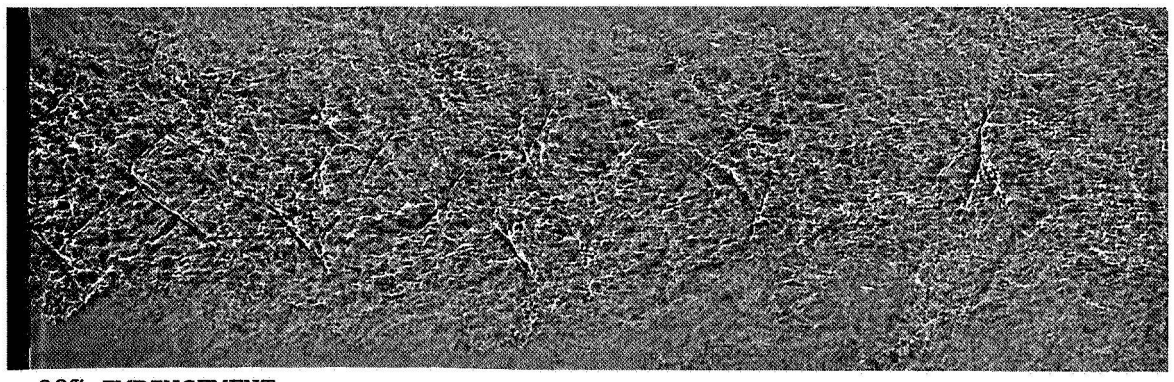

28% IMPINGEMENT

FIGURE 29, CONTINUED.

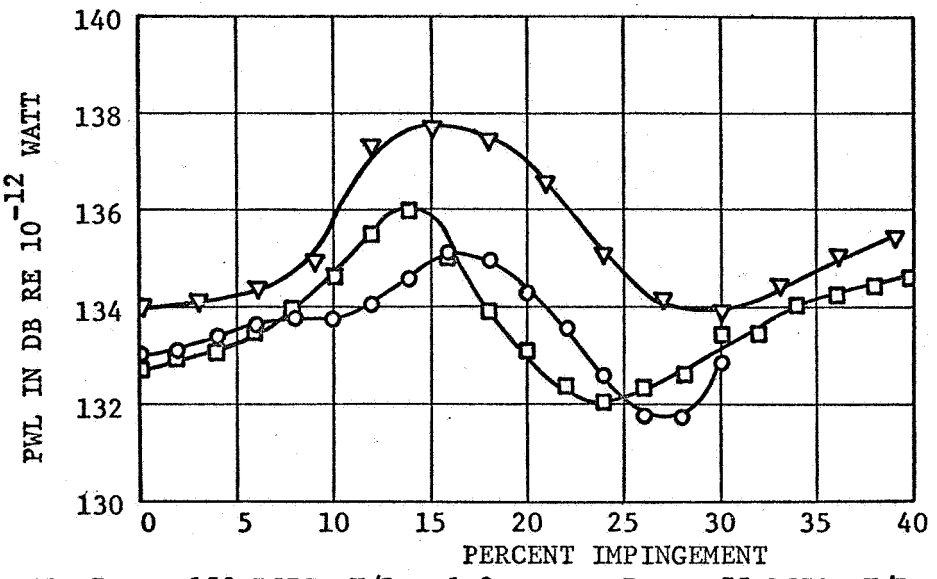

P_{TM} = 150 PSIG, X/D = 1.2. P_{TM} = 75 PSIG, X/D = 0.6.

P_{TM} = 100 PSIG, X/D = 0.8. ALL CURVES: $\frac{P_{TM}}{X/D}$ = 125.0

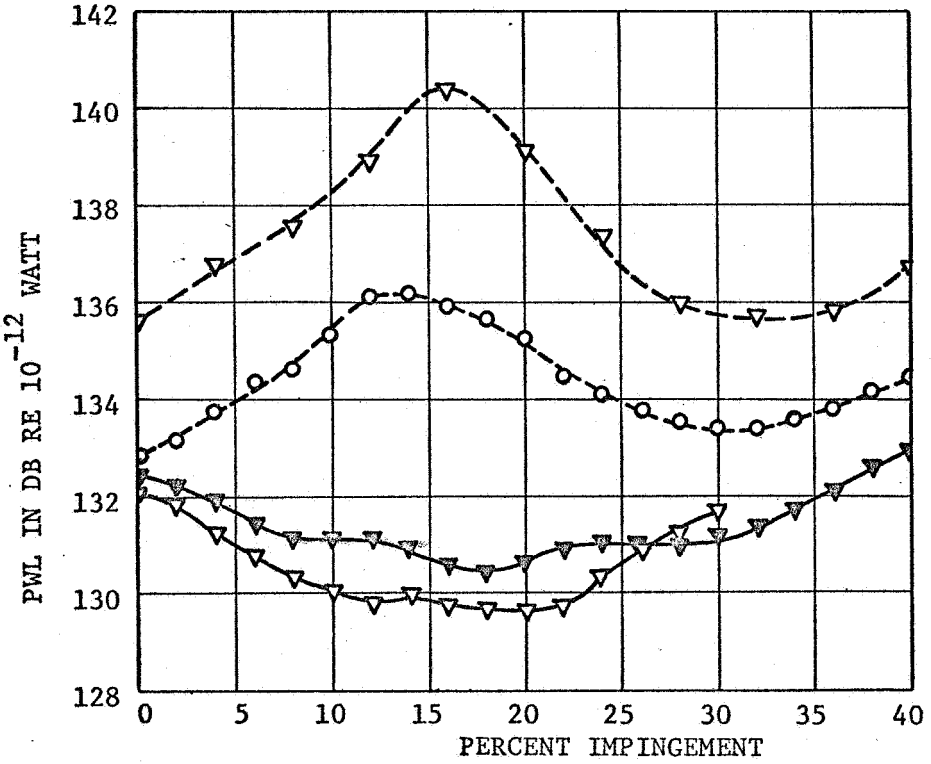

P_{TM} = 200 PSIG, X/D = 1.2. P_{TM} = 100 PSIG, X/D = 1.6.

P_{TM} = 100 PSIG, X/D = 0.6. P_{TM} = 75 PSIG, X/D = 1.2.

- - - - - - - $\frac{P_{TM}}{X/D}$ = 166.7 ——— $\frac{P_{TM}}{X/D}$ = 62.5

FIGURE 30. EFFECT OF MAIN JET TOTAL PRESSURE P_{TM} ON TOTAL ACOUSTIC POWER VARIATIONS WITH PERCENT IMPINGEMENT. NOZZLE ARRANGEMENT II.

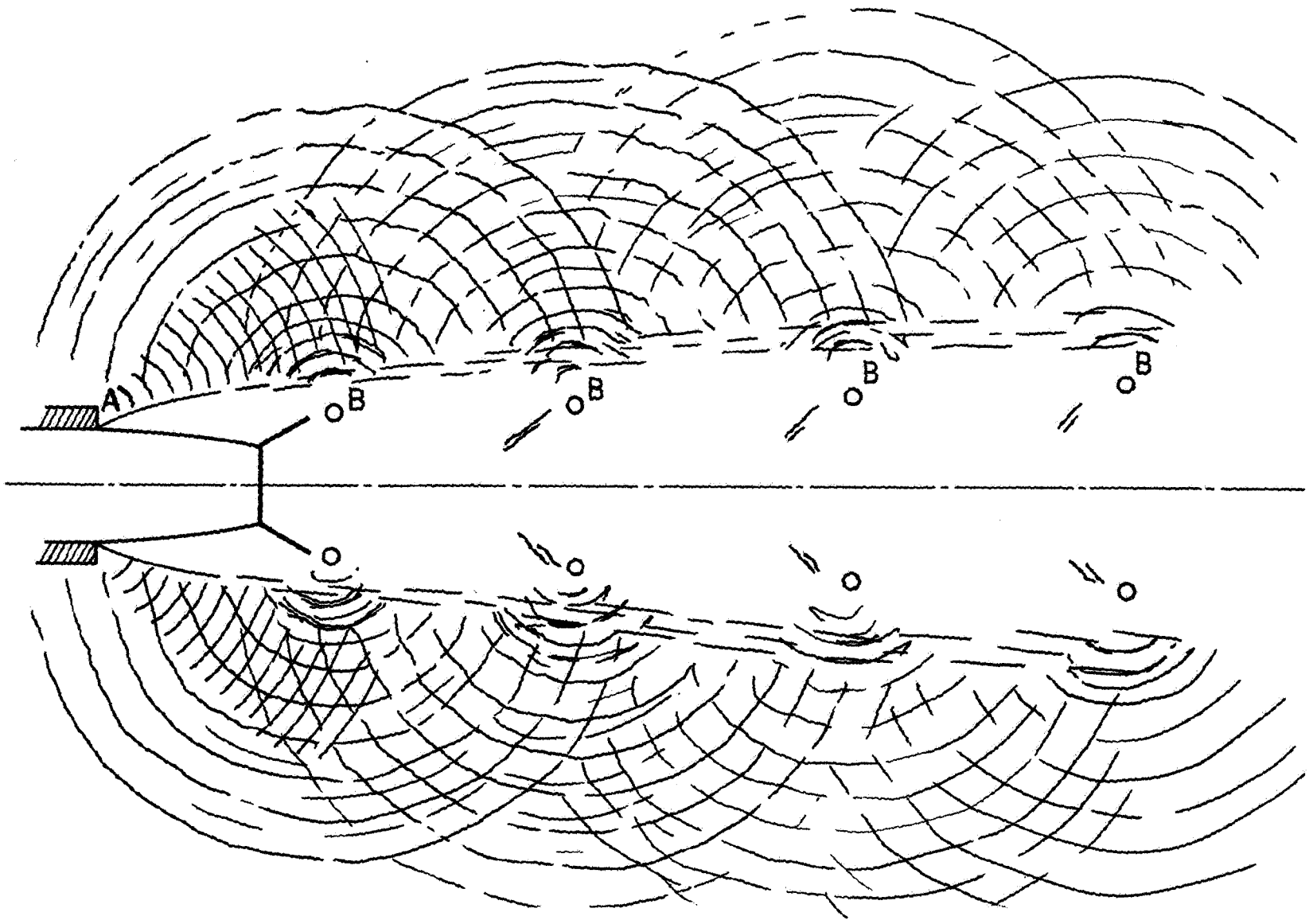

FIGURE 31. SKETCH OF TYPICAL ACOUSTIC EMISSIONS.
A. SOURCE OF DIRECTIONAL ACOUSTIC EMISSION.
B. SOURCE OF SPHERICAL ACOUSTIC EMISSION.

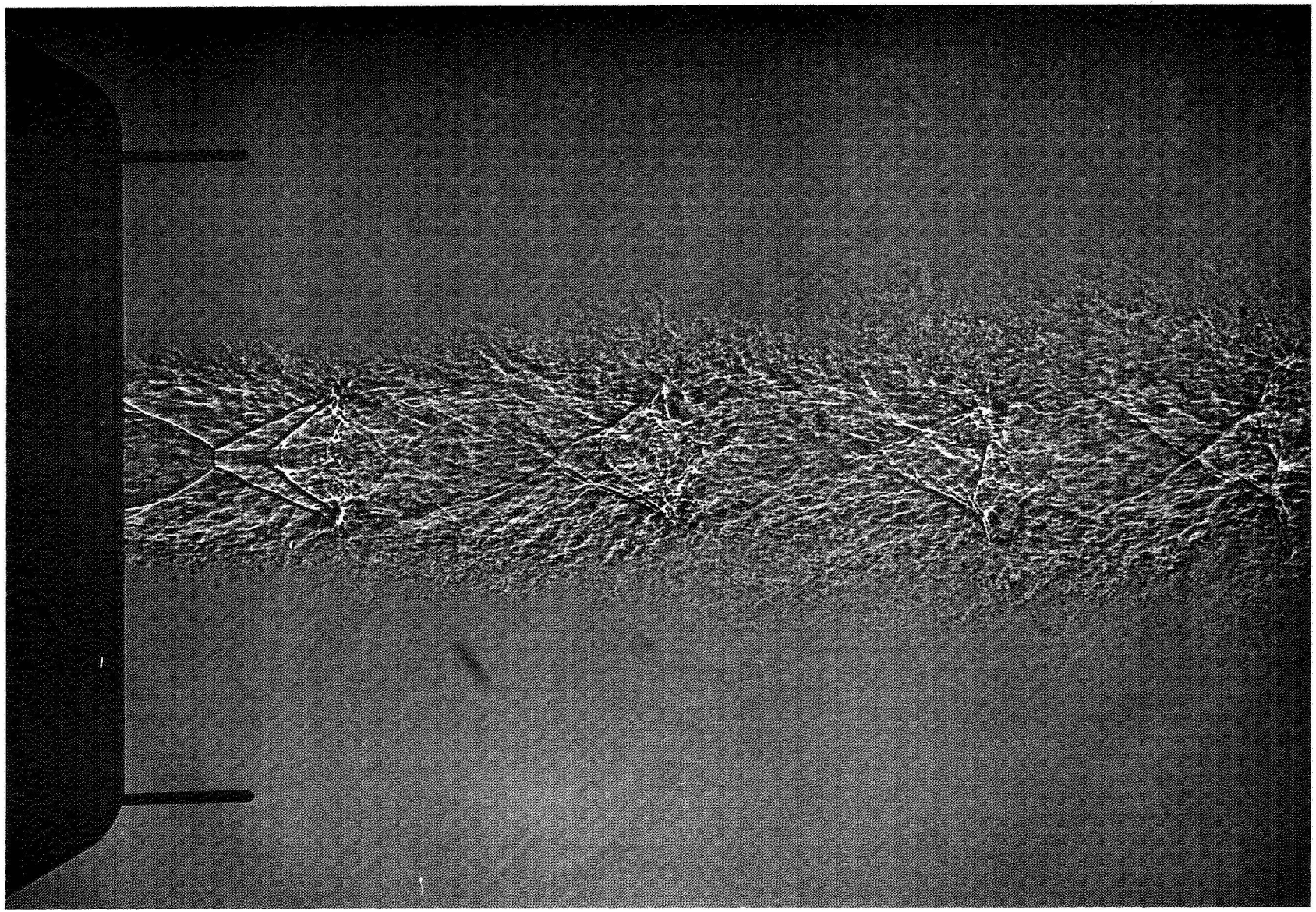

a) NOZZLE ARRANGEMENT I, X/D = 0.6, 8% IMPINGEMENT.

FIGURE 32. SHADOWGRAPHS FOR EACH NOZZLE ARRANGEMENT AT PEAK TOTAL ACOUSTIC POWER EMISSION SHOWING SOUND FIELDS. MAIN JET TOTAL PRESSURE = 100 PSIG.

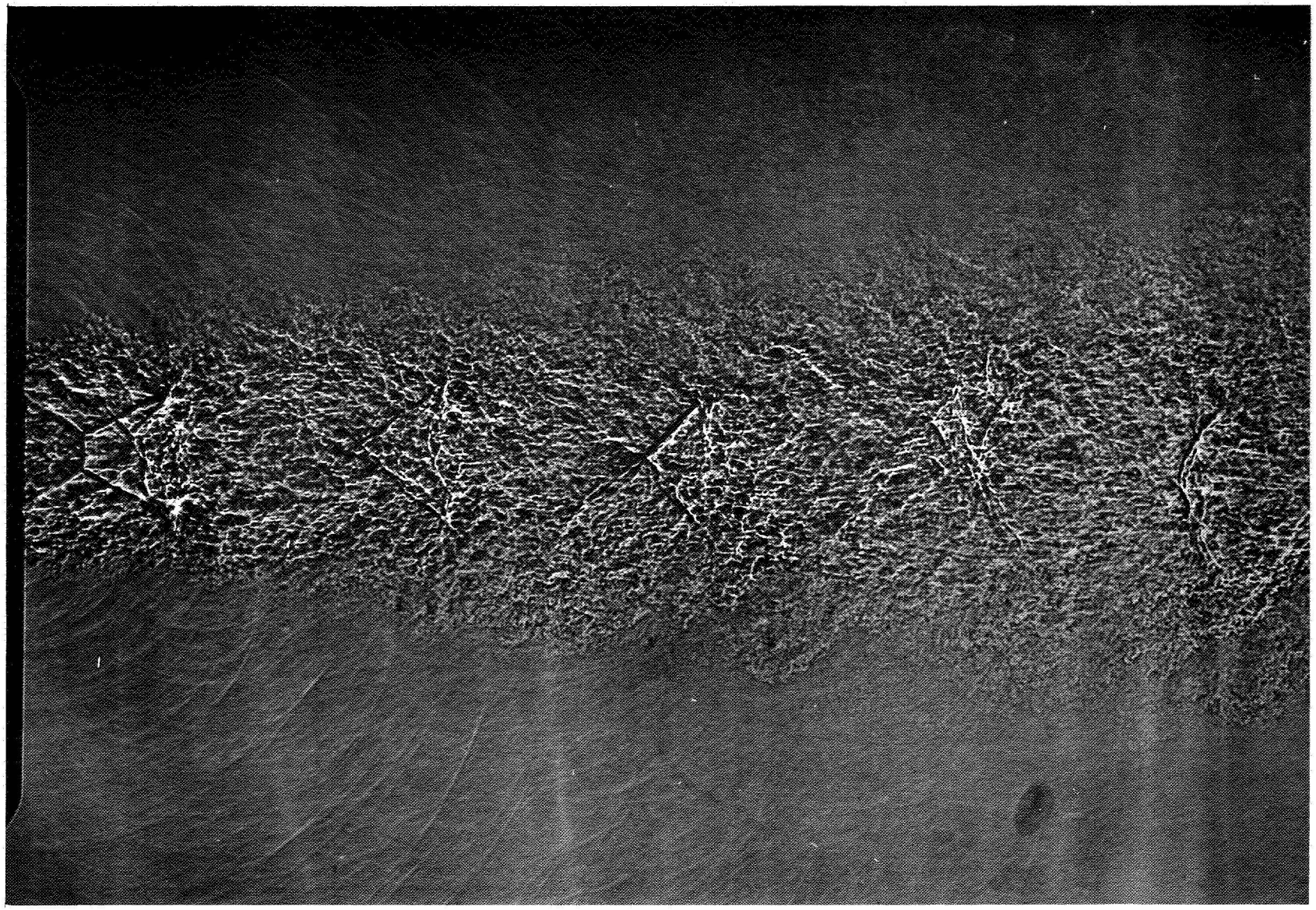

b) NOZZLE ARRANGEMENT II, X/D = 0.8, 14% IMPINGEMENT.

FIGURE 32, CONTINUED.

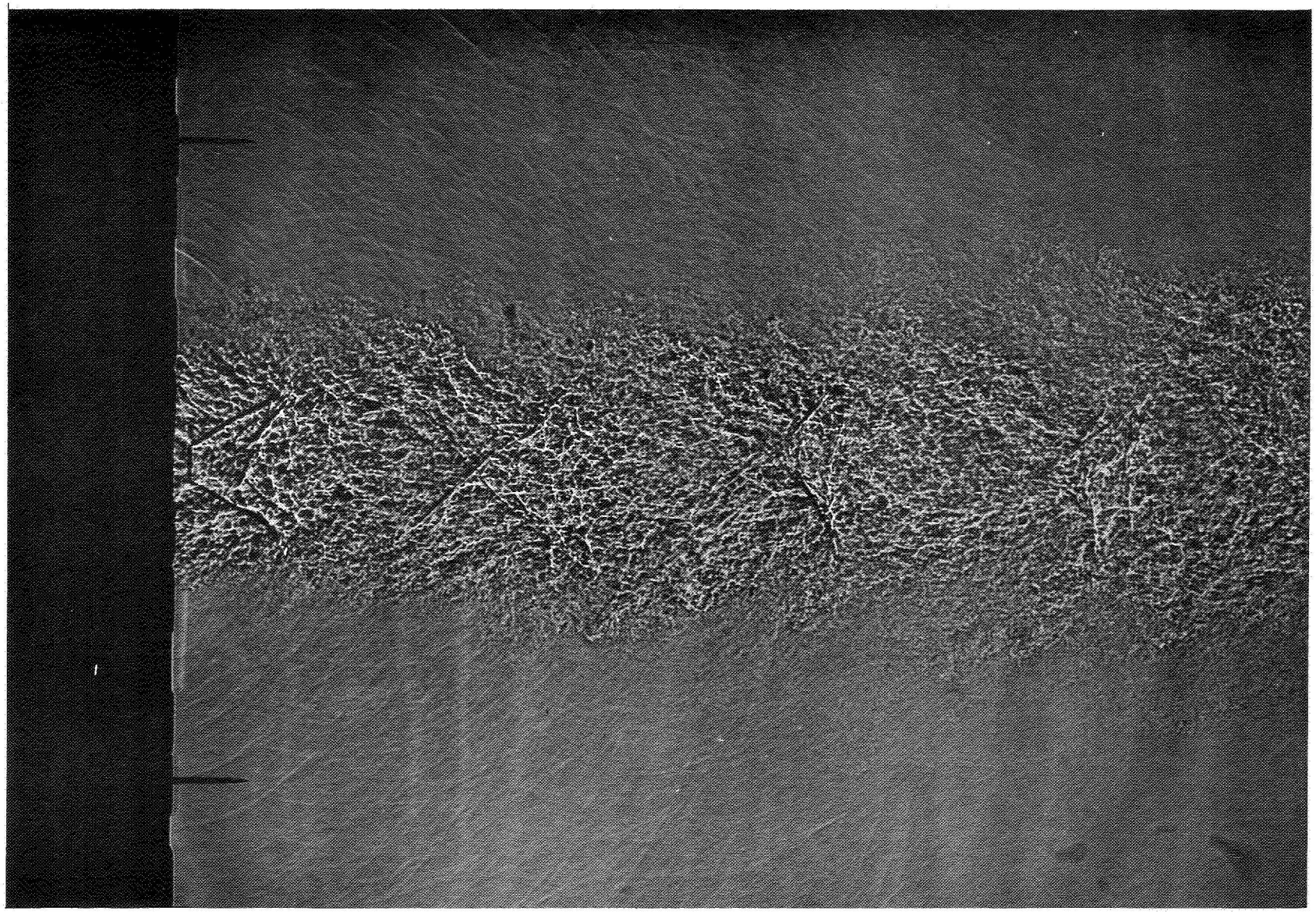

c) NOZZLE ARRANGEMENT III, X/D = 0.8, 12% IMPINGEMENT.

FIGURE 32, CONTINUED.

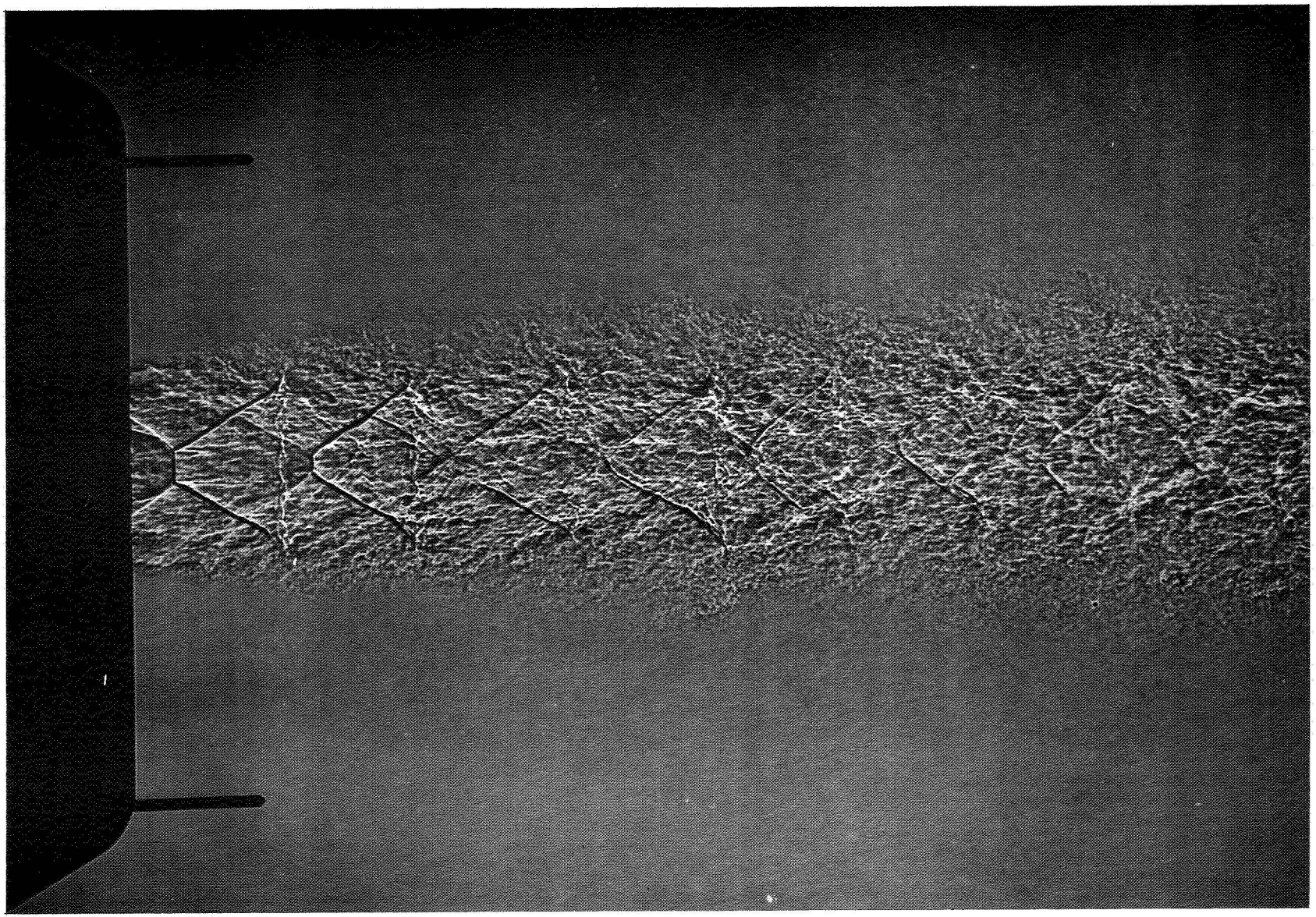

a) NOZZLE ARRANGEMENT I, X/D = 0.6, 18% IMPINGEMENT.

FIGURE 33. SHADOWGRAPHS FOR EACH NOZZLE ARRANGEMENT AT MINIMUM TOTAL ACOUSTIC POWER EMISSION SHOWING SOUND FIELDS. MAIN JET TOTAL PRESSURE = 100 PSIG.

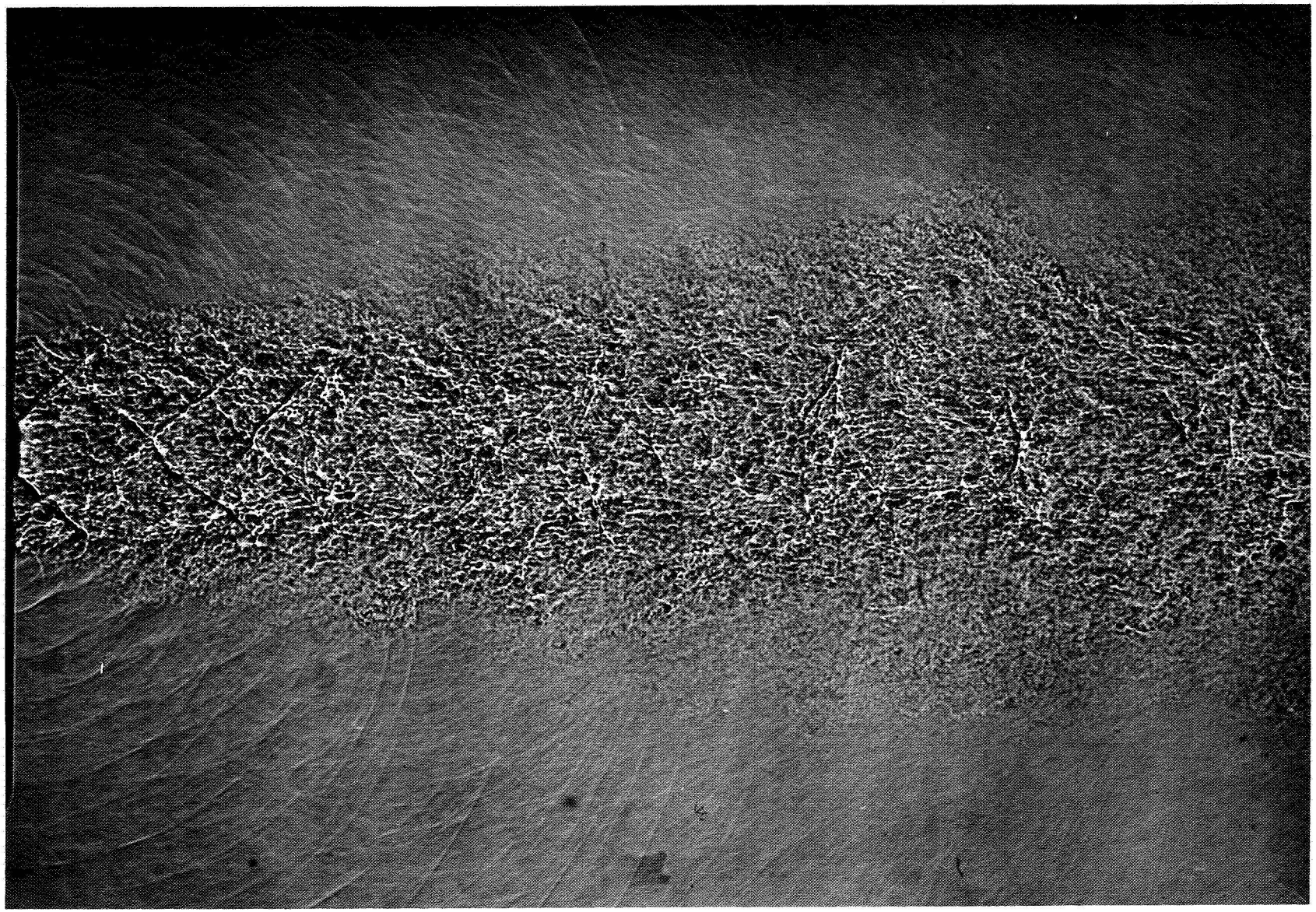

b) NOZZLE ARRANGEMENT II, X/D = 0.8, 24% IMPINGEMENT.

FIGURE 33, CONTINUED.

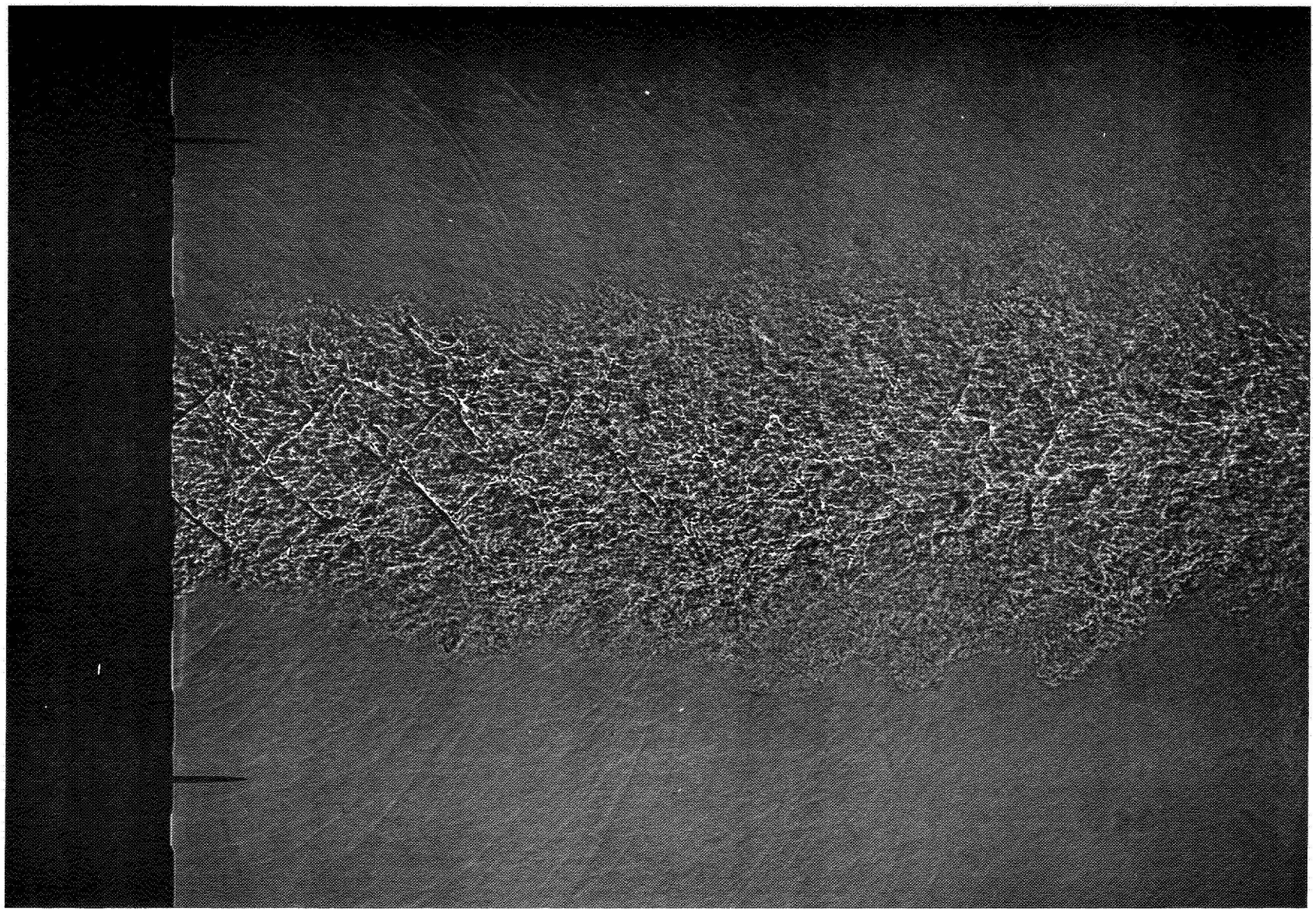

c) NOZZLE ARRANGEMENT III, X/D = 0.8, 24% IMPINGEMENT.

FIGURE 33, CONTINUED.

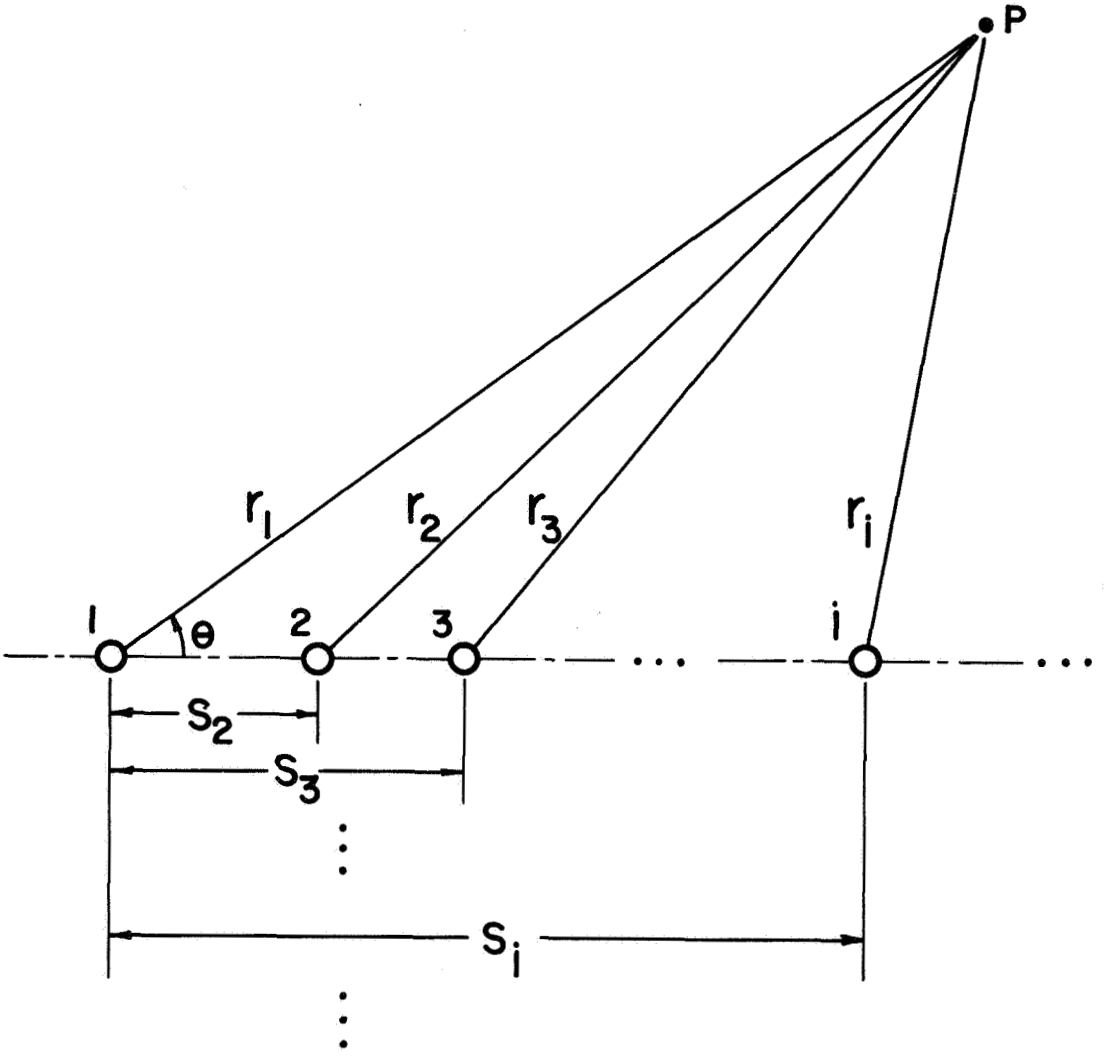

FIGURE 34. GEOMETRY OF LINE DISTRIBUTION OF MONOPOLE SOURCES.

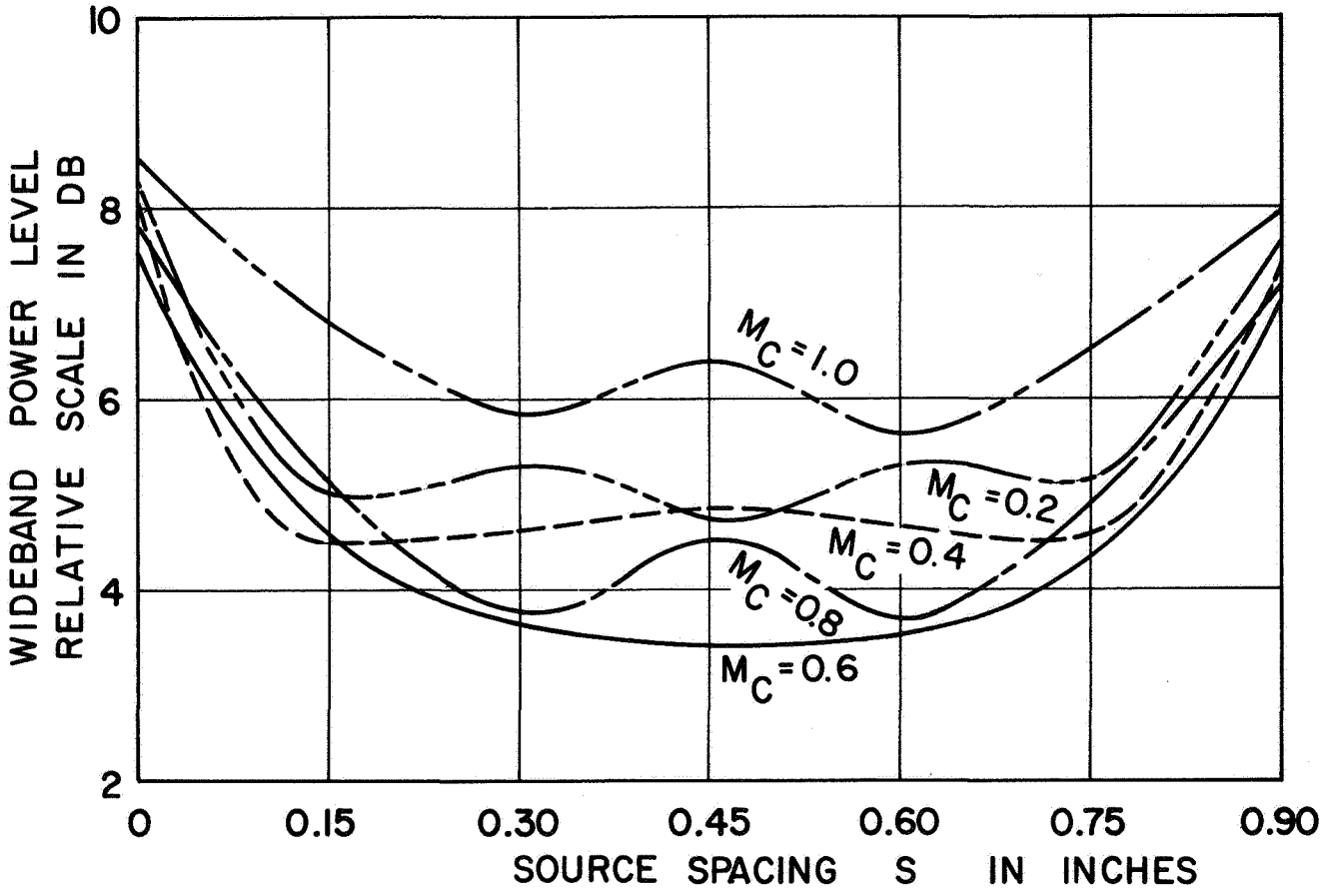

FIGURE 35. RELATIVE WIDEBAND POWER LEVEL VARIATIONS WITH SOURCE SPACING.

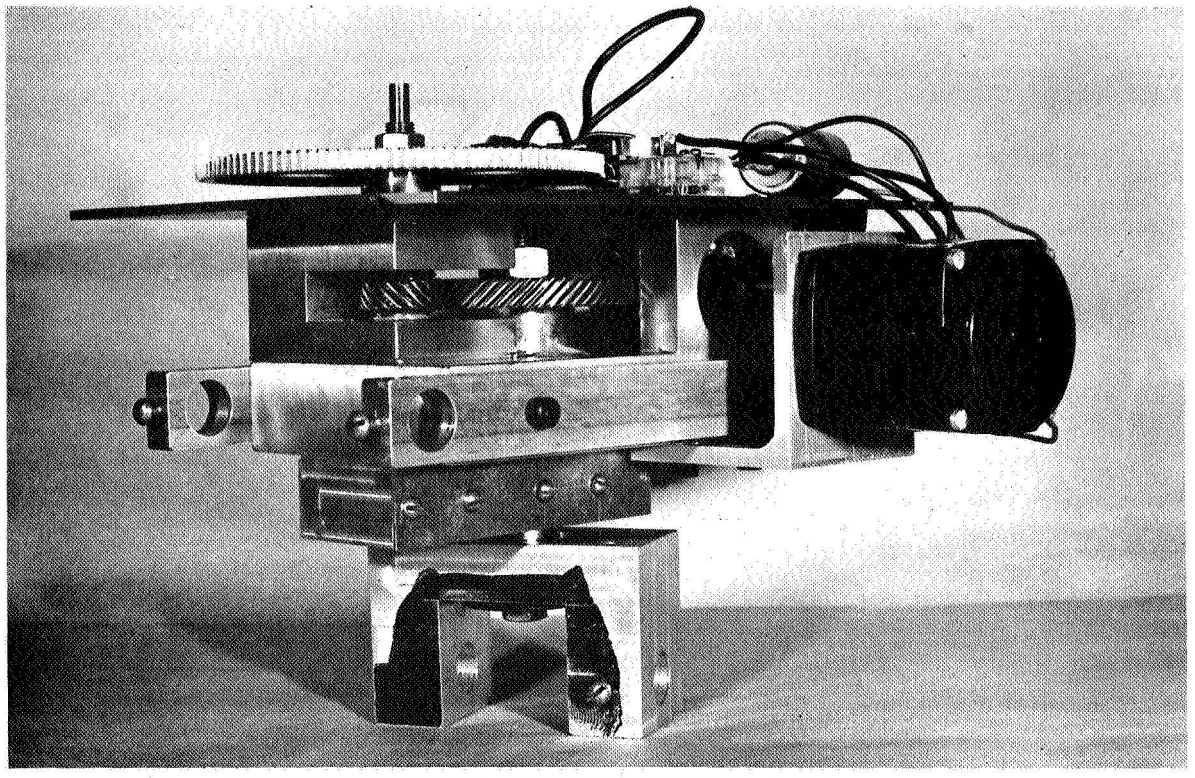

FIGURE 36. BASIC MICROPHONE BOOM POSITIONING ASSEMBLY.

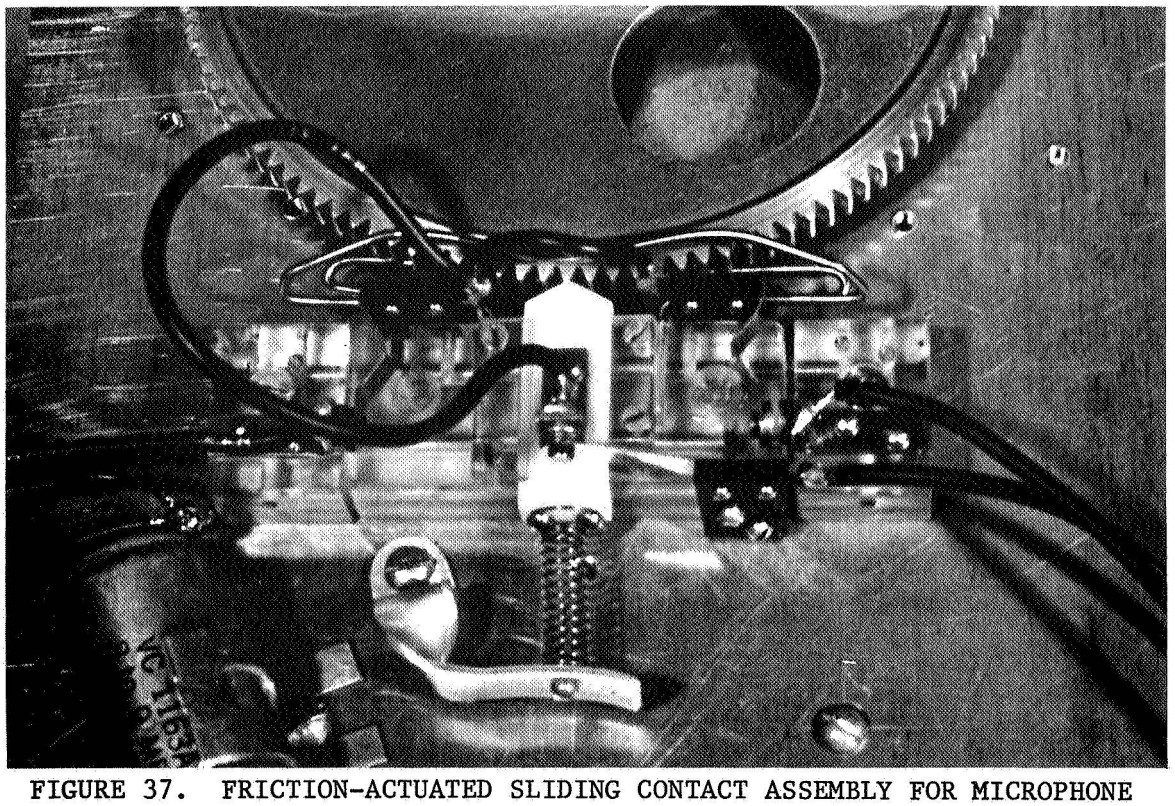

FIGURE 37. FRICTION-ACTUATED SLIDING CONTACT ASSEMBLY FOR MICROPHONE BOOM POSITION INDICATION.

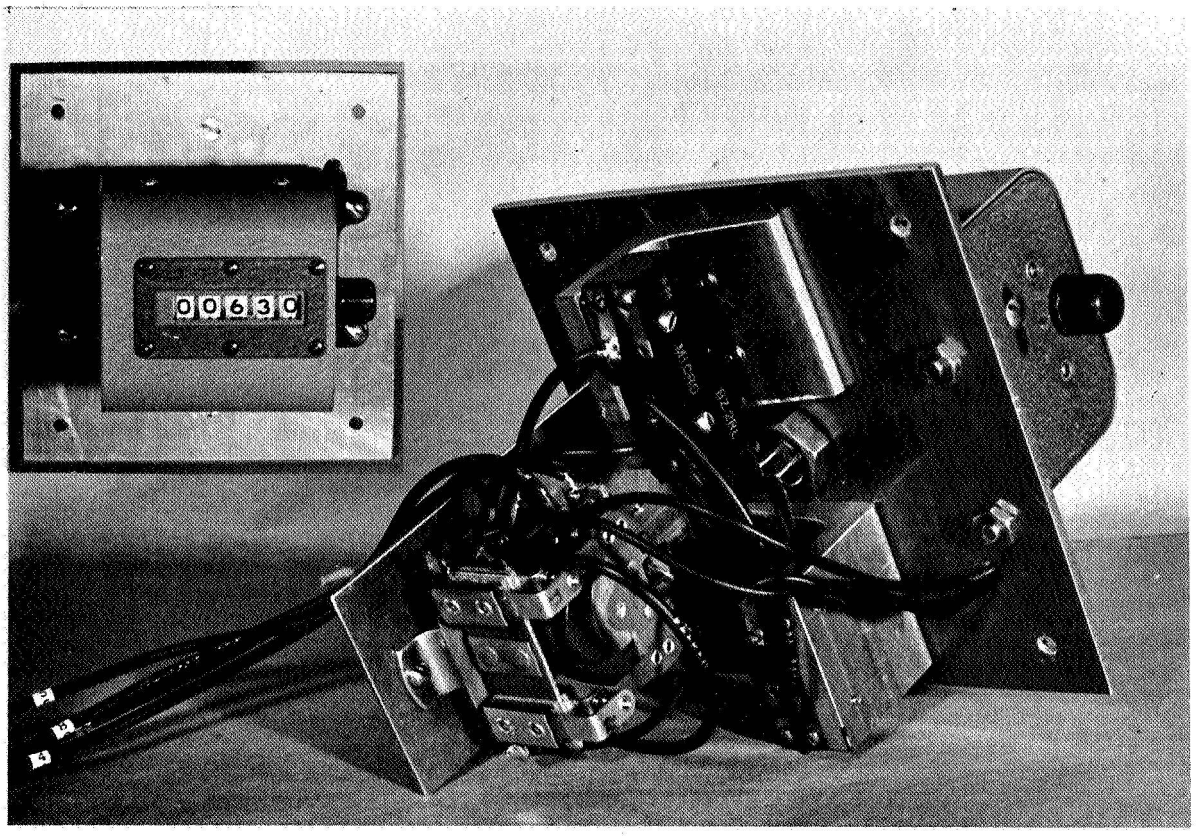

FIGURE 38. COUNT REGISTER ASSEMBLY. INSET SHOWS DIGITAL READOUT.